Title:	Assessment of existing structures based on elastic-plastic stress fields - Modelling of critical details and investigation of the in-plane shear transverse bending interaction
Authors:	Muttoni A., Fernández Ruiz M., Niketic F., Backes M.-R.
Published in:	Rapport OFROU
Volume: Pages:	N° 680 pp. 134
Country:	Switzerland
Year of publication:	2016
Type of publication:	Report

Please quote as:	Muttoni A., Fernández Ruiz M., Niketic F., Backes M.-R., *Assessment of existing structures based on elastic-plastic stress fields - Modelling of critical details and investigation of the in-plane shear transverse bending interaction*, Rapport OFROU, N° 680, Switzerland, 2016, pp. 134.

Schweizerische Eidgenossenschaft
Confédération suisse
Confederazione Svizzera
Confederaziun svizra

Eidgenössisches Departement für Umwelt, Verkehr, Energie und Kommunikation UVEK
Département fédéral de l'environnement, des transports, de l'énergie et de la communication DETEC
Dipartimento federale dell'ambiente, dei trasporti, dell'energia e delle comunicazioni DATEC

Bundesamt für Strassen
Office fédéral des routes
Ufficio federale delle Strade

Assessment of Existing Structures based on Elastic-Plastic Stress Fields

Modelling of Critical Details and Investigation of the In-Plane Shear Transverse Bending Interaction

Vérification de structures existantes par la méthode des champs de contraintes élastiques-plastiques Modélisation de détails critiques et analyse de l'interaction entre l'effort tranchant et la flexion transversale

Prüfung bestehender Bauwerke anhand der elastisch-plastischen Spannungsfeldmethode Modelle für kritische Details und Untersuchung der Interaktion von Längsschub und Querbiegung

École Polytechnique Fédérale de Lausanne (EPFL)
Laboratoire de construction en béton (IBETON)

Prof. Dr. A. Muttoni
Dr. M. Fernández Ruiz
F. Niketić
M.-R. Backes

Projet de recherche AGB 2009/009 sur demande de l'AGB Groupe de Travail Recherche en Matière des Ponts

October 2016 **680**

Schweizerische Eidgenossenschaft
Confédération suisse
Confederazione Svizzera
Confederaziun svizra

Eidgenössisches Departement für Umwelt, Verkehr, Energie und Kommunikation UVEK
Département fédéral de l'environnement, des transports, de l'énergie et de la communication DETEC
Dipartimento federale dell'ambiente, dei trasporti, dell'energia e delle comunicazioni DATEC

Bundesamt für Strassen
Office fédéral des routes
Ufficio federale delle Strade

Assessment of Existing Structures based on Elastic-Plastic Stress Fields

Modelling of Critical Details and Investigation of the In-Plane Shear Transverse Bending Interaction

Vérification de structures existantes par la méthode des champs de contraintes élastiques-plastiques Modélisation de détails critiques et analyse de l'interaction entre l'effort tranchant et la flexion transversale

Prüfung bestehender Bauwerke anhand der elastisch-plastischen Spannungsfeldmethode Modelle für kritische Details und Untersuchung der Interaktion von Längsschub und Querbiegung

École Polytechnique Fédérale de Lausanne (EPFL)
Laboratoire de construction en béton (IBETON)

Prof. Dr. A. Muttoni
Dr. M. Fernández Ruiz
F. Niketić
M.-R. Backes

Projet de recherche AGB 2009/009 sur demande de l'AGB Groupe de Travail Recherche en Matière des Ponts

October 2016 **680**

Impressum

Instance de recherche et équipe de projet

Direction du projet
Prof. A. Muttoni

Membres
F. Niketić
M.-R. Backes
Dr. M. Fernández Ruiz

Commission de suivi

Président
Jean-Christophe Putallaz

Membres
Dr. Manuel Alvarez
Stéphane Cuennet
Dr. Hans Rudolf Ganz

Auteur de la demande

Groupe de travail recherche en matière de ponts (AGB)

Source

Le présent document est téléchargeable gratuitement sur http://www.mobilityplatform.ch.

Table des matières

Résumé

La méthode des bielles-et-tirants et la méthode des champs de contraintes sont largement répandues dans la pratique et constituent la base de la norme SIA262:2013. Les deux méthodes conduisent à une borne inférieure de la résistance (selon la théorie de plasticité) et peuvent être aisément utilisées pour le dimensionnement d'éléments structuraux en béton armé et précontraint. Par contre, en ce qui concerne la vérification d'éléments structuraux existants, ces méthodes simples ne sont souvent pas suffisamment précises pour pouvoir démontrer la sécurité structurale. Dans ces cas, des méthodes avancées peuvent être utilisées. Les champs de contraintes élastiques-plastiques (EPSF, elastic-plastic stress fields) se sont montrés particulièrement appropriés pour ce type d'analyses. La méthode des EPSF permet d'établir des champs de contraintes licites (équilibre et condition de plasticité satisfaits, borne inférieure de la résistance) qui permettent au même temps la formation des mechanismes (borne supérieure de la résistance). Ainsi les EPSF remplissent simultanément les théorèmes statique et cinématique de la théorie de plasticité et constituent donc la solution exacte selon la théorie de plasticité. Il est à noter que selon la théorie de la plasticité, la solution exacte correspond à la résistance maximale possible de toutes les solutions basées sur les champs de contraintes. Vue la précision élevée/augmentée des champs de contraintes élastiques-plastiques, ils sont particulièrement intéressants pour l'analyse d'éléments structuraux critiques, car ils permettent éventuellement d'augmenter leur degré de conformité et ainsi d'éviter des renforcements onéreux.

La méthode des champs de contraintes élastiques-plastiques a été développée par Fernández Ruiz et Muttoni [12] et est implémentée dans un programme aux éléments finis nommé JCONC. JCONC est disponible gratuitement sous forme d'un applet sur le site web http://i-concrete.epfl.ch. Cet outil numérique est robuste et les résultats numériques ont montré un très bon accord avec les résultats d'essais d'une grande variété d'éléments structuraux et de cas de charge. Le présent rapport examine en détails un certain nombre de sujets liés aux EPSF qui n'avaient pas été abordés dans les premières publications :

- Recommandations pour des modèles aux éléments finis (EF) appropriés pour traiter des détails critiques de ponts tels que : entretoises, zones d'introduction de forces concentrées importantes et de forces de précontraintes, joints Gerber, poutres avec discontinuités géométriques etc. ;
- Adhérence béton-armature et éclatement du béton d'enrobage ;
- Examen critique de la méthode aux éléments finis (MEF): sensibilité au maillage et problèmes de localisation ;
- Validation rigoureuse et extensive de la MEF par une comparaison à des essais ;
- Discussion du format de sécurité à adopter pour ce type d'analyse non-linéaire.

La méthode des EPSF a été développée pour l'analyse d'éléments structuraux soumis à des sollicitations dans le plan (efforts membranaires). Or, dans de nombreux cas de la pratique, les efforts intérieurs réels sont une combinaison d'efforts membranaires et flexionnels (moments et efforts tranchants hors du plan). Un exemple spécifique est constitué par les âmes des ponts en caisson qui sont soumises simultanément à des efforts tranchants longitudinaux (dans le plan) et à des moments de flexion transversaux (hors du plan). Depuis les années 1970, des champs de contraintes appropriés pour ces cas de charge combinés ont été étudiés. Ces modèles, qui se basent généralement sur un champ rigide-plastique (RP), négligent certains aspects de l'interaction effort tranchant-flexion transversale, notamment la variation de l'inclinaison du champ de compression et du facteur de réduction k_c (pour la prise en compte de l'effet de la fissuration sur la résistance à la compression du béton) dans l'épaisseur de l'âme. Ainsi, ces modèles d'interaction RP donnent des estimations plutôt conservatrices de la résistance réelle. Dans le présent rapport, l'interaction entre l'effort tranchant et la flexion transversale dans les âmes de ponts en caisson est analysée selon une approche multicouches basée sur les EPSF. Des modèles d'interaction RP de la littérature sont présentés et leurs résultants sont comparés à la solution multicouches.

Le rapport est structuré en deux parties ; la première comporte la validation et l'application des EPSF pour divers détails critiques de ponts ; la deuxième traite l'action combinée de l'effort tranchant dans le plan et de la flexion transversale dans les âmes des ponts en caisson. Le contenu des deux parties est brièvement présenté ci-dessous.

Méthode des EPSF – Modèles aux éléments finis pour le traitement de détails structuraux critiques

Ce chapitre présente les principes des champs de contraintes élastiques-plastiques (EPSF) dont les résultats sont validés par une comparaison systématique à des résultats de campagnes expérimentales. Une série de détails structuraux spécifiques sont analysés et des recommandations pour leur modélisation appropriée sont données :

- Poutre en béton armé et béton précontraint ;
- Poutres avec joints Gerber et éléments avec discontinuité géométrique prononcée ;
- Entretoises et voiles croisés.

Cette section donne également des informations pratiques pour la modélisation de certains détails tels que les zones d'introduction de charges concentrées, les zones d'appui, l'ancrage des barres d'armatures, l'éclatement du béton d'enrobage etc. Des instructions claires pour le choix d'un maillage approprié sont données. Le sujet du format de sécurité à adopter pour un calcul EF non-linéaire est également traité dans cette section.

Finalement, 315 essais et les EPSF correspondants sont présentés et comparés. Les résultats et modèles EF ont été regroupés dans une base de données qui peut être consultée en ligne sur http://i-concrete.epfl.ch/epsf/.

Recommandations pour le maillage

Comme les champs de contraintes élastiques-plastiques sont développés de manière automatique par une méthode aux éléments finis, les résultats finaux peuvent être influencés par les propriétés du maillage et de l'élément fini utilisé. Afin d'évaluer la sensibilité des EPSF, une série d'éléments en béton armé soumis à des charges uniformes et non-uniformes ont été modélisés avec différents maillages. Les résultats numériques sont relativement constants, même si un léger effet de taille a pu être observé (*Fig. 13*).

A l'issue de cette analyse, il a été retenu que l'espacement des étriers peut être utilisé comme grille principale pour la construction du maillage. En plaçant quatre éléments finis entre deux étriers (*Fig. 11*), l'approximation du champ de contrainte réel est généralement suffisamment précise. De plus, il faut veiller à ce que la forme des EF triangulaires ne soit pas trop élancée, le rapport hauteur-largeur de 1:3 ne devant à cet effet pas être dépassé. Il est pourtant admissible que cette limitation ne soit pas respectée localement, p.ex. en cas de contraintes géométriques. En effet, les analyses ont montré que ce paramètre n'a généralement que peu d'influence sur le résultat global.

L'orientation des EF a par contre une très grande influence. Une orientation préférentielle de l'hypoténuse des EF doit être évitée. Il faut préférer des dispositions en forme de zigzag (*Fig. 16c*) ou en forme de bloc composé de quatre éléments (*Fig. 11*). Une orientation aléatoire de l'hypoténuse est également possible, mais demande aux moins 5 simulations afin d'obtenir une estimation fiable de la charge ultime (*Fig. 16c* à *Fig. 17*).

Convergence et nombre d'itérations

Le nombre d'itérations à effectuer doit être défini avant chaque calcul numérique. Les analyses ont montré que 250 itérations sont suffisantes pour obtenir des résultats satisfaisants. Le calcul a convergé après 250 itérations si l'erreur reste petite (*Fig. 18* courbe rouge), sinon le calcul a divergé (*Fig. 18* courbe noire). À la fin de chaque calcul numérique, un contrôle de l'équilibre global du modèle doit être effectué (réactions d'appuis - charges appliquées).

Particularités de la modélisation
Comme les EPSF sont utilisés pour l'analyse d'éléments structuraux dans un état de contraintes plan, quelques simplifications doivent être effectuées lors de la modélisation d'éléments réels.

- Géométrie des éléments finis pour le béton et les armatures.
  Les éléments structuraux en béton sont modélisés par des EF bidimensionnel (triangles plans) dont l'épaisseur correspond à l'épaisseur de l'élément structural (*Fig. 20a-b*). Si l'épaisseur réelle n'est pas constante (variation graduelle) sur la surface de l'EF triangulaire, l'EF prend une épaisseur moyenne. Les barres d'armatures qui sont situées à une même hauteur sont modélisées par une seule barre avec une section équivalente (*Fig. 20a-b*).
- Charges concentrées.
  Les charges concentrées et les appuis ne doivent pas être appliqués directement sur la surface de béton, parce qu'ils peuvent causer une rupture locale et donc la divergence du calcul numérique. Afin d'éviter ceci, les charges concentrées sont généralement introduites à l'aide d'une plaque en acier fictive (*Fig. 21*).
- Précontrainte.
  Le précontrainte est modélisée de la manière suivante :
  - Les forces d'ancrage de la précontrainte sont appliquées comme des charges concentrées à la surface du béton ;
  - Les forces de déviation sont appliquées comme des forces concentrées ou réparties;
  - Mise en place d'éléments-barres pour modéliser les câbles ou barres de précontrainte ;
  - Modification de la résistance (limite d'écoulement) dans les éléments-barres pour tenir compte de l'effet de la mise en tension (résistance résiduelle) ;
  - Réduction de l'épaisseur du béton pour prendre en compte la présence des gaines (*Fig. 22d*).

  Dans certains cas, la résistance du béton doit être augmentée localement afin d'éviter une rupture dans la zone d'ancrage. Ceci est possible grâce à l'état de compression triaxial dans cette zone (*Fig. 22a*).
- Longueur d'ancrage insuffisante.
  Dans ce cas, la rupture peut se produire à cause d'un manque d'adhérence. Afin de représenter ce comportement dans le modèle EF, la section de la barre d'armature est réduite linéairement en fonction de la relation adhérence-glissement (*Fig. 24*).
- Éclatement du béton d'enrobage.
  Pour les éléments de structure dont la rupture est causée par une délamination du béton d'enrobage dans la zone de compression, des EF additionnels doivent être introduits dans le modèle. Ces éléments fictifs sont mis en place dans la zone concernée et prennent en compte l'énergie de fissuration en admettant une loi de matériau élastique-plastique (*Fig. 26b* et *Fig. 27c*).

Format de sécurité
Pour les calculs avec la méthode des EPSF, le format de sécurité partiel, tel que défini dans la norme SIA262:2013, doit être appliqué aussi bien pour le dimensionnement de nouvelles structures que pour la vérification de structures existantes. Une méthode permettant d'adapter les facteurs de sécurité partiels pour les EPSF a été développée et est présentée dans cette section. Les facteurs de sécurité réduits qui en résultent doivent encore être utilisés avec beaucoup de précaution et uniquement si des investigations supplémentaires sont effectuées.

Exactitude de l'analyse par la méthode des EPSF
La méthode des EPSF permet d'obtenir une très bonne estimation de la charge de rupture réelle. La méthode a été comparée à un grand nombre d'essais effectués sur des éléments de types très variés par différents auteurs et à différentes périodes (1957-2015). La moyenne du rapport « charge de rupture mesurée sur charge de rupture calculée » est de 1.03 avec un coefficient de variation de 8%. Aucune tendance des résultats n'a pu être observée par rapport aux facteurs principaux (*Fig. 34*). De plus, la prédiction du mode de rupture de chaque élément correspond au mode observé lors de l'essai.

Âmes de poutres avec flexion transversale

Certains éléments structuraux, en particulier les âmes des ponts en caisson, ne peuvent pas être analysées en admettant un état de contrainte uniforme sur l'épaisseur. En effet, ces éléments sont constamment sollicités aussi bien par un effort tranchant longitudinal (dans le plan de l'âme) que par des moments et efforts tranchants transversaux (hors du plan de l'âme). Bien que ce type de sollicitation soit fréquent, il n'a que très peu été étudié dans le passé. Le petit nombre d'essais représentatifs disponibles dans la littérature montre quand même que la capacité portante peut être influencée de manière importante par la présence d'un moment transversal dans l'âme, en particulier si la résistance à la compression de l'âme est déterminante.

Par conséquent, le fait de négliger l'interaction entre l'effort tranchant et la flexion transversale et de faire des analyses indépendantes du comportement longitudinal et transversal des âmes de ponts caisson n'est pas en accord avec le comportement réel des âmes à la rupture. Ceci peut amener à des taux d'armature à l'effort tranchant excessifs et à une superposition inadmissible des contraintes de compression dans l'âme. Afin d'éviter cet effet, surtout dans le cas d'éléments soumis à d'importantes contraintes de compression et pour la vérification de structure existantes, les méthodes d'analyse doivent prendre en compte l'action simultanée (interaction) de l'effort tranchant et de la flexion transversale.

Le but de ce chapitre est donc d'étudier des modèles d'interaction existants et de proposer une approche avancée, basée sur les champs de contraintes élastiques-plastiques (EPSF), qui permet une étude détaillée de l'interaction effort tranchant-flexion transversale. Le chapitre commence avec une présentation de plusieurs modèles de la littérature, une importance particulière étant portée sur les modèles de Thürlimann [64] et Menn [65]. Thürlimann étend la méthode des champs de contrainte rigides-plastiques (RPSF) pour effort tranchant et flexion longitudinal au cas d'un moment de flexion transversal additionnel. Cette approche lui permet d'établir une expression explicite pour la résistance à l'effort tranchant maximal sous l'action d'un moment transversal donné. Plus tard, ce modèle d'interaction a été repris et modifié par plusieurs auteurs, dont Menn. Ces modèles d'interactions sont des modèles d'équilibre qui se basent sur le théorème statique (borne inférieure) de la théorie de plasticité et amènent donc à une estimation sécuritaire de la capacité portante. Les modèles d'interaction rigides-plastique (RP) sont simples et illustrent de manière élégante le transfert des efforts à l'intérieur de l'âme (en accord avec les observations d'essais). Cependant, ils prédisent une très forte interaction et donc une réduction importante de la résistance à l'effort tranchant sous l'action d'un moment transversal, même faible. Ce comportement des modèles RP s'explique en partie par leur champ de contraintes fortement simplifié, mais surtout par les hypothèses faites concernant l'inclinaison du champ de compression et la résistance effective du béton ($k_c \cdot f_{cp}$). Ces paramètres sont choisis selon les méthodes de dimensionnement classiques pour l'effort tranchant (sans flexion transversale) et admis constants sur l'épaisseur de l'âme. Ainsi, les modèles d'interaction RP conduisent à une estimation conservative de la résistance (borne inférieure) et à un effet très prononcé de la flexion transversale sur la résistance à l'effort tranchant.

Dans une seconde partie, une méthode affinée pour l'analyse de l'interaction entre l'effort tranchant longitudinal et la flexion transversale est présentée. Il s'agit d'un modèle élastique-plastique multicouches (ML-EP) dont chaque couche respecte les conditions des champs de contraintes élastiques-plastiques. Le modèle ML-EP permet une meilleure utilisation des réserves de résistance de l'âme et conduit donc à une estimation plus précise de la capacité portante réelle. L'approche ML-EP montre que l'interaction est sensiblement moins prononcée, surtout pour des moments transversaux faibles, ce qui augmente notablement la prédiction de résistance sous l'action combinée d'effort tranchant et de flexion transversale. La capacité portante globale augmente davantage, grâce à une résistance à l'effort tranchant initial (sans flexion transversale) plus élevée.

Le modèle ML-EP comporte un champ de contraintes plus détaillé permettant une distribution non-uniforme des contraintes, ainsi que des facteurs de réduction (k_c) et des inclinaisons variables à travers l'épaisseur de l'âme. Grâce aux conditions de compatibilité

cinématiques, les champs de contraintes dans les différentes couches peuvent développer des inclinaisons qui vont au-delà des limites conventionnelles et l'effet, généralement positif, de la compression flexionnelle sur la résistance effective du béton est ainsi également pris en compte. Les facteurs de réduction (k_c) calculés sur la base de l'état local de déformation sont généralement plus élevés que ce qui est admis dans les analyses RP. Malgré un coût de calcul plus important, l'approche ML-EP est une alternative intéressante dans les cas où une évaluation plus détaillée de la résistance à l'effort tranchant en présence d'un moment transversal est requise.

Finalement, une approche simplifiée est présentée. Elle combine l'outil numérique (JCONC) pour la génération des champs de contraintes élastiques-plastiques plans (constants dans l'épaisseur) avec les principes des modèles d'interactions RP. Cette approche simplifiée permet d'obtenir une information sur le comportement globale de l'élément tout en prenant en compte, de manière simplifiée, l'effet de la flexion transversale sur le champ de contraintes et donc la résistance à l'effort tranchant. Cette approche conduit généralement à une résistance plus élevée que les modèles d'interaction RP, mais donne tout de même une borne inférieure de la résistance réelle. Le rapport donne finalement un aperçu sur une extension de la méthode des champs de contraintes élastiques-plastiques qui consiste en un élément fini élastique-plastique multicouches.

Zusammenfassung

Die Bemessung von Stahlbeton- und Spannbetonträgern mittels Fachwerkmodellen und Spannungsfeldmethoden ist in der Praxis weit verbreitet. Beide Betrachtungsweisen führen, gemäss dem statischen Grenzwertsatzes der Plastizitätstheorie, zu einem unteren Grenzwert der Traglast und können somit zur einfachen und sicheren Bemessung von Betonelementen verwendet werden. Bei der Prüfung von bestehenden Bauteilen sind solch einfache Spannungsfelder (oder Fachwerkmodelle) jedoch oft unzureichend um die Tragsicherheit rechnerisch gewährleisten zu können. Erweiterte Spannungsfeldmethoden, und insbesondere die elastisch-plastische Spannungsfeld-methode (EPSF), haben sich in solchen Fällen als besonders geeignet erwiesen. Unter Berücksichtigung elastisch-plastischer Materialgesetze, leitet die EPSF Methode ein statisch zulässiges Spannungsfeld her, welches unter Bruchlast zu einem mit den Randbedingungen verträglichen Bruchmechanismus führt. Die EPSF erfüllen gleichzeitig den unteren und den oberen Grenzwertsatz der Plastizitätstheorie und führen daher zu exakten Lösungen der Traglast. Diese Traglast ist somit gleichzeitig die maximal mögliche Traglast eines Spannungsfeldes. Insbesondere bei der Prüfung kritischer Bauwerkteile ist die Anwendung der EPSF Methode von grossem Vorteil, da durch ihre erhöhte Präzision kostspielige Verstärkungen und Instandsetzungen eventuell vermieden werden können.

Die von Fernández und Muttoni [12] entwickelte EPSF Methode wurde in das Finite-Elemente (FE) Programm JCONC implementiert und kann als kostenloses Applet von der Internetseite http://i-concrete.epfl.ch heruntergeladen werden. Das FE Programm zeigt eine konsequente und gute Übereinstimmung mit den Versuchsergebnissen einer grossen Anzahl verschiedener Bauwerksteile und unterschiedlicher Traglasten auf. Verschiedene Themen wurden jedoch nicht detailliert oder explizit in den ersten Veröffentlichungen behandelt und werden deshalb in dem vorliegenden Bericht genauer untersucht:

- Richtlinien zur angemessenen Modellbildung von kritischen Brückentragwerkselementen: Querträger, Krafteinleitungszonen grosser Einzellasten und Vorspannkräfte, Gerber-Gelenke, Träger mit geometrischen Diskontinuitäten, gekreuzte Wände usw.;
- Verbund von Bewehrungsstahl-Beton und Abplatzungen der Betonüberdeckung;
- Kritische Auseinandersetzung mit der angewendeten FE Technik: Einfluss der Netzgeometrie auf die Ergebnisse und Lokalisierungsprobleme;
- Ausgedehnter Nachweise der Zuverlässigkeit der FE Methode mittels Vergleichen zu Versuchsergebnissen;
- Diskussion zum Sicherheitsformat für nicht-lineare Berechnungsverfahren.

Die EPSF Methode wurde zur Bemessung von 2D-Bauteilen in ebenem Spannungszustand entwickelt. In vielen praktischen Beispielen liegt jedoch eine kombinierte Beanspruchung aus Membran- und Querkräften vor. Ein besonderes Beispiel hierfür sind Hohlkastenträger von Brücken deren Stege gleichzeitig durch Längsschub und Querbiegung beansprucht werden. Seit den 1970ger Jahren wurden für solche Fälle geeignete Spannungsfelder erforscht. Die meist starr-plastischen Bemessungsvorschläge vernachlässigen jedoch gewisse Aspekte der kombinierten Beanspruchung und liefern somit eine eher konservative Näherung des tatsächlichen Schubwiderstandes unter Querbiegung. Der Grund hierfür liegt vor allem darin, dass die Neigung des Druckfeldes und der Beiwert k_c, zur Errechnung der effektiven Betondruckfestigkeit bei Rissbildung, über die Stegbreite konstant angenommen werden. Folgender Bericht enthält deshalb nicht nur eine Untersuchung der Interaktion von Längsschub und Querbiegung anhand der klassischen starr-plastischen Modelle, sondern ebenfalls eine detaillierte Analyse mittels einer erweiterten EPSF Methode (Schichtmodell).

Der vorliegende Bericht ist in zwei Teile gegliedert; der Erste behandelt die Prüfung und Anwendung der EPSF im Falle von kritischen Brückentragwerkselementen in ebenem Spannungszustand; der Zweite befasst sich mit der kombinierten Membran- und Querbeanspruchung welche in Stegen von Hohlkastenträgern auftreten. Der Inhalt beider Kapitel wird im Folgenden kurz zusammengefasst.

EPSF Methode – Modellbildung für die Behandlung kritischer Tragwerkselemente in ebenem Spannungszustand

Dieses Kapitel befasst sich mit den Grundlagen der EPSF Methode und dem systematischen Nachweise der numerischen Ergebnisse anhand von Vergleichen mit Versuchsergebnissen. Es werden ebenfalls eine Reihe spezifischer Bauteile untersucht für welche detaillierte Richtlinien zur angemessenen Modellbildung vorgeschlagen werden:

- Stahlbeton- und Spannbetonträger;
- Gerber-Gelenke und Träger mit geometrischen Diskontinuitäten;
- Brückenquerträger und gekreuzte Wände.

Des Weiteren werden praktische Empfehlungen für die FE-gerechte Darstellung von Krafteinleitungszonen grosser Einzellasten und Vorspannkräfte, Auflagerbereiche, Verankerung von Bewehrungsstäben und Abplatzen der Betonüberdeckung gegeben. Die FE-Modell-Beispiele werden zusätzlich durch klare Anleitungen zur Auswahl eines geeigneten Netzes ergänzt. Die Anwendung des Sicherheitsformats bei nicht-linearen Berechnungen mit der EPSF FE Methode wird ebenfalls behandelt. Der vorliegende Bericht enthält ebenfalls eine Diskussion über das Sicherheitsformat welches bei nicht-linearen Berechnungen mit der EPSF FE Methode angewendet werden soll.

Schlussendlich werden 315 Beispiele von EPSF Modellen vorgestellt und mit den zugehörigen Versuchsergebnissen verglichen. Diese Daten stehen in einer online Datenbank zur Verfügung: http://i-concrete.epfl.ch/epsf/.

Empfehlungen zur geeigneten Netzbildung für die EPSF Analyse

Da die EPSF automatisch anhand einer Finiten-Elemente-Methode generiert werden, können die Ergebnisse sowohl durch die Element- als auch durch die Netzeigenschaften beeinträchtigt werden. Um den Einfluss Letzterer auf die EPSF zu untersuchen wurde eine Reihe von Elementen unter gleichmässigem und ungleichmässigem Spannungszustand mittels verschiedener Netze untersucht. Die Ergebnisse waren relativ konstant, obwohl einen leichter Massstabseffekt festgestellt werden konnte (*Fig. 13*).

Es wurde festgehalten, dass der Schubbewehrungsabstand als Hauptgitter für die Netzbildung verwendet werden sollte. Mit vier Beton-Finiten-Elemente (Dreiecken) zwischen zwei Bewehrungsstäben (*Fig. 11*) kann entsprechend eine genügend genaue Näherung des Spannungsfeldes erreicht werden. Desweitern sollte darauf geachtet werden, dass die FE-Dreiecke das Verhältnis Höhe-zu-Breite von 1:3 nicht überschreiten. Ist dies jedoch unvermeidlich (z.B. durch geometrische Vorgaben) darf die Begrenzung punktuell verletz werden, da die Untersuchungen nur einen sehr geringen Einfluss dieses Parameters auf das Gesamtergebnis aufgezeigt haben.

Im Gegenteil zur Form der FE-Dreiecke, hat die FE Ausrichtung einen sehr grossen Einfluss auf das Endergebnis. Eine für das gesamte Modell bevorzugte Neigungsrichtung der FE-Hypotenusen sollte möglichst vermieden werden. Ein zick-zack Anordnung (*Fig. 16c*) oder Blöcke, bestehend aus vier Elementen (*Fig. 11*), sind zu bevorzugen. Eine aleatorische Anordnung der Elemente ist auch möglich, in diesem Fall werden jedoch mindestens 5 Simulationen benötigt um die Traglast verlässlich ermitteln zu können (*Fig. 16c* bis *Fig. 17*).

Konvergenz und Anzahl der Iterationen

Für die numerische Berechnung der EPSF muss die Anzahl der durchzuführenden Iterationen im Vorfeld festgelegt werden. Die vorliegenden Untersuchungen haben gezeigt, dass 250 Berechnungsschritte ausreichend sind. Eine FE-Berechnung konvergiert wenn der Fehler nach der 250ten Iteration klein bleibt (siehe rote Linie in *Fig. 18*). Ist dies nicht der Fall (siehe schwarze Linie in *Fig. 18*) ist das Modell divergiert. Am Schluss der Berechnung ist immer eine Kontrolle des Gesamtgleichgewichts (Auflagerkräfte) empfohlen.

Hauptaspekte der Modellbildung mit der EPSF Methode
Die EPSF wurde zur Analyse von Spannungsfeldern in ebenem Spannungszustande entwickelt. Dies entspricht in den meisten Fällen jedoch nicht exakt der Realität, weshalb gewisse Vereinfachungen bei der Modellbildung vorgenommen werden müssen.

- Modellgeometrie.
  Das Stahlbetontragwerk wird anhand von zweidimensionalen FE dargestellt. Die Dicke der FE entspricht der Stärke des jeweiligen Betonelementes (*Fig. 20a-b*). Ist die Elementstärke über die Fläche des FE-Dreieckes variabel, nimmt die FE Dicke den Durchschnittswert an. Bewehrungsstäbe welche sich auf gleicher Höhe befinden werden anhand eines einzelnen FE-Bewehrungsstabes mit äquivalenter Querschnittsfläche dargestellt (*Fig. 20a-b*).
- Lasteintragungszonen.
  Grosse Einzellasten und Auflagerkräfte sollten nicht direkt an die Betonoberfläche aufgebracht werden, da dies zu lokalem Versagen des FE Modells führen kann. Um dies zu vermeiden wird üblicherweise eine virtuelle Stahlplatte zur Lasteinleitung verwendet (*Fig. 21*).
- Vorspannung.
  Die Modellbildung für Spannbetonträger wird wie folgt durchgeführt:
  - Aufbringen einer konzentrierten Kraft zur Berücksichtigung der Verankerungskraft;
  - Verteilte und/oder konzentrierte Umlenkkräfte;
  - Spannglieder werden anhand von Bewehrungselementen dargestellt;
  - Reduzierung der Fliessgrenze der Spannelemente im FE Modell zur Berücksichtigung des verbleidenden Widerstandes (nach Vorspannung);
  - Verminderung der Stegdicke entlang der Spanngliedführung (*Fig. 22d*).

  In manchen Fällen muss die Betondruckfestigkeit in der Verankerungszone erhöht werden um die günstige Wirkung des dreiachsigen Spannungszustandes zu berücksichtigen und somit einen lokalen Betondruckbruch zu vermeiden (*Fig. 22a*).
- Unzureichende Verankerungslänge von Bewehrungsstäben.
  In solchen Fällen kann sich ein Verbundbruch ausbilden. Im FE Modell wird dies durch eine lineare Abminderung des Bewehrungsquerschnittes gemäss einer Verbund-Stahldehnung-Beziehung (*Fig. 24*) dargestellt.
- Abplatzen der Betonüberdeckung.
  Im Falle von Bauteilen die durch Abplatzungen der Betonüberdeckung in der Druckzone versagen (*Fig. 26a*) müssen spezielle Finite-Elemente, welche die Bruchenergie des Risses berücksichtigen, im betroffenen Bereich angebracht werden (*Fig. 26b* und *Fig. 27c*).

Sicherheitsformat
Bei numerischen Berechnungen mit der EPSF Methode sollte das Sicherheitsformat mit partiellen Faktoren gemäss der Norm SIA262:2013 sowohl zur Bemessung neuer Bauteile als auch beim Tragsicherheitsnachweis bestehender Elemente angewandt werden. Ein Verfahren zur Anpassung der Teilsicherheitsbeiwerte für die EPSF Methode wird vorgestellt. Die daraus folgenden verminderten Sicherheitsbeiwerte sollten jedoch nur mit grösster Vorsicht und unter Voraussetzung zusätzlicher Nachforschungen eingesetzt werden.

Genauigkeit der EPSF Analyse
Mit der EPSF Methode kann eine sehr gute Näherung der Traglast und des Bruchmechanismus erreicht werden. The EPSF Modelle wurden mit einer Vielzahl von Versuchsergebnissen verschiedenartiger Elemente, von verschiedenen Autoren und aus verschieden Perioden (1957 - 2015) verglichen. Das durchschnittliche Verhältnis von gemessener zu berechneter Traglast beträgt 1.03 mit einem Variationskoeffizient von 8%. Des Weiteren konnten keine Tendenzen in den Ergebnissen festgestellt werden (*Fig. 34*).

Querbiegebeanspruchung von Brückenstegen

In einer grossen Anzahl von Tragwerkselementen, wie zum Beispiel den Stegen von Hohlkastenbrücken, sind die Voraussetzungen zur Annahme eines über die Stegdicke konstanten Spannungszustandes nicht geben. Solche Elemente werden sowohl durch

Längsschub als auch durch Querbiege- und Querschublasten beansprucht. Obwohl diese kombinierte Beanspruchung sehr häufig vorkommt, wurde dieses Thema in der Vergangenheit nur sehr wenig erforscht. Es sind nur eine sehr begrenzte Anzahl an repräsentativen Versuchsergebnissen sind verfügbar, sie zeigen jedoch auf, dass der Schubwiderstand des Steges durch ein zusätzliches Querbiegemoment negativ beeinflusst werden kann. Dies gilt in besonderem Masse bei hoher Beanspruchung im Druckfeld.

Eine getrennte Ermittlung der Tragsicherheit beider Tragwirkungen (Längsschub und Querbiegung) stimmt demnach nicht mit dem wirklichen Tragverhalt des Steges im Bruchzustand überein. Ein solches Verfahren kann deshalb zu sehr hohen Bewehrungsgraden und unzulässigen Überlagerungen von Betondruckspannungen im Steg führen. Um dies zu vermeiden sollten Bemessungsverfahren womöglich die kombinierte Beanspruchung aus Schub und Querbiegung im Steg berücksichtigen. Dies gilt insbesondere für den Tragsicherheitsnachweis bestehender Tragwerkselemente mit potentiell sprödem Bruchverhalten.

Das Ziel der vorliegenden Arbeit ist es bestehende Modelle zur Interaktion von Längsschub und Querbiegung zu analysieren und ein erweitertes, auf der EPSF beruhendes, Modell vorzuschlagen. Zuerst werden aus der Literatur entnommene Interaktionsmodelle vorgestellt, mit besonderem Augenmerk auf die Modellvorschläge von Thürlimann [64] und Menn [65]. Thürlimann erweitert die starr-plastische Spannungsfeldmethode für Längsschub, Biegung und Torsion für den Fall eines zusätzlich angreifenden Querbiegemomentes und leitet daraus eine Interaktionsbeziehung zwischen dem maximalen Schubwiderstand und dem Querbiegemoment im Steg ab. Dieses Modell beruht auf dem statischen Grenzwertsatz der Plastizitätstheorie und führt somit zu einem unteren Grenzwert des Tragwiderstandes. Das Modell wurde später von mehreren Autoren (unter anderem Menn) übernommen und erweitert. Die starr-plastischen Modelle sind einfach zu handhaben und erläutern auf elegante Weise die Schubtragwirkung unter Querbiegung (in Übereinstimmung mit den Versuchen). Sie prognostizieren jedoch eine übermässig starke Interaktion und somit eine substantielle Abminderung des Schubwiderstandes, dies bereits für geringe Querbiegemomente. Der Grund hierfür liegt, zum Teil in dem sehr stark vereinfachten Spannungsfeld, hauptsächlich jedoch in den Annahmen die effektive Betondruckfestigkeit ($k_c f_{cp}$) und die Neigung der Druckstrebe betreffend. Die entsprechenden Werte werden gemäss dem klassischen Bemessungsverfahren bei Schubbeanspruchung (ohne Querbiegung) gewählt und führen deshalb zu eher konservativen Tragwiderständen (unterer Grenzwert) und einer ausgeprägten Interaktionsbeziehung zwischen Längsschub und Querbiegung.

Im zweiten Teil wird eine erweiterte, auf den EPSF beruhende, Methode zur Untersuchung der Wechselwirkung von Schub und Querbiegung vorgestellt. Dieses elastisch-plastische (EP) Schichtmodell erlaubt eine grössere Ausnützung der Kapazität und somit eine genauere Näherung der tatsächlichen Traglast von Stahlbetonträgern. Das EP Schichtmodell zeigt teilweise eine deutlich geringere Abminderung des Schubwiderstandes auf (als die starr-plastischen Modelle), was im Allgemeinen zu einem signifikant höheren kombinierten Tragwiderstand für Längsschub und Querbiegung führt, insbesondere im Bereich schwacher Querbiegemomente. Der kombinierte Tragwiderstand wird zusätzlich durch einen bedeutend höheren Anfangs-Schubwiderstand (ohne Querbiegung) positiv beeinflusst.

Das EP Schichtmodell verfügt über ein weitaus detaillierteres Spannungsfeld, mit über die Stegbreite variablen Spannungen, Druckfeldneigungen und effektiven Betondruckfestigkeitsfaktoren, als die starr-plastischen Modelle. Auf Grund der Verträglichkeitsbedingungen können sich zulässige Spannungsfelder mit Neigungswinkel ausserhalb der gebräuchlichen Neigungsgrenzen entwickeln. Des Weiteren wird der meist positive Einfluss der Querbiegedruckkraft auf die effektive Betondruckfestigkeit berücksichtigt. Die anhand der Dehnungszustände errechneten effektiven Betondruckfestigkeitsfaktoren sind im Allgemeinen deutlich höher als was bei starr-plastischen Berechnungen angenommen wird. Somit ist das EP-Schichtmodell, trotz erhöhtem Zeit- und Rechenaufwand, eine interessante Alternative für Fälle in denen eine detaillierte Auswertung des Schubwiderstandes unter Querbiegung erforderlich ist.

Im dritten Teil wird ein vereinfachtes Verfahren zum Nachweis der Tragsicherheit unter kombinierter Schub- und Querbiegebeanspruchung ganzer Tragwerkselemente vorgeschlagen. Die FE Methode zur automatischen Erstellung von EPSF wird mit den Hauptprinzipien der starr-plastischen Interaktionsmodelle kombiniert um den Einfluss des Querbiegemomentes auf vereinfachte Weise im FE Modell berücksichtigen zu können. Dieses Verfahren führt im Allgemeinen zu einer höheren Schubtragfähigkeit als starr-plastische Interaktionsmodelle mit konstanten Betondruckfestigkeitsfaktoren (k_c) und stellt dennoch einen unteren Grenzwert der Traglast dar. Schliesslich wird ein Ausblick auf ein neues, erweitertes Verfahren der EPSF Methode gegeben. Bei Letzterem handelt es sich um ein elastisch-plastisches Schicht-Finite-Element.

Summary

Stress fields and strut-and-tie models can be used to analyse reinforced and prestressed concrete members with transverse reinforcement. Both provide lower bound solutions of the failure load according to limit analysis and can be used for design of structural concrete members in a simple and reliable manner. With respect to the assessment of existing structures, simple stress fields (or their corresponding strut-and-tie models) might not be sufficient to ensure the strength of the structure. In this case, enhanced stress fields can be used. To this purpose, the use of elastic-plastic stress fields (EPSF) has revealed to be a suitable tool. The EPSF provides licit stress fields (lower-bound solution of the strength) respecting compatibility conditions of the materials (upper-bound solution of the strength). The EPSF fulfil simultaneously the upper-bound and lower-bound theorem of the theory of plasticity and therefore, they provide exact solutions according to the limit analysis. It can be noted that the exact solution represents the theoretical maximal load carrying capacity which can be calculated using stress fields. The use of EPSF is thus very convenient for the assessment of critical existing structures as their enhanced accuracy can potentially avoid unnecessary strengthening of structures or minimize the degree of rectifying required by them.

The EPSF were originally developed by Fernández Ruiz and Muttoni [12] and implemented in a finite element program (JCONC, which has been integrated as an applet into an educational web site http://i-concrete.epfl.ch and is free for download). This tool has been proven to be robust and consistent when compared to a large variety of structural members and failure loads. A certain number of topics were however not covered or detailed in the original works and are extended in the present report:

- Guidelines for suitable modelling (with the finite element method) of critical details of bridges such as diaphragms, introduction of prestressing forces, dapped-end members and others;
- Considerations of rebar-to-concrete bond and concrete cover spalling;
- Critical review of the finite element technology used (mesh sensitivity and localizations);
- Extensive validation of the tool against test data;
- Discussion on the suitable safety format for this type of nonlinear analysis.

The EPSF were developed as a tool to analyse plane stress problems. However, in many engineering situations, the in-plane inner forces are combined with out-of-plane forces (bending moments and shear). Particularly for box-girder bridges, the webs are subjected to in-plane shear and to transverse bending moments. Suitable stress fields for these elements were investigated since the 1970's. They correspond however to rigid-plastic solutions which neglect several issues (as the varying angle of the compressive stresses within the thickness of the panel and the resulting variable concrete strength reduction factor k_c accounting for cracking) and may be rather conservative. This topic is also reviewed in detail in this report on the basis of the EPSF. The classical approaches are presented and their results are compared to an EPSF solution of multiple layers.

This report is structured in two parts, the first covering the validation and application of EPSF to plane cases of critical details of bridges. It is followed by a second part dealing with the consideration of transverse bending and out-of-plane actions in the webs of bridges. The content of each part is briefly detailed below.

The EPSF method - Modelling techniques for plane stress critical details

In this part, the EPSF principles are presented and its results are validated by means of systematic comparison to test data. A series of specific details are also investigated and guidelines for their modelling are provided:

- Prestressed and reinforced concrete beams;
- Dapped-end beams and Gerber joints;
- Bridge diaphragms and crossed walls.

This section also offers some practical recommendations for modelling structural concrete members, such as load introduction zones, support regions, anchorage of reinforcement, concrete cover spalling etc. In addition to this, it gives clear recommendations on how to select a suitable mesh for a model and how to introduce the safety format to a nonlinear finite element analysis.

Finally, 315 practical examples of EPSF models are presented and compared to test. The results have been collected in a database, which is available online at http://i-concrete.epfl.ch/epsf/.

Mesh related recommendations for EPSF analysis

Given the fact that the EPSF are developed in an automatic manner using a finite element method, the final results can be influenced by mesh properties and element technology. In order to evaluate the sensitivity of EPSF models, a series of reinforced concrete members subjected to uniform and non-uniform stress states were modelled using different meshes. The EPSF proved to be quite stable, although some size effect was observed (refer to *Fig. 13*).

It is concluded that the actual stirrup spacing should be used as the main grid for the meshing. Four concrete finite elements should be placed in between each two stirrups (*Fig. 11*) in order to have a good representation of the reality. In addition to this, the shape of the finite element triangles should not be too distorted and the maximal height-to-side ratio of the triangle should not be more than 1:3. If it is unavoidable (due to geometrical constrains), this limit can be locally not respected, since the models showed very little sensitivity regarding this parameter.

The finite element orientation however has an important influence on the final result. Preferential inclinations of the finite element hypotenuses should be avoided. They should rather be disposed in a zig-zag manner (*Fig. 16c*) or in a block of 4, forming a square (*Fig. 11*). An aleatory hypotenuse inclination is acceptable, but requires at least 5 simulations in order to accurately assess the ultimate load of a structure (*Fig. 16c and Fig. 17*).

Model convergence and number of iterations

The number of iterations needs to be predefined for every simulation. The present investigation has shown that 250 steps are sufficient to obtain satisfying results. A model converged after 250 steps if the error stays low (refer to the red line in *Fig. 18*). If not, the model diverged (refer to the black line in *Fig. 18*). As an additional check, in order to accept an EPSF as a correct solution, the reaction forces from the model shall be checked to ensure that they correspond with the applied forces.

Modelling aspects of the EPSF method

Since the EPSF method is used to analyse plane stress state problems, some simplifications from the reality need to be performed when the actual structural members are analysed:

- Concrete and reinforcement geometry.
  Finite elements placed over a specific region of a structural concrete element should assume the thickness of that region (*Fig. 20*a and *b*). If the thickness of a structural concrete member is changing over the area of the finite element triangle, the finite element should assume the average thickness. The area of the reinforcement bars placed at the same height in a cross-section should be put together forming an

equivalent reinforcement bar. The reinforcement is then introduced as such to a finite element model (*Fig. 20*a and *b*).

- Concentrated loads.
  Concentrated loads and supports should not be placed directly on a surface of a structural concrete member, since they could cause local failure of the model (depending on their intensity). Instead, they should be applied to the model using a virtual steel plate (*Fig. 21*).
- Prestressing.
  In order to model a prestressed concrete element with the EPSF method, the following modifications need to be considered:
  - Applying a concentrated load on the element's surface to act as an anchorage force;
  - Introducing the deviation forces;
  - Introducing bar elements to account for the presence of the prestressing cables;
  - Modifying the yield limit of the tendon's high strength steel to account for the fact that they are initially under tension (residual strength);
  - Reducing locally the thickness of the concrete due to the presence of the duct (*Fig. 22d*).

  Since the size of the anchorage plate is well defined by the producer, the concrete compression strength sometimes needs to be locally increased to account for the beneficial effect of the tri-axial state of stress and thus to avoid local failure (*Fig. 22a*).
- Insufficient anchorage length.
  In case the rebars are not properly developed, a bond failure may happen. In this case, the section of the bars should be linearly reduced according to the bond strength (*Fig. 24*).
- Concrete cover spalling.
  In case the structural concrete elements are failing due to spalling of the concrete cover in the compression zone (as presented in *Fig. 26a*) special spalling elements need to be introduced in this zone (*Fig. 26b*). These elements account for the fracture energy of the spalling crack assuming an elastic-plastic material law (*Fig. 27c*).

Safety format
The partial safety format presented in SIA262:2013 should be applied with the EPSF simulations for the design and the assessment of structural concrete members. A procedure for tailoring partial safety factors for the EPSF method has been developed and presented. However, such reduction of partial safety factors should still be used with care and only when additional investigations are performed.

Accuracy of the EPSF analysis
The EPSF method is able to accurately estimate failure loads of structural concrete members. The elements varied in geometrical as well as mechanical properties, and were tested by various authors starting from 1957 to 2015. The average measured-to-predicted strength is equal to 1.03 with a coefficient of variation of only 8%. No trends in the results were observed for the most characteristic parameters (*Fig. 34*). In addition to this, each element failed accordingly to what was observed in the experimental campaigns.

Beam webs with transverse bending

Many structural elements such as the webs of box-girder bridges cannot be analysed under the assumption of a constant stress state (over the thickness) since they are subjected to transverse bending moments and out-of-plane shear. Despite the significance of this topic, only scanty research has been performed on it in the past. Yet, although only a small number of representative tests are available in the literature, it is that the bearing capacity of beams might be significantly influenced by the action of the transverse bending moment, especially in cases where concrete crushing is governing.

Consequently, neglecting the interaction of in-plane shear and transvers bending and performing independent analysis of the longitudinal and transverse behaviour of box-girder elements is not consistent with the actual behaviour of the webs at failure. It potentially leads to excessive amounts of shear reinforcement and to inconsistent and unsafe superposition of concrete compressive stresses. If, in the past, the interaction between

transverse bending and in-plane shear was often neglected (or treated in a simplified manner) in the design procedure, it is becoming of crucial importance for the assessment of existing structures.

The objective of this section is to study existing methods and to propose new ones grounded on the EPSF allowing for a detailed evaluation of the interaction effect. The section starts by presenting several in-plane shear transverse bending interaction models from the literature, with special emphasis on the models by Thürlimann [64] and Menn [65]. Thürlimann extended the classical rigid-plastic stress field (RPSF) approach for longitudinal shear, bending and torsion for the case of additional out-of-plane (transverse) bending. This allowed him to derive an explicit interaction relationship between the maximum in-plane shear resistance and the acting transverse bending moment. Thürlimann's model was later adopted and extended by several authors (including Menn). These are equilibrium based models that ground on the lower bound theorem of the theory of plasticity and thus lead to a safe estimate of the bearing capacity. The RPSF interaction models are simple and elegantly illustrate the shear transfer action under transverse bending (consistent with observations from tests). It is however observed that such rigid-plastic (RP) interaction models predict a very strong interaction and thereby a substantial reduction of the web shear resistance, already for small transverse moments. This is partly due to the strongly simplified stress-field, but above all it is due to the hypotheses on the concrete strength reduction factor and the inclination of the compression field. The latter are selected to be on the safe side according to what is known from the classical shear design (without transverse bending) leading thus to a conservative estimate of the shear strength (lower bound) and to a pronounced effect of the transverse bending moment.

In a second part, a refined method for the investigation of the in-plane shear transverse bending interaction is proposed. The proposed multi-layered elastic-plastic (ML-EP) panel element, in which every layer respects the conditions of the EPSF, takes account for the entire reserve capacity of the web segment, leading thus to a more accurate estimate of the failure load. The ML-EP approach showed that the actual interaction is noticeably weaker, thereby leading to a significantly higher combined in-plane shear transverse bending resistance of the web. This holds true particularly in the range of small transverse bending moments. Additionally, the predicted overall resistance greatly increases due to significantly higher initial in-plane shear strength (when no transverse bending moment is acting).

The ML-EP panel approach provides a more detailed stress-field allowing for the variation of stresses, inclinations and reduction factors over the width of the web. Due to the kinematic compatibility conditions, stress fields can develop inclinations beyond the conventional values/limitations and the mostly beneficial effect of the bending compression on the concrete strength reduction factor is taken into account. Additionally, the concrete strength reduction factors, which are computed from the local state-of-strain, are generally higher than what is admitted in RP approaches. Thus, although of higher computational cost, the ML-EP panel approach is an interesting alternative to the RP interaction models if a reduction of the uncertainty on the shear strength predictions under transverse bending is required.

Finally, a simplified verification method is presented. It is based on the finite element method for plane EPSF and thus provides information on the global behaviour and the bearing capacity of an entire structural element. The effect of the transverse bending moment on the stress-field, and thus on the in-plane shear resistance, is accounted for in a simplified manner by making use of the principles of the RP interactions models. This approach generally leads to higher shear strength for beams subjected to transverse bending than RP interaction models with constant concrete strength reduction factors (k_c). Nevertheless, it still provides a lower bound value of the actual failure load. Eventually, an outlook on an enhanced solution of the plane EPSF method, consisting of a multi-layered EPSF finite element method, is presented.

1 The use of elastic-plastic stress fields for the assessment of plane-stress members

The stress field method (SF) [1,2,3] and strut-and-tie models (STM) [4,5,6,7,8] are widely used for design and assessment of structural concrete members. Both techniques provide lower-bound solutions according to limit analysis and thus a variety of solutions can be proposed for the same structural member under specific actions. Selecting the most suitable lower-bound is a challenging task, which is usually related to cost optimization and to the type of analysis that needs to be performed.

When designing a new structural, element load-carrying models that are in equilibrium with the external actions at Ultimate Limit State (ULS) and provide simple reinforcement layouts should be selected. At the same time, the models must provide a suitable behaviour under Serviceability Limit State (SLS). On the other hand, when assessing the ultimate strength of an existing member (serviceability behaviour can be checked on site provided that no change in the actions occurs), avoiding or minimizing its strengthening should be the main priority. Therefore an optimal solution for a given case is reached through iterations starting from simple SF and STM. The models are gradually refined whenever calculated strength proves to be insufficient with respect to applied loads. At the final step, the model accounting for the actual failure mechanism of the investigated member governs the highest possible strength (exact solution) according to limit analysis [9,10].

This concept of gradual model refinement is known as the Levels-of-Approximation approach (LoA) [11], and is presented in *Fig. 1*. The idea behind it is to reach a satisfying accuracy of a model (for design or assessment) starting from simple solutions. Through this refinement, one can compare the results between simple and complex simulations in order to avoid any potential mistakes while saving time and resources (if a model based on a lower LoA provides satisfying behaviour, there is no need to pass to the higher LoA).

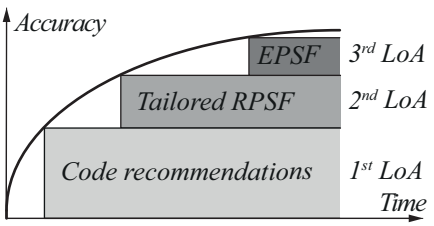

***Fig. 1** Levels of approximation approach*

As presented in *Fig. 1*, the lower LoA models take less time to develop but give more conservative solutions when compared to test results. As the level of approximation increases, so does the models computational time and accuracy. The 1st LoA is usually based on code recommendations (verifying the flexural or shear resistance on the basis of a cross-sectional approach for example). These expressions are quite general since they cover a wide range of practical problems (structural members having different cross-section shape and size, having different type of load, different arrangement of the supports etc.). 2nd LoA are usually based on tailored Rigid Plastic Stress Field (RPSF) method [3]. It accounts for specific characteristics of analysed elements thus giving more precise results (for example additional shear transfer in beams with double T cross section due to the presence of inclined flanges). Finally, the 3rd LoA is grounded on Elastic-Plastic Stress Field (EPSF) method [12] which gives exact solutions according to limit analysis by bringing together upper and lower bound theorem of the theory of plasticity [2].

It is important to keep in mind that every model is only a representation of the reality, meaning that the actual behaviour will always be slightly different. This justifies the idea that the appropriate model is not always the most complex one (accounting for all potential load carrying mechanisms). In fact it is the simplest solution which ensures a positive structural behaviour [13].

Even though SF and STM share a lot of similarities, they originate from two completely different approaches.

Strut-and-tie models were developed from the truss models introduced by Ritter in 1899 [4]. Truss models were founded on pure intuition, and used to describe the behaviour of beams. They allowed equilibrating the external actions and calculating the internal forces (tension and compression). It was later shown that the load-carrying models do not necessary have form a truss, but can also follow the shape of a funicular model in equilibrium [6]. This discovery set the beginning of the modern STM which were mainly developed in Stuttgart during the eighties [7,8]. Further studies focused on how to select an optimal position of the struts and ties in a model. Since at that time the elastic uncracked stress fields could be easily obtained by means of photo-elasticity or linear FEM, it was convenient to ground the shape of STM on such solutions [8]. Finally it was shown that the STM are consistent with lower-bound theorem of the limit analysis, and some procedures for the automatic development of the models were proposed [14].

On the other hand, the stress fields were directly developed from the theory of plasticity. The initial work in this field was done in 1936 by Gvozdev. In his publication which was later translated in English in 1960 [1], he formulated the upper and lower bound theorem, yield surface and the flow rule. One year later (in 1961) Drucker [2] developed a stress field for a simple supported beam subjected to point and distributed loading which respected both the upper and the lower bound theorem of the limit analysis (governing the exact solution). The stress fields were later mostly developed in Denmark [10] and Switzerland [15,3], where they are still used today as basic tools for structural design and assessment.

Despite their different origins the methods share many analogies and are in agreement with the limit analysis. Since they respect the yield condition at any point and are in equilibrium with applied loads, SF and STM can be treated as lower-bound solutions. Nevertheless if one could find a lower-bound solution compatible with a licit mechanism, this solution would be considered as the exact solution according to the theory of plasticity [13,16].

The stress field and strut-and-tie methods are complementary (they express the same physical phenomenon in different manners), and in practice they are usually combined to obtain licit solutions (refer to *Fig. 2*). Stress fields (presented in *Fig. 2a*) provide an accurate representation of a stress state inside an analysed member. They allow engineers to determine the size of the compression struts and therefore to obtain the value of compression stress in concrete. In addition to this, SF can indicate if smeared reinforcement is necessary and where [17,18], and are particularly useful when it comes to detailing in general (determining the nodal size or minimal space required to pass a strut for example). Finally SF can account for a variable angle of a compression field (fan region). Unfortunately, the process of developing a complete stress field can be time consuming, which leads us to main advantage of STM (refer to *Fig. 2b*). Given a fact that each force of a STM is nothing else but a resultant of a corresponding stress field simplifies the calculation of the model's equilibrium. Reinforcement amount can be directly determined and the critical regions can be indicated (nodes close to the edge of the element for example). Such regions however still require further study using SF method.

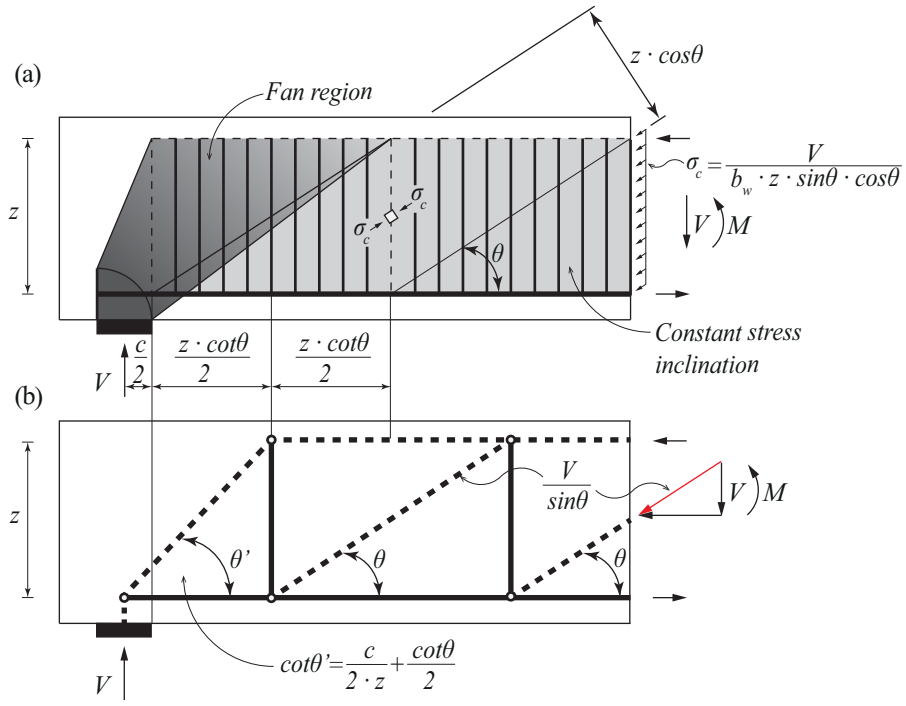

***Fig. 2** Stress field (a) and strut-and-tie model (b) of a beam*

In order to have a clear view of the actual stress state in structural concrete elements (cracked non-elastic stress fields), Fernández Ruiz and Muttoni [12] developed Elastic-Plastic Stress Field method (EPSF) and implemented it in a Finite Element (FE) program (JCONC – which has been integrated as an applet into an educational web site http://i-concrete.epfl.ch/). According to this approach stress fields are obtained iteratively for each load step by assessing the stresses in concrete and reinforcement based on constitutive laws (elastic-plastic material behaviour) and imposed deformations. EPSF method accounts for the upper and lower bound solution at the same time, which means that stress fields obtained at the ultimate load step are exact solutions according to the theory of plasticity [9].

This chapter contains practical guidelines on how to develop EPSF for plane stress state problems (beams and walls in reinforced and prestressed concrete). Basic principles and assumptions of EPSF method are presented and discussed; mesh related and convergence problems are attended (in regard to FE aspect of EPSF method analysis), and all relevant modelling techniques are given (introduction of bearings, concentrated loads, accounting for the insufficient reinforcement anchorage length etc.).

With respect to given recommendations, the document also provides chapters which address the behaviour of prestressed concrete beams failing in shear, elements with Gerber joins and bridge diaphragms.

Examples of various EPSF models are given in a form of an online database, and are available for downloading at http://i-concrete.epfl.ch/epsf/epsf.html. The database contains 315 elements tested by various authors (references corresponding to each experimental campaign are provided) and gives some basic information regarding elements geometrical and mechanical properties and observed failure modes. Ultimate strength of each element obtained using EPSF analysis (Q_{EPSF}) is compared to the failure load measured during the test (Q_{TEST}). The database also gives the average Q_{TEST}/Q_{EPSF} value for each experimental campaign along with the corresponding Coefficient of Variation (COV).

Finally safety format issues are addressed along with their implementation in the EPSF models.

1.1 Principal assumptions of the EPSF method

In order to better understand EPSF method and show its compatibility with Rigid-Plastic Stress Field (RPSF) analysis, the following section presents constitutive laws for steel, concrete and bond. In addition to this, it gives a brief description of the algorithm used to obtain the stress fields.

1.1.1 Constitutive laws

Reinforcing steel is assumed to behave as an elastic-plastic material in tension and compression with the possibility to account for strain hardening behaviour (refer to *Fig. 3a*). Its response is governed by the yield strength of the material (f_s), its elastic modulus (E_s) and its hardening modulus (E_h).

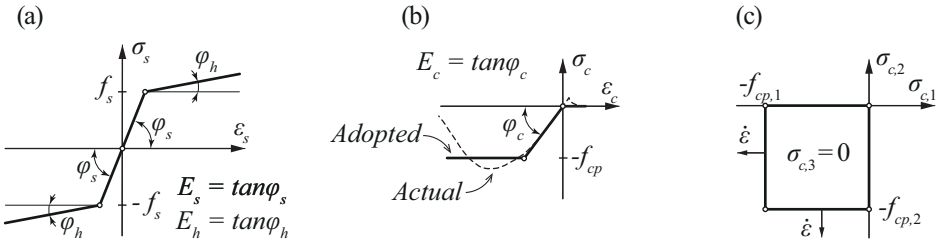

Fig. 3 *Constitutive law of steel (a); concrete (b); and yield surface for plane stress state in concrete (c)*

The concrete constitutive law is presented in *Fig. 3b*. Its behaviour under compression is assumed to be elastic-perfectly plastic, whereas its tensile strength is completely neglected. Concrete modulus of elasticity (E_c) is adopted as secant modulus of the material, and plastic concrete strength (f_{cp}) is calculated according to equation (1).

$$f_{cp} = f_c \cdot \eta_{fc} \tag{1}$$

f_{cp} represents the plastic compressive strength of the concrete [MPa];

f_c represents the uniaxial concrete compressive strength [MPa] obtained from a standard cylinder test (150 mm in diameter and 300 mm in height);

η_{fc} represents the concrete compressive strength reduction factor [19], which accounts for its brittle behaviour and can be calculated according to equation (2).

$$\eta_{fc} = \left(\frac{f_{co}}{f_c} \right)^{1/3} \leq 1 \tag{2}$$

f_{co} is equal to 30 MPa in case of normal strength concrete [21].

In addition to this the concrete compressive strength is reduced due to the presence of the transverse strain. This phenomenon is taken into account through an efficiency factor η_ε which can be evaluated on the basis of the compression-softening law proposed by Vecchio and Collins [22] (see equation (4)), as presented in equation (3).

$$f_{cp,eff} = f_{cp} \cdot \eta_\varepsilon \tag{3}$$

$$\eta_\varepsilon = \frac{1}{0.8 + 170 \cdot \varepsilon_1} \leq 1 \tag{4}$$

ε_1 represents the transverse strains in concrete;

$f_{cp,\,eff}$ represents the effective concrete compressive strength [MPa].

In-plane concrete strength can be represented using a Mohr-Coulomb yield surface with a tension cut-off (refer to *Fig. 3c*). The effect which transverse strains have on material strength can be understood as shrinkage in the yield surface with respect to the positive transverse strain increase. It should be noted that plastic concrete strength (f_{cp}) cannot be increased due to application of negative transverse strains (concrete confinement).

It is important to emphasize that in JCONC, concrete compressive strength reduction factor (defined in equation (2)) needs to be introduced manually by setting the concrete compressive strength equal to its plastic value (as defined in equation (1)). On the other hand, the concrete compressive strength efficiency factor (refer to equation (4)) is accounted for by the program, in an automatic manner. This value will change for every FE depending on its strain state (in case of FE subjected to pure compression for example, the efficiency factor will be equal to 1.0 since there are no transverse tensile strains present in the concrete).

Finally, bond between the reinforcement and surrounding concrete is assumed to be perfect, meaning that these two materials have equal strains in the direction of reinforcement ($\varepsilon_s = \varepsilon_c$) resulting in zero slip.

1.1.2 Finite element implementation

Implementation of the previous constitutive laws into a nonlinear Finite Element method (FEM) analysis can be performed by means of two different types of element: link elements and constant strain triangles.

Reinforcement bars and prestressing tendons are modelled using link (1D) finite elements with uniaxial behaviour (neglecting the dowel effect) as presented in *Fig. 4*. Based on a given displacement and the length of a FE (refer to *Fig. 4.a*), strain state of the structural steel member can be obtained directly (*Fig. 4b*). This value is then used as an input parameter to determine the stress state (refer to *Fig. 4c*) based the constitutive law presented in *Fig. 3a*. The stresses can then be used to determine the nodal forces ($F_{s,i}$) by means of simple integration over the cross-section surface of the analysed element (refer to *Fig. 4d*).

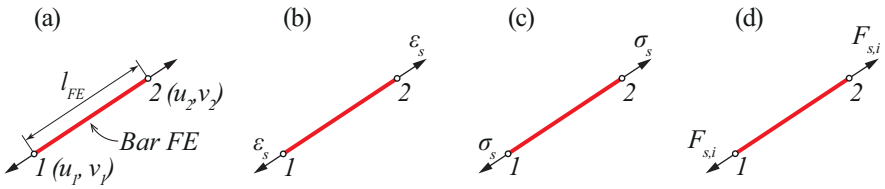

Fig. 4 *Bar finite element (a); its strain state (b); stress state (c); and nodal forces (d)*

Concrete is modelled using constant strain triangles. Once again, a displacement field is imposed on a concrete FE (refer to *Fig. 5a*) which is then used to obtain a strain state (ε_x, ε_y, γ_{xy}).

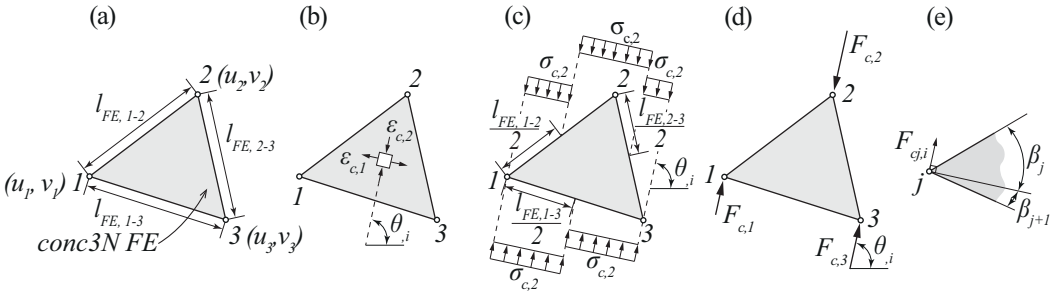

Fig. 5 *Concrete finite element (a); ist strain state (b); stress state (c); nodal forces (d); and characteristic angle β in j-node (e)*

By means of basic Mohr's transformations the principle strains (ε_1 *and* ε_2) are obtained as well as their principle direction θ_i (refer to *Fig. 5b*). Assuming that the principal stresses are parallel to the principal strains, concrete stresses can be directly calculated (refer to *Fig. 5c*) using the constitutive law defined in *Fig. 3b*. Finally as presented in *Fig. 5d* and *c,* nodal forces can be derived using an equation (5).

$$F_{cj,i} = \sigma_i \cdot \left(\frac{l_j}{2} \cdot \cos\left(\beta_j\right) - \frac{l_{j+1}}{2} \cdot \cos\left(\beta_{j+1}\right) \right), \text{ for } i = \{1,2\} \text{ and } j = \{1,2,3\} \tag{5}$$

$F_{cj,i}$ represents the nodal force in j-node and i-principle stress direction [N];

$\sigma_{c,i}$ represents the concrete stress in i-principle direction [MPa];

l_j represents the length of j-side of the FE triangular [m];

β_j represents the characteristic angle in j-node presented in [°].

The iterative process for obtaining EPSF for a given load, geometry and reinforcement layout starts with a linear elastic FEM calculation, in which both materials (concrete and steel) have infinite strength in tension and compression. This is done in order to obtain an initial displacement field, which is then imposed back to the model. This time however, the materials are assuming elastic-plastic behaviour (as presented *Fig. 3*). Strains, stresses and nodal forces coming from the bar and concrete FE are obtained (as described above), after which equilibrium of each node is checked. This usually results in having some residual (un-equilibrated) forces. The intensity and the direction of these forces are then used to correct the initial displacement field, by moving the nodes at a certain rate by using Newton-Raphson algorithm. This defines a second displacement field, which is then reused in the same manner. The entire process is repeated for a predefined number of steps until a convergence is reached (a point in which residual forces become insignificant). If the applied load proves to be greater than the model's strength, calculation will diverge. In order to easily follow the convergence process, a relative error based on the intensity of un-equilibrated forces is plotted after each iteration step (detail analysis of factors affecting models convergence will be presented in chapter 1.2.4).

As described above, the method verifies the equilibrium of the system and the yield condition everywhere (lower bound theorem is respected). It also respects compatibility conditions and eventually becomes a failure mechanism (upper bound theorem is respected). According to the theory of plasticity, this means that the final solution is the exact solution. One major advantage of the EPSF is the fact that the failure kinematics of an analysed member is clearly visible (refer to *Fig. 6*a), and can be used to develop an upper bound solution according the RPSF to verify the results (failure mechanism which can be assumed when developing the tailored RPSF is given in *Fig. 6b* - the entire procedure can be found in [13]).

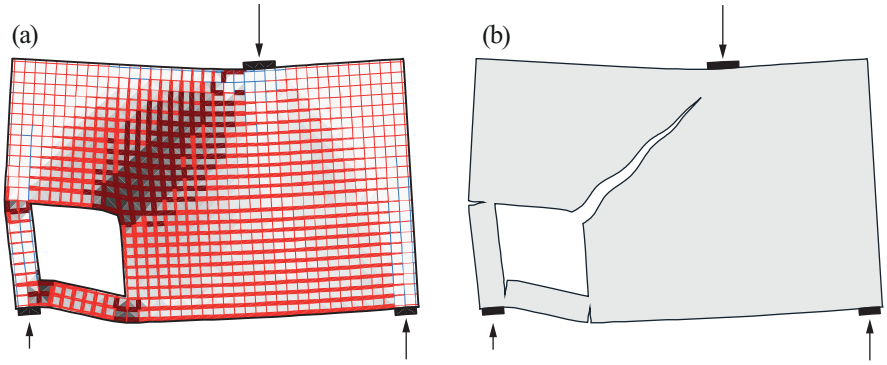

Fig. 6 *Licit failure mechanism: obtained using EPSF method (a); obtained using RPSF method (b)*

1.2 Sensitivity analysis of JCONC models

Considering the fact that EPSF are developed using FEM analysis, it is important to investigate the sensitivity of the models with respect to the mesh properties. In other words, it is necessary to show how size, shape and finite element orientation affect the final results; what are the limits in which satisfactory accuracy is ensured; and how much error is introduced in case optimal meshes cannot be applied?

When developing an EPSF, the number of iterations used to perform a nonlinear FE analysis needs to be predefined, which could also play an important role in the accuracy of the results. This is why special attention is given to this parametric study, with a goal to determine the minimal number of iterations required to obtain satisfactory results.

1.2.1 Finite element size

The effect which finite element size has on EPSF at the ULS was investigated using four groups of numerical models. First three consisted of elements subjected to a uniform stress state (pure compression, pure tension and pure shear), whereas the forth consisted of reinforced concrete beams subjected to four-point bending test. The idea behind it was to investigate a realistic model which combines all three stress states in a structure with potential redistributions amongst the elements.

Four types of meshes (M1 to M4) were applied within each group. Meshes were kept uniform (all FE had identical shape and orientation), and varied only in area of applied FE triangles (refer to *Fig. 7*). This allowed a direct comparison of the results and avoided the influence of undesired mesh parameters (such are presence of skewed FE and local mesh refinement)

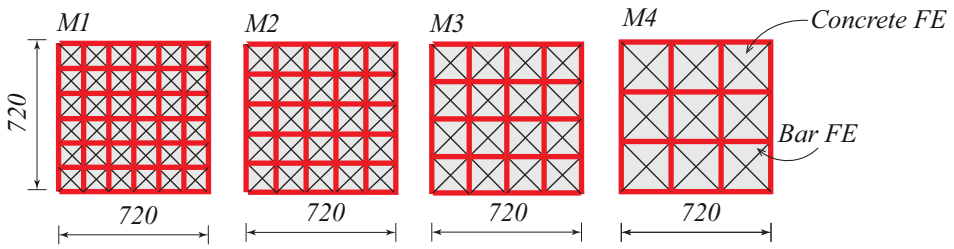

Fig. 7 *Geometrical properties of applied FE meshes*

Elements subjected to pure compression

The sensitivity of EPSF method when applied to elements subjected to pure compression was investigated using an element presented in *Fig. 8*. Plastic compressive strength of applied concrete was 38 MPa, and steel yielding strength was 550 MPa. External loads were introduced over the two facing edges of the element in each node of the mesh.

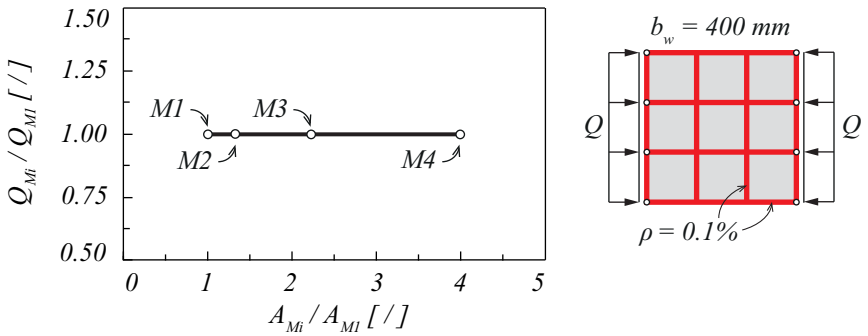

Fig. 8 *Sensitivity of the JCONC results for elements subjected to pure compression – FE size*

The element was modelled using four meshes presented in *Fig. 7* (M1 to M4), and the corresponding ultimate loads were compared (all 4 models are available to download at http://i-concrete.epfl.ch/epsf/epsf.html).

The results are presented in *Fig. 8*. As it can be observed there is no mesh dependency. The horizontal axis shows normalized area of applied FE (area of applied FE triangles was divided with the area of the FE applied in M1-mesh), and vertical axis shows the normalized failure loads (Q_{ult} of each simulation was divided with the Q_{ult} obtained after applying the M1-mesh).

Elements subjected to pure tension

The sensitivity analysis of EPSF method was further spread on elements subjected to pure tension. For this purpose an element presented in *Fig. 9* was used. After applying the meshes given in *Fig. 7* no difference in the governing ultimate load was observed (refer to *Fig. 9*). Once more the two axis show normalized values of the FE area and failure load and the models can be downloaded at http://i-concrete.epfl.ch/epsf/epsf.html.

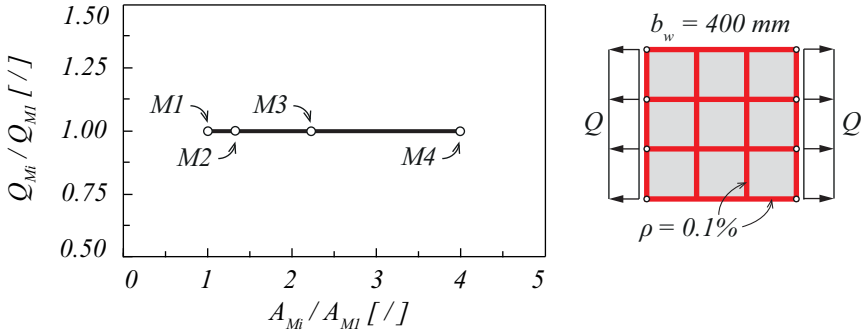

Fig. 9 *Sensitivity of the JCONC results for elements subjected to pure tension – FE size*

Elements subjected to pure shear

The method proved to be quite stable in case of elements subjected to uniform shear stress state as well. This was investigated using panels tested by Vecchio and Collins in 1979 (specimen PV4) [22]. No difference in the ultimate shear stress was observed between the models - they all failed at 2.56 MPa (compared to the measured 2.86 MPa). Element's geometry properties and the results of the EPSF analysis are presented in *Fig. 10*. Concrete compressive strength was 26.6MPa, and structural steel yielded at 242 MPa. Same as before, horizontal and vertical axis are normalized and the applied models can be found at http://i-concrete.epfl.ch/epsf/epsf.html.

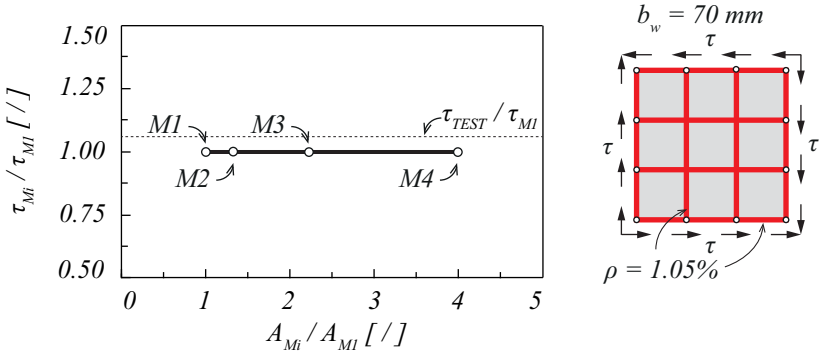

Fig. 10 *Sensitivity of the JCONC results for elements subjected to pure shear – FE size*

Beams subjected to shear

In order to extend the investigation of JCONC mesh sensitivity on structural members with potential stress redistributions (as is usually the case in real structures), the meshes presented in *Fig. 7* were used to model a reinforced concrete beam with double T cross-section subjected to four-point bending (refer to *Fig. 11*).

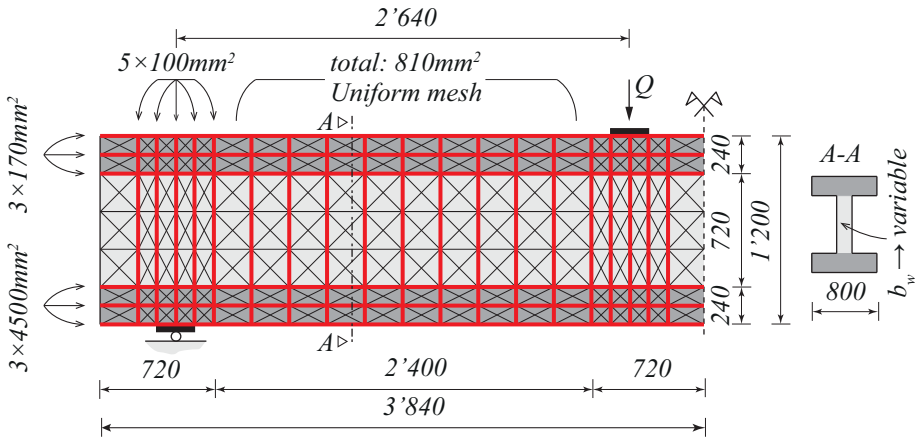

Fig. 11 *Geometry properties of analysed double T cross-section RC beam*

The beam was designed to fail in shear in its central (web) region. The web provided a space with uniform geometrical properties which allowed for the direct application of meshes M1 to M4. The total amount of transverse steel in the web (810 mm^2) was kept constant for all investigated models. Each time the steel was smeared between the concrete finite elements as presented in *Fig. 7* (4 concrete FE triangles were placed between 2 bar FE). It is important to emphasize that in this case (contrary to previous investigations on elements subjected to pure compression, tension and shear), applied meshes could not be 100% uniform due to the presence of the flanges where slightly elongated finite elements needed to be applied. However, by forcing the failure of the beam in the web region this influence became negligible.

In order to cover a wide range of shear failure modes (starting from the failure governed by the yielding of the stirrups, to the failure governed by the crushing of the concrete) 4 beams having 4 different web thicknesses were analysed: $b_w = 200\ mm$ corresponding to $\rho_w = 0.17\%$; $b_w = 100mm$ corresponding to $\rho_w = 0.34\%$; $b_w = 50mm$ corresponding to $\rho_w = 0.68\%$; and $b_w = 30mm$ corresponding to $\rho_w = 1.13\%$; where ρ_w presents the transverse shear reinforcement ratio (refer to *Fig. 11*).

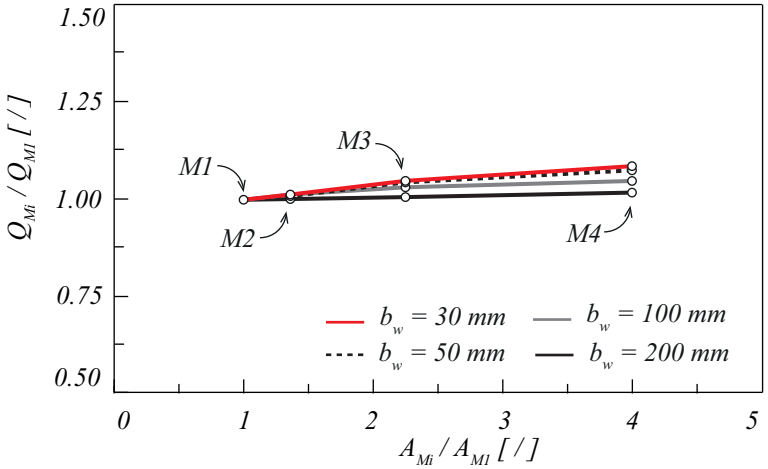

Fig. 12 *Sensitivity of the JCONC results for elements subjected to nonuniform stress state – FE size*

As it can be seen in *Fig. 12*, the models show some mesh dependency. In general, meshes using smaller FE govern lower failure loads. In addition to this there is also a difference between the elements failing purely due to the crushing of the concrete ($\rho_w = 1.13\%$, where the difference between the ultimate loads obtained using meshes M1 and M4 was almost 9%) and the elements failing due to the crushing of the concrete and yielding of the stirrups ($\rho_w = 0.34\%$ and $\rho_w = 0.17\%$, in which case this difference dropped down to around 5% and 2%).

The reason for having the trend in the results can be observed in *Fig. 13* which shows the stress fields (SF), and the concrete compressive strength efficiency factors (η_ϵ) for 16 analysed models (4 different web thicknesses times 4 meshes M1 to M4, available for download at http://i-concrete.epfl.ch/epsf/epsf.html). All models failed locally due to the crushing of the concrete in the web close to one of the flanges (compressed flange in case of models with higher transverse reinforcement ratio and flange under tension in case of the beams with lower transverse reinforcement ratio). In this zone, the compressive strength of concrete was locally reduced due to the presence of transverse strains. As the zone became smaller, the reduction of the concrete strength became bigger - in other words, strain localization was observed.

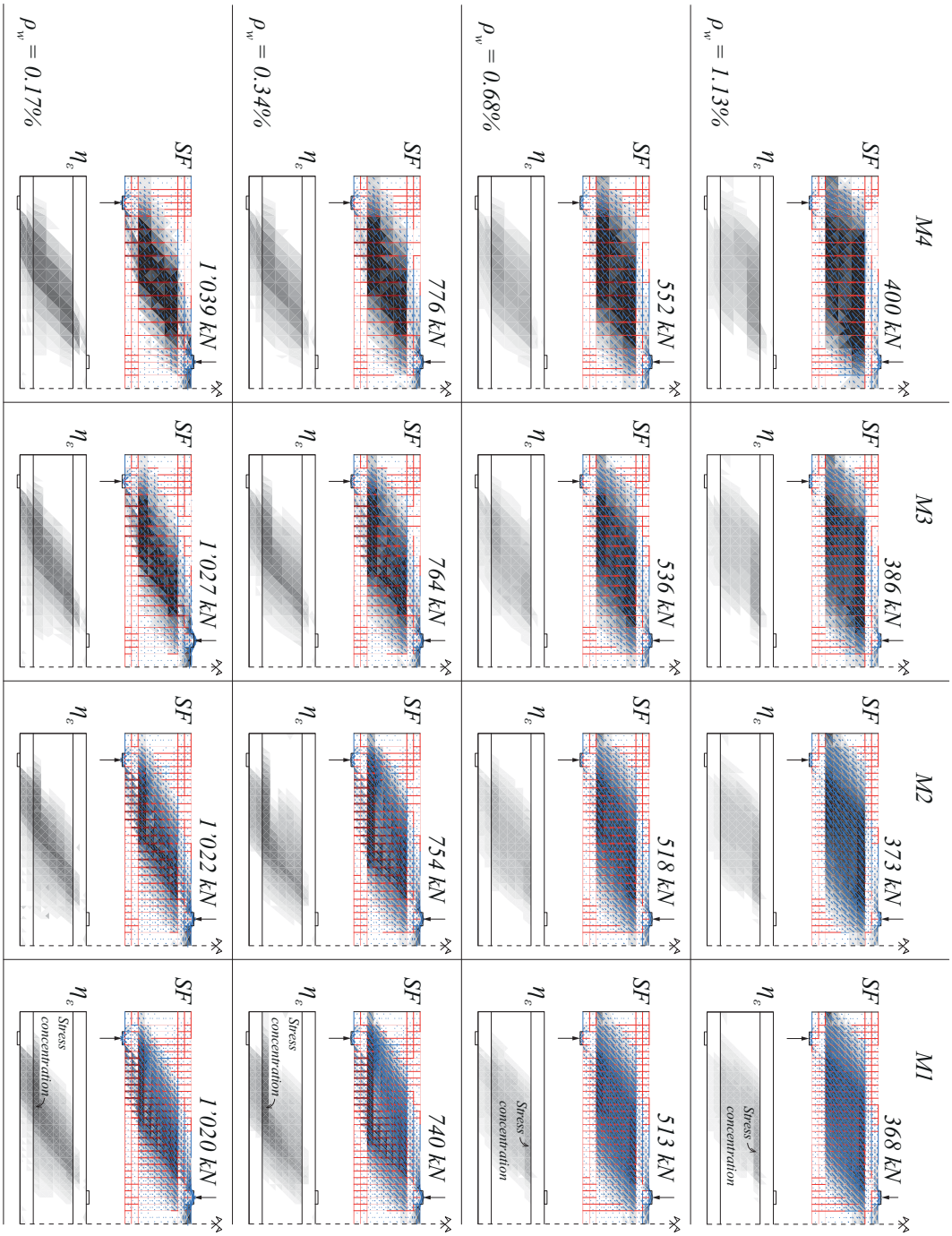

Fig. 13 *Stress fields and concrete compressive strength reduction factor of TT cross-section beams*

Considering the fact that the area of applied FE in M1 models is 4 times smaller than the one in M4 proves that the results are reasonably stable even in case of non-uniform stress fields. The higher drop in ultimate load was observed on a series of beams which had

significantly high amount of transverse reinforcement (more than 1%), which is usually not the case in reality. When this ratio dropped down 0.4% or less, the results were much more stable.

Recommendations concerning the finite element size

It can be concluded that the EPSF method gives stable results for various sizes of applied FE. A general recommendation when selecting an optimal FE size is to use the stirrup spacing as the main grid for meshing, and place two concrete FE triangles in between (as presented in *Fig. 11*). Using this criterion along with the recommendations concerning the FE shape and FE orientation (that will be presented in the following chapters) the models will give a realistic representation of the actual behaviour of investigated members. This is in fact the manner in which the database was generally modelled.

1.2.2 Finite element shape

The shape of applied finite elements is another parameter which affects the EPSF analysis. In order to investigate its significance and provide practical recommendations for meshing, a reinforced concrete beam with web thickness of $b_w = 100mm$, corresponding to $\rho_w = 0.34\%$ (presented in *Fig. 11*) was investigated using 5 additional meshes ($M_{def,ref}$ to $M_{def,4}$) given in *Fig. 14*.

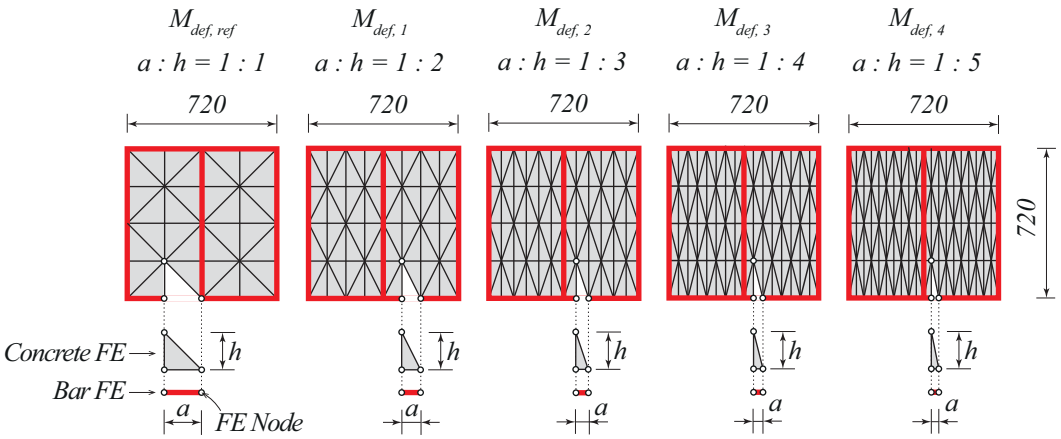

Fig. 14 *Distorted finite element meshes*

The finite element distortion was defined as ratio between the height of a constant strain triangle and the length of its corresponding side (a:h ratio presented in *Fig. 14*). As it can be seen this ratio varied from 1:1 to 1:5.

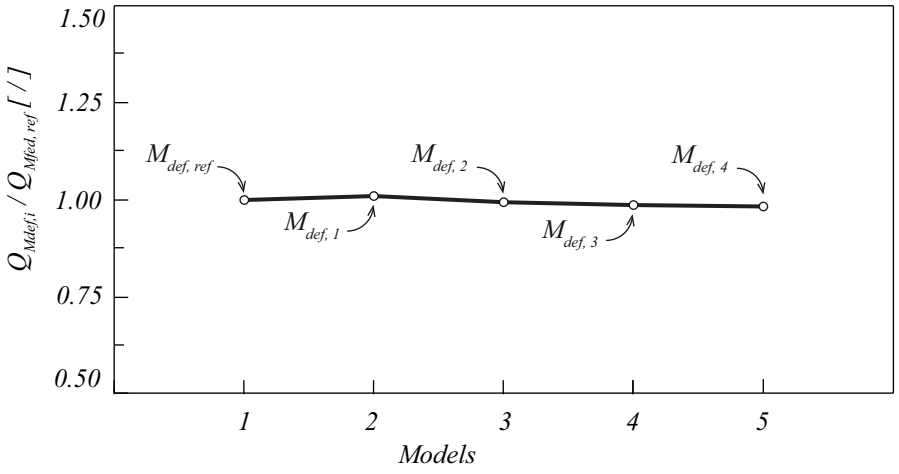

Fig. 15 *Sensitivity of the JCONC results for elements subjected to nonuniform stress state – FE shape*

The results of JCONC analyses are given in *Fig. 15*, which shows that the ultimate load was quite stable. The maximal difference between the reference model ($M_{def,ref}$) and the most distorted one ($M_{def,\ 4}$) was approximately 2%, proving that the presence of distorted FE has little influence on the simulation.

Based on the general recommendations for FE analysis found in literature [23], the maximal triangle height-to-side ratio used in practice should not be greater than 1:3. A fact that the difference in results is not too big even if finite elements have height-to-side ratio higher than the recommended value in case of JCONC is definitely reassuring, but should be avoided if possible. Meshes containing zones with distorted finite elements due to the complex formwork of reinforcement geometry for example can be locally accepted. Similarly to previous cases, all 5 models can be inspected at http://i-concrete.epfl.ch/epsf/epsf.html.

1.2.3 Finite element orientation

Orientation of finite element triangles forming a mesh has an effect on the final results. The fact that the hypotenuses of the constant strain triangles are parallel throughout a model affects the shape of the ultimate EPSF as well as the estimation of the ultimate strength.

In order to investigate this phenomenon, the reinforced concrete beam presented in *Fig. 11* (with web thickness of $b_w = 100mm$, corresponding to $\rho_w = 0.34\%$) was modelled once more, using a regular mesh formed out of triangles with 1:2 height-to-side ratio. Triangles were first orientated in a way which allowed their hypotenuses to descend from top left to bottom right corner, then vice versa. Zig-zag FE orientation was also analysed and finally, a mesh with random FE triangle orientation was applied. *Fig. 16* shows 4 different meshes that were applied along with their corresponding stress filed at ULS and concrete compressive strength effectiveness factor.

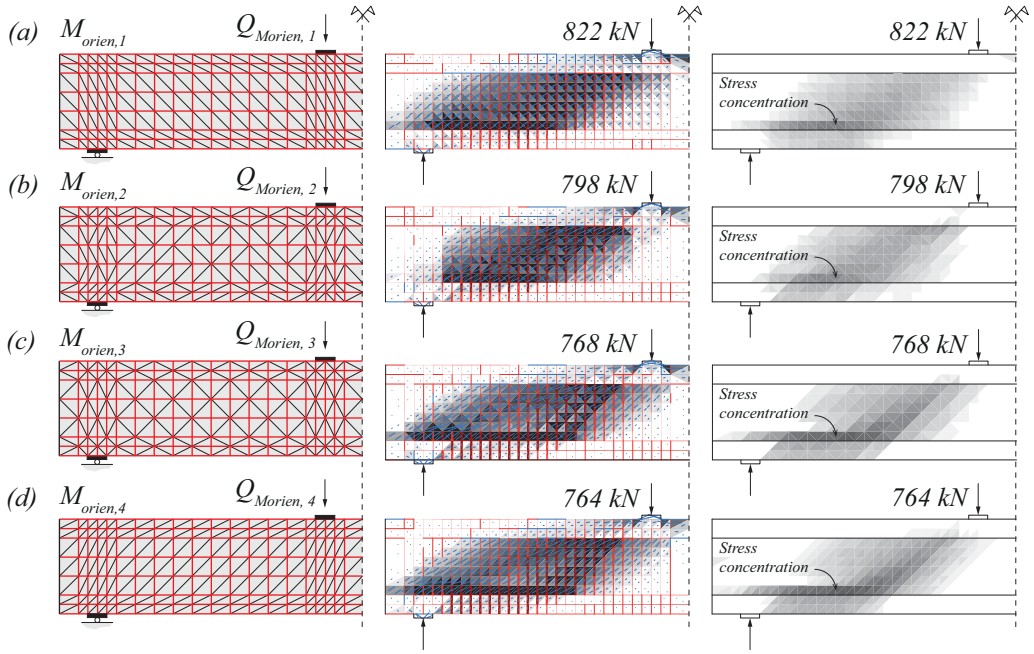

Fig. 16 *Mesh shape, stress field and concrete compressive strength effectiveness factor of analysed TT cross-section beam using different FE orientation (a) to (d)*

As it can be observed the difference between the ultimate loads is not negligible and can be as high as 8% (between $M_{orien,1}$ and $M_{orien,4}$). A difference in shape of the three EPSF can be also observed.

In case the angle between the hypotenuses of the concrete FE triangles and the direction of the principle compressive stresses is smaller, the compressive stress field tends to be more concentrated governing a lower ultimate load (refer to $M_{orien,4}$).

On the other hand if the finite element hypotenuses are almost perpendicular to the principle compressive stresses, the stresses field tends to spread over a wider web area, governing a higher ultimate load (refer to $M_{orien,1}$).

The explanation for this behaviour lies in the process of deriving the nodal forces. It depends on the angle between the principle stress direction and each side of the constant strain triangles (refer to *Fig. 5*).

In order to overcome this, the FE mesh should not have any preferential hypotenuses inclination. Instead, zig-zag FE (refer to $M_{orien,3}$) random FE inclination is preferred (refer to $M_{orien,2}$). However it is important to mention that in case of random inclination more than one simulation need to be performed in order to obtain a consistent result (refer *to Fig. 17*). In this case an average value of 5 different simulation was taken as representative.

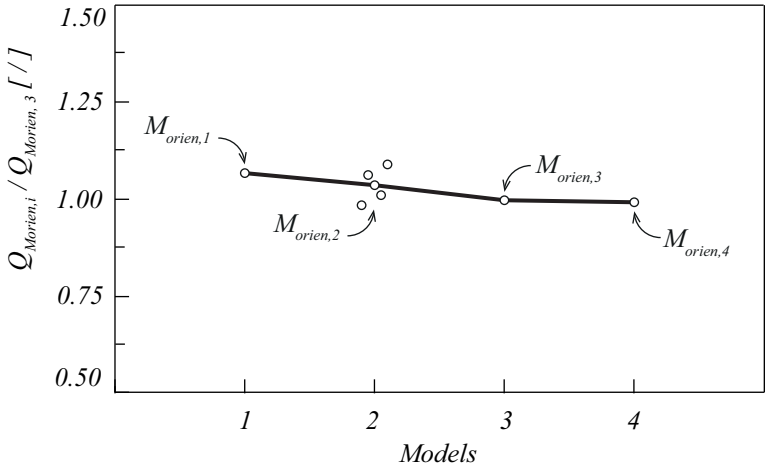

Fig. 17 *Sensitivity of the JCONC results for elements subjected to nonuniform stress state – FE orientation*

Therefore it can be concluded that using meshes which favour certain FE orientation should be avoided as much as possible. Instead of this, meshes with zig-zag inclination of hypotenuses or the ones with horizontal and vertical FE hypotenuses (presented in *Fig. 7*) should be selected. In case a random FE orientation is applied average value of at least 5 different simulations should be taken as representative (this approach gives satisfying results, but depending on the size of an analysed model it can be time consuming). All 8 FE models investigate in this chapter can be found at http://i-concrete.epfl.ch/epsf/epsf.html.

1.2.4 Model convergence

EPSF are developed based on the imposed displacement fields, which are obtained through iterations. This process can lead to the convergence of the model (an exact solution according to the theory of plasticity is reached) or its divergence (failure of the element). Convergence process is expressed through an error (a relative amount of the residual forces present in the model). In case the error is gradually reduced reaching a stable asymptotic value, the analysed model converged. Otherwise the model diverged indicating that the applied loads are too high. *Fig. 18* shows the development of an error over 250 iteration steps for 2 simulations.

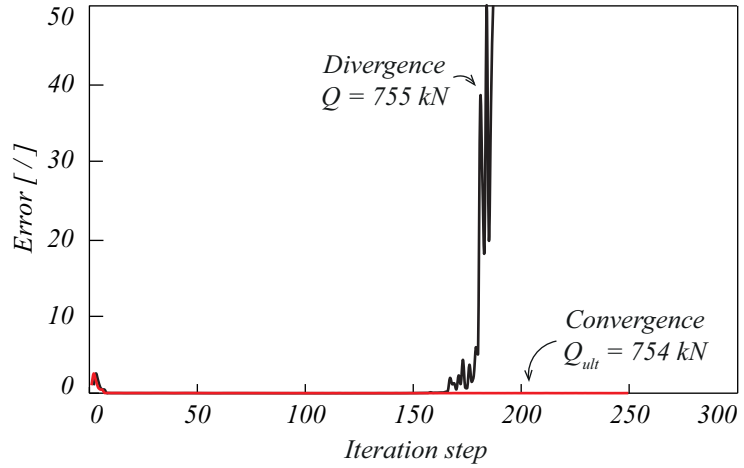

Fig. 18 *Convergence and divergence of a JCONC simulation*

The element in question is a reinforced concrete beam from *Fig. 11* ($b_w = 100mm$, corresponding to $\rho_w = 0.34$), applying the M2 mesh (refer to *Fig. 7*). The model converged under 754 kN load but diverged under 755 kN (as presented in *Fig. 18*), thus indicating that its ultimate strength is equal to 754 kN. Aside from looking at the error and visual validation of obtained stress field, one more check should be performed in order to validate if the EPSF truly converged or not. The sum of the reaction forces should be obtained by means of hand-calculations, and the values should be compared to the ones retrieved directly from the EPSF. In case there is a mismatch, applied load needs to be reduced until all three checks are satisfied.

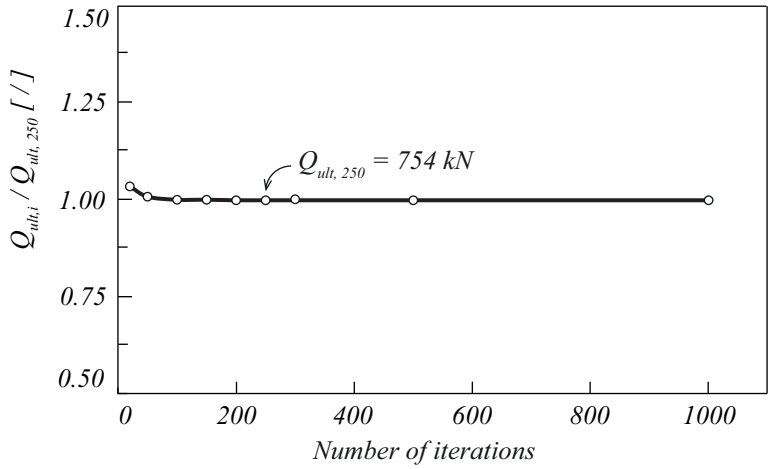

Fig. 19 *Ultimate strength of a TT reinforced concrete beam depending on different number of iterations*

The graph presented in *Fig. 18* can rise a bit of concerns, since there are no indications the model will diverge until the 155th step. This could lead to a conclusion that in case the number of predefined iterations was 150 instead of 250 steps for example, the analysed

load case would converge and therefore overestimate elements strength. This is why a sensibility analysis of this parameter was investigated.

Ultimate strength of reinforced concrete beam was estimated using different number or iterations. The obtained results are presented in *Fig. 19*.

It can be seen that the difference in estimated ultimate load obtained with 250 and 1000 iterations is negligible (in this case there is no difference at all). Time wise performing a calculation with 1000 iterations can be very costly depending on size of the mesh. Therefore general recommendation for the number of iterations used to obtain satisfying results is 250 steps.

1.3 Modelling aspects of EPSF method

This chapter provides modelling guidelines used to obtain suitable EPSF for various structural elements. Apart from introducing some basic geometrical characteristics of the element into the model (for example web thicknesses or multiple reinforcement bars) the chapter also focuses on some peculiar details, like the introduction of concentrated loads, introduction of prestressing and insufficiently anchored reinforcement bars. Special attention was given to the aspect of concrete cover which spalls off from the compression zones and directly governs their ultimate strength (in the case of the dapped-end beams for example).

1.3.1 Concrete and reinforcement geometry

The EPSF method is used to solve 2D stress state problems. This means that there can be no variations in the geometry properties of the model throughout its thickness. In other words real, 3D structural concrete elements need to be represented in a simplified manner.

The thickness of the concrete is a parameter which requires little or no modifications, and can usually be directly implemented into the model. In case a specific region of the element has a constant thickness, the corresponding FE triangles should simply be assigned with this value (as presented in *Fig. 20 a* and *b*). On the other hand, if a region has variable thickness, each FE should be defined using an average thickness obtained over the area of that particular FE.

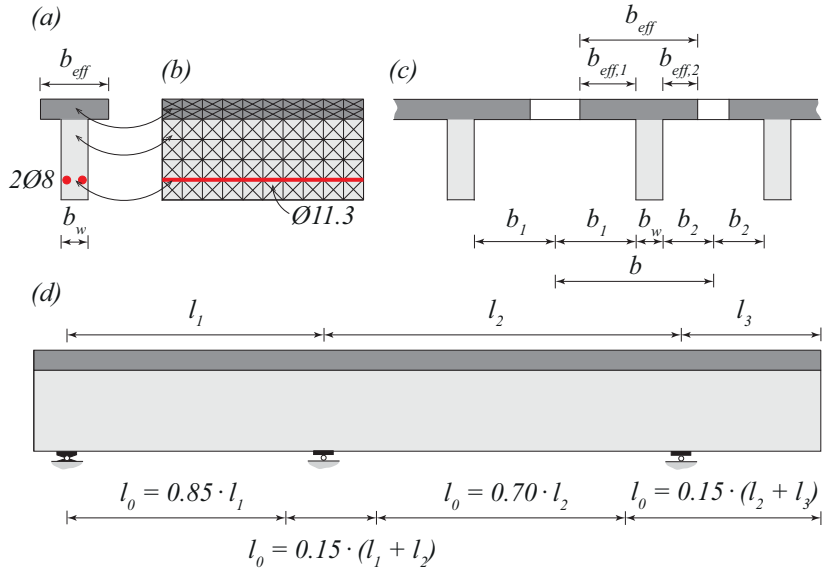

Fig. 20 *Modelling the cross-section geometrical properties – cross-section geometry (a); example of a FE mesh (b); effective flange width (c); relevant l_0 distances (d)*

It is important to mention that there are also cases in which the geometry properties of analysed elements are not clearly defined. Typical example is the flange width of a beam cast in situ with a slab. In such cases, the recommendations for estimating the flange width given by SIA262:2013 [24] should be applied.

The effective with can be estimated using equation 6.

$$b_{eff} = \Sigma b_{eff,i} + b_w \leq b \tag{6}$$

b_{eff} represents the effective slab width [m];

$b_{eff,i}$ represents concrete slab contribution to effective width left and right from the analysed rib [m];

b_w represents the thickness of the rib [m];

b represents distance between the midpoints of slabs left and right from the rib [m]

The effective width of the slab, left or right from the rib can be estimated using the following equation:

$$b_{eff,i} = 0.2b_i + 0.1l_0 \leq 0.2l_0 \tag{7}$$

b_i represents the distance between midpoints of a slab and rib side closer to it [m] (refer to *Fig. 20c*);

l_0 represents the distance between the zero points on the moment diagram along the rib [m] (refer to *Fig. 20d*).

It is important to emphasize that the cantilever length in the previous figure is less than one half of the adjacent span and the ratio between adjacent spans is between 1 and 1.5.

Reinforcement bars can vary in number and diameters throughout an elements thickness and need to be merged into one equivalent re-bar. Area of such bar has to be equal to sum of all re-bar areas originally placed at that specific height. For example, in order to model the *2Ø8* re-bars presented in *Fig. 20a* one *Ø11.3* bar elements needs to be introduced into the model (refer to *Fig. 20b*). With respect to the thickness to be considered in presence of post-tensioning ducts, this aspect is discussed in section 1.3.3

1.3.2 Introduction of external load and supports

As it was previously presented EPSF are developed explicitly by imposing the displacements and equilibrating the nodal forces (refer to chapter 1.1.2). These forces are obtained though integration of stresses over two sides of FE triangles connected in a single node (refer to equation 5 and *Fig. 5*). If the forces cannot be equilibrated, no convergence (solution) can be found.

Local concrete crushing caused by concentrated loads can be easily understood by looking at the previous procedure in an opposite direction. The applied forces, based on their intensity and the FE size, govern stresses in the surrounding concrete. In case the finite elements are sufficiently small and the applied loads are sufficiently high, the compressive strength of the concrete can be locally reached. In order to prevent this from happening, concentrated forces need to be spread over multiple nodes, which is usually done by introducing the loads over support plates, or using multiple (smaller) forces instead of a single (big) one.

Area over which a single load should be spread can be determined using equation 8.

$$A = \frac{Q_i}{f_{cp}} \tag{8}$$

A represents the area of the spreading zone [mm^2];

Q_i represents the applied load (external force or reaction, for example) [N];

f_{cp} represents plastic compressive strength of the concrete [MPa] (refer to equation 1)

The size of the plate itself is based on previously calculated area. One of its sides is equal to the thickness of analysed element (b_w), and the other is determined using equation 9.

$$b = \frac{A}{b_w} \tag{9}$$

b represents the width of the steel plate [mm];

b_w represents the width of the analysed element [mm];

A represents the area of the spreading zone [mm^2] calculated using equation 8.

The support plate is usually modelled using perfectly elastic steel with infinite tensile and compressive strength (refer to *Fig. 21a*).

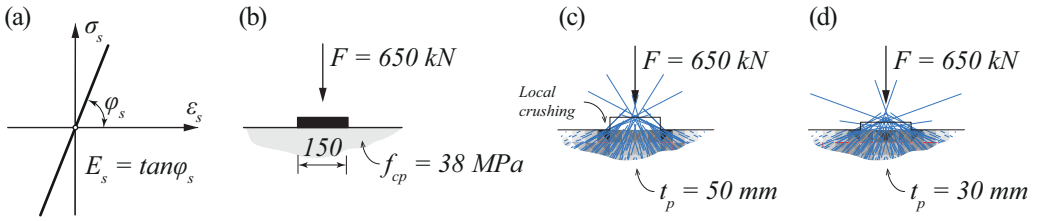

Fig. 21 *Modelling the concentrated loads in JCONC – constitutive law of steel plate (a); width of the steel plate (b); local concrete crushing due to increased stiffness of the steel plate (c); correct concentrated load introduction (d)*

The thickness of the plate can be determined is necessary through iterations. It can be assumed as 25% of the smallest plate size and then decreased in case the plate proves to be too rigid causing uneven stress distribution.

In order to clarify the previous considerations, the introduction of concentrated loads is presented in *Fig. 21b* to *d*. Plastic concrete compressive strength is equal to 38 MPa, and reinforcement steel yields at 550 MPa. 650 kN concentrated force was applied on the surface of 120 mm thick element. The load was initially introduced using $150 \times 120 \times 50\ mm$ steel plate (refer to *Fig. 21b* and *c*). High compression stresses next to its corners and relatively low compression stresses in the mid-section below the steel plate indicate that the assumed thickness is too large. The plate acts as a rigid body by pushing the concrete with it edges. The thickness was later reduces from $50\ mm$ to $30\ mm$ (see *Fig. 21d*) and evenly distributed compressive stresses in the concrete were observed, meaning that the proposed solution can be accepted.

1.3.3 Prestressing

The effects of prestressing can be taken into account by:

- Applying a concentrated load on the elements surface to act as an anchorage force;
- Introducing the deviation forces;
- Introducing bar FE to account for the presence of the prestressing tendons;
- Modifying the yield limit of the tendon to account for the fact that they are initially under tension;
- Reducing locally the thickness of the concrete due to the presence of the duct

The anchorage forces are obtained through integration of the initial prestress over the area of cable. Their direction is parallel to the direction of the cables at the anchorage point (as presented in *Fig. 22a*).

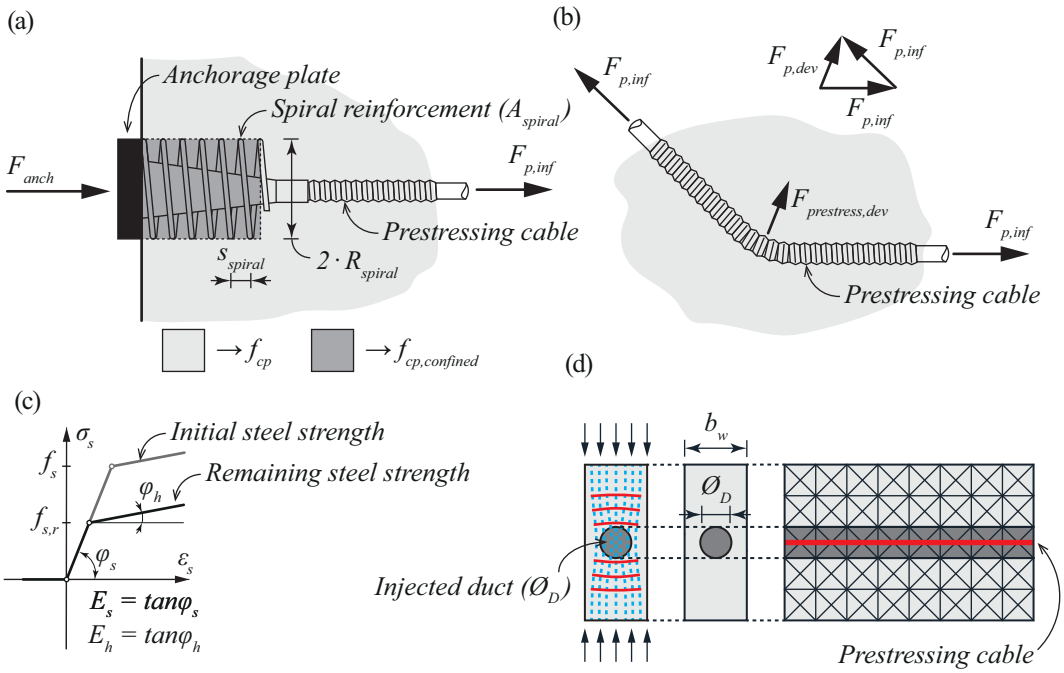

Fig. 22 *Modelling the effects of prestressing in JCONC – anchorage of the prestressing cables (a); introduction of deviation forces (b); constitutive law of prestressing steel (c); modelling of the prestressing duct (d)*

The intensity and the direction of the deviation forces can be directly determined by equilibrium. As presented in *Fig. 22b*, the deviation force is the resultant of the two tensile forces coming from the prestressing tendon acting on each side of the analysed free-body.

The problem of applying the concentrated forces into the model has already been discussed, and the recommendations given in chapter 1.3.2 apply in this case as well. However, there are some differences.

In contrast to classical external loads where one could define the size of the redistribution steel plate using equations 8 and 9, size of the anchorage plate is well defined by the producer (refer to *Fig. 22a*). Depending on the level of the prestress, its surface can be sufficient to prevent the local crushing of the concrete or not. In case the concrete crushing does occur, its compressive strength needs to be locally increased based on the geometry and the amount of confinement (spiral) reinforcement. (see *Fig. 22a*)

The EPSF method does not automatically account for an increase in concrete compression strength due to the presents of confining pressure. However this value can be easily estimated using the Theory of Plasticity and Mohr-Coulombs failure criteria in the following manner [10]:

$$f_{cp,confined} = f_{cp} + \frac{1+\sin\varphi}{1-\sin\varphi} \cdot \left|\sigma_{conf}\right| \tag{10}$$

f_{cp} presents the plastic compressive strength of the concrete, defined in equation 1 [MPa];

φ presents the internal concrete friction angle [°];

σ_{conf} presents the confinement compression stress [MPa].

Internal concrete friction angle is usually estimated to be 37° [10]. Therefore the previous equation becomes:

$$f_{cp,confined} = f_{cp} + 4 \cdot \left| \sigma_{conf} \right| \tag{11}$$

The maximal intensity of confining stresses can be estimated by assuming that the entire spiral reinforcement is yielding. This governs a following equation:

$$\sigma_{conf} = \frac{f_s \cdot A_{spiral}}{R_{spiral} \cdot s_{spiral}} \tag{12}$$

σ_1 presents the confining compression stress [MPa];

f_s presents the yielding strength of the steel [MPa];

A_{spiral} presents the cross-section area of the bar forming the spiral [mm^2] (refer to *Fig. 22a*);

R_{spiral} presents the radius of the spiral [mm] (refer to *Fig. 22a*);

S_{spiral} presents the spiral step [mm] (refer to *Fig. 22a*).

Concrete which is within the spiral reinforcement should be modelled with an increased compressive strength, whereas the one outside of it should be modelled using its standard plastic compressive strength (refer to *Fig. 22a*).

High-strength steel used to fabricate the wires is assumed to behave as an elastic-plastic material. However its yielding strength needs to be reduced to compensate for the fact that the cables are under initial prestress (refer to *Fig. 22c*). Based on previous considerations:

$$f_{s,r} = f_s - \sigma_{p,\inf} \tag{13}$$

$f_{s,r}$ presents the reduced steel yielding strength;

f_s presents the initial steel yielding strength;

$\sigma_{p,inf}$ presents the prestress in the cable at an infinite point in time.

Introducing both anchorage and deviation forces as well as the reduction of tendon yield strength can be performed automatically in JCONC by using a "*cable*" finite element to model a prestressing cable instead of a "*bar*" finite element.

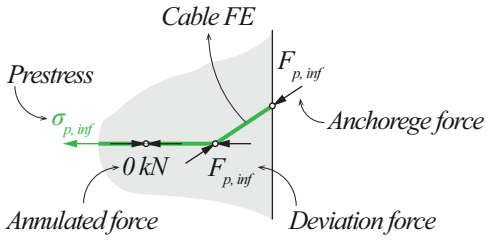

Fig. 23 *Application of cable finite element into a JCONC model*

The two elements work in the same manner (refer to *Fig. 4*), but the "*cable*" FE requires one additional input parameter called "*sigma_0*" which corresponds to $\sigma_{p,inf}$ in equation 13. Based on this value, the element automatically reduces the attributed yield strength of the steel (as described in equation 13) and integrates the $\sigma_{p,inf}$ over the area of the cables cross-section in order to obtain the prestress force. After that, it adds the prestress force in both nodes which define a cable FE itself, in the direction of the finite element (refer to *Fig. 23*). In this way if the two neighbouring cable FE have the same direction, the prestress force will be compensated, if not a deviation force be automatically introduced.

Another aspect which needs to be accounted for within EPSF analysis is related to presence of the ducts. Hollow or injected steel or plastic tubes create disturbance in the compression stress transfer by deviating stress trajectories away or towards the duct (refer to *Fig. 22d*). In both cases, the effective web thickness is locally reduced which needs to be reflected within EPSF models.

This means that the mesh needs to be formed in a way which allows FE triangles positioned over the duct to assume reduced web thickness according to the following equation:

$$b_{w,eff} = b_w - k_c \cdot \Sigma \Phi_D \tag{14}$$

$b_{w,eff}$ presents the reduced (nominal) web thickness [mm];

b_w presents the initial web thickness [mm];

$Ø_D$ presents the diameter of the duct [mm];

k_c presents the web width reduction factor, which can be taken according to SIA262:2013 [24] (0.5 for grouted steel ducts; 0.8 for grouted plastic ducts; 1.2 for non-grouted plastic ducts).

Previous recommendations concerning web width reduction are presented in *Fig. 22d.* The light grey indicated parts of the structure which should be modelled using the initial thickness of the element (b_w), whereas the dark grey indicates parts of the structure which should apply the nominal web thickness ($b_{w,nom}$). Additional results regarding the investigation of k_c factor are discussed in chapter

1.3.4 Bond and anchorage

The EPSF method assumes perfect bond behaviour. There is no displacement between the nodes of the concrete and bar (or cable) FE. This assumption differs from reality, where a complex stress-transfer mechanism between the two materials exists; a slip can occur and in some cases it might govern the strength of an analysed member.

Bond stresses should nevertheless be considered as they govern the reinforcement anchorage length. If the re-bars are not properly anchored, they cannot yield at the ULS. This reduces the amount of tensile stress taken by the member and therefore governs its strength. In order to account for the insufficient anchorage length, reinforcement bars have to be modified before the implementation in EPSF models.

This can be done accounting for a rigid-plastic bond behaviour described by the Tension Chord Model (TCM) [25].

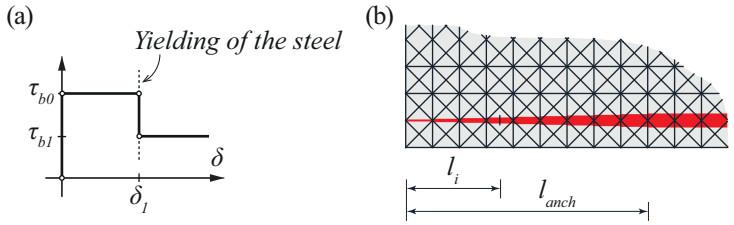

Fig. 24 *Modelling the insufficient anchorage length of a re-bar: constitutive law for concrete to steel bond stresses (a); varying the bar FE area over the anchorage length to account for the unperfected steel to concrete bond (b)*

The TCM adopts a simplified bond stress-slip relationship (presented in *Fig. 24a*). It assumes a constant transition of the bond stress between the reinforcement and the concrete equal to:

$\tau_{b0} = 2 \cdot f_{ctm}$, for ordinary ribbed bars prior to yielding [MPa], and (15)

$\tau_{b1} = f_{ctm}$, for ordinary ribbed bars after yielding [MPa]. (16)

In equations 15 and 16 f_{ct} represents the mean tensile strength of concrete which can be assessed using following equation:

$$f_{ctm} = 0.3 \cdot \left(f_c\right)^{2/3} \tag{17}$$

f_c represents the uniaxial concrete compressive strength obtained from the standard cylinder compressive tests ($150\ mm$ in diameter and $300\ mm$ in height).

The minimal anchorage length can easily be calculated assuming bond stress equal to τ_{b0} (refer to equation 15) as presented in following equation:

$$l_{anch} = \frac{\Phi}{8} \cdot \frac{f_s}{f_{ctm}} \tag{18}$$

l_{anch} presents the anchorage length of a bar [mm];

Ø presents the re-bar diameter [mm];

f_s presents yielding strength of the reinforcing steel [MPa];

f_{ctm} presents the average tensile strength of concrete [MPa] (refer to equation 17).

In case the applied anchorage length is equal or larger than l_{anch}, the reinforcement bars can be modelled using equivalent re-bar diameter (refer to *Fig. 20a* and *b*) through its entire length, keeping the model as simple as possible. Otherwise, the equivalent reinforcement diameter needs to be reduced linearly over l_{anch} starting from its full size until 0 as presented in *Fig. 24b.*

Since the reduction cannot be smooth (one link FE cannot have different characteristics on opposite sides), this needs to be in steps. Each FE would assume the average diameter of the bar over its length using the following equation:

$$\Phi_{equi,i} = \Phi_i \cdot \sqrt{\frac{l_i}{l_{anch}}} \tag{19}$$

$Ø_i$ presents the diameter of a re-bar in i^{th} FE [mm];

$Ø_{equi}$ presents the equivalent re-bar diameter [mm];

l_{anch} presents the necessary anchorage length [mm];

l_i presents the distance between the beginning of the bar and the mid-point of the i^{th} FE [mm].

The reduction of the re-bar diameter limits the amount of the tension forces that can be taken by the reinforcement at a specific point on the re-bar, thus limiting the concrete stresses in these regions to safe values.

Smooth re-bars have completely different behaviour compared to ribbed re-bars. Considering the fact that they cannot transfer stresses to surrounding concrete in a mechanical manner, means that at ultimate limit state smooth re-bars can slip (refer to *Fig. 25*), which can govern the ultimate strength of an analysed member. One of the main

assumptions of EPSF method is that there is no slip between steel and concrete within a model, which is the opposite of reality in this case. Additional problem with smooth reinforcement is that it can locally crush the concrete in the zones where the bars are bent-up (to take the shear force), and in the zones where they are anchored with hooks (as indicated in *Fig. 25*).

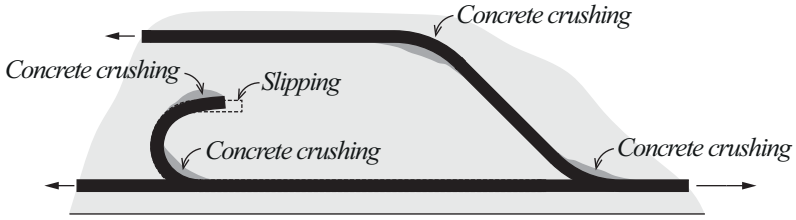

***Fig. 25** Behaviour of smooth reinforcing bars at ultimate limit state*

Undergoing research indicates that in such cases concrete compressive strength needs to be locally increased (in order to prevent concrete from crushing), and that based on obtained stresses in the re-bars, additional verifications need to be performed in order to determine if local failures have occurred prior to that moment or not.

1.3.5 Concrete cover spalling

Cover spalling failures can affect the members with concrete covers subjected to compressive actions. This means columns, nodal regions of concrete frames or dapped-end beams (refer to *Fig. 26*a). Even though the EPSF method is able to predict cover spalling failures without any specific considerations, the results are quite conservative.

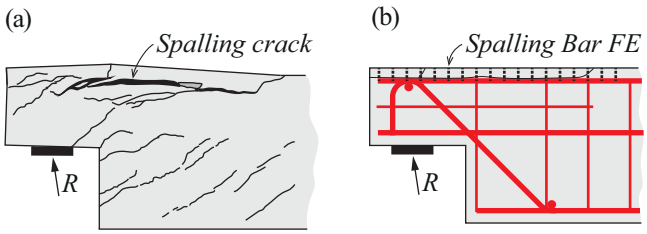

***Fig. 26** Spalling failure of a dapped end beam (a); Introduction of spalling FE (b)*

The reason for this is grounded on the fact that the tensile strength of concrete cover is neglected by the EPSF method. This means that the transverse tensile strains that appear in the cover (refer to *Fig. 26b*) are not equilibrated. By means of η_ε effectiveness factor, concrete compressive strength within the cover is severely reduced (as ε_1 increases without control), and the EPSF models are not able to reach the actual failure loads (a safe estimation of the failure load is obtained).

A link FE connecting the potential spalling crack with the edge of the element (*Fig. 26b*) is used to introduce this missing fracture energy [40]. The area of this element should be equal to the equivalent concrete area.

Spalling bar elements can be arranged each time over all concrete covers. However, for modelling simplification, it is recommended to arrange them only in the critical spalling region (see example for dapped-end beams in *Fig. 26b*). The development and implementation of this element can be consulted elsewhere [40].

Fracture energy (G_f) depends on several factors and requires experimental tests for an accurate determination. If no experimental data is available it is suggested to use MC-2010 [21] estimation of fracture energy (refer to equation 20).

$$G_f = 73 \cdot f_{cm}^{0.18} \tag{20}$$

G_f represents the fracture energy [N/m];

f_{cm} represents the mean compressive strength of [MPa].

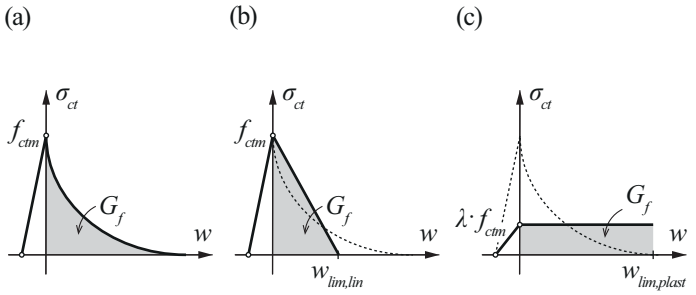

Fig. 27 *Tensile strength laws for spalling cracks: exponential softening law (a); linear softening law (b); elastic-plastic softening law (c)*

Different tensile laws for the spalling elements were analysed, as indicated in *Fig. 27*. It was observed that the spalling process is mainly dependent on the fracture energy introduced in the system with a limited influence of the shape of the considered law. This is why the most suitable model is the elastic-plastic approach (presented in *Fig. 27c*). In this case the plastic tensile strength of the cover is defined as a fraction (λ) of the mean concrete tensile strength (f_{ctm}). λ should be based on the fracture energy and a limit spalling crack width (w_{lim}) in following manner:

$$\lambda \cdot f_{ctm} = \frac{G_f}{w_{\lim}} \tag{21}$$

G_f represents the fracture energy [N/m];

f_{ctm} represents the mean tensile strength of concrete in [MPa] (refer to equation 17);

w_{lim} represents the width of the spalling crack at failure in [mm];

λ represents a redistribution factor.

If no specific recommendations for the spalling crack width of the analysed element are available, a pertinent value can be obtained using the following equation [40] (given by MC-2010 [21]):

$$w_{\lim} = \frac{5 \cdot G_f}{f_{ctm}} \tag{22}$$

w_{lim} represents the width of the spalling crack at failure [mm];

G_f represents the fracture energy [N/m];

f_{ctm} represents the mean tensile strength of concrete in [MPa] (refer to equation 17).

This limit crack width leads to a value of λ factor equal to 0.2. Hence, a plastic tensile strength of 20% of the mean concrete cover tensile strength (f_{ctm}) should be taken into account in order to model cover spalling.

This approach has proved to lead to very consistent results [40] as it will be presented later on in chapter 1.5.

1.3.6 Safety format

The level of risk within a strength prediction varies a lot depending on the amount of available information regarding structural usage and properties. Analysis of new elements involves less information (more uncertainty) regarding material properties, load level, load history, geometry and reinforcement layout than analysis of existing structures. It also uses more conservative assumptions compared to approaches which are usually applied when assessing the state of existing structures. In order to ensure the same probability of failure for each analysed member over its expected lifetime, every simulation applies a certain type of safety format. This chapter discusses on different types of safety formats that could be combined with the EPSF method (global and partial safety format) and gives recommendations on which type is best suited for design and assessment of structural concrete members. Finally, it introduces a compliance factor based on which it discusses on the amount and urgency of modification that need to be done in order to maintain the usage of a structure.

When dealing with global nonlinear FE analysis in practice there is always a question of the correct implementation of structural safety. There are two main approaches:

- Partial Safety Format (PSF), and
- Global Safety Format (GSF).

PSF implies reducing the material resistance vales (f_{ck} and f_{sk}) in order to obtain the design values (f_{cd} and f_{sd}), which are then used to determine the design resistance of analysed members. In other words:

$$f_{cd} = \frac{f_{ck}}{\gamma_c} \tag{23}$$

$$f_{sd} = \frac{f_{sk}}{\gamma_s} \tag{24}$$

$$R_d = f(f_{cd}; f_{sd}; a_{nom}) \tag{25}$$

f_{ck} represents the characteristic strength of plastic concrete compressive strength (5% fractile on a normal distribution);

f_{cd} represents the design strength of concrete;

γ_c represents the partial safety factor for concrete equal to 1.50 [24];

f_{sk} represents the characteristic yield strength of steel (5% fractile on a normal resistance distribution);

f_{sd} represents the design strength of steel;

γ_s represents the partial safety factor for steel equal to 1.15 [24];

R_d represents the design resistance of an element;

a_{nom} represents the nominal geometry values.

On the other hand, GSF uses mean values of material properties and nominal values of geometry properties in order to determine the mean elements resistance, after which a single (global) safety factor is applied in order to determine the design resistance values in following manner:

$$R_m = f(f_{cpm}; f_{sm}; a_{nom}) \tag{26}$$

$$R_d = \frac{R_m}{\gamma_d} \tag{27}$$

R_m represents the mean resistance of an element;

R_d represents the design resistance of an element;

γ_d represents the global safety factor.

Since the PSF uses different reduction factors for steel and concrete strength, this means that in case of global nonlinear FE analyses internal stress redistribution is not necessarily reproducing the most probable one, but the one of the governing (potentially most brittle) failure mode. This is the main reason why some of the modern codes (for example EC2 [26,27]) recommend that only GSF should be applied when conducting a global nonlinear FE analysis. The main question which arises from these considerations is which type of failure is the most adequate for limit analysis: the most probable one or the most critical one? In addition to this it is not that evident what to do in case of RPSFs, since they present a global nonlinear calculation method as well, and such they already take into account the internal stress redistributions between steel and concrete.

According to subsection 7.11.3 of MC2010 [21] PSF can be applied for global non-linear analyses giving a safe estimate of a design resistance. This approach is also consistent and leads to the same results obtained (by hand) using RPSF. Thus, the classical partial safety factors (γ_c = 1.5 and γ_s = 1.15) should be applied when designing new structures with EPSF method. When it comes to assessment of the existing structures it is pertinent to keep the same safety format but one can note that such approach gives slightly conservative results.

In order to take advantage of the enhanced accuracy of EPSF, a method for tailoring partial safety factors to be applied with EPSF calculations is being developed. So far this methodology has shown that it is in agreement with the code recommendations but is sensitive to scatter of concrete compressive strength (systematic assessment of actual material properties on site is required for this approach). Therefore, the reduction of the partial safety factors should be taken with caution. Further analysis is currently undergoing. Therefore, one should consult the PhD thesis of Filip Niketic [28] in order to obtain the final results.

With respect to the uncertainties there are two groups that participate in the final value of partial safety format for steel and concrete:

- Uncertainties related to material properties (γ_C for concrete and γ_S for steel);
- Uncertainties related to model and geometrical dimensions ($\gamma_{Rd,c}$ and $\gamma_{Rd,s}$).

The two factors are multiplied in order to obtain the final value in following manner:

$\gamma_c = \gamma_C \cdot \gamma_{Rd,c}$, for the concrete partial safety factor (28)

$\gamma_s = \gamma_S \cdot \gamma_{Rd,s}$, for the steel partial safety factor (29)

In the previous equations (28 and 29) the material uncertainty safety factors can be determined using expressions from equations 30 and 31.

$$\gamma_C = \frac{f_{ck}}{f_{cm} \cdot e^{-\alpha \cdot \beta \cdot (COV)_{fc}}} \geq 1.00 \text{ for the concrete} \tag{30}$$

$$\gamma_S = \frac{f_{sk}}{f_{sm} \cdot e^{-\alpha \cdot \beta \cdot (COV)_{fs}}} \geq 1.00 \text{ for the steel, where} \tag{31}$$

f_{ck} and f_{cm} respectively represent the characteristic and the mean value of concrete compressive strength (assuming a log-normal distribution of the variable);

$(COV)_{fc}$ represents the coefficient of variation of concrete compressive strength;

α represents the sensitivity factor;

β is the reliability index.

The notation for the steel safety factors is the same except the index letter "S" indicating steel instead of "C" indicating concrete.

The reliability index depends on the acceptable probability of failure (p_f) and the corresponding reference period (n) in years. For a standard design case acceptable probability of failure is equal to 10^{-6} [29] and the design reference period is equal to 50 years [29]. The reliability index can be calculated in following manner:

$$\beta_1 = \Phi^{-1}(1 - p_f) \tag{32}$$

$$\beta = \Phi^{-1}(\Phi(\beta_1)^n) \tag{33}$$

Φ represents the normal distribution function;

β_1 represents the reliability index for one year reference period.

After introducing the recommended values to equation 32 the reliability index for one year is equal to 4.75. Based on equation 33 the same index for 50 year reference period is equal to 3.89. Appendix B of SIA269 [30] also gives recommendations for estimating the reliability index for one year reference period based on the ratio between the costs of structural failure and cost of its redistribution (ρ *coefficient*), and the reduction of risks as the result of reduction (EF_M). This value can then be combined with equation 33 to calculate the reliability index for the requested reference period. MC2010 [21] recommends a value of 3.80 for the reliability index (50-year reference period), which was assumed for the purpose of this research.

The sensitivity factor is separating dominating uncertainties from nondominating uncertainties. The final value of a partial safety factor (refer to equations 28 and 29) will be obtained assuming that one of the two sub-factors is dominating (due to the material uncertainties or modelling uncertainties) and the other one is not. Out of the two combinations the one governing the maximal value of the total partial safety factor will be selected. According to SIA269 [30] in case the variable uncertainty is of key importance (dominant variable) it should assume sensitivity factor equal to $\alpha = 0.80$; otherwise $\alpha = 0.30$.

As it was already indicated, the most significant parameter (the one having the strongest impact on the final value of the partial safety factor) is the coefficient of variation of the materials. For steel, this scatter is not very high and a value of 0.055 is assumed as fixed (according of SIA 262 [24]). The COV was back-calculated assuming lognormal distribution of the variable with $f_{sk} = 500\ MPa$ and $f_{sm} = 550\ MPa$. Variation of the concrete compressive strength on the other hand is something which is much less uniform. In addition to this, quality control systems have changed a lot over the past century, so it is very difficult to give general recommendations. This is why it is very important to conduct a thorough

statistical analysis of concrete compressive strength for each particular structure which is being assessed. However, in order to have an idea of the scatter of concrete compressive strength, a literature review has been conducted based on information for concrete cast in the 1960's [31, 32, 33] and presented in *Fig. 28*.

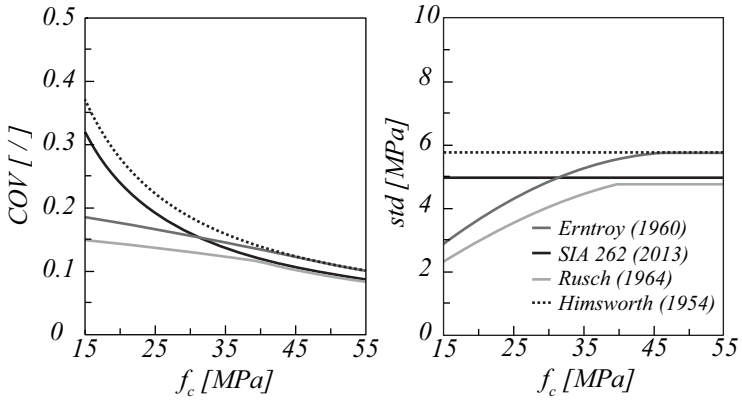

Fig. 28 *Coefficient of variation and standard deviation of concrete compressive strength according to various authors*

Fig. 28 compares the results from three different authors (Himsworth [31], Erntoy [32] and Rusch [33]) to modern code recommendations (SIA262:2013 [24]).

Geometry and model uncertainties governing the value of partial safety coefficient can be expressed in following manner:

$$\gamma_{Rd,c} = \frac{\left(Q_{TEST} / Q_{MODEL}\right)_k}{\left(Q_{TEST} / Q_{MODEL}\right)_m \cdot e^{-\alpha \cdot \beta \cdot \sqrt{(COV_{MODEL})^2 + (COV_{geometry,c})^2}}} \geq 1.00 \tag{34}$$

$$\gamma_{Rd,s} = \frac{\left(Q_{TEST} / Q_{MODEL}\right)_k}{\left(Q_{TEST} / Q_{MODEL}\right)_m \cdot e^{-\alpha \cdot \beta \cdot \sqrt{(COV_{MODEL})^2 + (COV_{geometry,s})^2}}} \geq 1.00 \tag{35}$$

$(Q_{TEST}/Q_{MODEL})_m$ represents the average ratio between the actual (tested) and estimated resistance for a specific calculation method;

COV_{MODEL} represents the corresponding coefficient of variation;

$(Q_{TEST}/Q_{MODEL})_k$ represents the characteristic value of the model uncertanty (corresponding to 5% fractile on a log-normal distribution);

$COV_{geometr,c}$ represents the coefficient of variation of the geometry properties which are relevant for the resistance strength of concrete (external cross section dimensions and effective depth);

$COV_{geometr,s}$ represents the coefficient of variation of the geometry properties which are relevant for the resistance strength of steel (effective depth and reinforcement diameter).

The first three parameters $(Q_{TEST}/Q_{MODEL})_m$, COV_{MODEL} and $(Q_{TEST}/Q_{MODEL})_k$ can be estimated using the elements from online database (refer to http://i-concrete.epfl.ch/epsf/epsf.html). All analysed members can be divided into two groups:

- Members failing in flexure
- Members failing in shear.

For each of these groups average Q_{TEST}/Q_{MODEL} ratio and COV_{MODEL} can be estimated using EPSF method. Reinforced cconcrete elements from the same database have been

assessed using the recommendations from SIA262:2013 [24] in order to compare the final values of partial safety coefficient. It is expected that the PSF for EPSF will be lower (due to the higher accuracy of the method) compared to code recommendations, and that the PSF for code recommendations should be equal to $\gamma_c = 1.5$ and $\gamma_s = 1.15$. *Tab. 1* shows the results of EPSF analysis and code recommendations of the database. It is important to emphasise that the following test campaigns were selected from the database for the purpose of this research, in order to account only for the specimens that had clear flexural and shear failures (Vecchio F.J., Shim W., 2004.; Yoon Y.S., Cooc W.D., Mitchell D., 1996.; Sagaseta J., Vollum R.L., 2011.; Sorensen H.C., 1974.; Leonhardt F., Walter R., 1963.; Kaufmann W., Marti P., 1996.; Kaufman M.K., Ramirez J.A., 1988.; Kuchma, D. et al. – without specimen G10, 2008.; Rupf, M., Muttoni, A., 2012. - without specimen SR31B, Moore A. M., 2014 and Fernandez Ruiz M., Muttoni A., 2008.). The speciments which failed differently during the experiment compared to what the models have predicted were discarded.

Tab. 1 *Accuracy of SIA262:2013 and EPSF based on analysis on the members from the online database*

	EPSF		**SIA262:2013**		
	Flexural failure	Shear failure	Flexural failure	Shear failure LoA1	Shear failure LoA2
Q_{TEST}/Q_{MODEL}	1.075	1.048	1.059	1.439	1.223
COV_{MODEL}	0.060	0.083	0.080	0.212	0.168

When it comes to variation of geometry properties applied COV are given in *Tab. 2* [34]. All variable assume normal distribution.

Tab. 2 *Main parameters for geometrical probabilistic models*

Variable	R_k/R_m*	*COV*
External cross-section	1.000	0.030
Effective depth	1.000	0.040
Reinforcement diameter	1.000	0.020

*Bias value – ratio between characteristic and mean value of a variable

Final values of PSF for concrete are presented in *Fig. 29* to *Fig. 31* (which applied SIA262:2013 equations when assessing the database) and Fig. 32 to *Fig. 33* (which applied EPSF method). Shear resistance of the elments has been estimated using both first and second Level of Approximation (LoA) from SIA262:2013. In each of the graphs, the red line gives the value of the partial safety factor for concrete assuming that the material uncertainties are dominant. On the other had, black line gives the same values assuming that model and geometry uncertainties are dominant. The PSF are given in a function of concrete compressive strength. Each of the 4 graphs in *Fig. 29* to *Fig. 33* assumes different scatter of concrete compressive strength (indicated each time in the upper right corner of the graph).

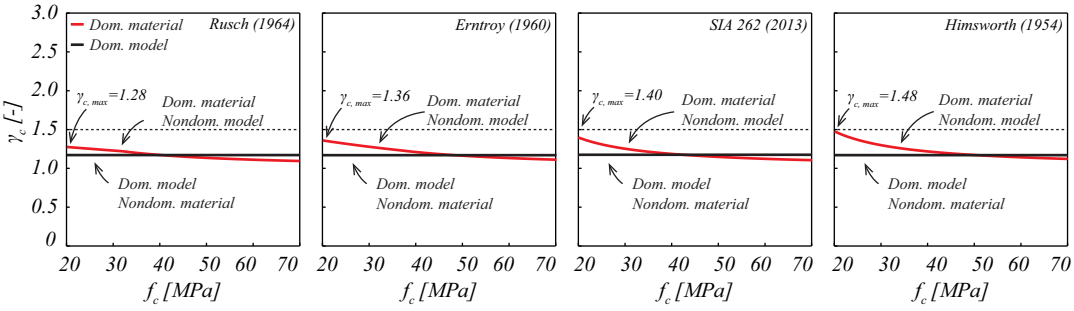

Fig. 29 *Tailored partial safety factors for concrete – Flexural failure estimated with SIA262:2013*

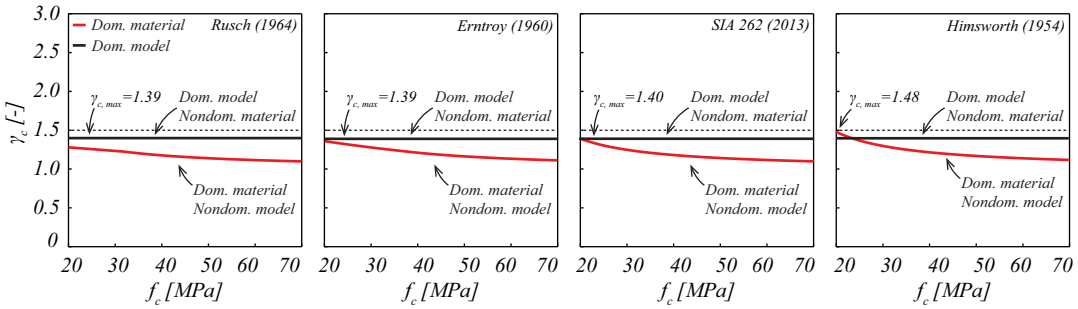

Fig. 30 *Tailored partial safety factors for concrete – Shear failure estimated with SIA262:2013 LoA1*

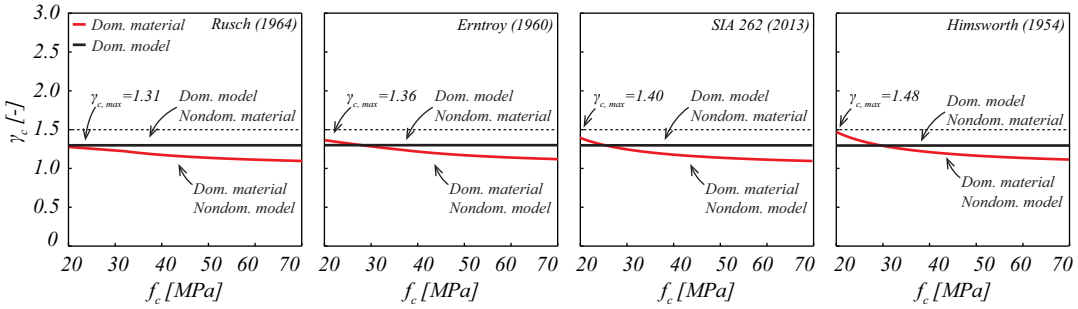

Fig. 31 *Tailored partial safety factors for concrete – Shear failure estimated with SIA262:2013 LoA2*

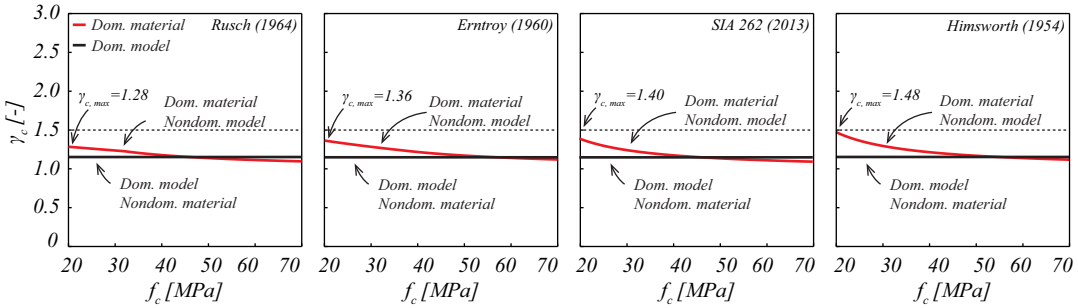

Fig. 32 *Tailored partial safety factors for concrete – Flexural failure estimated with EPSF*

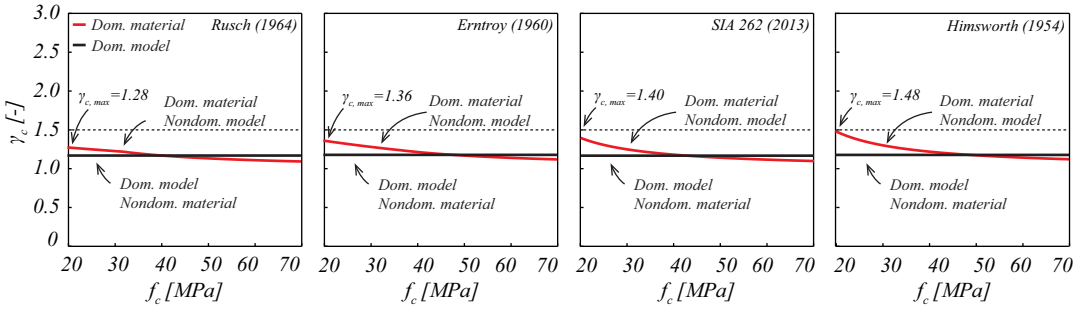

Fig. 33 *Tailored partial safety factors for concrete – Shear failure estimated with EPSF*

In case the structural analysis is based on equations presented in SIA262:2013 [24], maximal partial safety factor for the concrete is equal to 1.48 (which is close to 1.50 indicated by the codes) for elements failing in flexure and shear. This value is determinant each time for the low strength concrete (around 20 MPa) if the dispersion of the concrete compressive strength is assumed according to Himsworth [31]. In case of elements failing in flexure, it can be observed that the PSF for concrete can be reduced as the concrete compressive strength increases, due to the low COV of concrete compressive strength and high accuracy of the applied model. Elements failing in shear, on the other hand, do not experience the same reduction. This is due to the fact that the applied model is much less accurate compared to the one for flexure (refer to *Tab. 1*). In addition to this, it can be

observed that the first level of approximation for shear according to SIA262:2013 governs higher partial safety factor for concrete (γ_c=1.39) compared to the second level of approximation γ_c=1.31 for higer concrete compressive strength, which is to be expected. In order to keep a uniform value of the PSF for concrete, the maximal obtained should be selected (referring to 1.48 in this case), which indicates that the tailoring procedure is in agreement with the code regulations.

For the EPSF method partial safety factors are simmilar for both failure modes (refer to Fig. 32 and *Fig. 33*), due to high model accuracy for both types of failure (refer to *Tab. 1*). Simmilary to elements failing in flexure estimed with SIA262:2013, the material uncertainties are dominant in case of lower strength concrete (around 20 MPa), and govern the maximal value of PSF (γ_c=1.48). It can be observed that this value is highly dependent on COV of concrete compressive strength (according to Rusch [33] for example the maximal PSF for concrete is $\gamma_{c,max}$=1.28). This is why it is crusial to accurately estimate the level of concrete compressive strength dispersion. PSF tailored for EPSF method can be reduced as the concrete compressive strength increases (refer to Fig. 32 and *Fig. 33*). According to the proposed procedure, it can be as low as 1.17 in case of 70 MPa concrete, at which point it becomes almost equal to PSF for steel, indicating that the partial safety factor practicaly becomes global safety factor.

The final value of partial safety factor for concrete that should be used with EPSF method is not explicitly given in this chapter. Similarly to LoA approach, one should first apply $\gamma_c = 1.5$. In case this simulation does not give satisfying accuracy, the value of PSF for concrete can be reduced accoriding to the proposed procedure. Thorough statistical analysis needs to be conducted in order to verify the scatter of concrete compressive stretgth for a given element. In addition to this, the value of sensitivity coefficients needs to be revised in order to make sure that the 0.3 and 0.8 are pertinent values for that particular case. It should be mentioned once more that the tailoring procedure for PSF is still under development, and that the presented results should be taken with reserve.

Partial safety factor for steel has also been calculated, but since the dispersion of the tensile strength is much less, the results are not presented in a form of a graph. *Tab. 3* summarizes the obtained results.

***Tab. 3** Tailored partial safety factors for steel*

	Flexural failure	**Shear failure**
SIA262:2013	1.17	Non
EPSF	1.15	1.16

It can be observed that the PSF for steel are much more uniform and are not that different from 1.15 indicated by the codes. The reason why the PSF for steel was not calculated in case of elements failining in shear for the SIA262:2013 is due to the fact that in reality, failure of the tested speciments was always gowerned by the simultaneous failure of concrete and reinforcement. Eventhough the codes have predicted a few simulatinous failures of elements in shear, the avaleable number of such elements was not sufficient for a pertinent statistical analysis.

When assessing the strength of the existing structures design failure load are usually compared to necessary load requirements. This ratio is called degree of compliance [30] of compliance factor and is defined in following manner:

$$n = \frac{Q_{Rd}}{Q_d} \tag{36}$$

n presents the compliance factor;

Q_{Rd} presents the load governing element's strength;

Q_d presents the required load.

Naturally, if the compliance factor is 1.0 and above, the analysed structure does not need any strengthening and it fully satisfies usage requirements.

1.4 EPSF validated with test database

In order to provide some practical examples of EPSF models, and to validate the applicability of the method itself, a database containing 315 structural concrete elements was formed and placed online at http://i-concrete.epfl.ch/epsf/epsf.html. All FE models are available for download and can be used to clarify the recommendations given in chapters 1.2 and 1.3. In addition to this the database was use to obtain the results presented in chapters 1.5, 1.6 and 1.7. Finally, by running the models one can study their behaviour (observe the failure modes; determine the inclination of the compression field etc.). The investigations have shown that the kinematics of the EPSF models were always in agreement with the test results.

Tab. 4 contains a list of all investigated experimental campaigns (all the references can be found on the indicated web page). It also indicates the type of structural concrete that was used, the number of specimens involved in each campaign, cross section geometry and the static system of the test setup.

***Tab. 4** Summary of the online database*

N°.	Reference	Struct. conc.	Specimen N°	Cross-section	Test setup
1	Vecchio F.J., Shim W., 2004.	RC	9	Rec. CS	3PB
2	Yoon Y.S., Cooc W.D., Mitchell D., 1996.	RC	9	Rec. CS	3PB
3	Sagaseta J., Vollum R.L., 2011.	RC	7	Rec. CS	3PB/CLCB
4	Mansur M.A. et al., 1991.	RC	8	Rec. CS	CLCB
5	Hong S.G. et all., 2002.	RC	7	Rec. CS	4PB
6	Sorensen H.C., 1974.	RC	10	T CS	4PB
7	Leonhardt F., Walter R., 1963.	RC	16	T CS	4PB
8	Kaufmann W., Marti P., 1996.	RC	4	TT CS	PB
9	Nagrodzka-Godycka K., Piotrkowski P., 2012.	RC	12	Dapped-end	4PB
10	Mata Falcón, 2015.	RC	50	Dapped-end	3PB
11	Chan T., 1979.	RC	8	Dapped-end	3PB
12	Khan T., 1981.	RC	9	Dapped-end	3PB
13	Cook W.D., 1987.	RC	3	Dapped-end	3PB
14	Zhu R.R.H. et all.., 2003.	RC	6	Dapped-end	3PB
15	Herzinger R., 2008.	RC	18	Dapped-end	4PB
16	Campana S., Muttoni A., 2011.	RC	13	Corner elem.	PB
17	Placas A., 1969.	RC	23	Rec. CS + T CS	3PB
18	Bach F., Nielsen M.P., Braestrup M.W, 1980.	RC	12	T CS	4PB
19	Leonhardt F., Walther R., 1966.	RC	2	Rec. CS	SBCL
19	Leonhardt F., Walter R., 1966.	RC	2	Cross-beam	3PB
20	Leonhardt F., Walter R., Diliger W. 1968.	RC	5	Cross-beam	4PB
21	Baumann T., Rüsch H., 1970	RC	7	Cross-beam	4PB
22	Saqan E. I., Frosch R. J., 2009.	PC	9	Rec. CS	3PB
23	Kaufman M.K., Ramirez J.A., 1988.	PC	6	TT CS	4PB
24	Kuchma, D. et al., 2008.	PC	19	TT CS	SBCL
25	Rupf, M., Muttoni, A., 2012.	PC	13	TT CS	CLCB
26	Fernandez Ruiz M., Muttoni A., 2008.	PC	6	TT CS	4PB
27	Moore A.M., 2014.	PC	11	TT CS	3PB
28	De Wilder K. et al., 2015.	PC	6	TT CS	4PB

29	Leonhardt F., Koch R., Rostasy F., 1973.	PC	3	Cross-beam	3PB
30	Büeler C., Thoma K., 2010.	PC	2	Cross-beam	3PB

RC: Reinforced concrete
PC: Prestressed concrete

Rec. CS: Rectangular cross section
T CS: T cross section
TT CS: Double T cross section

Dapped-end : Dpped end beam
Cross-beam : Crossed beams

3PB: Three point bending
4PB: Four point bending
CLCB: Concentrated load on a continuous beams

PB: Pure bending
SBCL: Simple beam continuous load

The strength of each EPSF model (Q_{EPSF}) was compared to the measured values (Q_{TEST}) (refer to http://i-concrete.epfl.ch/epsf/epsf.html). The following table gives an average Q_{TEST}/Q_{EPSF} ratio with corresponding COV for each experimental campaign and the entire database.

***Tab. 5** Synthesis of the ultimate load results estimated using the EPSF method*

N°.	Reference	Q_{TEST}/Q_{EPSF}	COV
1	Vecchio F.J., Shim W., 2004.	1.03	0.05
2	Yoon Y.S., Cooc W.D., Mitchell D., 1996.	0.95	0.07
3	Sagaseta J., Vollum R.L., 2011.	1.03	0.09
4	Mansur M.A. et al., 1991.	0.99	0.06
5	Hong S.G. et all., 2002.	1.06	0.05
6	Sorensen H.C., 1974.	1.16	0.06
7	Leonhardt F., Walter R., 1963.	1.11	0.06
8	Kaufmann W., Marti P., 1996.	1.03	0.03
9	Nagrodzka-Godycka K., Piotrkowski P., 2012.	0.98	0.07
10	Mata Falcón, 2015.	0.99	0.07
11	Chan T., 1979.	1.02	0.05
12	Khan T., 1981.	1.03	0.07
13	Cook W.D., 1987.	0.99	0.04
14	Zhu R.R.H. et all.., 2003.	1.06	0.07
15	Herzinger R., 2008.	0.99	0.06
16	Campana S., Muttoni A., 2011.	0.97	0.06
17	Placas A., 1969.	1.04	0.14
18	Bach F., Nielsen M.P., Braestrup M.W, 1980.	1.14	0.12
19	Leonhardt F., Walther R., 1966.	1.02	0.04
20	Leonhardt F., Walter R., Diliger W. 1968.	1.01	0.04
21	Baumann T., Rüsch H., 1970	1.06	0.06
22	Saqan E. I., Frosch R. J., 2009.	1.23	0.10
23	Kaufman M.K., Ramirez J.A., 1988.	1.07	0.07
24	Kuchma, D. et al., 2008.	1.09	0.07
25	Rupf, M., Muttoni, A., 2012.	1.06	0.05
26	Fernandez Ruiz M., Muttoni A., 2008.	0.98	0.05
27	Moore A.M., 2014.	1.00	0.07
28	De Wilder K. et al., 2015.	0.98	0.04

29	Leonhardt F., Koch R., Rostasy F., 1973.	1.05	0.03
30	Büeler C., Thoma K., 2010.	1.01	0.01
		Total: 1.04	0.10

The same results are also presented in *Fig. 34*. The 4 for graphs presents the results in function of concrete compressive strength (f_c), longitudinal reinforcement ratio (ρ – refer to equation 37), cross-section prestress level ($\sigma_{p,inf}$ – refer to equation 38) and transverse reinforcement ratio (ρ_w – refer to equation 39). The figure also shows a moving average of the point of clouds in order to determine any trends in results (in this particular case every point on the sliding average line corresponds to 10 point in the cloud).

$$\rho = \frac{A_{SL}}{b \cdot d} \tag{37}$$

$$\sigma_{p,\text{inf}} = \frac{F_{p,\text{inf}}}{A} \tag{38}$$

$$\rho_W = \frac{A_{SW}}{b_W \cdot s} \tag{39}$$

A_{SL} represents the total area of longitudinal flexional reinforcement [mm^2];

b represents the width of the flexural compression zone [mm]

d represents the static height of the section with maximal bending moment [mm]

A_{SW} represents the total area a stirrup [mm^2];

b_W represents the web width [mm]

s represents the spacing between the stirrups [mm]

$F_{p,inf}$ represents the total prestress force [N];

A presents the cross-section area [mm^2].

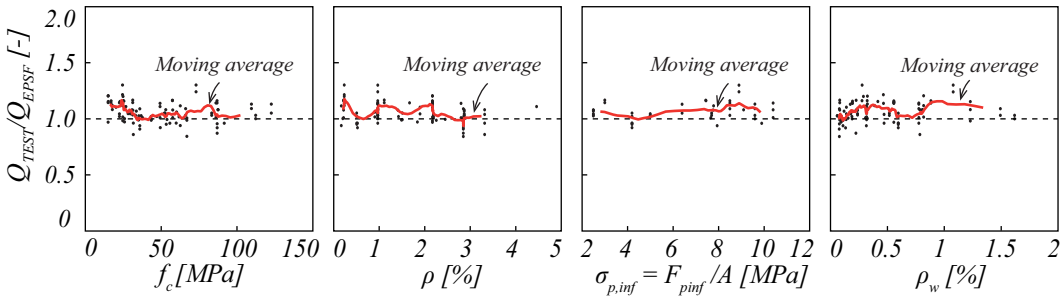

Fig. 34 *Results of the EPSF analysis*

All previous considerations validate the accuracy and the generality of the approach. Keeping this in mind, the following chapters will point out the representative results from the database, which are related to specific problems often found in bridge structures.

1.5 Specific considerations regarding dapped-end beams

Dapped-end beams (DEB), also known as Gerber joints are common concrete details extensively used in precast concrete structures, generated when precast girders reduce their depth near to the ends or to introduce hinges only to transfer shear forces. This detail allows a depth reduction of the structure and is an easy way of assembly different structural precast elements or to generate expansion joints. Because of the reduced depth, significant stress and crack concentration develop nearby the discontinuity section. Thus, specific considerations have to be done in order to achieve safety and durability of DEB. This chapter summarizes the most significant aspects developed by Jaime Mata-Falcón [40].

The main potential failure modes in DEB (refer to *Fig. 35*) are:

- Shear failure of the full-depth section;
- Diagonal tension from the re-entrant corner;
- Shear failure over the extended end;
- Spalling off of the upper concrete cover.

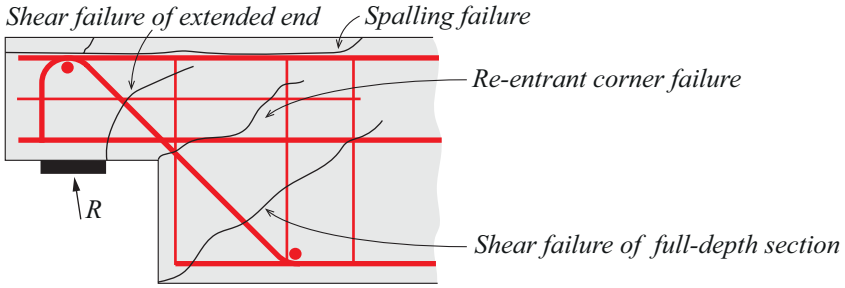

***Fig. 35** Failure mechanisms of dapped-end beams*

EPSF models are able to safely predict all failure modes. However, the spalling failure can be predicted in an excessive safe mechanism by EPSF. In these cases specific modelling of the compression cover as described in section 1.3.5 has to be carried out in order to obtain accurate results.

In order to validate the application of EPSF in DEB following experimental campaigns were modelled according to the guidelines given in this report:

- Chan (1979) – 8 tests [36]
- Khan (1981) – 9 tests [37]
- Cook & Mitchell (1987) – 3 tests [38]
- Zhu et al. (2003) – 6 tests [39]
- Herzinger (2008) – 18 tests [40]
- Mata-Falcón (2015) – 50 tests [40]
- Nagrodzka-Godycka K., Piotrkowski P. (2012) – 12 tests [41]

It is important to mention that the spalling finite elements were applied in all the cases independently from the fact that the spalling was detected or not.

A brief description of the experimental studies analysed is presented in *Fig. 38*. It shows geometry of the dapped-end region, the shape of reinforcement cage, type of loading, longitudinal and transverse reinforcement ratio and concrete compression strength.

The JCONC files to reproduce these elements can be downloaded from http://i-concrete.epfl.ch/epsf/epsf.html. Two cases are for instance given in *Fig. 36* that shows a spalling failure and a re-entrant corner failure. More details can be found in [40].

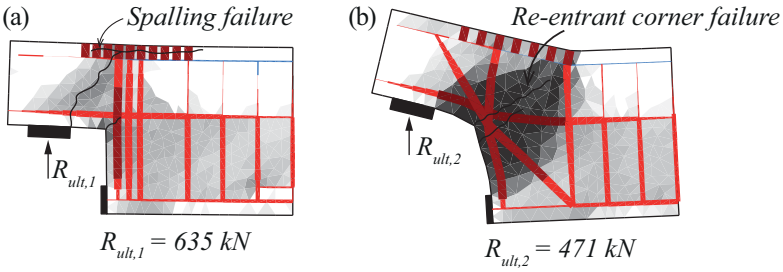

Fig. 36 *Failure mechanism of dapped-end beams: spalling failure – DEB 1.6 (a) re-entrant corner failure – DEB 2.1 (b) tested by Mata-Falcon [40]*

Fig. 37 shows the ratio between the experimental ultimate vertical load at the support (Q_{TEST}) and the transverse reinforcement ratio using the EPSF models (Q_{EPSF}). Average and coefficient of variation of this ratio is shown for each series in *Tab. 5*.

The prediction, with a general average of the ratio between experimental and predicted load for the selected series of 1.00 and a coefficient of variation of 0.07, can be considered to be sufficiently accurate. The accuracy is similar for all the studied series, independent from the different geometric and material characteristics.

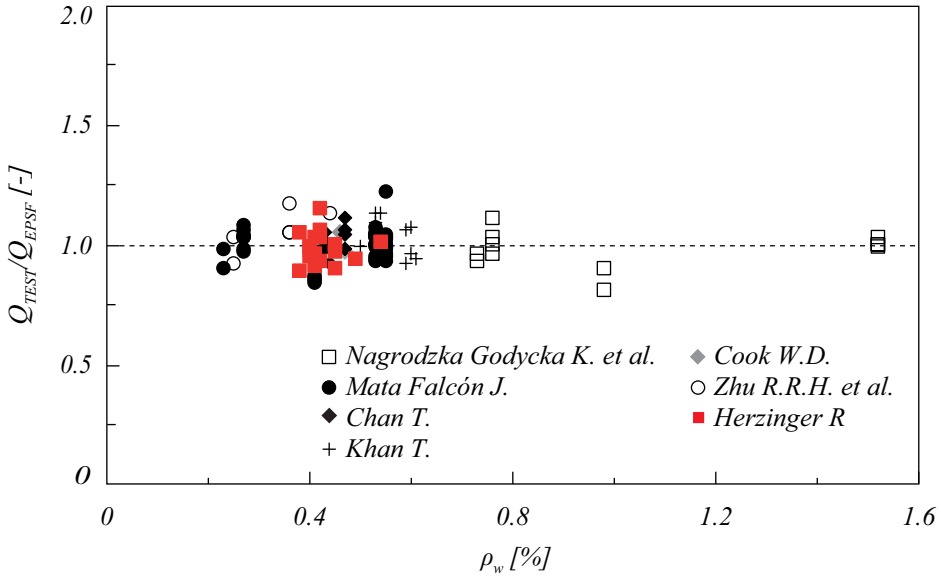

Fig. 37 *Ultimate loads of dapped-end beams estimated using EPSF method*

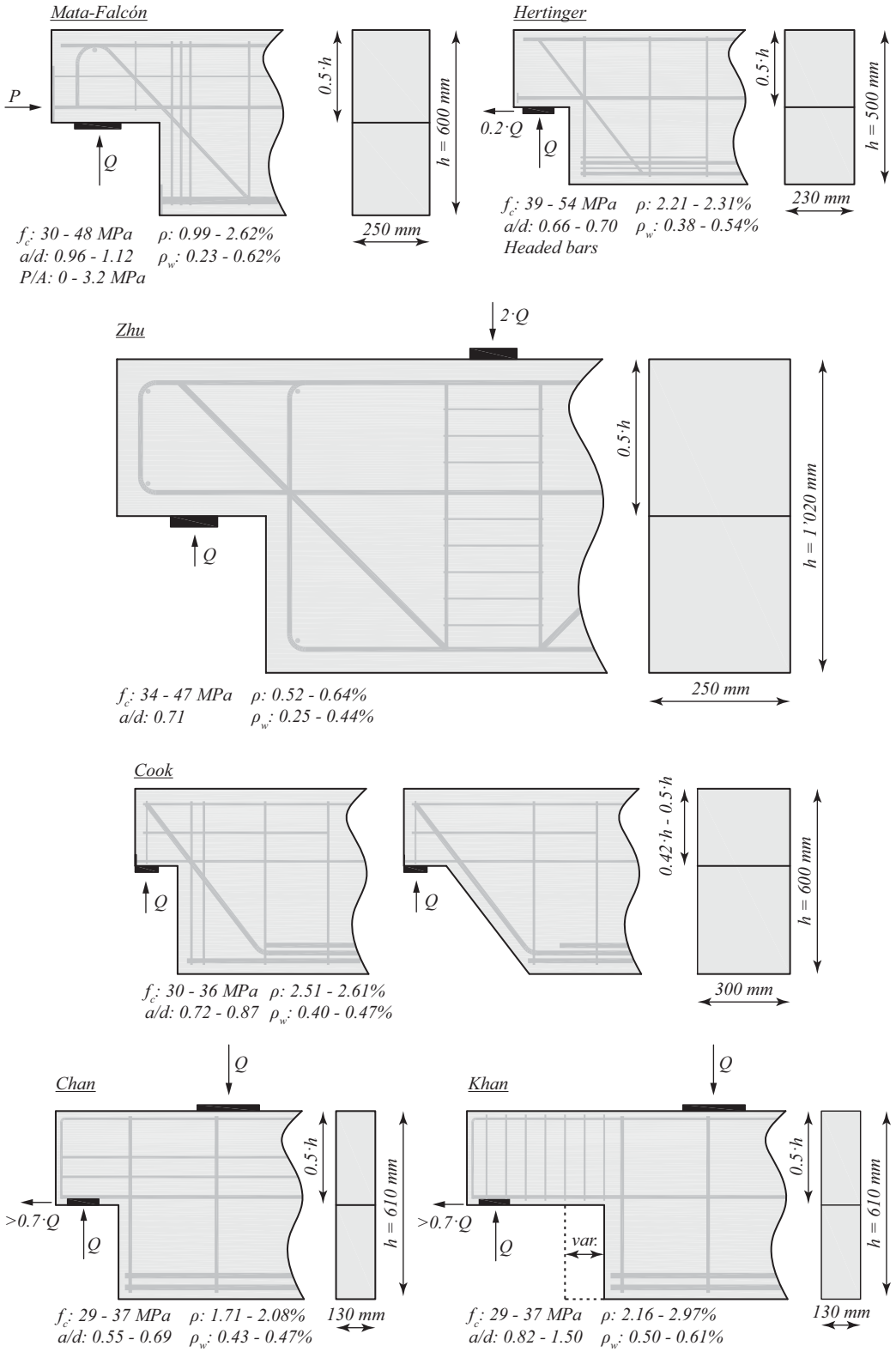

Fig. 38 *The main characteristics of the dapped-end beams used to validate EPSF method*

1.6 Prestressed beams

The assessment of prestressed girders with EPSF is one of its most interesting applications. This is due to the fact that a number of parameters can be calculated in an automatic manner, namely:

- The angle of compression field (below 25° in many cases);
- The value of k_c (above 0.55 in many cases);
- The increase of the force of the prestressing tendon in the critical region;
- The contribution of the flanges due to shear compression.

With respect to the EPSF modelling, one of the most controversial issues is the reduction of the web thickness due to the presence of the ducts ($k_D\,factor$). Some national codes (like ACI [42] for example) indicate that this reduction is not necessary, whereas the others (SIA262:2013 [24], EC2 [27], MC2010 [21] and AASHTO [43]) clearly state that this effect needs to be accounted for. However, the reduction values are different in all 4 codes (refer to *Tab. 6*).

***Tab. 6** Reduction of the web thickness due to the presence of prestressing ducts (k_D)*

Code	Grouted steel duct	Empty steel duct	Grouted plastic duct	Empty plastic duct
SIA262:2013	0.5	1.2	0.8	1.2
EC2	0.5	1.2	1.2	1.2
ACI 318 – 11	0	0	0	0
AASHTO LRFT	0.25	0.5	0.25	0.5
AASHTO Seg. Gird.	0.5	1.0	0.5	1.0
MC 2010	0.5	1.2	0.8	1.2

In order to determine the most appropriate value which needs to be applied, following experimental campaigns were modelled with EPSF method (more details can be found in [47]):

- Rupf, M. (2013, 2014) – 10 tests [44, 45]
- Moore A.M. (2014) – 10 tests [46]

Basic mechanical properties of the specimens are presented in *Tab. 7*.

***Tab. 7** Basic mechanical properties of prestressed concrete beams*

Rupf, M. (2014)					Moore A.M. (2014)				
Spec. n°	Name	f_c [MPa]	ρ_w [%]	$F_{p,inf}/A$ [MPa]	Spec. n°	Name	f_c [MPa]	ρ_w [%]	$F_{p,inf}/A$ [MPa]
1	SR21	30.8	0.09	2.5	11	62-1S	73.1	0.93	11.8
2	SR22	33.7	0.13	2.5	12	62-2S	82.7	0.93	12.3
3	SR23	35.3	0.06	2.5	13	62-2N	82.7	0.93	12.3
4	SR24	31.3	0.25	2.5	14	62-4S	95.8	1.4	12.5
5	SR25	33.1	0.09	5.0	15	62-4N	93.8	1.4	12.5
6	SR26	36.9	0.06	5.0	16	62-5S	86.2	0.31	12.5
7	SR27	28.3	0.19	5.0	17	62-5N	86.2	0.31	12.5
8	SR29	29.8	0.25	2.5	18	62-6S	85.5	1.14	13
9	SR30	31.4	0.25	2.5	19	62-6N	91	1.14	13
10	SR31	31.3	0.09	3.0	20	62-7S	84.1	1.14	13

Tab. 8 gives the average ratio between the experimental ultimate shear force (Q_{test}) and the estimated maximal shear using the EPSF models (Q_{EPSF}) for the two experimental

campaigns, applying the reduction factors from *Tab. 6*. It also gives the corresponding coefficient of variation.

Tab. 8 *Synthesis of the ultimate loads of prestressed concrete beams estimated using EPSF method and different web width reduction factors (k_D - factors)*

Code	Q_{TEST}/Q_{EPSF} – Steel ducts	COV– Steel ducts	Q_{TEST}/Q_{EPSF} – Plastic ducts	COV – Plastic ducts
SIA262:2013	1.04	0.07	0.99	0.02
EC2	1.04	0.07	1.09	0.05
ACI 318 – 11	1.00	0.09	0.83	0.03
AASHTO LRFT	1.00	0.09	0.84	0.03
AASHTO Seg. Gird.	1.04	0.07	0.91	0.02
MC 2010	1.04	0.07	0.99	0.02

It shows that the SIA262:2013 [24] recommendations are in best agreement with test observations. The Rupf series shows less variation in the ultimate load than Moores, which was due to the fact that the specimens had smaller amount of the transverse shear reinforcement and lower amount of prestresses. This means that the overall response of the beam was softer, and thus the importance of the web reduction parameter is lower.

The web reduction factor has a big influence on the failure mechanism of the element. The investigation has shown that a wrong failure mode was obtained in each model in case the web reduction factor was not applied (refer to *Fig. 39*). As it can be seen the model which did not apply any web width reduction failed due to the crushing of the web in the region close to the flanges that was not observed during the experimental campaign. The same conclusion was drawn after modelling the entire Rupf test series as well at the test series of Moore (refer to *Fig. 40*).

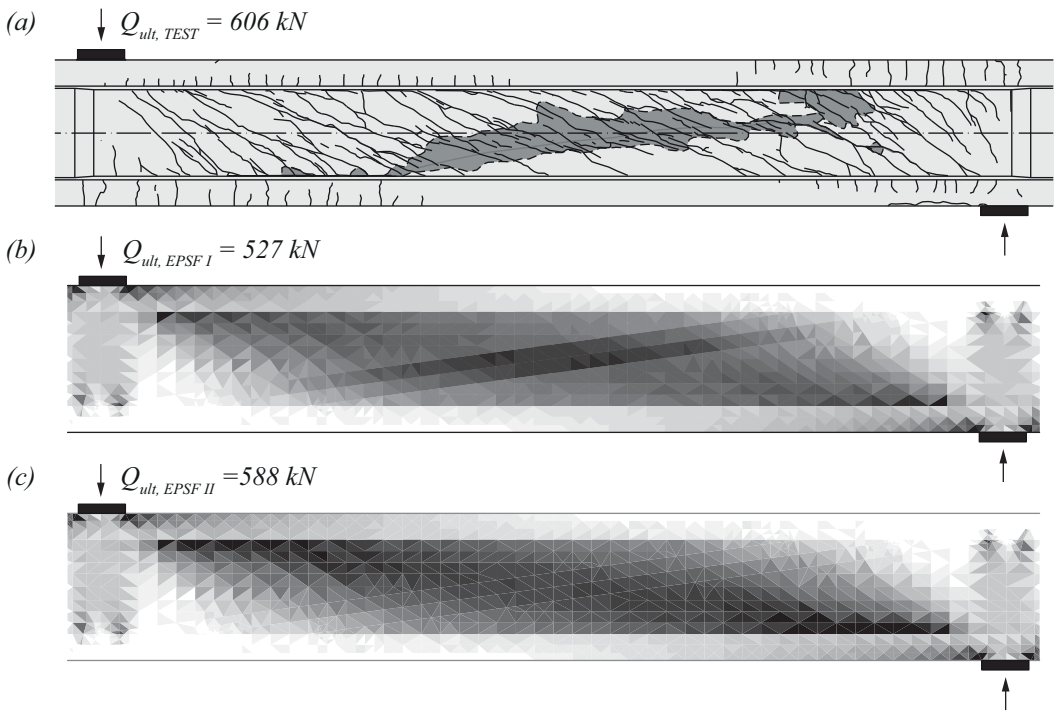

Fig. 39 *Prestressed beam SR27 tested by Rupf – observed failure mechanism (a); failure mechanism obtained with EPSF method after applying the kc factor according to SIA262:2013 (b); failure mechanism obtained with EPSF method with no reduction of the web thickness (c)*

The *Fig. 40* shows the ultimate load of the beam *TX62-6* estimated using EPSF method after applying different k_D - *factors*. The beam was tested twice (once on each side) using a

different material for the prestressing duct (plastic and steel). As it can be seen in the *Fig. 40a*, this had a significant influence on the beams ultimate strength (15.4% difference between the 2 specimens was observed) and it governed its failure mode (crushing above the duct - see *Fig. 40b*). When it comes to EPSF analysis it gave different results as the k_D - *factors* increased. At first ($k_D = 0$) the model had a wrong failure mode (similar to the one presented in *Fig. 39c*) and it overestimated the actual failure load (refer to *Fig. 40a*). As the k_D - *factor* increased the failure mechanism changed which can be clearly seen in the graph (the black dot in *Fig. 40a*. The red points show the failure loads obtained using the k_D - *factors* recommended by SIA262:2013 for steel and plastic ducts, which gave an excellent correlation with the experimental campaign.

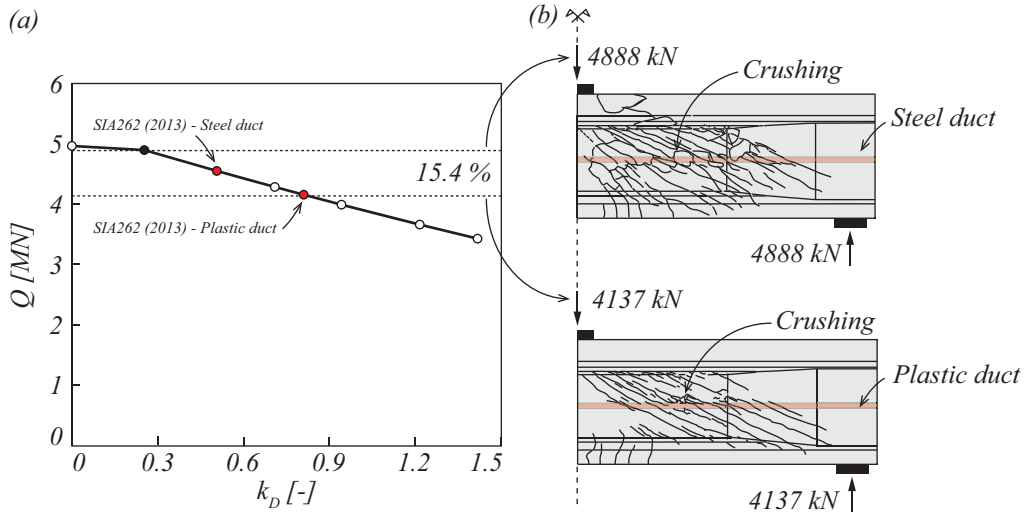

Fig. 40 *Prestressed beam TX62-6 tested by Moore – the results of EPSF analysis (a); the observed failure modes and measured ultimate load (b)*

Based on these results it was clear that k_D - *factors* need to be applied in order to obtain a correct failure mode of the prestressed beams and in order not to overestimate their strength. The recommendation given by SIA262:2013 and MC 2010 gave the best results.

In order to validate the application of EPSF, additional experimental campaigns were modelled:

- Kaufman M.K., Ramirez J.A. (1988) – 6 tests [48]
- Saqan E. I., Frosch R. J. (2009). – 9 tests [49]
- Kuchma, D. et al. (2008) – 19 tests [50]
- Fernandez Ruiz M., Muttoni A. (2008) – 6 tests [51]
- De Wilder K. et al. (2015) – 6 tests [52]

A brief description of experimental studies analysed is presented in *Fig. 41.* It shows geometry of the presress cable, the shape of reinforcement cage, type of loading, longitudinal and transverse reinforcement ratio and concrete compression strength.

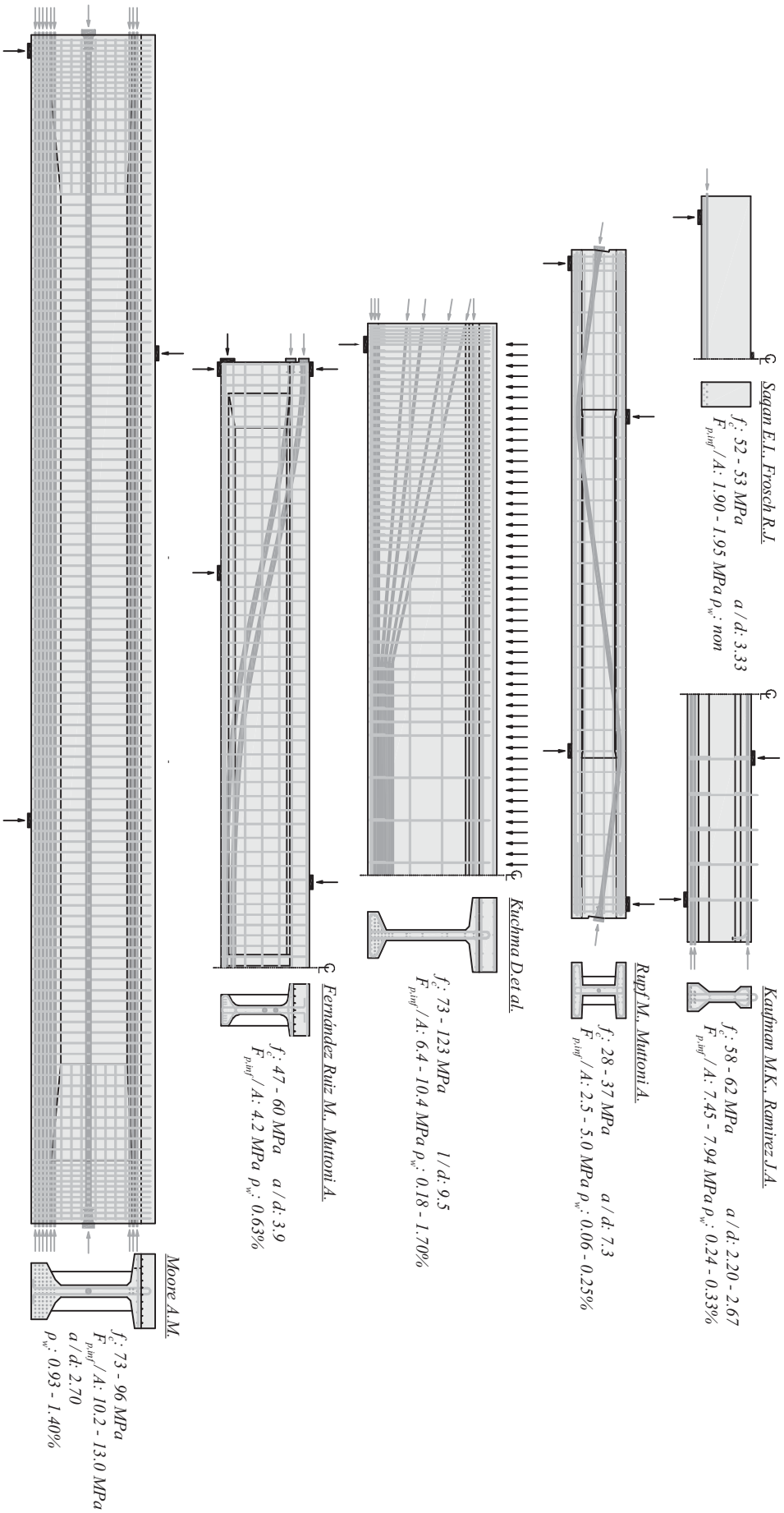

Fig. 41 *The main characteristics of the prestressed beams used to validate EPSF method*

Fig. 42 presents the ratio between the experimental ultimate shear force (Q_{TEST}) and the estimated maximal shear force using the EPSF models (Q_{EPSF}) in function of transverse reinforcement ratio (ρ_w).

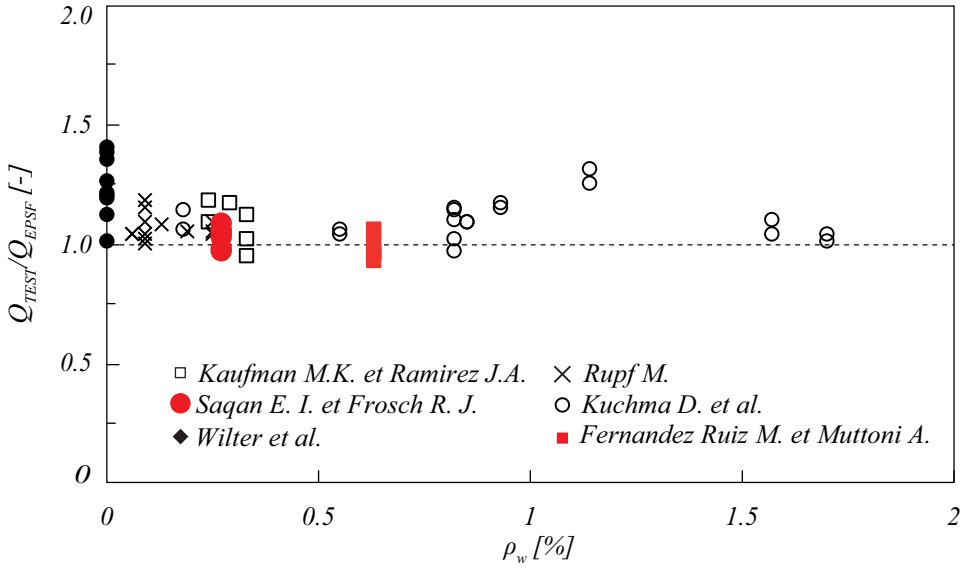

***Fig. 42** Ultimate loads of prestressed beams estimated using EPSF method*

An average general ratio between the experimental and predicted failure load for the selected specimens of 1.07 and a coefficient of variation of 0.10, can be considered as sufficiently accurate. The EPSF method showed similar accuracy for all investigated series except the series of Saqan and Frosh (2009). This was due to the fact that the prestressed beam had no transverse shear reinforcement. Since the concrete FE did not have any steel to control the transverse deformations, the η_ε reduction factor (refer to equation 4) was overestimated, thus governing lower strength of the beams. In general the EPSF method is not applicable in case of the elements with no transverse reinforcement, meaning that the results did not come as a surprise.

1.7 Bridge diaphragms

Bridge diaphragms allow supporting bridges not only under their webs. The box-girder bridges, they also allow to develop uniform torsion conditions, so to resist in more efficient manner torsion actions. However, these elements are complex to design - they are not in plane of the webs and are subjected to complex stress states.

As presented in *Fig. 43*, the internal forces are deviated from the longitudinal webs, through suspension reinforcement to the bridge diaphragm in order to reach the support. In the perspective of EPSF method, this means that two simultaneous simulations are required in order to analyse the stress states of the members in different planes and to correctly distribute the shear force transfer from one element to another (assuming that the entire shear force is applied in point A - *Fig. 43* can be too conservative while assuming that it is only applied in the point B - *Fig. 43*, might be unsafe for example). In addition to this, placing the suspension reinforcement exactly in the crossing zone of longitudinal and transversal elements can be physically impossible (due to the amount of re-bars or construction site constrains). In such cases reinforcement is distributed over a wider zone which brings up a question whether such arrangement can still effectively transfer the shear force, and if this can this affect the failure mechanism of the system. However, the most important question which will be addressed in this chapter is can the EPSF method be used to correctly predict the ultimate capacity and failure mechanisms of such systems and with what accuracy.

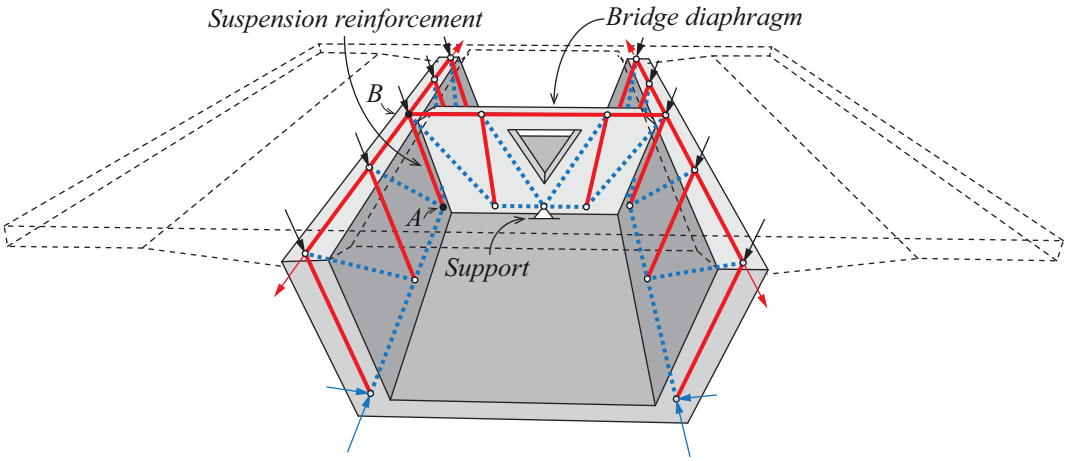

***Fig. 43** Bridge diaphragm – principle function and strut-and-tie model*

For the purpose of this research a database containing 19 results form 5 different experimental campaigns was compiled:

- Leonhardt F., Walther R. (1966) – 2 test [6];
- Leonhardt F., Walther R., Dilger W. (1968) – 5 tests [53];
- Baumann T, Rüsch H. (1970) – 7 tests [54];
- Leonhardt F., Koch R., Rostasy F. (1973) – 3 tests [55];
- Büeler Ch., Thoma K. (2010) – 2 tests [56].

The first three experimental programs contain only reinforced concrete specimens, whereas the last two apply prestressed concrete beams (tests performed by Büeler Ch. and Thoma K. were designed specifically of the purpose of ORFOU rapport AGB Forschungsbericht No. 660 [57]). All 5 experimental campaigns were conducted in order to better understand the mechanism of beam to beam shear transfer action, and as such are adequate to simulate behaviour of bridge diaphragms (reinforcement details and main parameter are given in *Fig. 44*).

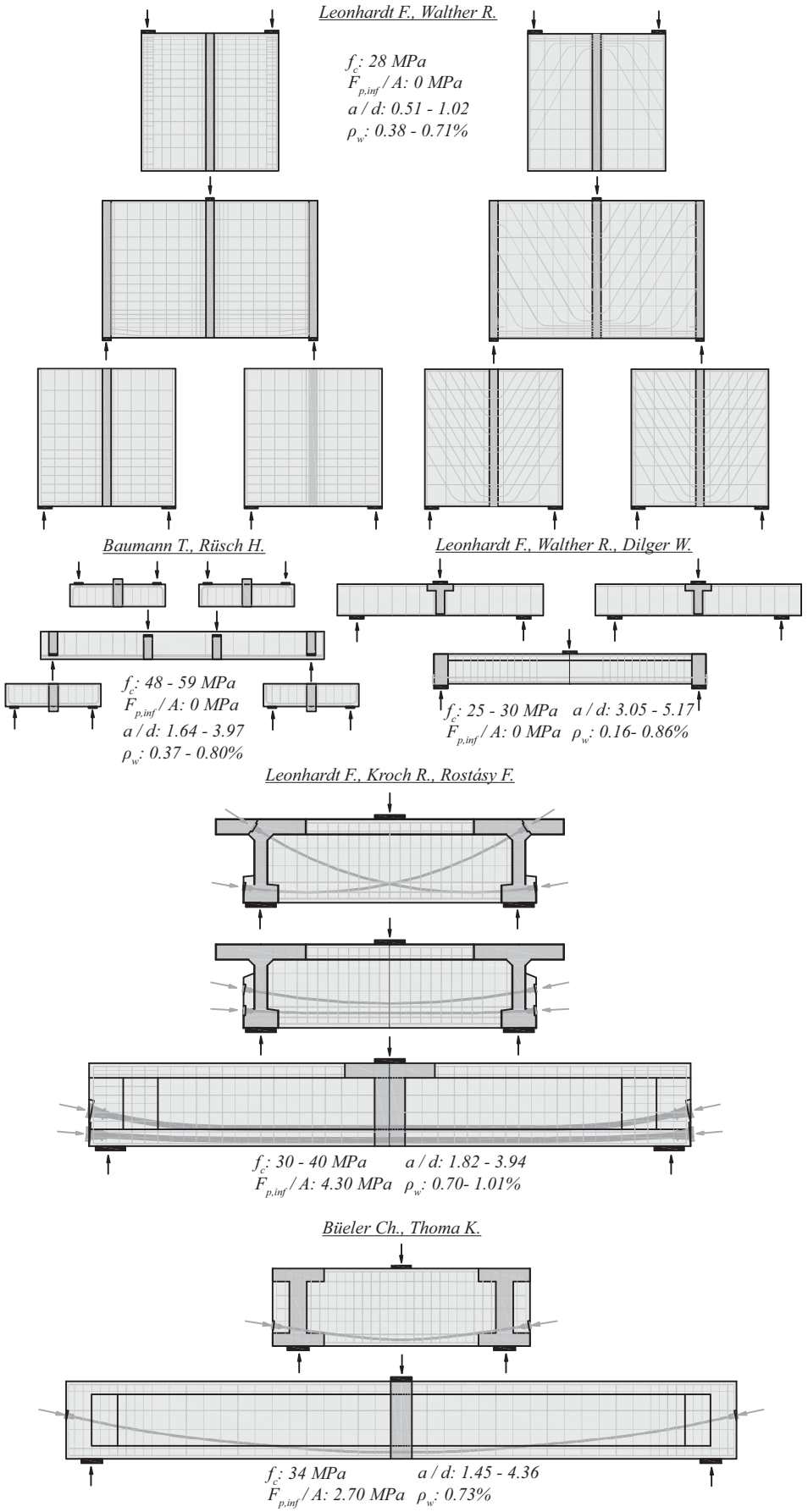

Fig. 44 *Main characteristics of the members used to validate EPSF method*

The modelling technique which was applied in order to analyse crossed members by means of EPSF method is presented in *Fig. 45*.

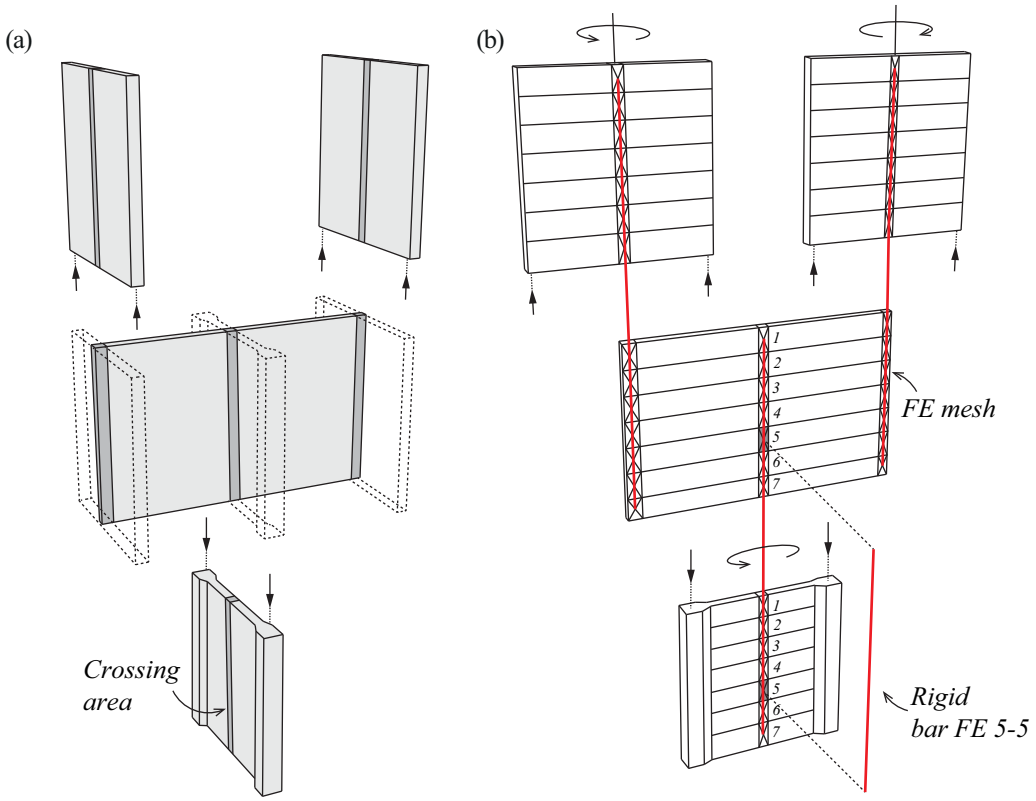

Fig. 45 *Modelling technique for crossed-beam members using EPSF method: decomposition of the analysed specimen (a); connecting the crossed-beams members with rigid bar FE (b)*

In this figure, a tested specimen and its corresponding modelling are presented (the test was a part of an experimental campaign conducted by Leonhardt F. and Walther R. in 1966 [6]) consists of 4 elements: 3 transverse walls connected by a longitudinal wall (refer to *Fig. 45a* – the dashed specimen). The 2 exterior transverse elements act as supports while the load is applied indirectly via central transverse wall. In order to analyse the entire system using EPSF method all specimens need to be placed in a single plane (as presented in *Fig. 45b*). In a given example this means that the transverse members need to be rotated by 90° (refer to Fig. 45*b*) and placed above the longitudinal element in case they serve as supporting members, or below it in case they introduce the loads. Finally finite elements in the crossing zone need to be linked node-by-node using rigid bars in order to impose equal nodal displacement between the elements (refer to *Fig. 45b* - for example the node 5 in the longitudinal wall needs to be connected to node 5 of the transversal wall using a rigid bar FE 5-5). It was observed that the best results are obtained in case the linking in done in a single line where the symmetry axes of the two elements are crossing each other. This also implies that the meshes of the connecting region need to have equal number of FE over their height (as presented in *Fig. 45b*).

Very satisfactory results have been obtained after applying the described modelling technique**.** On average EPSF method yielded 4% lower values of specimen's ultimate strength when compared to what was measured during the tests. In addition to this the results showed very little scatter (COV = 5%) and no trends presented as a function of 4 basic mechanical parameters (concrete strength, prestress level, longitudinal and transverse reinforcement ratio as given in *Fig. 46*).

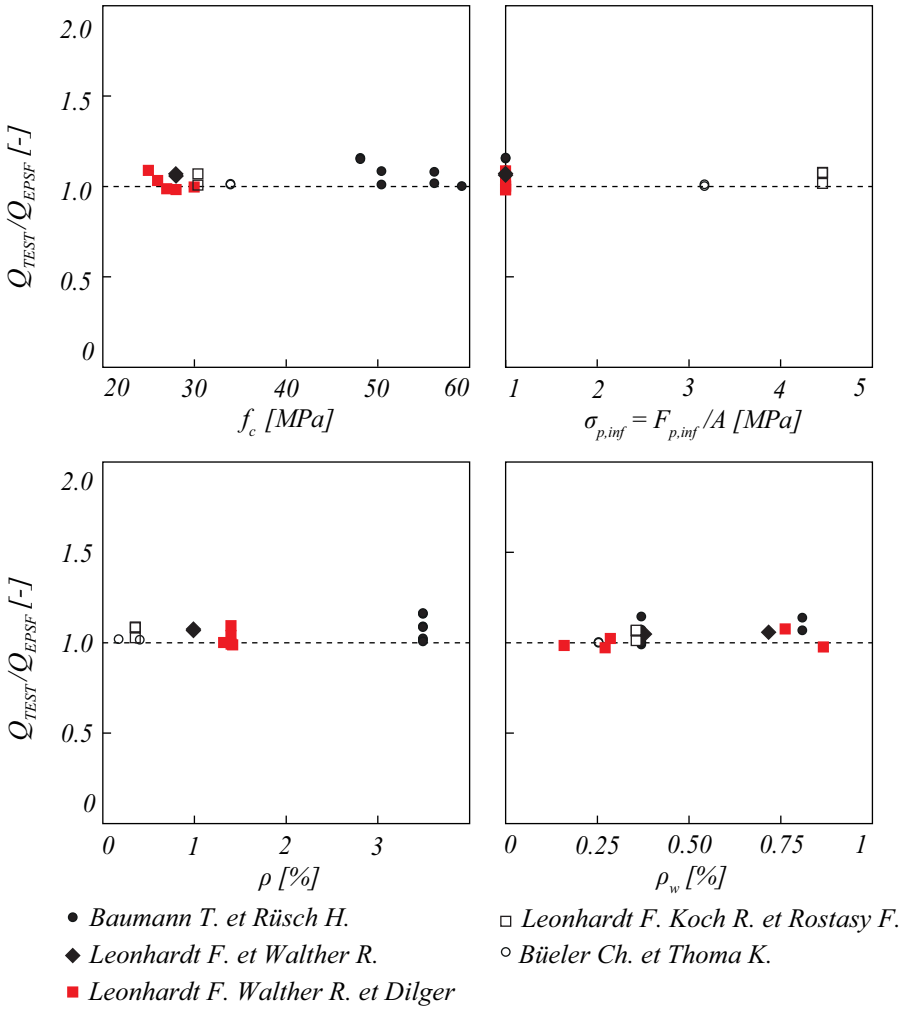

Fig. 46 *Ultimate loads of crossed-beam members estimated using EPSF method*

In terms of failure mechanisms, each EPSF model predicted that the specimens will fail accordingly to what was observed in the experimental campaigns. The method proved capable of correctly predicting the failure mechanism of reinforced and prestressed concrete elements. In some cases the failures occurred in one of the crossed-beams (refer to *Fig. 47*), while the others failed in the connecting region (see *Fig. 48*).

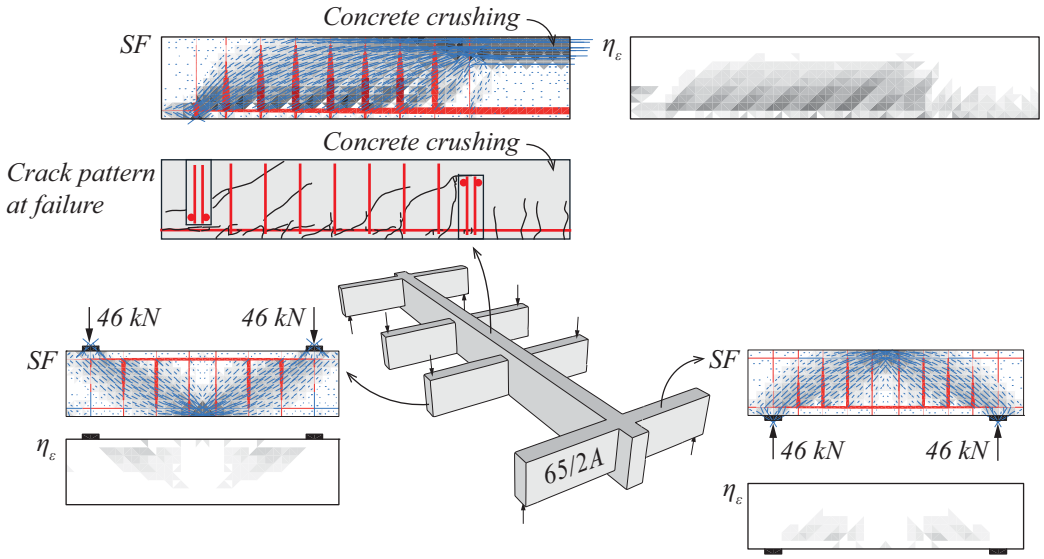

Fig. 47 *Results of the EPSF analyses performed on a 65/2A specimen tested by Baumann – governing flexural failure of the member*

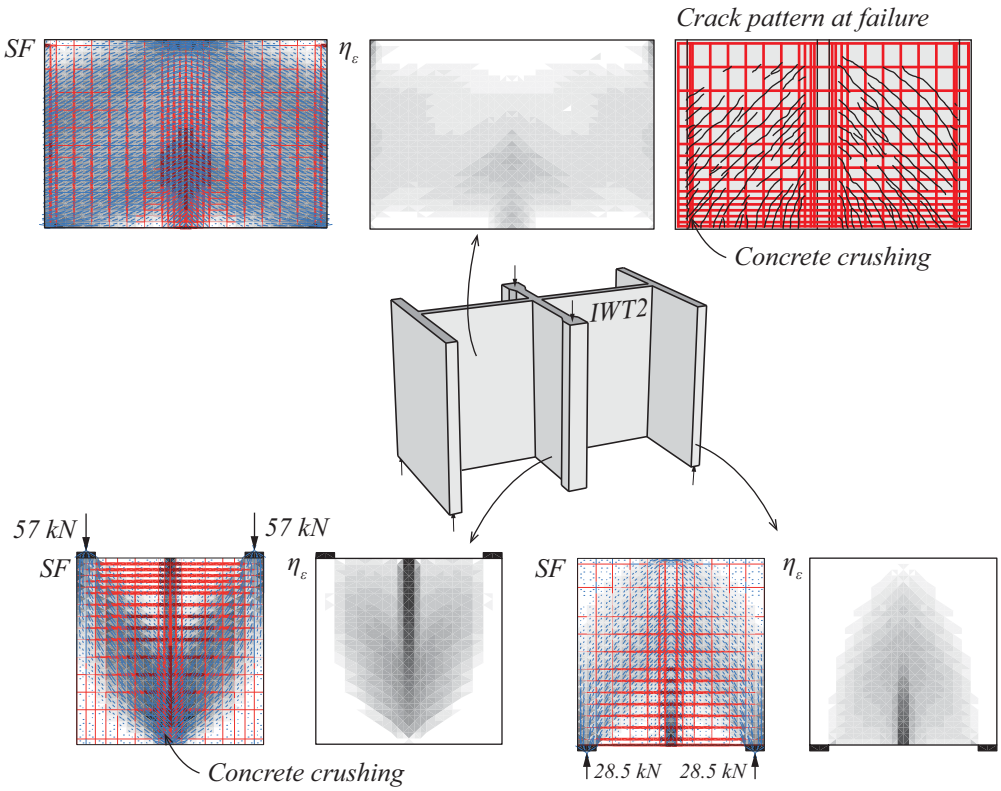

Fig. 48 *Results of the EPSF analyses performed on a IWT2 specimen tested by Leonhardt and Walter – governing local failure of the member*

Based on presented results the EPSF method has proved to be efficient and accurate tool for simulating behaviour of crossed-beam members capable of predicting the correct ultimate load and failure kinematics both on local and global level.

2 Strength and behaviour of beam webs with transverse bending

2.1 Introduction

The design of structural concrete elements subjected to longitudinal shear and longitudinal bending, where equilibrium-based solutions as stress fields can be consistently used when stirrups are arranged, has been extensively studied over the past century and has been thoroughly reviewed in chapter 1 of this report. A topic where less research effort has been devoted to is the interaction between in-plane (longitudinal) shear and out-of-plane (transverse) bending, which nevertheless is present in numerous structures and in particular in box-girder bridges (*Fig. 49*). In the longitudinal direction, the girder webs are mainly subjected to membrane (in-plane) actions due to longitudinal shear and torsion. In the transverse direction, the webs can be subjected to significant transverse (out-of-plane) bending moments, depending on the span ratios of the deck slab, the bending stiffness ratio between the deck slab and the web, as well as the eccentricity and level of live load acting on the cantilever (*Fig. 49b*). Additionally, in case of none or insufficient transverse stiffeners the effect of torsion leads to a substantial increase of the transverse moment in the web. In principle, box girder webs are thus always subjected to a combination of in-plane shear and out-of-plane bending moments. Tests on beams and shell elements ([58], [59], [60], [61], [62], [63]) have shown that the membrane state-of-stress in the element (resulting from in-plane shear) can be significantly disturbed by the presence of out-of-plane bending moments, which leads to a reduced shear resistance, especially if a brittle failure due to crushing of concrete is to be expected. Consequently, neglecting their interaction and performing independent analyses for longitudinal shear and transverse bending, and then summing the required shear reinforcement, is not consistent with the actual behaviour of the web at failure. Furthermore, it potentially leads to excessive amounts of reinforcement and to inconsistent and unsafe superposition of concrete compressive stresses.

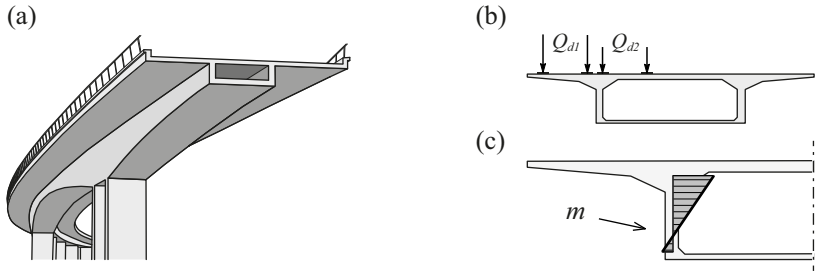

Fig. 49 *Interaction of in-plane shear and transverse bending in the webs of (a) box-girder bridges; (b) transverse cross section with typical traffic load; (c) transverse bending moment in the web.*

For the assessment of beam webs under combined action of in-plane shear and transverse bending, a number of consistent design approaches grounded on the lower bound theorem of the theory of plasticity are proposed in the literature ([64], [65], [66], [61]). The shear-transverse bending interaction is investigated by means of equilibrium based models while assuming rigid-perfectly plastic behaviour for concrete and steel. The models are based on the classical rigid-plastic stress field (RPSF) approach (basis of the Swiss code SIA262:2013 [24] and illustrated in [3]) that is then adapted to account for transverse bending. The principle consists essentially in shifting the compression field in the web towards the bending compression side of the web width and by this equilibrating a transverse bending moment. The additional equilibrium condition for the transverse bending moment thus allows formulating a rigid-plastic (RP) interaction model for in-plane shear and transverse bending that is typically represented by means of shear-transverse bending interaction diagrams. Such diagrams then allow evaluating the actual shear strength of the web as a function of the acting transverse bending moment. Chapter 2.2 gives an overview on different RP interaction models and investigates two of them in detail.

Alternatively, the design of reinforced concrete members subjected to membrane and bending actions can also be performed using sandwich models as proposed in *fib* Model Code 2010 [21] and EN 1992-2:2005 [67]. Sandwich models, as for example proposed by Marti [68], Mancini [69], Figueiras [70] and Seelhofer [71], are useful tools for the ultimate limit state design of reinforced concrete slabs. They are however less adapted for the analysis of beam webs where high membrane loads (due to shear) are expected. Sandwich models normally neglect the contribution of the sandwich core in the load transfer of membrane actions, which leads to safe but conservative estimates of the combined resistance for in-plane shear and transverse bending (see Mancini [72], Seelhofer [71]). Furthermore, the sandwich model approach, where the compression fields are normally assumed to act in the two outer layers, is not consistent with the actual behaviour of the web as it has been observed in the tests, i.e. shifting of the compression field towards the bending compression side. Consequently, the sandwich model approach will not be further developed in this report.

The RPSF approaches provide lower bound estimates of the strength of a member [3]. A more general procedure for automatic development of stress fields that is based on the elastic-plastic stress field (EPSF) method has been proposed by Fernández Ruiz and Muttoni [12] and is presented in detail in chapter 1.1. This method respects the equilibrium conditions, compatibility conditions and the yield criteria of materials. Consequently, the EPSF method leads to exact solutions according to the theory of plasticity and thus to a more accurate estimate of the actual strength of reinforced concrete members. An application of the EPSF method to the problem of panels and beams subjected to shear and transverse bending is presented in chapter 2.3. This is done by means of a multi-layered elastic-plastic (ML-EP) panel element, in which every layer respects the conditions of the EPSF. This approach is applied to the case of in-plane shear and transverse bending in beam webs which allows a detailed modelling of the in-plane state-of-stress in the web and a better insight into the actual in-plane shear transverse bending interaction. It is shown that the ML-EP panel approach usually leads to larger capacities than conventional RP interaction models. The ML-EP panel element confirms the basic principles of the RP interactions models, but also stresses out significant differences in the underlying stress fields.

The RP and ML-EP panel solutions allow for a local verification of the resistance of the web cross-section. In order to investigate the global behaviour and the actual bearing capacity of the entire structural element, a simplified verification approach that is based on the finite element method for plane EPSF (Fernández Ruiz and Muttoni [12]) is proposed in chapter 2.4. The effect of the transverse bending moment on the plane EPSF, and thus the in-plane shear resistance, is accounted for in a simplified/indirect manner by making use of the principles of the RP interaction models. This approach generally leads to higher shear strength for beams subjected to transverse bending than RP interactions models, but still provides a lower bound solution of the actual failure load. An outlook on an enhanced solution of the EPSF method consisting of a multi-layered EPSF element will eventually be introduced in chapter 2.5.

2.2 Panel solutions based on the rigid-plastic stress field method

The issue of longitudinal shear and transverse bending in beam webs was early addressed by Kupfer in 1969 (as cited by Ewald [60]). Kupfer assumed that under the action of a transverse bending moment the compression field in the web inclines towards the bending compression side. For a given shear load Kupfer computed a maximum admissible concrete compressive stress at the web-flange section which allowed him to formulate a limitation for the transverse bending moment (in the uncracked state). In 1973 (as cited by Ewald [60]), Jungwirth and Baumann adopted his principle, i.e. that the transverse bending moment can be resisted only by the vertical component of the inclined compression forces (due to longitudinal shear) that is eccentric relative to the web axis. They additionally proposed a formulation to determine a supplementary vertical bending reinforcement. Although the equilibrium of forces and moments is fulfilled at the considered web section, the assumptions are not/poorly consistent with the actual behaviour of web at failure and no effect of the transverse bending moment on the actual shear strength is considered.

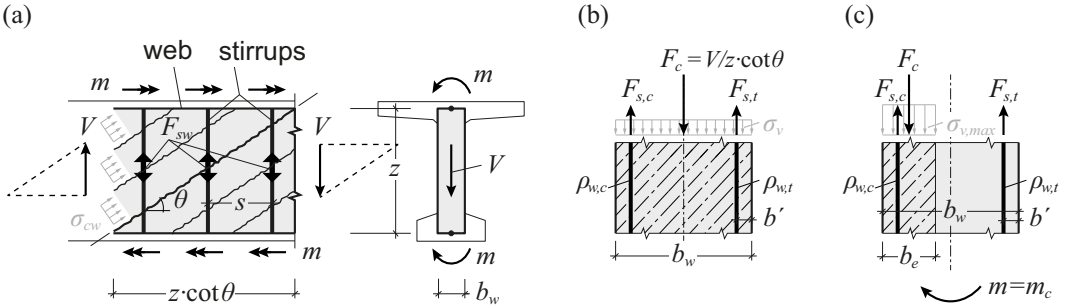

Fig. 50 *The RPSF for shear design of webs with transverse bending: (a) elevation with stress field and web cross section with loads; (b) equilibrium of a web segment cross section in pure shear; (c) equilibrium with a moderate transverse bending moment.*

In engineering practice the design of reinforced and prestressed concrete members is generally performed using a stress field approach and in particular the rigid-plastic stress field (RPSF) method, which constitutes the basis of the Swiss code SIA 262:2013 [24]. In chapter 1, the present report already illustrated the origins, the subsequent developments and the theoretical background of the RPSF method. In 1977, Thürlimann [64] extended the classical RPSF approach for longitudinal shear, bending and torsion to the case of additional transverse (out-of-plane) bending and deduces from this an interaction relationship between the in-plane shear resistance and the acting transverse bending moment. Similarly to Kupfer's idea, the inclined compression field for shear is shifted towards the exterior face of the web such that the transverse bending moment is equilibrated by the vertical component of the concrete compressive stresses. Thürlimann's model allows carrying additional transverse bending moments by rearranging the tensile forces between the stirrups on both sides of the web. This approach which is grounded on the lower bound theorem of the theory of plasticity (static theorem) was later adopted and extended by several authors. In the following the rigid-plastic (RP) interaction models by Thürlimann [64], Menn [65], Stucchi [66] and Gaspar [61] will be developed in particular.

The rigid-plastic (m - V) interaction models ([64], [65], [66], [61]) are a direct application of the RPSF method, thus they have to satisfy the equilibrium and yield conditions of the materials. *Fig. 50a* shows the rigid-plastic stress field that is assumed to develop in the web at failure, where V is the in-plane shear force and m the out-of-plane bending moment. The stress field in the web section (*Fig. 50b-c*) illustrates the principal of shifting the compression field in order to account for transverse bending. The vertical component of the concrete compressive stress resultant per unit length, $F_c = V/(z\cdot\cot\theta)$, is always equilibrated by the stirrup forces at each side of the web, $F_{s,t}$ and $F_{s,c}$ (per unit length). In pure shear conditions (*Fig. 50b*), the stirrup forces are equal, $F_{s,t} = F_{s,c}$, and the resultant F_c is centred in the width of the web. A transverse bending moment m can then be resisted by shifting the resultant F_c towards the bending compression side of the web, *Fig. 50c*. No changes in the stirrup forces are required. The maximum moment m_c that can be

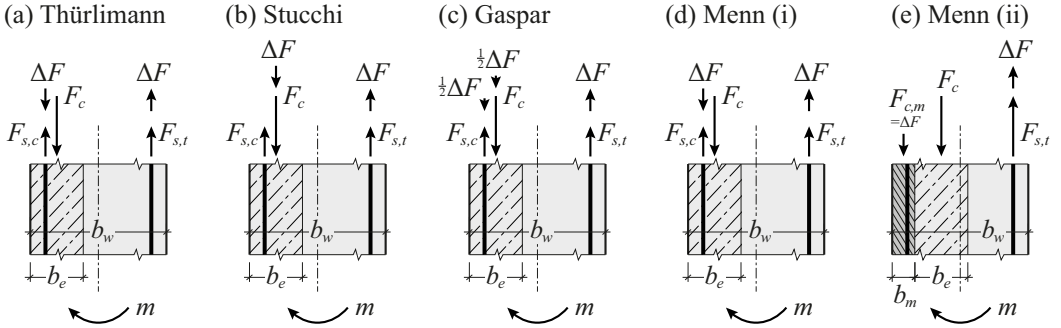

Fig. 51 *Schematic representation of the vertical equilibrium of a web segment subjected to a high transverse bending moment, according to: (a) Thürlimann [64]; (b) Stucchi [66]; (c) Gaspar [61] and (d)-(e) Menn [65].*

equilibrated by the eccentricity of the compression field is limited by the minimum web width b_e required to resist the shear force V. The two equilibrium conditions for vertical forces and transverse moments thereby allow for the establishment of an explicit interaction model for shear and transverse bending (m - V).

It should be noted that in such RP interaction models, the eccentricity relative to the web axis of the inclined compression due to shear generates additional torsion and bending moments in the longitudinal direction of the web (about the vertical axis). They are considered as generalized reaction forces and they potentially lead to a slight modification of the stress distribution in the upper and lower flanges of the beam before being transferred to the transverse supports of the structural element.

For higher levels of transverse bending moments ($m > m_c$) some authors ([64], [65], [66], [61]) propose different modifications to the previous stress field (*Fig. 50c*) in order to equilibrate the supplementary transverse moment $\Delta m = m - m_c$. Thürlimann [64] assumes that the additional moment Δm can be resisted by changes in the stirrup forces, *Fig. 51a*. Stucchi [66] recommends increasing the force in the stirrups on the flexural tension side by ΔF. The equilibrium of forces is maintained by applying an equivalent compression force ΔF on the shear strut, *Fig. 51b*. The tensile force $F_{s,c}$ in stirrups on the bending compression side remains unchanged. In order to account for a more realistic kinematic bending behaviour of the web Gaspar [61] proposes a solution that combines the previous ideas by Thürlimann and Stucchi, *Fig. 51c*. Gaspar's model equilibrates the addition tensile force ΔF, due to Δm, at the same time by an increase of the concrete compression force on the shear strut and a reduction of the stirrup force $F_{s,c}$ on the bending compression side. Menn [65] proposes to distinguish between two different situations: (i) predominant shear and (ii) predominant transverse bending. In the first case, the additional moment Δm is balanced by variations in the stirrup forces, *Fig. 51d*. This procedure is equivalent to Thürlimann's proposal, but it is only applicable as long as the stirrups on the bending compression side are still in tension, $F_{s,c} > 0$. For higher transverse bending moments (situation (ii)), the tensile force $F_{s,c}$ vanishes and is replaced by a compressive force $F_{c,m}$ acting on the outer layer of the flexural compression faces. As a consequence, the resultant of the concrete compressive force due to shear F_c shifts towards the centre of the web width, *Fig. 51e*.

The comparison of the different rigid-plastic interaction models from the literature is shown by means of the shear-transverse bending (m - V) diagram in *Fig. 52*. The overall behaviour of the models is very similar. Stucchi's model is the most conservative, whereas Thürlimann's and Menn's models are more favourable, especially for larger bending moments. Gaspar's model, that is a combination of Thürlimann's and Stucchi's model, is consequently predicting a behaviour mid-way between the previous models.

In general, the effect of the transverse bending moment m on the in-plane shear strength V is significant. For example, in case of a transverse moment of 30% of the pure flexural

strength m_{R0} of the web the models predict a loss of up to 20% of the initial in-plane shear strength V_{R0}.

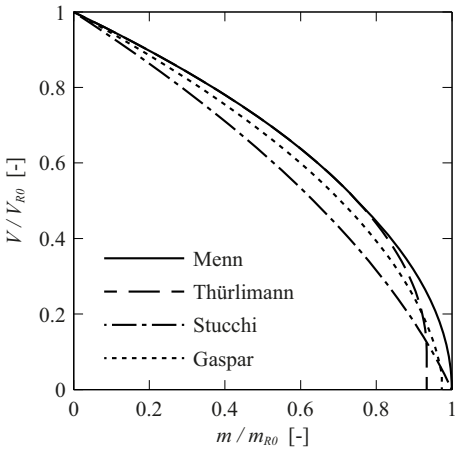

Fig. 52 *Comparison of RP shear - transverse bending interaction models for* $\theta = 30°$, $k_c = 0.55$, $f_{cd} = 20$ *MPa,* $f_{sd} = 435$ *MPa,* $\rho_w = 0.6\%$, $\rho_{w,c}/\rho_{w,t} = 1.0$, $b'/b_w = 0.1$.

A more detailed examination of this phenomenon, presented later in this report, on the basis of a ML-EP panel element will show that RP approaches potentially have a high level of conservatism and that the actual interaction is less pronounced. In the following, a detailed discussion of this issue is presented. First, the RPSF solutions will be presented in sections 2.2.1 - 2.2.3, with a special focus on that of Thürlimann and Menn (out-of-all the lower bound solutions, these models predict the highest combined resistance). A detailed discussion on the main hypotheses leading to the previously mentioned excessively safe (m - V) interaction of RPSF approaches is presented in section 2.2.4. Later, the methodology of the ML-EP approach will be presented and discussed in chapter 2.3. Comparisons between the ML-EP approach and the RPSF approaches are presented in section 2.3.4.

2.2.1 Analysis of webs with rigid-plastic stress-fields

In-plane shear

The present chapter briefly describes the internal forces and the state-of-stress developing in the rigid-plastic stress field of a beam web at failure, when no transverse bending moment is applied. For the analysis it is assumed that the longitudinal reinforcement is sufficient to avoid a bending failure. Thus, failure is governed by shear.

The shear force V acting on the web is carried by an inclined (θ) compression field (*Fig. 50a*), where σ_{cw} is the concrete compressive stress in the direction θ of the strut and τ the nominal tangential stress.

$$\sigma_{cw} = \frac{V}{b_w \cdot z \cdot \sin\theta \cdot \cos\theta} = \frac{\tau}{\sin\theta \cdot \cos\theta} \tag{40}$$

$$\tau = \frac{V}{z \cdot b_w} \tag{41}$$

The shear force per unit length F_c, i.e. the vertical component of resultant of the inclined compressive stresses σ_{cw}, is given by the equation (42). The vertical component σ_v (equation (43)) of the compressive stress σ_{cw} is distributed uniformly over the width of the web, see *Fig. 50b*.

$$F_c = \frac{V}{z \cdot \cot\theta} \tag{42}$$

$$\sigma_v = \frac{F_c}{b_w} = \frac{V}{z \cdot b_w \cdot \cot\theta} = \tau \cdot \tan\theta = \sigma_{cw} \cdot \sin^2\theta \tag{43}$$

The forces in the stirrups are determined along a section in the web that is inclined at an angle θ (see *Fig. 50a*). If the stirrups are vertical, the stirrup force per unit length F_s is determined by equation (44), where F_{sw} is the force per stirrup and s the spacing between stirrups. The stirrup force F_s is in equilibrium with the shear force per unit length F_c (*Fig. 50b*).

$$F_s = \frac{F_{sw}}{s} = \frac{V}{z \cdot \cot\theta} \tag{44}$$

At failure, the shear reinforcement is assumed at yielding, $F_s = F_y$. For design, the yield strength of the shear reinforcement per unit length F_y is defined by the equation (45.a), where $\rho_w = A_{sw}/(b_w \cdot s)$ is the reinforcement ratio of the web. The yield strength of the shear reinforcement on the bending tension side and on the bending compression side is indicated by $F_{y,t}$ and $F_{y,c}$, with the respective reinforcement ratios $\rho_{w,t} = A_{sw,t}/(b_w \cdot s)$ and $\rho_{w,c} = A_{sw,c}/(b_w \cdot s)$.

$$F_y = F_{y,t} + F_{y,c} = \rho_w \cdot b_w \cdot f_s \tag{45.a}$$

$$F_{y,t} = \rho_{w,t} \cdot b_w \cdot f_s \tag{45.b}$$

$$F_{y,c} = \rho_{w,c} \cdot b_w \cdot f_s \tag{45.c}$$

The shear resistance of the concrete $V_{R,c}$ and the shear resistance of the stirrups $V_{R,s}$ are defined according to the SIA262:2013 [24], with the equivalent plastic strength $f_{cp} = \eta_{fc} \cdot f_c$. The shear strength of the reinforced concrete element is thus given by $V_R = \min(V_{R,c}; V_{R,s})$.

$$V_{R,c} = k_c \cdot f_{cp} \cdot b_w \cdot z \cdot \sin\theta \cdot \cos\theta \tag{46}$$

$$V_{R,s} = f_s \cdot \rho_w \cdot b_w \cdot z \cdot \cot\theta \tag{47}$$

The highest shear strength V_{R0} is obtained for $V_{R,c} = V_{R,s}$ and the corresponding inclination of the compression field is designated by θ_0.

$$V_{R0} = f_s \cdot \rho_w \cdot b_w \cdot z \cdot \sqrt{\frac{k_c \cdot f_{cp}}{f_s \cdot \rho_w} - 1} \tag{48}$$

$$\sin^2(\theta_0) = \frac{f_s \cdot \rho_w}{k_c \cdot f_{cp}} \tag{49}$$

Transverse bending

The transverse bending strength m_{R0} of the web cross section is defined according to equations (50), where the shear reinforcement ratio on the bending tension side is defined by $\rho_{w,t} = A_{sw,t}/(b_w \cdot s)$ and b' is the position of the reinforcement in the width of the web, see *Fig. 50b*.

$$m_{R0} = f_s \cdot \rho_{w,t} \cdot b_w \cdot \left(b_w - b' - \frac{f_s \cdot \rho_{w,t} \cdot b_w}{2 \cdot f_{cp}} \right) \tag{50}$$

2.2.2 The RPSF approach for shear and transverse bending by Thürlimann

The work presented by Thürlimann in 1977 [64] was a supplement to the new Recommendation 34 of the SIA162:1976 [73] at the time. The SIA162, as well as the CEB Model Code (1977) [74], had introduced new design rules based on the RPSF method for reinforced concrete beams under longitudinal shear, bending and torsion. Thürlimann proposed to extend the analysis to cases with out-of-plane, i.e. transverse, bending in order to obtain a consistent RP design procedure that is conforming to the new recommendations.

According to the usual approach for beam design, Thürlimann splits the beam into a tension chord, a web and a compression chord. The analysis is then performed on a shear panel representing the web of the reinforced concrete beam failing in shear due to yielding of the shear reinforcement. The results are applicable to beams and box girders if the internal forces due to shear and torsion are known. In his work, Marti [75] extends Thürlimann's model for general cases in order to account for potential failure due to yielding of the longitudinal reinforcement (not developed in this report). In a first approach, Thürlimann studied the effect of the location of the compression field in the width of the web on the transverse bending resistance. Later, he formulated a more general expression allowing for changes in the reinforcement tensions and asymmetrical shear reinforcement layouts. He validates his model by comparing it to the tests performed by Kaufmann and Menn [59].

Transverse bending moment due the eccentricity of the compression field

The state-of-stress in the cross section of the web without transverse bending is shown in *Fig. 53a*. The two stirrup forces are identical, $F_{s,t} = F_{s,c} = F_y/2$, and in equilibrium with the vertical component of the concrete compressive force due to shear, $F_c = V/(z \cdot \cot\theta) = F_y$. The resultant F_c is centred in the web width b_w and the compression field is distributed uniformly over the entire width of the web.

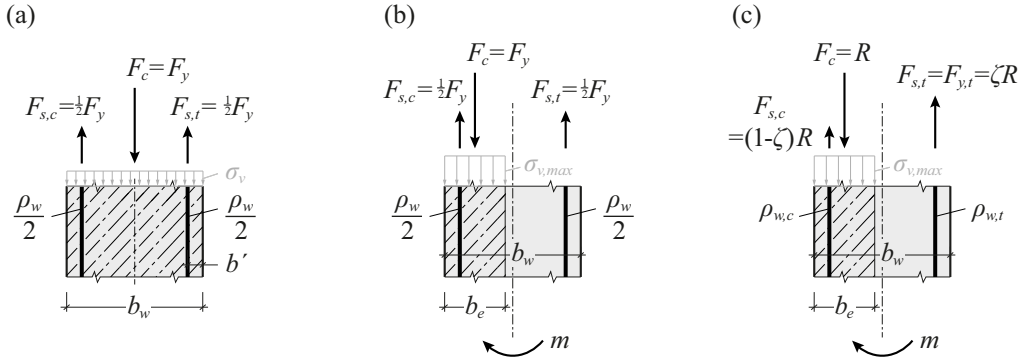

Fig. 53. *Equilibrium of a web segment according to Thürlimann [64]: (a) without a transverse bending moment; (b) with a transverse bending moment; (c) the general case.*

The presence of an out-of-plane bending moment m in the shear wall requires a modification of the initial state-of-stress in order to ensure the equilibrium between external and internal forces. A possible solution is proposed by Thürlimann [64], see *Fig. 53b*. The inclined compression field and thus also its vertical resultant F_c are shifted towards the bending compression side within the web width b_w. The compressive stress distributions for σ_v and σ_{cw}, are approximated by a uniform stress block on the width b_e while the stirrup forces remain unchanged (compared to the state-of-stress for $m = 0$, *Fig. 53a*). The transverse moment that can be equilibrated by this procedure is highest when the width of the compression field is reduced to the minimum width b_e necessary to transfer the shear force while respecting the maximum allowable stress in the concrete. It must be noted that Thürlimann established his model according to the recommendations at that time

(SIA162:1976 [73] and CEB Model Code 1976 [74]) which refer to concrete stresses in terms of nominal tangential stresses τ that should not exceed the value of τ_{max}. The maximum tangential stress τ_{max} recommended by the SIA162:1976 is approximately equivalent to the concrete strength of the compression field $V_{R,c}$ (SIA262:2013 [24]) when assuming an inclination of $\theta = 45°$.

$$\tau_{\max} \cong \frac{V_{R,c,\mathrm{SIA\,262:2013}}(\theta = 45°)}{z \cdot b_w} = \frac{1}{2} \cdot k_c \cdot f_{cp} \tag{51}$$

The width b_e can thus be determined according to *Fig. 53a-b*, where $F_c = b_w \cdot \sigma_v = b_e \cdot \sigma_{v,max}$ and $\sigma_{v,max} = \tau_{max} \cdot \tan(\theta)$ according to equation (43).

$$\frac{b_e}{b_w} = \frac{\sigma_v}{\sigma_{v,\max}} = \frac{\tau}{\tau_{\max}} = \frac{2 \cdot V}{z \cdot b_w \cdot k_c \cdot f_{cp}} \tag{52}$$

The transverse bending moment m per unit length can thus be computed from the state-of-stress shown in *Fig. 53b*. Since both stirrup forces are identical ($F_y/2$), only the vertical resultant F_c is considered in the computation of the moment. With $F_c = F_y$ (equilibrium of vertical forces) and F_y according to equation (45) the transverse bending moment m can then be expressed as a function of the acting shear force V.

$$m = m_c = F_c \cdot \left(\frac{b_w}{2} - \frac{b_e}{2} \right) = \frac{1}{2} \cdot \rho_w \cdot b_w^2 \cdot f_s \cdot \left(1 - \frac{2 \cdot V}{z \cdot b_w \cdot k_c \cdot f_{cp}} \right) \tag{53}$$

General shear-transverse bending interaction model

Although the ($m - V$) relation presented in equation (53) allows to evaluate the effect of a transverse bending moment on the shear strength, Thürlimann [64] points out that it does not cover the general case where the shear reinforcement of the web cross section is unsymmetrical ($\rho_{w,t} \neq \rho_{w,c}$). In addition, Thürlimann suggests that, particularly if m is high, the model should consider the possibility that only the shear reinforcement on the bending tension side reaches its yielding strength, $F_{s,t} = F_{y,t}$, while the stirrups on the bending compression side only carry the remaining shear load, $F_{s,c} \leq F_{y,c}$. In order to account for this, Thürlimann [64] proposes a more general configuration of the internal force distribution that is shown in *Fig. 53c*. Respecting the equilibrium of forces and the plastic strength of material, this stress field fulfils the conditions of the static theorem of the theory of plasticity and can thus be used to determine a lower bound value of the failure load.

If R designates the resultant force of the both stirrup forces and ζ the percentage of the total vertical load carried by the stirrups on the bending tension side, then the internal forces of the general rigid-plastic stress-field can be expressed by the following set of equations.

$$R = F_{y,t} + F_{s,c} \qquad = F_c = \frac{V}{z \cdot \cot\theta} \tag{54}$$

$$F_{s,t} = \zeta \cdot R \qquad = F_{y,t} \tag{55}$$

$$F_{s,c} = (1 - \zeta) \cdot R \qquad \leq F_{y,c} \tag{56}$$

$$\zeta = \frac{F_{y,t}}{R} \tag{57}$$

Thürlimann limits the values for the parameter ζ to a range from ½ to 1 (equation (58)). The lower bound $\zeta = ½$ represents the symmetrical case, where the stirrups on the bending tension and bending compression side carry the same amount of load, $F_{s,t} = F_{s,c} = R/2$.

When $\zeta = 1$, the entire shear load is carried by the reinforcement on the bending tension side, $F_{s,t} = R$ and $F_{s,c} = 0$. This configuration will lead to the highest transverse bending moment. Thürlimann neglects the cases where $\zeta > 1$, the contribution of the compression force in the stirrups, $F_{s,c} < 0$, to the transverse bending moment is considered to be negligible.

$$\frac{1}{2} \le \zeta \le 1 \tag{58}$$

The transverse bending moment m is thus computed according to *Fig. 53c*.

$$m = m_s + m_c = \left(F_{s,t} - F_{s,c}\right) \cdot \left(\frac{b_w}{2} - b'\right) + R \cdot \left(\frac{b_w}{2} - \frac{b_e}{2}\right) \tag{59.a}$$

The moment m can be expressed as a function of ζ and V by substituting $F_{s,t}$ and $F_{s,c}$ according to equations (55)-(56), R according to equation (57) with $F_{y,t}$ from equation (45.b) and b_e by equation (52).

$$m = \frac{\rho_{w,t} \cdot b_w^2 \cdot f_s}{2\zeta} \cdot \left[(2\zeta - 1) \cdot \left(1 - 2\frac{b'}{b_w}\right) + \left(1 - \frac{2 \cdot V}{z \cdot b_w \cdot k_c \cdot f_{cp}}\right) \right] \tag{59.b}$$

The general expression for the (m - V) interaction as proposed by Thürlimann (equation (59.b)), shows two main components in the equilibrium of moments. The second term in the brackets denotes the transverse bending moment generated by the eccentricity of the compression field, m_c. The first term in the brackets is the contribution of the shear reinforcement to the transverse bending moment, m_s. This term shows the beneficial effect of having a difference in the stirrups forces on the bending tension side relative to the bending compression side. The higher the difference ($\zeta > ½$), the higher is the transverse bending moment m_s that can be resisted. This shows that a considerable increase of the transverse bending moment can be achieved by rearranging a symmetric reinforcement layout ($\zeta = ½$ where $\rho_{w,t} = \rho_{w,c}$) into a asymmetrical layout where $\zeta > ½$, or by adding reinforcement on the bending tension side such that $\rho_{w,t} > \rho_{w,c}$.

The (m - V) interaction diagrams resulting from equation (60) are represented in *Fig. 54* (solid lines). The transverse bending moment m and the shear force V are normalized by the shear strength V_{R0} (equation (48)) and the bending strength m_{R0} (equation (50)). The ratio between the reinforcement strength and the equivalent plastic strength of concrete is expressed by $r_f = f_s / \eta_{fc} \cdot f_c$.

$$\frac{m}{m_{R0}} = \frac{\dfrac{b'}{b_w} + \left(1 - 2\dfrac{b'}{b_w}\right) \cdot \zeta - \left(\dfrac{\rho_w \cdot r_f}{k_c} \cdot \sqrt{\dfrac{k_c}{\rho_w \cdot r_f} - 1}\right) \cdot \dfrac{V}{V_{R0}}}{\left(1 - \dfrac{b'}{b_w} - \dfrac{\rho_{w,t} \cdot r_f}{2}\right) \cdot \zeta} \le \frac{\overline{m}}{m_{R0}} \tag{60}$$

For low shear forces, $\tau/\tau_{max} = b_e/b_w \le 2b'/b_w$, Thürlimann limits the transverse moment to the bending strength $\overline{m} = \rho_{w,t} \cdot b_w^2 \cdot f_s \cdot (1\text{-}2b'/b_w)$. The maximum shear force that can be applied is limited to $V_{max} = \tau_{max} \cdot z \cdot b_w$, according to Thürlimann [64].

Comments on Thürlimann's (m - V) interaction diagrams

The (m - V) interaction formula from equation (59.b), resp. equation (60), is the original formulation presented by Thürlimann in 1977. This formulation is established on the basis of a concrete shear strength expression (τ_{max} according to SIA162:1976, equation (51)) that is different from the recent code recommendations ($V_{R,c}$ according to SIA262:2013 [24], equation (46)). Consequently, the concrete shear strength when defined by $V_{R,c} = \tau_{max} \cdot z \cdot b_w$

is independent of the actual inclination of the compression field θ and generally leads to an overestimation of the shear strength according to SIA262:2013 (see *Fig. 54*, curves higher than V/V_{R0} = 1). The original formulation by Thürlimann can be adapted to today's code recommendations by replacing the expression for the required web width b_e from equations (52) by equation (61), where b_e is derived from $V_{R,c}$ according to SIA262:2013. The adapted (m - V) interaction is shown in *Fig. 54* (dashed curves). In the range of small transverse bending moments, the (m - V) interaction predicted according to the adapted formulation is similar to Thürlimann's original formulation. However, for high transverse bending moments this formulation leads to a significant reduction of the shear strength.

In general, with both formulations (original and adapted) is not possible to reach the plastic bending strength m_{R0} when no shear force is applied. This shows that the underlying RPSF (*Fig. 53*) is not appropriate for high transverse bending moments. Menn, chapter 2.2.3, has taken into account this issue when developing his interaction model.

Practical application

Thürlimann [64] also proposes design and assessment procedures based on the previous interaction model.

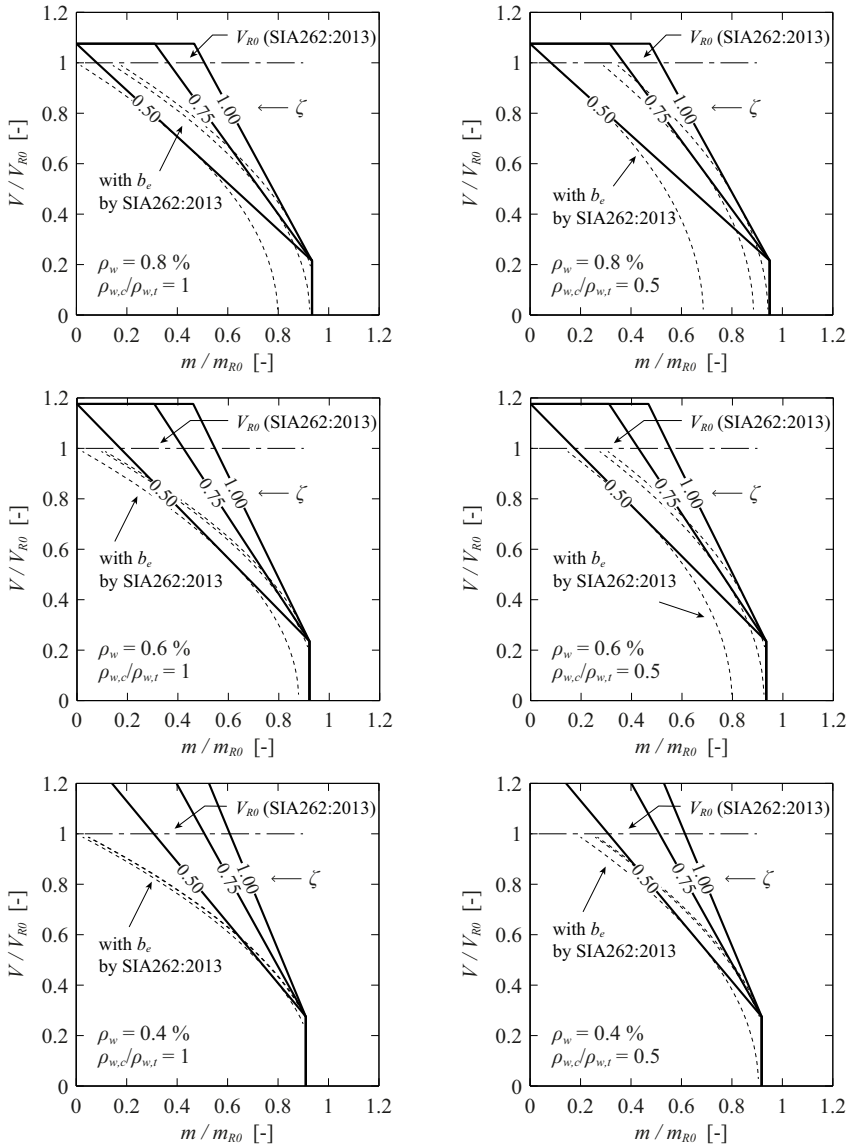

Fig. 54 *Interaction diagrams by Thürlimann [64] (solid lines) and adaptation to the SIA262:2013 [24] (dashed lines), for f_{sd} = 435MPa, f_{cd} = 20MPa, k_c = 0.55 and b'/b_w = 0.1.*

The design shear force V_d and the design transverse bending m_d acting on the web of the box-girder are determined by an elastic analysis of the structure. In a first step, a symmetrical shear reinforcement is designed to carry V_d ($F_{y,t} = F_{y,c} = 0.5 \cdot V_d/z \cdot \cot\theta$). The design of the longitudinal reinforcement has to account for the horizontal component of the shear force V_d. The inclination of the compression field is selected according to the general web design method (SIA162:1976 [73] $30° \leq \theta \leq 60°$; SIA262:2013 [24] $30°(25°) \leq \theta \leq 45°$). The width of the web b_w should be selected larger than the minimum width b_e, especially if the transverse moment m_d is important. The transverse bending strength $m/m_{Rd,0}$ can then be computed from the interaction diagram (*Fig. 54*) along the curve $\zeta = ½$. If the bending strength is insufficient, Thürlimann proposes to redesign the shear reinforcement for a one-sided reinforcement layout ($\zeta = 1$ and $F_{y,t} = V_d/z \cdot \cot\theta$). The stirrups on the bending tension side carry the entire shear load and the required amount of shear reinforcement on the tension side $\rho_{w,t}$ is doubled compared to the previous situation. If the bending strength with $\zeta = 1$ is still insufficient, the cross section of the web has to be increased. If the required bending strength lays between the two previous values (for $\zeta = ½$ and $\zeta = 1$), the reinforcement on the tension side only needs to be partially increased (compared to $\rho_{w,t}$ for $\zeta = ½$). In the next iterations the parameter ζ is progressively increased (from $\zeta > ½$), the tension $F_{s,t}$ (resp. $\rho_{w,t}$) increases while $F_{s,c}$ (resp. $\rho_{w,c}$) decreases, until the computed bending strength corresponds to the design moment m_d.

For the assessment of existing structures, the web cross section, the shear reinforcement and the loads are known. First the total reinforcement tensions R, equation (54), have to be determined from V_d and θ. Next, it is assumed that the reinforcement on the tension side is yielding, $F_{s,t} = F_{y,t} = \rho_{w,t} \cdot b_w \cdot f_{sd}$, and the parameter ζ can be computed form equation (57). The transverse bending strength of the cross section can thus be read from the interaction diagram, respectively computed from equation (59.b).

2.2.3 The RPSF approach for shear and transverse bending by Menn

In [65], Menn clarifies again the fact that the superposition of the required reinforcement to resist each load (shear and transverse bending) separately is not consistent with the actual behaviour of the web at failure. The required reinforcement should be determined by a model that accounts for the effect of a combined load situation. This statement is confirmed by tests performed by Kaufmann and Menn [59] that show a modification of the shear transfer action under the effect of the transverse bending moment. It was observed that the resultant of the compressive force due to shear shifts towards the flexural compression side of the web, which, in the context of in-plane truss models and RPSFs, can be regarded as an out-of-plane inclination of the diagonal compression strut. Kaufmann and Menn's tests [59] showed as well that the stresses in both stirrups are not identical under the action of the transverse moment; the bending tension side usually had higher tension stresses than the compression side of the shear reinforcement. For the beams that failed in shear with yielding of the shear reinforcement, it was observed that the stirrups on the bending tension side started yielding first, but at failure the stirrups on both sides had reached the yield strength. In beams that failed due to concrete crushing, the stirrups on the bending compression side did not yield. Based on these observations, Menn [65] proposed a rigid-plastic stress field model for the design of reinforced concrete webs under shear and transverse bending. The interaction model takes advantage of the excess capacity of the web (if $b_e < b_w$) and resists additional moments by varying the stirrup forces (*Fig. 55b*) or, when the transverse moment is high, by an increase of the total concrete compressive force in the web (*Fig. 55c*).

The internal state-of-stress for the different equilibrium conditions is shown in *Fig. 55*. The concrete compressive stress distribution is modelled as a uniform stress block, the concrete tensile strength is neglected and the stirrups are assumed to be vertical. Contrary to the hypothesis made by Thürlimann, see chapter 2.2.2, Menn assumes that the inclination angle of the compression strut θ is known and that the forces in the stirrups on the tension and compression side adjust accordingly.

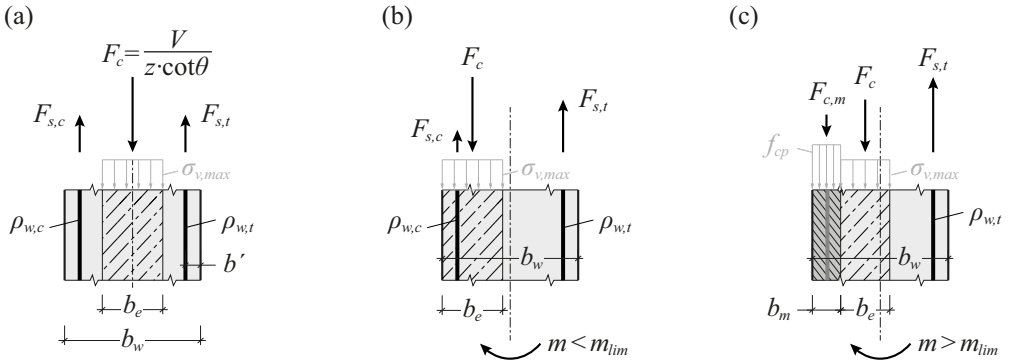

Fig. 55 *Equilibrium of a web segment according to Menn [65]: (a) in pure shear; (b) with a small transverse bending moment; (c) with a large transverse bending moment.*

The minimum width b_e required to resist the shear force V is computed according to equation (61). Note that this formulation, taken from the second edition of Menn [65] dating from 1990, originally computed the shear resistance of concrete $V_{R,c}$ using the reduced concrete compressive strength $f_{c,red}$ (SIA162:1989 [76]). In equation (61) $f_{c,red}$ is replaced by $k_c{\cdot}f_{cp}$, consistently to the notation of the SIA262:2013 [24].

$$\frac{b_e}{b_w} = \frac{V}{z \cdot b_w \cdot k_c \cdot f_{cp} \cdot \sin\theta \cdot \cos\theta} \tag{61}$$

Based on the previous considerations and the equilibrium conditions presented in *Fig. 55b-c*, Menn derives the forces in the shear reinforcement, on the bending compression and on the bending tension side, $F_{s,c}$ and $F_{s,t}$, that equilibrate the applied set of internal loads (V, m). As previously mentioned, Menn [65] distinguishes between two cases: (i) predominant shear and (ii) predominant transverse bending.

Case (i): Predominant shear

The equilibrium of a web segment subjected to a shear load V and a small transverse bending moment $m \leq m_{lim}$ is shown in *Fig. 55b*. The resultant of the concrete compression force $F_c = V/z{\cdot}\cot\theta$, is shifted to the bending compression side. Additionally the stirrup forces on the tension side $F_{s,t}$ are increased (relative to *Fig. 55a* $m = 0$) and the tension forces in the stirrups on the compression side $F_{s,c}$ are reduced. The equilibrium conditions of vertical forces and transverse moments are then formulated as follows:

$$\frac{V}{z \cdot \cot\theta} = F_{s,t} + F_{s,c} \tag{62}$$

$$m = F_{s,t} \cdot (b_w - 2b') - \frac{V}{z \cdot \cot\theta} \cdot \left(\frac{b_e}{2} - b'\right) \tag{63}$$

Equation (62) and (63) allow computing the stirrup forces as a function of V and m:

$$F_{s,t} = \frac{V}{z \cdot \cot\theta \cdot (b_w - 2b')} \cdot \left(\frac{b_e}{2} - b'\right) + \frac{m}{(b_w - 2b')} \tag{64}$$

$$F_{s,c} = \frac{V}{z \cdot \cot\theta \cdot (b_w - 2b')} \cdot \left(b_w - b' - \frac{b_e}{2}\right) - \frac{m}{(b_w - 2b')} \geq 0 \tag{65}$$

As described in Menn's model [65], the present state of equilibrium is only applicable if a net tensile force remains in the stirrups on the compression side, $F_{s,c} \geq 0$. Thus in case of high transverse bending moments, or small shear loads, the internal forces have to be

computed according to the equilibrium conditions for predominant transverse bending (case(ii)).

Case (ii): Predominant transverse bending

In case of predominant transverse bending, *Fig. 55c*, the forces in the reinforcement on the compression side are assumed to be equal to zero, $F_{s,c} = 0$. In order to ensure the equilibrium of forces an additional compressive force $F_{c,m}$ is applied to the web cross section. $F_{c,m}$ represents a pure bending compression force and is acting in the vertical direction at the outermost position of the web width. As a consequence, the resultant of the inclined compression field due to shear, F_c, is shifted towards the centre of the web cross section. The width b_m required to resist the compressive force $F_{c,m}$, is computed according to equation (66). Note that in this case no concrete strength reduction factor k_c intervenes (respectively k_c = 1.0).

$$b_m = \frac{F_{c,m}}{f_{cp}} \tag{66}$$

The equilibrium conditions can thus be established:

$$\frac{V}{z \cdot \cot\theta} = F_{s,t} - F_{c,m} \tag{67}$$

$$m = F_{s,t} \cdot \left(b_w - b' - \frac{b_m}{2} \right) - \frac{V}{z \cdot \cot\theta} \cdot \left(\frac{b_e}{2} + \frac{b_m}{2} \right) \tag{68}$$

The unknown compressive force $F_{c,m}$ and the tension force in the shear reinforcement $F_{s,t}$ are then given by:

$$F_{s,t} = \frac{1}{\left(b_w - b' - b_m/2 \right)} \cdot \left[\frac{V}{z \cdot \cot\theta} \cdot \left(\frac{b_e + b_m}{2} \right) + m \right] \tag{69}$$

$$F_{c,m} = \frac{1}{\left(b_w - b' - b_m/2 \right)} \cdot \left[\frac{V}{z \cdot \cot\theta} \cdot \left(\frac{b_e + b_m}{2} \right) + m \right] - \frac{V}{z \cdot \cot\theta} \tag{70}$$

Explicit (*m* - *V*) expression and corresponding interaction diagrams

For a given amount of shear reinforcement ($\rho_{w,t}$, $\rho_{w,c}$) and a given inclination of the compression field θ, the relation between V and m can be expressed explicitly and represented in an interaction diagram (*Fig. 56*). In order to establish the explicit equation $m = f(V)$, the tension forces in the stirrups, $F_{s,t}$ and $F_{s,c}$, must be selected. The highest transverse moment can be resisted when the reinforcement on the tension side is yielding, $F_{s,t} = F_{y,t} = \rho_{w,t} \cdot b_w \cdot f_s$. For the case (i) of predominant shear load, m can be derived from equation (63) with $F_{s,t} = F_{y,t}$ and b_e according to equation (61). For the case (ii) where the transverse bending force is important, the (m - V) interaction is derived from equation (68) with $F_{s,t} = F_{y,t}$, b_e from equation (61), b_m from equation (66), where $F_{c,m}$ is obtained from equation (67). The explicit (m - V) interaction formulas for both cases are shown hereafter.

Case (i) : predominant shear ($m \le m_{lim}$)

$$m = \rho_{w,t} \cdot b_w \cdot f_s \cdot \left(b_w - 2b'\right) - \frac{1}{2} \cdot \frac{V}{z \cot\theta} \cdot \left(\frac{V}{z \cdot k_c \cdot f_{cp} \cdot \sin\theta \cdot \cos\theta} - 2b' \right) \quad \text{if } V \geq V_{lim} \tag{71}$$

Case (ii) : predominant transverse bending ($m \geq m_{lim}$)

$$m = \rho_{w,t} \cdot b_w \cdot f_s \cdot \left(b_w - b' - \frac{\rho_{w,t} \cdot b_w \cdot f_s}{2 f_{cp}} \right) - \frac{1}{2} \cdot \left(\frac{V}{z \cdot \cot\theta} \right)^2 \cdot \left(\frac{1}{k_c \cdot f_{cp} \cdot \sin^2\theta} - \frac{1}{f_{cp}} \right) \quad \text{if } V \leq V_{lim} \tag{72}$$

The (m - V) interaction for case (i), that is derived from the state-of-equilibrium for predominant shear, is only applicable if the stirrups on the compression side are in tension, $F_{s,c} \geq 0$. This condition permits establishing the shear force V_{lim}, resp. the transverse bending moment m_{lim}, defining the limit state between the two cases. They are computed from the equilibrium equations (62) and (63) when $F_{s,c} = 0$ and $F_{s,t} = F_{y,t}$.

$$V_{lim} = \rho_{w,t} \cdot b_w \cdot f_s \cdot z \cdot \cot\theta \tag{73}$$

$$m_{lim} = \rho_{w,t} \cdot b_w \cdot f_s \cdot \left(b_w - b' - \frac{1}{2} \frac{\rho_{w,t} \cdot b_w \cdot f_s}{k_c \cdot f_{cp} \cdot \sin^2\theta} \right) \tag{74}$$

Design procedure

The amount of shear reinforcement, $\rho_{w,t}$ and $\rho_{w,c}$, necessary to resist a given design load (m_d, V_d) can be determined, either using the previous expressions for $F_{s,t}$ and $F_{s,c}$, or the pre-calculated (m - V) interaction diagrams.

If the shear reinforcement is computed based on the stirrup tension forces, $F_{s,t}$ and $F_{s,c}$ are first computed for the case of predominant shear (case (i)). If the stirrups on the bending compression side are not in tension, $F_{s,c} < 0$, the equations for predominant transverse bending (case (ii)) must be used instead. The latter require some iterations in order to determine the necessary width b_m for the bending compressive force $F_{c,m}$. The necessary amount of shear reinforcement is eventually computed by the known relations $\rho_{w,t} = F_{s,t}/(b_w \cdot f_{sd})$ and $\rho_{w,c} = F_{s,c}/(b_w \cdot f_{sd})$.

Alternatively, (m - V) interaction diagrams that have been established for multiple reinforcement ratios can be used. The required amount of shear reinforcement is read in the interaction diagram at the point defined by the design load (m_d, V_d). Menn suggests using linear interpolation between curves from one diagram as well as between different interaction diagrams.

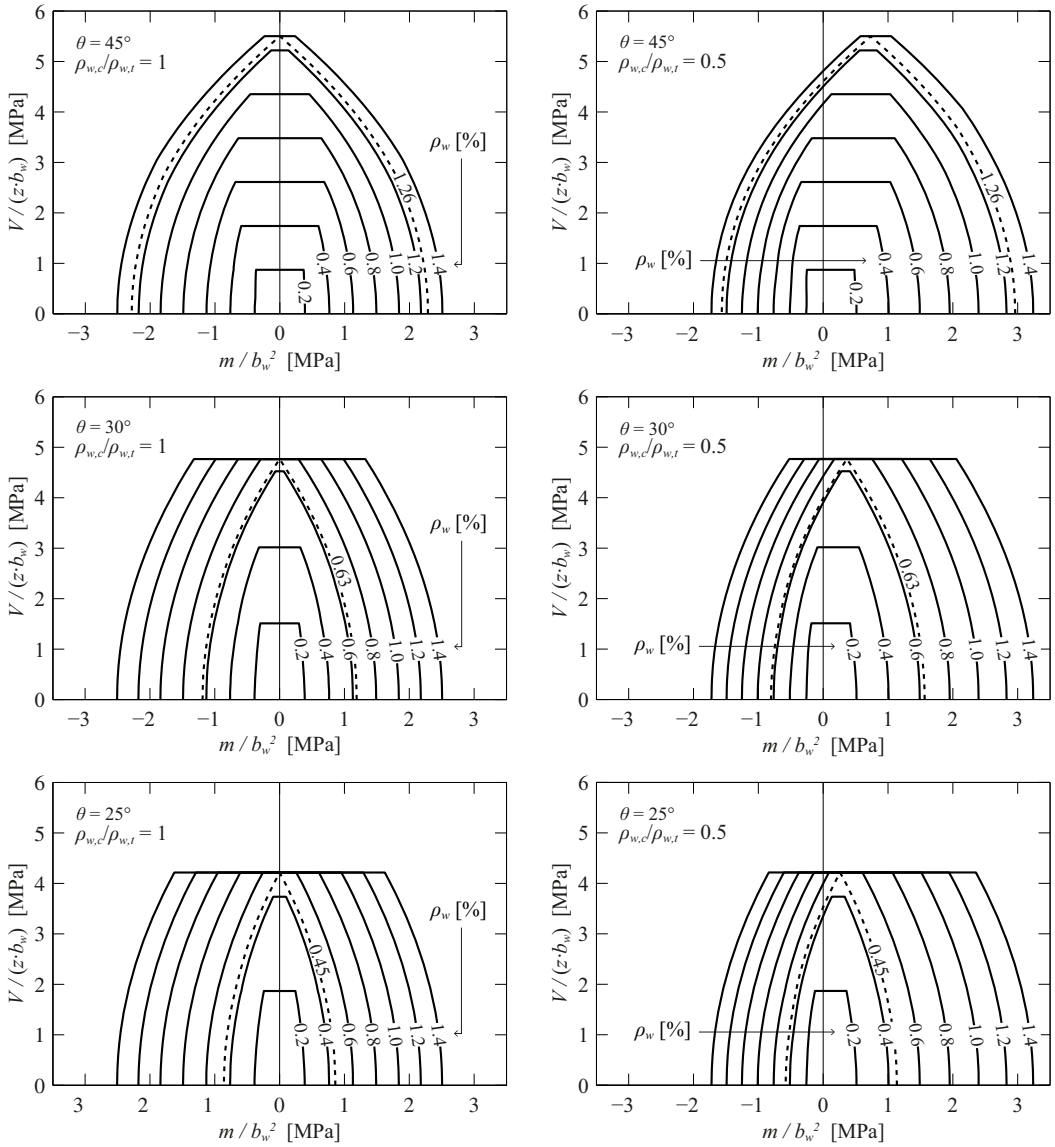

Fig. 56 *RP interaction diagrams by Menn [65], for f_{sd} = 435 MPa, $f_{cd} = \eta_{fc} \cdot f_{ck}/\gamma_c$ = 20 MPa, k_c = 0.55 and b'/b_w = 0.1.*

2.2.4 Comments on the RP interaction models

All the models proposed in the literature are RP equilibrium solutions that tailor the stress-field distribution in the transverse direction in order to account for the out-of-plane bending moment. They are ground on the same basic principle that consists in arranging the compression field on a minimum web width and then shifting it to the bending compression side. Differences in the models are observed when regarding the forces in the stirrups and for high levels of transverse bending. The investigations performed on the basis of the RP models by Thürlimann and Menn show that the RPSF approach is an elegant method to illustrate the shear transfer action under transverse bending and to identify the key factors in the assessment of the maximum combined shear-transverse bending resistance: the reserve capacity of the web width ($b_w > b_e$) and the potential difference between the forces in the stirrups on the bending compression and the bending tension side ($\Delta F = F_{s,t} - F_{s,c} \geq 0$, resp. $\rho_{w,t} \geq \rho_{w,c}$). Another advantage of the RP interaction models is that they can be easily adapted for any specific case (shear reinforcement and location, web geometry) and their practical application can then be implemented by means of explicit (m - V) interaction formulas or diagrams.

However, the previously presented RP interaction models predict a very strong interaction between in-plane shear and transverse bending leading to a substantial loss in shear strength (*Fig. 52*). Particularly in the range of small transverse moments the effect on the in-plane shear strength is surprisingly high. For some models, a bending moment of 30% of m_{R0} (pure bending resistance) leads to a loss of up to 20% of the initial shear strength. While this safe estimate of the shear strength could be acceptable for the design of new structures, it might be too penalizing when assessing the shear strength of existing structures and consequently leading to costly and probably unnecessary strengthening.

For this reason, it should be kept in mind that the RP interaction models by Menn [65] and Thürlimann [64], as any other model based on the RPSF approach, make a number of hypotheses that will influence the shear strength of the web. The most arguable assumptions in the context of transverse bending are made regarding the inclination of the compression field θ and the concrete strength reduction factor k_c. First, the inclination θ and the factor k_c are assumed to be constant over the width of the web, for simplicity reasons and by simple extrapolation from the classical stress field approach. Second, the values for θ and k_c are chosen according to recommendations for reinforced concrete members subjected to in-plane shear only. However, the previous chapters have shown that the equilibrium conditions and the state-of-stress in the concrete in the transverse direction are subject to significant modifications in order to account for the transverse bending moment. This observations, and the fact that the proposed RPSF models predict an unexpectedly strong (m - V) interaction, leads to the conclusion that the classical assumptions for θ and k_c are too penalizing in the context of in-plane shear and transverse bending, in particular for the assessment of existing structures. An improvement of the web behaviour could be obtained if the factors θ and k_c account for the mostly positive effect of the transverse bending moment, as for example the effect of the bending compression (vertical) on the inclination of the compression field θ ($\theta \uparrow$) and the concrete strength reduction factor k_c for cracking ($k_c \uparrow$). However, the questions on how to correctly assess the superposition of the bending compression and the inclined shear field and to what extent the values of k_c and θ should be adapted remain. Some effort in this direction has been done by Menn [65] (additional compression zone when m is high) and Stucchi [66] (bending compression partially added to vertical component of the shear force) but the effect on the overall resistance was not significant.

In the following, a refined analysis of the (m - V) interaction is presented using a multi-layered elastic-plastic (ML-EP) approach (chapter 2.3) that is based on the EPSF method presented earlier in this report. The proposed multi-layered approach assumes kinematic compatibility between the reinforcement and the concrete in the transverse direction of the web (Bernoulli hypothesis) and thus evaluates the inclination of the compression field θ and the concrete strength reduction factor k_c with respect to the prevailing state-of-strain (chapter 2.3.1). The ML-EP approach was then implemented into a panel element (chapter 2.3.2) in order to investigate the in-plane shear transverse bending interaction that develops in beam webs. The analyses show that the inclination of the compression field θ and the concrete strength reduction k_c vary significantly over the width of the web. Furthermore, their values and their variation over the web width are strongly dependent on the intensity of the transverse bending moment acting on the cross section. A detailed analysis of the internal state-of-stress and a detailed comparison to the RP interaction models can be found in chapter 2.3.3 to 2.3.4. The most valuable observation made with the ML-EP panel element is that the factors k_c and θ and the compression field (stress profile on b_w) are barely effected by small transverse moments leading thus to a weaker (m - V) interaction and significantly higher in-plane shear strength than predicted by the RP interaction models.

2.3 Multi-layered panel approach based on the elastic-plastic stress field method

The elastic-plastic stress field method (EPSF) that is presented in chapter 1.1 has proven to be a powerful tool for the assessment and design of reinforced concrete members subjected to a plane stress state. A major asset of the EPSF method is that it simultaneously respects the static and kinematic conditions of the theory of plasticity which leads to exact solutions. The resulting stress fields (exact solutions) account for kinematic compatibility between reinforcement and concrete and the associated state-of-strain is then used to assess the concrete and reinforcement stresses based on elastic-plastic material laws.

The EPSF method has been chosen to investigate the effect of transverse bending on the in-plane shear strength because it provides detailed information about the internal state-of-stress at failure. It has been seen from previous RP interaction models that the assumptions on the concrete strength reduction factor η_ε (k_c) and the inclination of the compression field θ might play a major role in the assessment of the actual shear strength under transverse bending. The EPSF method permits computing these parameters based on the actual state-of-strain associated to the prevailing state-of-stress and thus leads to a potentially more accurate evaluation of the shear-transverse bending interaction.

In order to apply the EPSF method to members subjected to out-of-plane loads, a multi-layered approach has been developed. The member thickness is divided into a finite number of layers. Each layer is in a plane state-of-stress which is defined by an individual EPSF. In contrast to the RP interaction models, the multi-layered approach allows representing a variable stress distribution (versus a uniform stress block) over the width of the element, as well as variable inclinations and concrete strength reduction factors.

The proposed multi-layered elastic-plastic stress field (ML-EPSF) is presented in detail in chapter 2.3.1. First, the ML-EPSF method has been applied to a panel element in order to investigate shear-transverse bending interaction based on a sectional analysis and to derive ($m - V$) interaction diagrams (chapter 2.3.2) that are comparable to the RP interaction models. Later, a finite element (FE) program was developed which extends the application of the ML-EPSF approach to the analysis of entire reinforced concrete members (chapter 2.5).

2.3.1 Formulation of a general multi-layered elastic-plastic stress field approach for in-plane loading and out-of-plane bending

The proposed ML-EPSF is an extension of the EPSF method developed by Fernández Ruiz and Muttoni [12] and therefore relies on the same principles and benefits from the same advantages. The approach allows considering compatibility conditions for determining the stress field in a structure. As a consequence, at failure the lower bound theorem and the upper bound theorem of the theory of plasticity are respected. The resulting stress field is thus in equilibrium with the applied loads, the yield criteria of the materials are respected and the failure mechanism is compatible with the boundary conditions. Since both theorems are fulfilled by such stress fields they can be regarded as exact solutions according to the theory of plasticity.

The ML-EPSF, as the EPSF, is a displacement based procedure where stresses are derived for a given state-of-strain by means of material laws. In the ML-EPSF method the reinforced concrete element is divided over its width into a finite number (n) of concrete layers which each behave according to the EPSF method, *Fig. 57a*. Additional layers are introduced for steel at the location of the reinforcement in the width of the element. The deformation of each layer is defined by a separate strain field ($\varepsilon_{x,i}$, $\varepsilon_{y,i}$, $\gamma_{xy,i}$), *Fig. 57e*. Thus, the effect of out-of-plane bending is accounted for by varying the deformation of every layer with respect to the Bernoulli-Navier hypothesis of plane sections, *Fig. 57d* ($\varepsilon_i = \varepsilon_0 + \chi \cdot z_i$, where χ is the curvature associated to the transverse bending moment). In the concrete layers the principal strains ($\varepsilon_{1,i}$, $\varepsilon_{2,i}$) and their orientation (θ_i) are determined using Mohr's

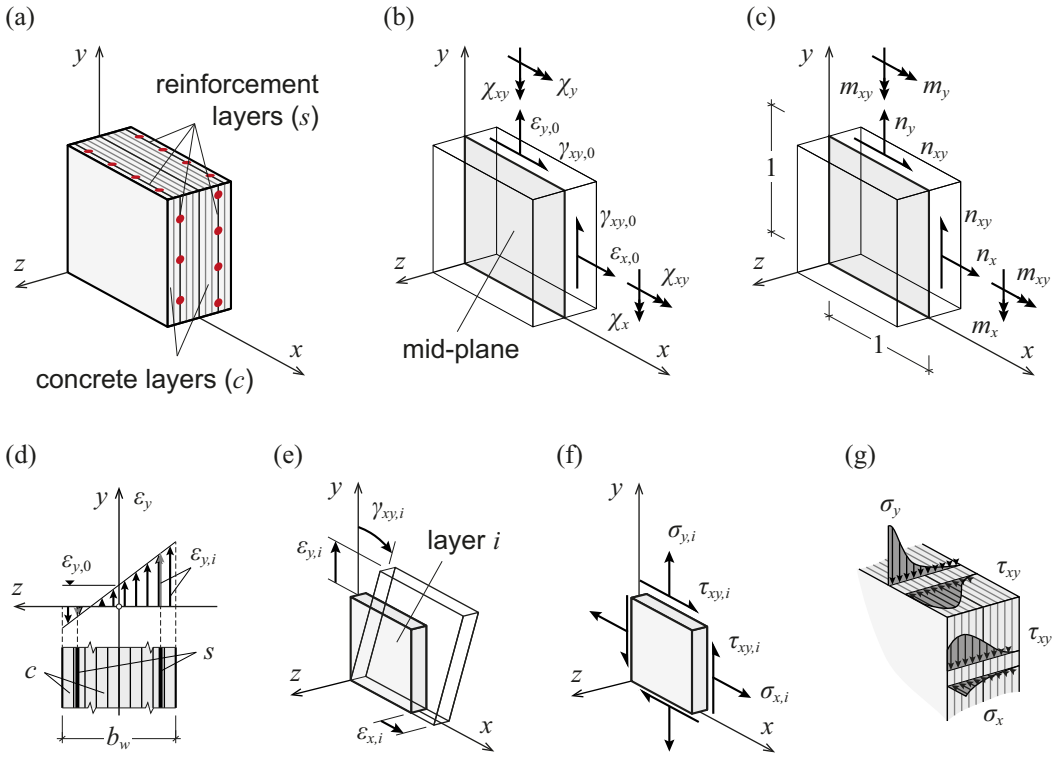

Fig. 57 *ML-EPSF model: (a) concrete and reinforcement layers; (b) deformations at mid-plane; (c) stress resultants; (d) strain profile in a cross section; (e) state-of-strain of each layer; (f) plane state-of-stress in each layer and (g) example of stress profile across the element thickness.*

circle. The concrete principal stresses are then computed from the principal strains assuming that the principal strain directions coincide with the principal stress directions. The applied material laws are the same as in the EPSF method and are presented in detail in chapter 1.1.1. The stress-strain relationship for both, concrete and steel, is assumed to be elastic-perfectly plastic and the concrete tensile strength is neglected (*Fig. 3*). The plastic concrete strength f_{cp} (equation (1)) is corrected by the concrete strength reduction factor η_ε that accounts for cracking due to transverse strain. The reduction factor $\eta_{\varepsilon,i}$ is computed individually for each layer according to the formula proposed by Vecchio and Collins [22] (equation (3) and (4)). The resulting stresses for the concrete and reinforcement layers (*Fig. 57f-g*) are then integrated over the element width to obtain the stress resultants/internal forces, *Fig. 57c*.

The general formulations that are used to derive the state-of-strain and the state-of-stress in the concrete and reinforcement layers, as well as the internal forces resulting from an imposed set of in-plane and out-of-plane deformations are presented hereafter.

The kinematics of the ML-EPSF are show in *Fig. 57b*, where ($\varepsilon_{x,0}$, $\varepsilon_{y,0}$, $\gamma_{xy,0}$) are the in-plane strains at the mid-plane of the element and (χ_x, χ_y, χ_{xy}) the out-of-plane curvatures. The state-of-strain in a plane located at a distance z from the mid-plane is then computed assuming the Bernoulli-Navier hypothesis of plane sections, *Fig. 57d*:

$$\varepsilon_x = \varepsilon_{x,0} - z \cdot \chi_x\,, \qquad \varepsilon_y = \varepsilon_{y,0} - z \cdot \chi_y\,, \qquad \gamma_{xy} = \gamma_{xy,0} - z \cdot \chi_{xy} \tag{75}$$

Concrete layers

The element width is divided into n concrete layers of equal width (b_w/n). The location of the i-th layer relative to the mid-plane is indicated by z_i (centre of the layer). The state-of-strain in each concrete layer ($\varepsilon_{x,i}$, $\varepsilon_{y,i}$, $\gamma_{xy,i}$) is then obtained from equation (75) when $z = z_i$. The associated principal strains $\varepsilon_{1,i}$ and $\varepsilon_{2,i}$ (with $\varepsilon_{1,i} \geq \varepsilon_{2,i}$) are computed using Mohr's circle of

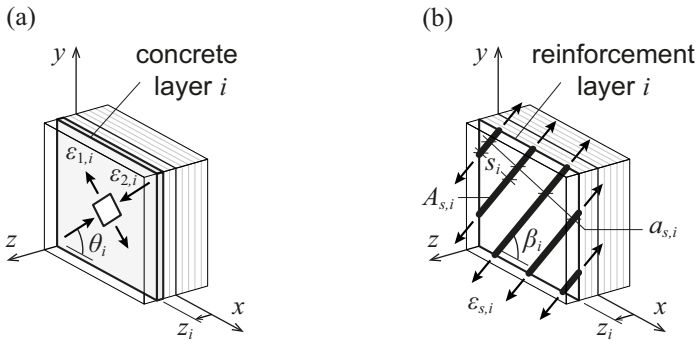

Fig. 58 *ML-EPSF layer strains: (a) principal strains a concrete layer; (b) axial strains in reinforcement layer.*

strains. The angle θ_i indicates the inclination of the principal compressive strain $\varepsilon_{2,i}$ relative to the x-axis, see *Fig. 58a*.

$$\tan\theta_i = \frac{\varepsilon_{y,i} - \varepsilon_{x,i} - \sqrt{\left(\varepsilon_{x,i} - \varepsilon_{y,i}\right)^2 + \gamma_{xy,i}^2}}{\gamma_{xy,i}} \tag{76}$$

$$\varepsilon_{1,i} = \varepsilon_{x,i} - \frac{1}{2}\cdot\gamma_{xy,i}\cdot\tan\theta_i, \qquad \varepsilon_{2,i} = \varepsilon_{y,i} + \frac{1}{2}\cdot\gamma_{xy,i}\cdot\tan\theta_i \tag{77}$$

Since it is assumed that the direction of principal stresses is parallel to with the direction of principal strains (Fernández Ruiz and Muttoni [12]), the concrete principal stresses $\sigma_{1,i}$ and $\sigma_{2,i}$ (with $\sigma_{1,i} \geq \sigma_{2,i}$) can be computed directly from the principal strains by means of the elastic-plastic material law presented in chapter 1.1.1. The maximum compressive stress in each layer is limited by its effective strength $f_{c,eff,i} = \eta_{\varepsilon,i} \cdot f_{cp}$.

$$\sigma_{1,i} = E_c \cdot \varepsilon_{1,i} \qquad \text{with } -f_{cp} \leq \sigma_{1,i} \leq 0 \tag{78.a}$$

$$\sigma_{2,i} = E_c \cdot \varepsilon_{2,i} \qquad \text{with } -\eta_{\varepsilon,i}\cdot f_{cp} \leq \sigma_{2,i} \leq 0 \tag{78.b}$$

The concrete strength reduction factor $\eta_{\varepsilon,i}$ accounting for the effect of transverse strain on the concrete compressive strength is computed according to Vecchio and Collins [22] (alternative approaches could also be used).

$$\eta_{\varepsilon,i} = \frac{1}{0.8 + 170\cdot\varepsilon_{1,i}} \leq 1.0 \tag{79}$$

It can be noted that in theory two reduction factors could be computed, one for each principal direction, $\eta_{\varepsilon 1,i} = \mathrm{f}(\varepsilon_{2,i})$ and $\eta_{\varepsilon 2,i} = \mathrm{f}(\varepsilon_{1,i})$, which would define the respective effective compressive strength $f_{c1,eff,i} = \eta_{\varepsilon 1,i} \cdot f_{cp}$ and $f_{c2,eff,i} = \eta_{\varepsilon 2,i} \cdot f_{cp}$. In fact, $f_{c1,eff,i} < f_{cp}$ will never be governing for $\sigma_{1,i}$ because this situation would only occur if both strains, $\varepsilon_{1,i}$ and $\varepsilon_{2,i}$, are positive ($\varepsilon_{1,i} \geq \varepsilon_{2,i} > 0$), but in this case, $\sigma_{1,i} = 0$ anyway (tensile strength neglected). If $\varepsilon_{1,i} \leq 0$, the second strain $\varepsilon_{2,i}$ is negative too which leads to $\eta_{\varepsilon 1,i} = 1.0$ and $f_{c1,eff,i} = f_{cp}$. This is the reason why equation (79) only computes the reduction factor associated to the second principal direction, $\eta_{\varepsilon,i} = \eta_{\varepsilon 2,i}$, and why in equation (78.a) the maximum compressive stress for the first principal direction is limited to the unreduced concrete plastic strength ($-f_{cp} \leq \sigma_{1,i}$).

The concrete principal stresses are rotated back into the global x-y coordinate system, where $\sigma_{cx,i}$ and $\sigma_{cy,i}$ are the concrete compressive stresses and $\tau_{cxy,i}$ are the concrete tangential stresses in each layer according to *Fig. 57f*.

$$\sigma_{cx,i} = \sigma_{1,i} \cdot \sin^2 \theta_i + \sigma_{2,i} \cdot \cos^2 \theta_i \tag{80.a}$$

$$\sigma_{cy,i} = \sigma_{1,i} \cdot \cos^2 \theta_i + \sigma_{2,i} \cdot \sin^2 \theta_i \tag{80.b}$$

$$\tau_{cxy,i} = \left(\sigma_{2,i} - \sigma_{1,i}\right) \cdot \sin \theta_i \cdot \cos \theta_i \tag{80.c}$$

Reinforcement layers

The reinforcement layers are placed at the actual position of the reinforcement in the width of the element (independently of position of the concrete layers). The state-of-strain ($\varepsilon_{x,i}$, $\varepsilon_{y,i}$, $\gamma_{xy,i}$) in the i-th reinforcement layer can thus be computed from equation (75) when $z = z_i$. The axial reinforcement strain $\varepsilon_{s,i}$ is computed by equation (81), where β_i indicates the orientation of the reinforcement bars relative to the x-axis, see *Fig. 58b*. The dowel action that can develop in reinforcement bars in case of shear or bending deformations is neglected in the ML-EPSF method (Fernández Ruiz and Muttoni [12]).

$$\varepsilon_{s,i} = \varepsilon_{x,i} \cdot \cos^2 \beta_i + \varepsilon_{y,i} \cdot \sin^2 \beta_i + \gamma_{xy,i} \cdot \sin \beta_i \cdot \cos \beta_i \tag{81}$$

The stress in the reinforcement bars $\sigma_{s,i}$ is computed in the bar direction using the elastic-plastic constitutive law for steel presented in chapter 1.1.1, where f_s is yielding strength of steel and E_s the modulus of elasticity.

$$\sigma_{s,i} = E_s \cdot \varepsilon_{s,i} \qquad \text{with } \left|\sigma_{s,i}\right| \le f_s \tag{82}$$

The stress of each reinforcement layer can then be expressed in x-y coordinates by the following equations, *Fig. 57f*:

$$\sigma_{sx,i} = \sigma_{s,i} \cdot \cos^2 \beta_i \tag{83.a}$$

$$\sigma_{sy,i} = \sigma_{s,i} \cdot \sin^2 \beta_i \tag{83.b}$$

$$\tau_{sxy,i} = \sigma_{s,i} \cdot \sin \beta_i \cdot \cos \beta_i \tag{83.c}$$

Stress resultants

The stress resultants (n_x, n_y, n_{xy}, m_x, m_y, m_{xy}), *Fig. 57c*, that result from the imposed set of deformations ($\varepsilon_{x,0}$, $\varepsilon_{y,0}$, $\gamma_{xy,0}$, χ_x, χ_y, χ_{xy}) are obtained by integrating the layer stresses over the element thickness b_w, *Fig. 57g*. The integration can be performed by summation since the stresses are constant in each layer. The stress resultants are computed per unit length.

The in-plane forces in x and y direction, n_x and n_y, and the in-plane shear force, n_{xy}, are computed according to equations (84.a-c). The summation is performed over the n concrete layers and the n_s steel layers, with $a_{s,i} = A_{s,i}/s_i$ being the reinforcement area per unit length ($A_{s,i}$ bar cross section, s_i rebar spacing) in the i-th rebar layer (see *Fig. 58b*).

$$n_x = \frac{b_w}{n} \cdot \sum_{i=1}^{n} \sigma_{cx,i} + \sum_{i=1}^{n_s} a_{s,i} \cdot \sigma_{sx,i} \tag{84.a}$$

$$n_y = \frac{b_w}{n} \cdot \sum_{i=1}^{n} \sigma_{cy,i} + \sum_{i=1}^{n_s} a_{s,i} \cdot \sigma_{sy,i} \tag{84.b}$$

$$n_{xy} = \frac{b_w}{n} \cdot \sum_{i=1}^{n} \tau_{cxy,i} + \sum_{i=1}^{n_s} a_{s,i} \cdot \tau_{sxy,i} \tag{84.c}$$

The out-of-plane moments, m_x and m_y, and the torsion moment, m_{xy}, are computed as follows:

$$m_x = -\frac{b_w}{n} \cdot \sum_{i=1}^{n} z_i \cdot \sigma_{cx,i} - \sum_{i=1}^{n_s} z_i \cdot a_{s,i} \cdot \sigma_{sx,i} \tag{85.a}$$

$$m_y = -\frac{b_w}{n} \cdot \sum_{i=1}^{n} z_i \cdot \sigma_{cy,i} - \sum_{i=1}^{n_s} z_i \cdot a_{s,i} \cdot \sigma_{sy,i} \tag{85.b}$$

$$m_{xy} = -\frac{b_w}{n} \cdot \sum_{i=1}^{n} z_i \cdot \tau_{cxy,i} - \sum_{i=1}^{n_s} z_i \cdot a_{s,i} \cdot \tau_{sxy,i} \tag{85.c}$$

2.3.2 Implementation of a ML-EPSF panel element for assessing the in-plane shear and transverse bending interaction in beam webs

In the present chapter the in-plane shear and transverse bending interaction that occurs in beams and box-girders is investigated by applying the ML-EPSF method to a panel element that represents a segment of the web, *Fig. 59a*.

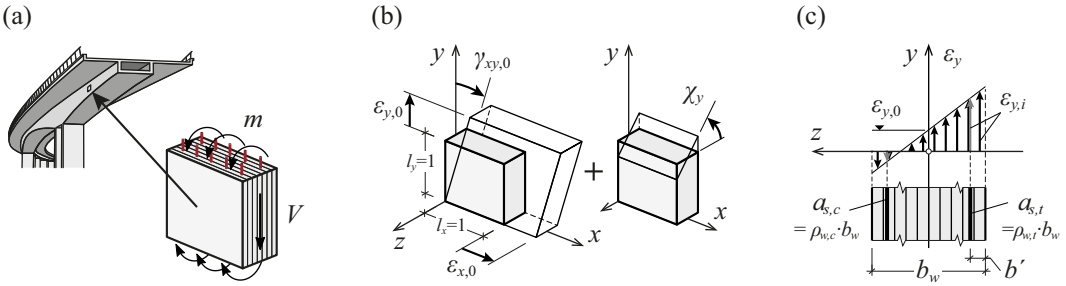

Fig. 59 *The ML-EPSF panel: (a) investigated forces; (b) panel in-plane and transverse deformations; (c) layered panel cross section with vertical deformation.*

The panel element, of unite size ($l_x = 1$, $l_y = 1$) and width b_w, is divided into n concrete layers and has two reinforcement layers ($n_s = 2$) that are placed at the location of the actual web reinforcement (on each face of the web), *Fig. 59*(c). In this study it is assumed that the orientation of the shear reinforcement is vertical ($\beta_1 = \beta_2 = 90°$).

The assumed panel kinematics is shown in *Fig. 59b* and in equation (86). The shear deformation γ_{xy} and the transverse curvature χ_y allow computing the in-plane shear force V ($= - l_y \cdot n_{xy}$) and the transverse bending moment m ($= m_y$). The longitudinal deformation of the web is assumed to be constant over the width ($\chi_x = 0$) and is represented by ε_x ($= \varepsilon_{x,0}$). The vertical deformation in the mid-plane of the web is designated by $\varepsilon_{y,0}$ and is used to compute the vertical deformation in the concrete and reinforcement layers while accounting for the transverse curvature χ_y. Thus, the state-of-strain in each layer, concrete or steel, is defined by the following equations, where z indicates the position of the layer centre relative to the panel mid-plane (*Fig. 59c*).

$$\varepsilon_x = \varepsilon_{x,0}\,, \qquad \varepsilon_y = \varepsilon_{y,0} - z \cdot \chi_y\,, \qquad \gamma_{xy} = \gamma_{xy,0} \tag{86}$$

In the present study, it is assumed that the web is only subjected to in-plane shear V and transverse bending m, *Fig. 59a*. No external vertical force (for example prestressing) is

acting on the web cross section, which allows formulating the condition that the sum of vertical stress must be equal to zero, $n_y = 0$.

$$n_y = \frac{b_w}{n} \cdot \sum_{i=1}^{n} \sigma_{cy,i} + \sum_{i=1}^{n_s} a_{sw,i} \cdot \sigma_{sy,i} = 0 \tag{87}$$

Finally, the shear force V and the transverse bending moment m that result from a shear deformation γ_{xy} and a transverse curvature χ_y are computed according to the iterative procedure illustrated in *Fig. 61* (light grey shaded area). For given panel characteristics (geometry and material) and a given state of deformation (γ_{xy}, χ_y), the state-of-stress fulfilling the equilibrium of vertical forces (equation (87)) can be calculated. To do this, the initially unknown vertical deformation $\varepsilon_{y,0}$ is varied until $n_y = 0$ is obtained. During the iterative procedure, the state-of-strain in each layer is given by equation (86), allowing to compute the state-of-stress in the concrete and reinforcement layers according to the ML-EPSF approach presented in chapter 2.3.1 (equation (76) to (85)). When $\varepsilon_{y,0}$ satisfies the condition $n_y = 0$, the computed stress field is in equilibrium with the combined action of in-plane shear and transverse bending. The internal forces V and m resulting from the imposed shear deformation γ_{xy} and transverse curvature χ_y are then computed as follows:

$$V = -l_y \cdot n_{xy} = -\frac{b_w}{n} \cdot l_x \cdot \sum_{i=1}^{n} \tau_{cxy,i} \tag{88.a}$$

$$m = m_y = -\frac{b_w}{n} \cdot \sum_{i=1}^{n} z_i \cdot \sigma_{cy,i} - \sum_{i=1}^{n_s} z_i \cdot a_{sw,i} \cdot \sigma_{sy,i} \tag{88.b}$$

In this approach, the panel deformation $\varepsilon_{x,0}$, that is representing the longitudinal deformation of the web, is assumed to be a fixed parameter of the web. In order to be representative for the investigated element, the value of $\varepsilon_{x,0}$ should consider the actual boundary conditions of the web and the effect of a possible longitudinal prestressing on the axial elongation of the web. For the analyses presented in this report, typical values for the average longitudinal strain have been chosen: $\varepsilon_{x,0} = 0.5‰$ for normal beams and $\varepsilon_{x,0} = 0.0‰$ for prestressed beams.

Building the (*m* - *V*) interaction diagram

Interaction curves for m and V are obtained by varying the transverse curvature χ_y for different shear deformation γ_{xy}, (*Fig. 60a*, thin lines). The (m - V) interaction diagram defining the maximum combined resistance for in-plane shear and transverse bending is given by the envelope of the curves established for various values of γ_{xy} (*Fig. 60a* bold line).

The different steps required to build the interaction diagram (bold curve in *Fig. 60a*) are illustrated in the flowchart in *Fig. 61*. They are classified into three major parts: Part 1: computing the (m, V) values for different curvatures while the shear deformation is maintained constant; Part 2: increasing the shear deformation; Part 3: determining the (m - V) interaction curve (the envelope). Detailed explanations regarding the different steps are provided in the following paragraphs.

Part 1: The shear force V and the transverse bending moment m are computed for increasing transverse curvatures χ_y while the shear deformation γ_{xy} is maintained constant and then plotted in a shear-transverse bending moment diagram, (*Fig. 60*, thin lines). *Fig. 61* Part1 illustrates the computational steps to determine V and m that are iterated in a loop over χ_y. Within each iteration the curvature is incremented by $\Delta\chi$ such that χ_y varies between 0 and χ_{max} ($0 \le \chi_y \le \chi_{max}$). The maximum curvature is reached when the increase of the transverse moment between two iterations is negligible ($m - m_{previous} <$ threshold) or when the deformation in a reinforcement or concrete layer reaches the ultimate deformation of the material ($\varepsilon_{s,i} = \varepsilon_{su}$ or $\varepsilon_{2,i} = \varepsilon_{cu} = -3.0‰$). *Fig. 60b-c* shows that for $\chi_y = 0$ the panel element is in a pure shear state ($V \ge 0$, $m = 0$) and that with increasing transverse curvature the shear force resisted by the cross section is decreasing. The transverse moment m is increasing with the transverse curvature and is maximum when $\chi_y = \chi_{max}$.

Part 2: This part consists in a loop over the shear deformation γ_{xy} which is varied between 0 and γ_1. After each iteration, the shear deformation is increased by $\Delta\gamma$ and Part 1 is repeated in order to obtain the (m, V) curve corresponding to the incremented shear deformation. The iterations are stopped when $\gamma_{xy} = \gamma_1$, where γ_1 is the shear deformation producing the highest shear force V when $\chi_y = 0$. The cases investigated in this report (with typical reinforcement ratios and material properties) showed no significant improvement of the (m - V) interaction curve (envelope) for higher shear deformations $\gamma_{xy} > \gamma_1$. From *Fig. 60b-c* it can be seen that the shear force V is increasing with the shear deformation, meanwhile the resisted transverse bending moment m is decreasing. Thus, in order to determine the maximum shear strength under the action of a transverse bending moment the results have to be combined in a shear-transverse bending moment diagram.

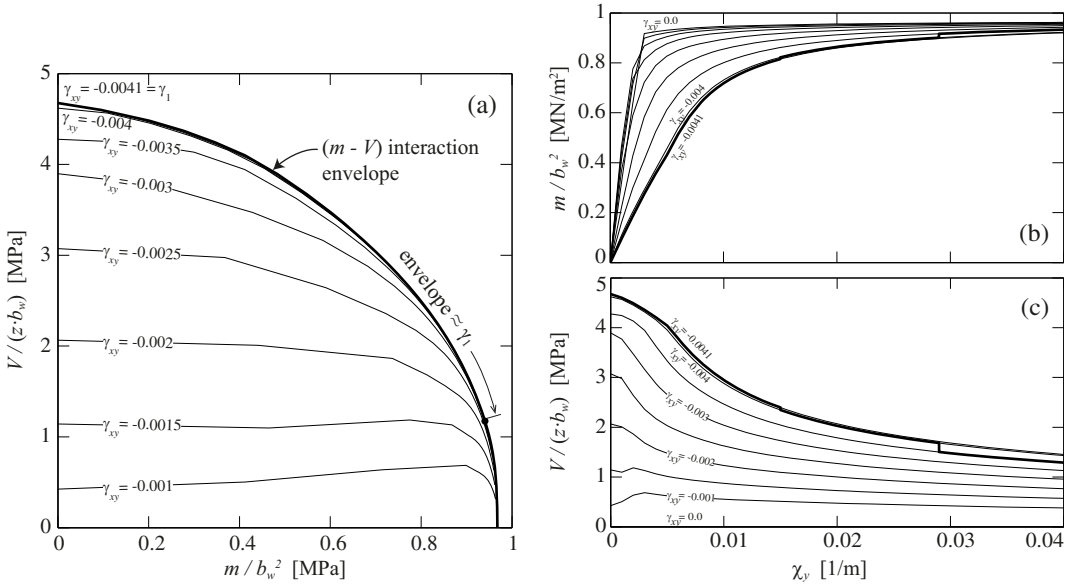

Fig. 60 *Establishment of an (m - V) interaction diagram: (a) transverse moment-in-plane shear curves for multiple γ_{xy} and the (m - V) envelope; (b) curvature-moment diagram; (c) curvature-in-plane shear force diagram, for f_{sd} = 435 MPa, $f_{cd} = \eta_{fc} \cdot f_{ck}/\gamma_c$ = 20 MPa, ρ_w = 0.5%, $\rho_{w,t}/\rho_{w,c}$ = 1.0, b'/b_w = 0.1 and ε_x = 0.5‰.*

Part 3: The (m - V) interaction curve defining the maximum combined resistance for in-plane shear and transverse bending is given by the envelope of all the curves for constant shear deformation, *Fig. 60a*. From *Fig. 60b-c* it can be seen that the envelope (in bold) intercepts multiple curves, for small curvatures $\gamma_{xy} = \gamma_1$ is determinant, but with increasing curvature the envelope is obtained for smaller shear deformations. In general, it has been found that the curve for $\gamma_{xy} = \gamma_1$ is a good approximation of the envelope curve. However, it is not covering the entire range of transverse moments that can be resisted by the web cross section (*Fig. 60a*), since the maximum moment is limited by the ultimate deformation of the material (resp. $\chi_{max} = f(\gamma_{xy})$). Thus for higher transverse bending moments (approximately $m > 0.8 \cdot m_{R0}$), the (m - V) interaction curve built from the various (m, V) curves computed in Part 2 has to be used.

For future analyses performed with the ML-EPSF panel element the only (m - V) interaction curve that is considered is the envelope curve such as it has been defined in the previous paragraph.

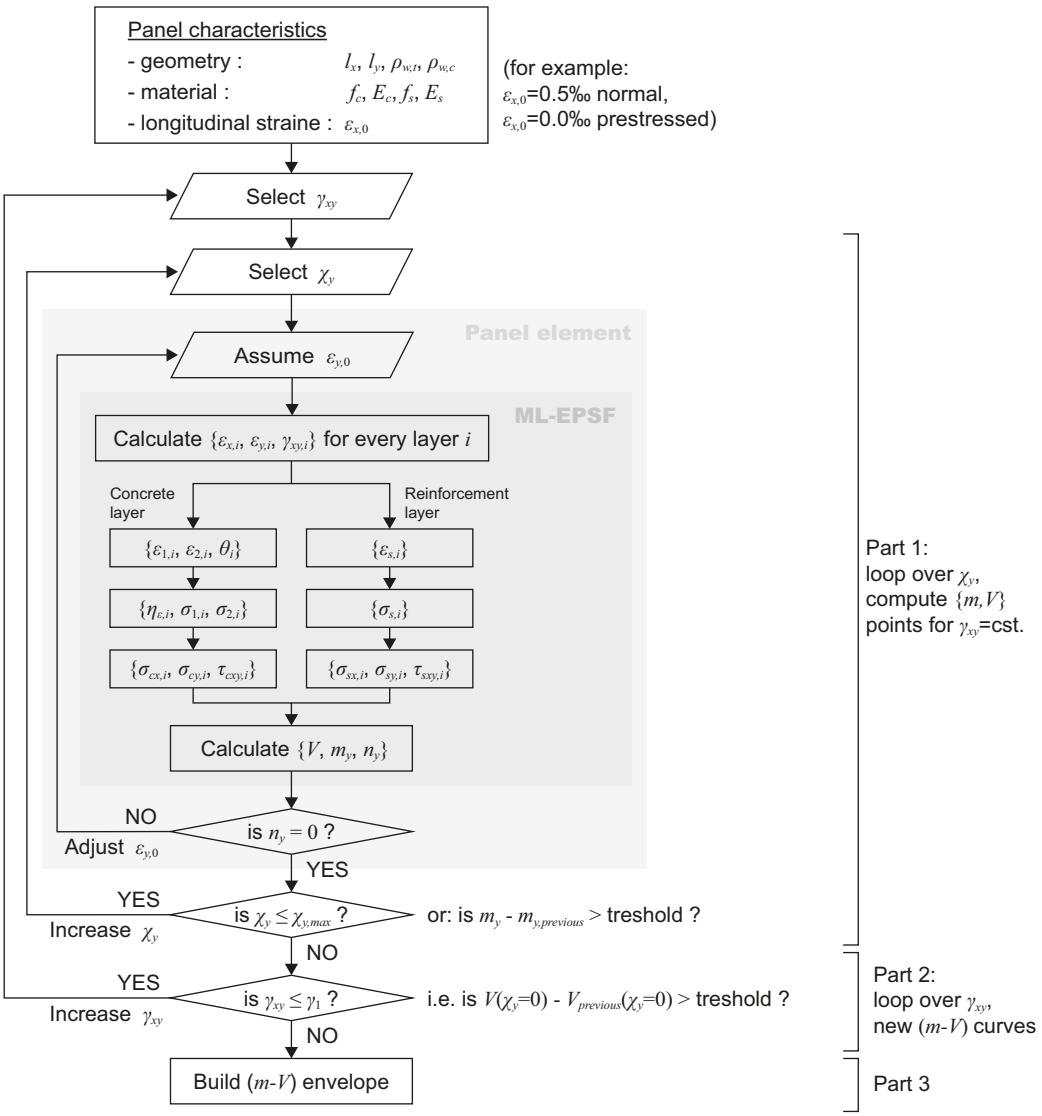

Fig. 61 *Flowchart for the development of the (m - V) interaction diagram according to the ML-EPSF panel element.*

2.3.3 Analysis of the (m - V) interaction in beam webs with the ML-EPSF panel element

In-plane shear transverse bending interaction diagrams according to the proposed ML-EPSF panel element

The application of the EPSF method to the multi-layered panel element allows assessing the combined resistance for in-plane shear and transverse bending that is then typically represented in (m - V) interaction diagrams. In *Fig. 62* are shown the (m - V) interaction curves obtained for various amounts of shear reinforcement (ρ_w) and different longitudinal deformations (ε_x). In general, it can be observed that the transverse bending moment leads to a significant reduction of the initial in-plane shear strength. However, it can be seen as well that in the range of small transverse moments the interaction is much weaker and the shear strength is only slightly reduced. For example, a transverse bending moment m of 30% of m_{R0} causes a reduction of the initial shear strength by only 10% (at most) which is significantly less than what has been predicted with the RP interaction models for comparable cross sections (see detailed comparison between the RPSF and ML-ESPF interaction models in chapter 2.3.4).

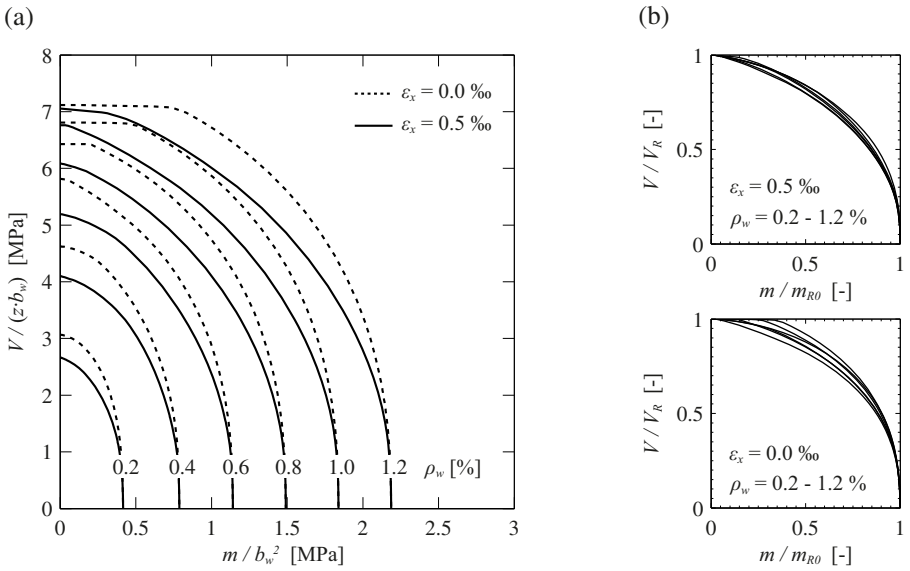

Fig. 62 *In-plane shear-transverse bending interaction according to the ML-EPSF panel element, for f_{cd} = 20 MPa, f_{sd} = 435 MPa, $\rho_{w,c}/\rho_{w,t}$ = 1.0, b'/b_w = 0.1: (a) (m - V) interaction diagram; (b) normalized diagrams for ε_x = 0.5‰ and ε_x = 0.0‰.*

Furthermore, the (m - V) interaction diagrams in *Fig. 62* show that the longitudinal strain ε_x has a non-negligible effect on the overall resistance of the element. In elements with no or only limited longitudinal deformation (prestressed beams $\varepsilon_x \approx 0$) the predicted initial shear strength (when $m = 0$) is significantly higher than for normal beams (ε_x = 0.5‰). This is mainly due to the fact that a restrained deformation ε_x can lead to a significant increase of the concrete strength reduction factor η_ε (up to 1.0), whereas in the RP approach this factor is assumed constant (SIA262:2013 [24]: $k_c = 0.55$, respectively $k_c \leq 0.65$ in case of a refined analysis). Besides the initial shear strength η_ε also has a positive effect on the overall shape of the (m - V) interaction curve (compare plots in *Fig. 62b*) making thereby the in-plane shear strength less sensitive to the transverse bending moment.

For high shear reinforcement ratios the (m - V) interaction curves presented in *Fig. 62*a show a horizontal plateau for small transverse bending moments. In this region, the shear resistance V is limited by the concrete strength ($V_{R,c} < V_{R,s}$); the shear reinforcement is not yielding ($\sigma_s < f_s$, see *Fig. 63b* for ρ_w = 1.2%) which allows carrying an increasing transverse bending moment m by changes in the stirrup forces with no or only little loss of shear resistance V. This phenomenon is even more pronounced for reduced longitudinal strain.

When the in-plane shear V goes to zero, the transverse bending resistance computed with the ML-EPSF panel element is equal to the classical transverse bending strength m_{R0} as defined by equation (50).

Analysis of the (m - V) interaction on the basis of the internal state-of-stress

The use of (m - V) interaction diagrams is a simple and compact way to represent the highly non-linear behaviour of a reinforced concrete web segment subjected to a combination of in-plane and out-of-plane loads. Although easily applicable for practical purpose, such condensate representations make it sometimes difficult to understand and validate the results (i.e. the (m - V) interaction diagrams) obtained by the multi-layered stress field approach. Thus, analysing the various parameters of the ML-EPSF on the cross section of the web element gives a better understanding of the actual internal state-of-stress and how the latter is influenced by the transverse bending moment. *Fig. 63* shows the state-of-stresses in the concrete and the shear reinforcement for different levels of transverse bending m/m_{R0} corresponding to the previously investigated (m - V) interaction curve for ρ_w = 0.6% and ε_x = 0.5‰ in *Fig. 62a*.

The state-of-stress in the concrete on the width of the web is illustrated in the plots of *Fig. 63a*, where the x-axis indicates the position z of the concrete layers relative to the web mid-

(a) State-of-stress in the concrete

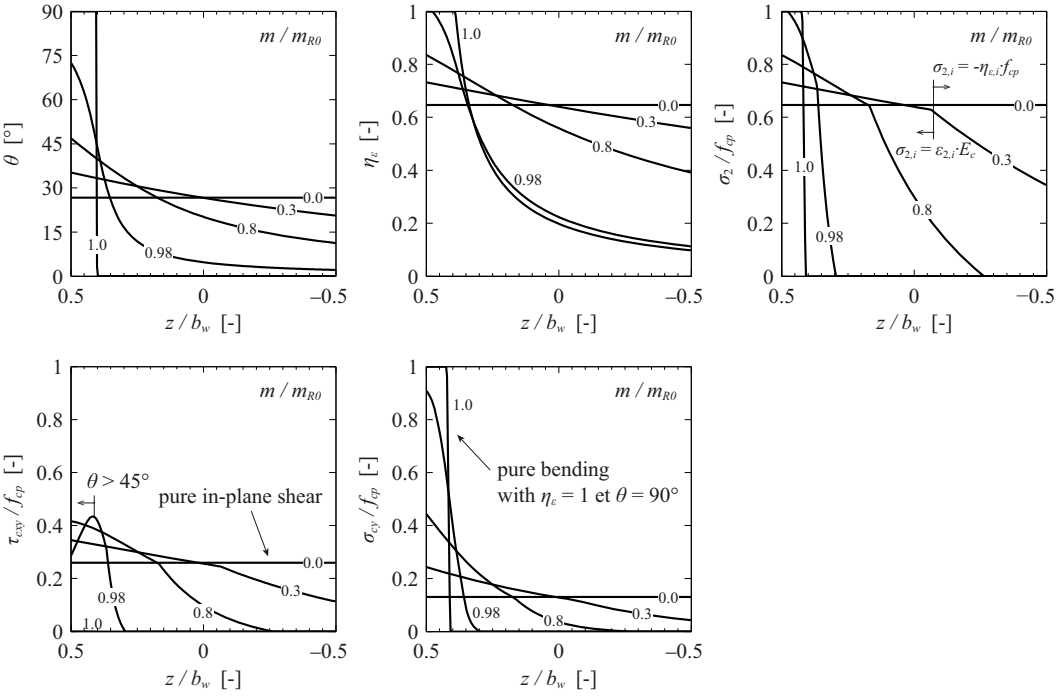

(b) Stirrup stresses

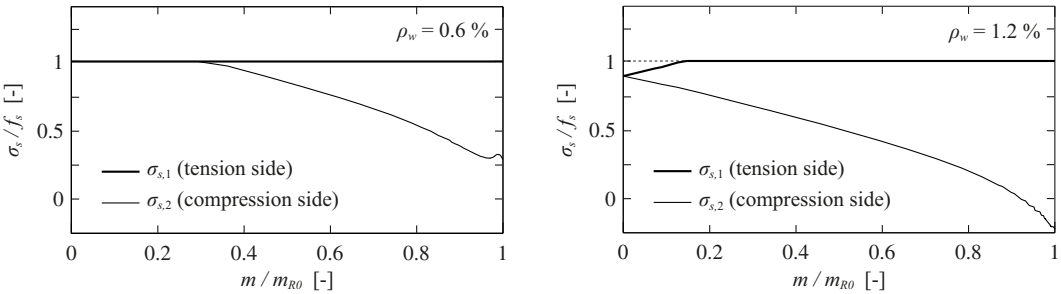

Fig. 63 *State-of-stress in the web cross section according to the ML-EPSF panel element for f_{cd} = 20 MPa, f_{sd} = 435 MPa, $\rho_{w,c}/\rho_{w,t}$ = 1.0, b'/b_w = 0.1 and ε_x = 0.5‰; (a) state-of-stress in the n concrete layers for ρ_w = 0.6% at different levels of transverse bending m/m_{R0}; (b) stress in the reinforcement layers.*

plane and the y-axis the value of the stress field parameter in the corresponding concrete layer. The investigated parameters are the inclination of the compression field θ, the concrete strength reduction factor η_ε, the principal compressive stress σ_2, the shear stress τ_{cxy} and the vertical component of the compressive stress σ_{cy} in the concrete. While establishing the (m - V) interacting curve (*Fig. 61*), these parameters have been evaluated for each concrete layer according to the elastic-plastic stress field approach described in section 2.3.1. The results are used to investigate how the internal stress-field, which is in equilibrium with the applied in-plane shear force V and the transverse bending moment m while respecting kinematic compatibility conditions, evolves with increasing levels of transverse bending moments m/m_{R0}. The stress distributions are shown for m/m_{R0} = {0, 0.3, 0.8, 0.98 and 1.0} which corresponds to several (m, V) cases along the interaction curve. They illustrate typical results that can be obtained with the ML-EPSF panel method in case of predominant in-plane shear (m/m_{R0} = 0.3) up to pure transverse bending states (m/m_{R0} = 1).

For small transverse bending moments (for example m/m_{R0} = 0 to 0.3) it can be seen from *Fig. 63a* that the behaviour of the element is still close to a pure shear behaviour; the shear stresses τ_{cxy} are relatively uniformly distributed over the entire width b_w of the web and the angles of inclination θ are almost constant. In addition, in the present example, it is found

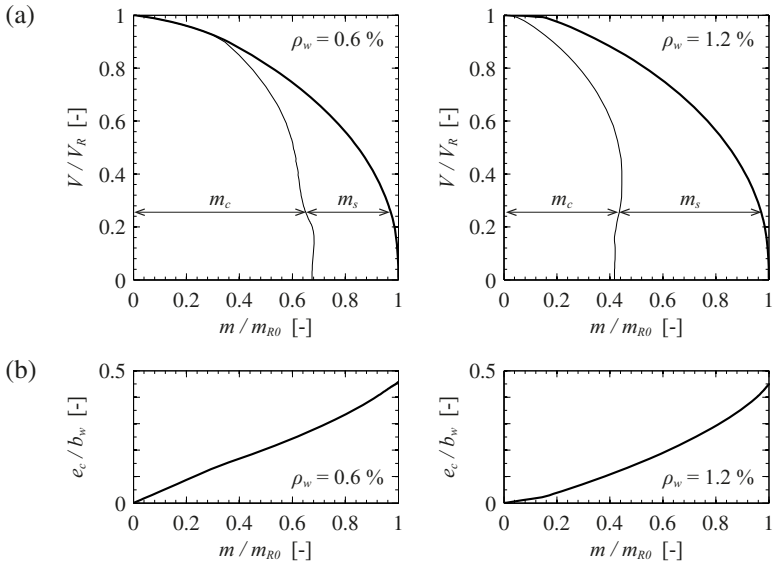

Fig. 64 *Contribution of the compression field to the transverse bending resistance, for f_{cd} = 20 MPa, f_{sd} = 435 MPa, $\rho_{w,c}/\rho_{w,t}$ = 1.0, b'/b_w = 0.1 and ε_x = 0.5‰: (a) moment equilibrated by the compression field (m_c) in the concrete and the stirrup forces (m_s); (b) eccentricity (e_c) of the compression field resultant (n_{cy}) relative to the web mid-plane.*

that the concrete strength reduction factor $\eta_\varepsilon \approx 0.65$ (= k_c), which is still higher than what is typically assumed for conventional rigid-plastic stress fields ($k_c = 0.55$), where no out-of-plane moment is considered. Consequently, the ML-EPSF leads to higher in-plane shear strength as conventional RPSF methods (see comparison to RPSF *Fig. 65* where $V_{\text{ML-EPSF}} > V_{R0}$). This is consistent with observations made with the classical elastic-plastic stress field method (for in-plane loading) by Fernández Ruiz and Muttoni [12].

When the transverse bending moment m is higher, the ML-EPSF approach allows to observe that the stress distribution on the cross section is not uniform anymore; the concrete compressive stresses (σ_2 and σ_{cy}) and the shear stresses (τ_{cxy}) increase towards the bending compression side ($z > 0$). At the same time, the width for the compression field diminishes, since some of the layers on the bending tension side ($z < 0$) have no stress. Indeed, the results of the ML-EPSF show that these layers are subjected to a state-of-strain of pure tension ($\varepsilon_1 > \varepsilon_2 > 0$) for which no concrete stresses can develop (concrete tensile strength being neglected in the EPSF method). Additionally, the multi-layered panel element shows that the inclination of the compression field θ in the outer layers increases significantly for high transverse moments, reaching up to 90° in some layers.

Finally, for very high levels of transverse bending (see *Fig. 63a* for m/m_{R0} = 0.98 to 1.0) the results of the ML-EPSF panel show that the web stress profile resembles more and more a typical plastic bending stress distribution. The outer concrete layers on the compression side, together with the stirrups on the tension side, behave as in pure flexion: the compression field is concentrated in a narrow segment and it's inclination θ approaches 90° (vertical), the compressive stresses σ_2 reach the plastic strength of concrete f_{cp} ($\eta_\varepsilon \rightarrow 1.0$) and the reinforcement on the bending tension side is yielding ($\sigma_{s,1} = f_s$, see *Fig. 63b*). At the same time, only a small shear force V can still be resisted by the web, of which most is carried by the inner concrete layers, see τ_{cxy} for $m/m_{R0} = 0.98$ in *Fig. 63a*. The outermost layers, that mainly contribute to m and for which the inclination of the compression field exceeds 45°, only carry a very small amount of the shear force. When the transverse moment eventually reaches m_{R0}, no more shear stresses are transferred by concrete layers.

A particular attention should be payed to the concrete strength reduction factor η_ε because it plays a significant role in the evaluation of the shear strength V in general (Fernández Ruiz [12]) and thus as well in the assessment of the combined (m - V) resistance of the web. For the following discussion it should be kept in mind that in the ML-EPSF approach (as in EPSF) the factor η_ε is computed directly from the acting state-of-strain in the different

concrete layers (see equation (79)). *Fig. 63a* shows that, with increasing transverse moments, the reduction factor η_ε (equal to k_c for RPSF), decreases rapidly towards the bending tension side (where the principal tensile strains ε_1 increase due to χ_y), and increases towards the bending compression side (where the ε_1 decrease due to χ_y). When the transverse bending moment is close to the pure bending strength m_{R0} (meaning χ_y high and thus ε_1 very small) $\eta_\varepsilon = 1$ in some of the outermost layers on the compression side. The effect of η_ε on the concrete compressive stress σ_2 ($\sigma_2 \leq -\eta_\varepsilon \cdot f_{cp}$), and consequently on the entire stress distribution on the cross section (σ_{cy}, τ_{cxy}), is clearly visible in the graphs of σ_2 in *Fig. 63a*. The sudden change in the stress profile indicates in which layers the compressive stress σ_2 is limited to the (local) effective compressive strength $f_{c,eff,i} = -\eta_{\varepsilon,i} \cdot f_{cp}$ (towards the bending tension side). The non-uniform distribution of η_ε thus largely contributes to the non-linear distribution of the shear stress τ_{cxy} and the vertical compressive stress σ_{cy} on the web cross section.

The evolution of the stresses in the shear reinforcement on the bending tension ($\sigma_{s,1}$) and on the bending compression side ($\sigma_{s,2}$) is show in *Fig. 63b*. While the shear force is still predominant (low transverse bending moments) the stirrups on both sides are yielding. With increasing transverse moments, the stresses in the stirrups on the compression side ($\sigma_{s,2}$) decrease which then contributes to equilibrate the transverse bending moment m. This phenomenon is clearly visible in *Fig. 64a* where the respective contributions of the compression field in the concrete (m_c) and the forces in the shear reinforcement (m_s) to the transverse bending resistance of the cross section are represented (m_c and m_s according to equation (85.b)).

Up to a certain level, the transverse moment can be entirely resisted by the compression field in the concrete, because the resultant compressive force is eccentric relative to the web mid-plane (see $e_c = n_{cy}/m_c$ in *Fig. 64b*, where n_{cy} is obtained from equation (84.b) when accounting for concrete stresses only). When the stress in the stirrups on the compression side starts reducing, the steel moment m_s begins to develop. For very high shear reinforcement ratios (in this case for example for $\rho_w = 1.2\%$) the shear reinforcement is initially not yielding (see *Fig. 63b*) because the concrete shear strength of the web is governing. Thus, in this case small transverse moments are mainly resisted by an increase of the tensile force in the stirrups on the tension side and a decrease of the force on the compression side (until $\sigma_{s,1} = f_s$) which leads to the plateau in the (m - V) interaction curve.

2.3.4 Comparison between the ML-EPSF panel element and the RPSF interaction models

The observations made on the basis of the proposed multi-layered elastic-plastic stress field panel element allow validating the basic principles and ideas of the rigid-plastic interaction models presented in literature. The out-of-plane bending moment m acting on the transverse web cross section causes the shear force resultant to shift towards the flexural compression side in order to maintain the equilibrium of moments (F_c in *Fig. 50b* and σ_{cy} in *Fig. 63a*). For high transverse bending moments the eccentricity of the compression field is not sufficient to equilibrate m (*Fig. 64*) and additional bending resistance is obtained by changes in the stirrups forces (ΔF in *Fig. 51* and σ_s in *Fig. 63*(b)). Furthermore, the ML-EPSF approach confirms Menn's model for predominant transverse bending (*Fig. 51e*) that assumes the presence of a pure compression zone (where $k_c = 1$ and $\theta = 90°$) in the outermost layers of the web (compare to σ_{cy} and η_ε in *Fig. 63a*).

Although the ML-EPSF approach leads to very similar in-plane shear transverse bending interaction mechanisms, the actual stress fields as well as the associated predicted strength differ significantly. These differences result naturally from the different types of stress fields used: equilibrium based rigid-plastic stress fields (RPSF) and kinematic compatible elastic-plastic stress fields (EPSF). In the RPSF interaction models the transverse stress distribution is tailored to equilibrate m and the compressive stress is assumed as a uniform stress bloc with $\sigma_{cw} = k_c \cdot f_{cp}$ (effective compressive strength of concrete). The stress field parameters (θ, k_c) are chosen based on recommendations for RPSF for in-plane shear design, typically $k_c = 0.55$ and $25° \leq \theta \leq 45°$ (SIA262:2013 [24]). They are assumed constant over the width of the web and their value does not depend on

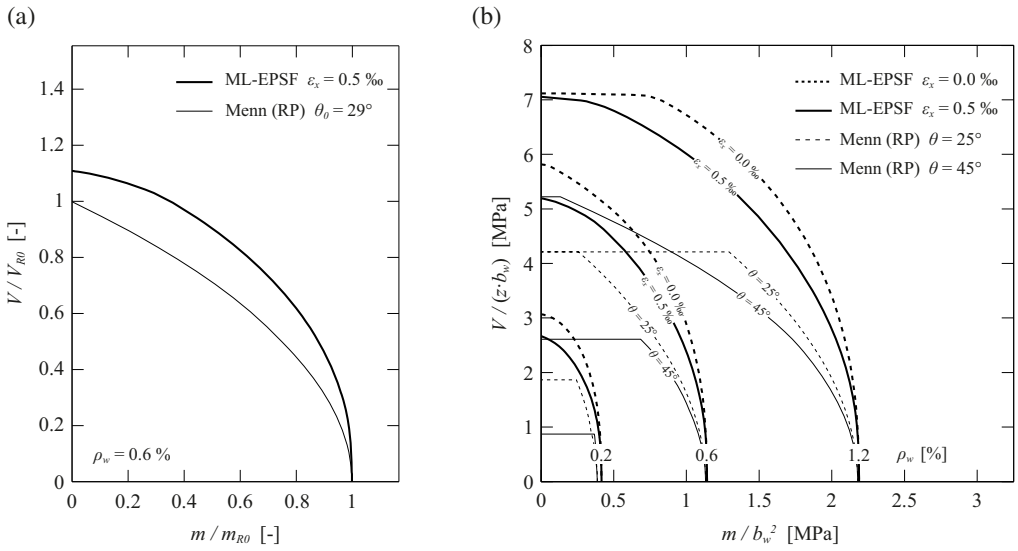

Fig. 65 *Comparison of (m - V) interaction diagrams according to the RP model by Menn [65] and the proposed ML-EPSF panel element for f_{cd} = 20 MPa, f_{sd} = 435 MPa, $\rho_{w,c}/\rho_{w,t}$ = 1.0 and b'/b_w = 0.1: (a) normalized diagram for ρ_w = 0.6%, Menn with $\theta = \theta_0$ = 29°, k_c = 0.55 and ML-EPSF with ε_x = 0.5‰; (b) range of diagrams for various ρ_w.*

the intensity of the transverse bending moment m. These hypotheses, however, are very different from what is observed when computing the stress field with respect to kinematic compatibility conditions. The ML-EPSF panel element shows that the inclination of the compression field θ is variable over the web width and changes with the intensity of the acting transverse moment m (see θ in *Fig. 63a*). For high shear forces, the ML-EPSF method (as EPSF in general) allows inclinations that are lower than the code recommendations. On the other hand, when the transverse bending moment m is strong, the inclination can reach up to 90° in the outer layers of the web. Similar observations are made for the concrete strength reduction factor η_ε ($= k_c$) that varies strongly, depending on the intensity of m and the position on the web width (see η_ε in *Fig. 63a*). Regarding the overall stress field distribution on the width of the web, the most significant difference is observed in the range of small transverse bending moments: in the RPSF approach the compression field is already concentrated on a minimum width and shifted towards the bending compression side (*Fig. 50c*), whereas in the ML-EPSF approach the compression field is still developed over the entire width of the web and the stress distribution is only slightly effected by the transverse bending moment (see σ_{cy} for m/m_{R0} = 0.3 in *Fig. 63a*). For higher transverse bending moments the ML-EPSF approaches the uniform stress distribution of the RPSF, but with different maximum stresses (due the different values for k_c resp. η_ε). Consequently, these differences between the RPSF and the ML-EPSF are clearly visible in the resulting (m - V) interaction diagrams, *Fig. 65*.

The (m - V) interaction curves resulting from the RP model proposed by Menn [65] and the proposed ML-EPSF panel element are plotted in *Fig. 65*. The interaction diagrams in *Fig. 65a* are established for $\theta = \theta_0$ = 29° (such that $V_{R,c} = V_{R,s} = V_{R0}$ for k_c = 0.55 and ρ_w = 0.6%) and normalized by the in-plane shear strength V_{R0} according to equation (48) and the transverse bending resistance m_{R0} according to equation (50). The overall behaviour (*Fig. 65a*) shows that the ML-EPSF approach predicts a weaker interaction between shear and transverse bending which results in a substantial increase of the combined in-plane shear transverse bending resistance. Especially in the range of small transverse bending moments the reduction of the shear strength is considerably lower (weaker slope and higher curvature of the (m - V) curve). As already discussed earlier, the difference between these two interaction curves can be mainly explained by the fact that in the RPSF models the values for k_c and θ are constant (over b_w and independent of m) and selected to be on the safe side (for example for beams k_c = 0.55 and 25° ≤ θ ≤ 45°), whereas, in the ML-EPSF method, these values are computed directly from the static and kinematic compatibility conditions. Consequently, the values for the concrete strength reduction factor η_ε are generally significantly higher than those assumed for k_c in RPSFs which leads to higher in-

plane shear strength. This mainly explains why in *Fig. 65a* $V_{\text{ML-EPSF}}/V_{R0}$ > 1.0 (for $V_{\text{ML-EPSF}}$ η_ε = 0.65 when m = 0, whereas for V_{R0}, computed according to RPSF, k_c = 0.55). More details regarding the issue of the initial EP in-plane shear strength are given in the next paragraph. Furthermore, the positive effect of the bending compression on the strut inclination θ and on the factor k_c is not accounted for in the RP models, which leads to additional conservatism in the prediction of the combined shear transverse bending strength. From *Fig. 65b* it can be seen that the difference between the RPSF and the ML-EPSF interaction diagrams is even more prominent for high shear reinforcement ratios (significant difference in the slops for ρ_w = 1.2% when $m/b_w^2 > 1.5$).

Besides the general shape of the (m - V) interaction curves, the initial in-plane shear strength (when m = 0) plays a major role for the combined (m - V) resistance. The ML-EPSF method predicts substantially higher initial shear strength (+12% for ρ_w = 0.6% in *Fig. 65a*) which leads to an overall increase of the in-plane shear strength under transverse bending (curve shifted upwards). This difference is again mostly due to the concrete strength reduction factor which is chosen to be on the safe side for the RPSF method (k_c = 0.55), whereas in the EPSF method this factor is computed on the basis of the panel kinematics which leads to less penalizing values (for example η_ε = 0.65 for *Fig. 65a*, when m = 0). This difference becomes even more pronounced for high shear reinforcement ratios (η_ε = 0.75 for ρ_w = 1.2% in *Fig. 65b*). For very low shear reinforcement ratios the concrete strength reduction factor for both methods (RP and EP) is very similar (~0.55), nevertheless the EPSF predicts higher initial shear strength (*Fig. 65b* ρ_w = 0.2%) because, in these cases, the computed inclination of the compression field decrease below 25° (recommended inferior limit by SIA262:2013 [24] for the RPSF approach).

To summarize, the shear strength of a web under in-plane shear and transverse bending can be assessed with both, the RPSF and ML-EPSF, interactions models. The underlying force transfer mechanisms reflect the correct behaviour of the web and allow performing local verification along the web of a beam. The RPSF interaction model presented by Menn [65] is easy to apply, however, since it bases on the static theorem of the theory of plasticity (equilibrium of forces), hypotheses on θ and k_c as well as strong simplifications of the internal state-of-stress have to be made. The RPSF interaction model thus leads to a lower bound value of the actual in-plane shear strength under transverse bending. The ML-EPSF panel element on the other hand requires a high computational cost but leads to an accurate analysis of the internal state-of-stress and to significantly higher in-plane shear strength, especially in the range of small transverse bending moments.

2.4 The plane EPSF method with a simplified approach for transverse bending in beam webs

The Swiss code SIA262:2013 [24] recommends assessing the shear strength of beams with stress field approaches. The elastic-plastic stress field (EPSF) method, which is implemented into a finite element method (Fernández Ruiz and Muttoni [12]) and which is presented extensively in this report, allows obtaining a more precise estimation of the ultimate strength of reinforced concrete members than the classical rigid-plastic stress field approach. Thus, this method is selected in order to investigate the in-plane shear strength of beams and box girder beams subjected to out-of-plane (transverse) bending moments in addition to the in-plane shear loading.

The EPSF method however is only applicable to reinforced concrete members which are in a plane state-of-stress (i.e. subjected to forces acting in the element plane). The transverse bending moment m can thus not be modelled explicitly in the FE model. By making use of the principles of the RP interaction models presented earlier in this report, the effect of m on the in-plane shear strength can however be considered by:

- Reducing the web thickness
- Reducing the shear reinforcement cross section, only applied for very high transverse bending moments.

These aspects are discussed in the following sections.

2.4.1 Reduction of the web width

From the previous analyses performed on the basis of the RPSF and the ML-EPSF panel elements (chapter 2.2 and 2.3) it was found that the transverse bending moment m leads the compression field to concentrate in a limited area on the bending compression side of the web cross section ($b_e \leq b_w$ in *Fig. 50* and σ_2 in *Fig. 63*). Thus, only a part of the web width b_w is available to transfer the shear force V when a transverse bending moment m is acting. In order to account for this in the finite element model, the web width is reduced to an effective web width $b_{w,eff} = b_w - \Delta b_w$. The reduction of the web width Δb_w is computed as follows:

$$\Delta b_w = 2 \cdot z \cdot \cot\theta \cdot \frac{m_{Rd,c}}{V_d} \tag{89}$$

With,

$$m_{Rd,c} = m_d - m_{Rd,s} \tag{90}$$

Where z is the lever arm, θ the average inclination of the compression field in the concerned region (obtained, by iteration, from the previous computation with the EPSF method), m_d is the transverse bending moment acting on the web, $m_{Rd,s}$ the transverse bending resistance provided by the shear reinforcement and V_d the shear force acting in the plane of the web (accounting for the longitudinal shear force and the torsional moment in box girder cross sections, see SIA 262 [24] for further details).

The equation (89) is derived from the equilibrium of a web segment subjected to a shear load V_d and a transverse bending moment m_d, *Fig. 66*: the compression field is only acting on a limited width $b_{w,eff}$ on the bending compression side of the web width and its inclination θ is assumed constant over $b_{w,eff}$, the vertical component of the resultant of the compression field $V_d/(z \cdot \cot\theta)$ is acting at $e_c = (b_w - b_{w,eff})/2 = \Delta b_w/2$ from the web centre and thus contributes to the transverse bending resistance $m_{Rd,c} = V_d/(z \cdot \cot\theta) \cdot \Delta b_w/2$. The shear reinforcement on both sides of the web is assumed to be yielding and the resisted moment is then computed

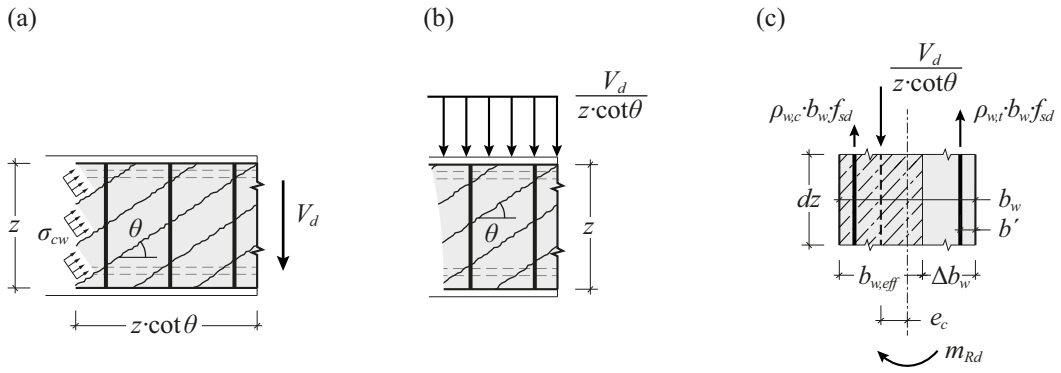

Fig. 66 *Concept of the web width reduction: (a) web elevation with in-plane shear; (b) web elevation with the vertical componant of the shear force per unit length; (c) transverse cross section of the web with equilibrium between the stirrup forces and the compression field.*

by $m_{Rd,s} = f_{sd} \cdot (\rho_{w,t} - \rho_{w,c}) \cdot b_w \cdot (b_w/2 - b')$. Knowing the acting transverse moment m_d and the resistance provided by the shear reinforcement $m_{Rd,s}$, the required resistance $m_{Rd,c}$ can derived (equation (90)) and by this the necessary eccentricity e_c of the compression field resultant. Consequently, the required width $b_{w,eff}$ and eventually the width reduction Δb_w can be computed (equation (89)).

Note that in this simplified verification approach the required web width is computed based on equilibrium considerations only, whereas in the previous RP interaction models (section 2.2) the required width is determined on the basis of the shear resistance of the compression strut. In order to emphasize this difference, a different notation for the required web width was chosen in the simplified verification method: $b_{w,eff}$ compared to b_e in the RP models (see section 2.4.3 for further information on this issue).

2.4.2 Reduction of the effective shear reinforcement

The width reduction Δb_w obtained according to equation (89) is reasonable for transverse bending moments m_d up to the magnitude of $m_{Rd,s}$, but it is very conservative for higher transverse moments.

The RP interaction models presented in the literature (in particular Thürlimann [64] and Menn [65]) suggest that, in case of high transverse bending moments, additional resistance can be obtained by reducing the tension force in the shear reinforcement on the bending compression side ($\sigma_{s,c} < f_s \rightarrow m_{R,s}$ increases). This behaviour is confirmed by the proposed ML-EPSF panel element (chapter 2.3.3) where the internal state-of-stress is computed with respect to the panel kinematics. The reinforcement stress ($\sigma_{s,2}$ in *Fig. 63*) reduces with an increasing moment, which leads to a higher contribution of the shear reinforcement to the transverse bending resistance (*Fig. 64* $m_{Rd,s}/m_{Rd}$ increases with m_d).

The behaviour of the web is significantly improved when this additional bending resistance provided by the reduced stress in the shear reinforcement is taken into account. In the present simplified verification method this leads to a less penalizing reduction of the web width, but requires a reduction of the effective shear reinforcement area on the bending compression side. This is considered by the factors λ which represent the amount of reinforcement that is actually used (activated), relative to the available shear reinforcement:

$$\begin{cases} \rho_{w,t,eff} = \lambda_t \cdot \rho_{w,t} = \lambda_t \cdot a_{sw,t} / b_w \\ \rho_{w,c,eff} = \lambda_c \cdot \rho_{w,c} = \lambda_c \cdot a_{sw,c} / b_w \end{cases} \quad \text{with,} \quad \begin{matrix} \lambda_t = 1 \\ 0 \le \lambda_c \le 1 \end{matrix} \tag{91}$$

$$\lambda_m = \frac{\lambda_t \cdot \rho_{w,t} + \lambda_c \cdot \rho_{w,c}}{\rho_{w,t} + \rho_{w,c}} = \frac{\lambda_t \cdot a_{sw,t} + \lambda_c \cdot a_{sw,c}}{a_{sw,t} + a_{sw,c}} \tag{92}$$

Where $\rho_{w,c,eff}$ and $\rho_{w,t,eff}$ are the effective amount of shear reinforcement, $a_{sw,c}$ and $a_{sw,t}$ the available reinforcement area per unit length on the bending compression, respectively tension, side of the web and λ_m the reduction factor to apply when modelling the effective reinforcement area in the FE model ($\lambda_m \cdot a_{sw}$).

If the factor λ_c is selected smaller than 1.0, the transverse bending resistance provided by the shear reinforcement increases, $m_{Rd,s} = f_{sd} \cdot (\lambda_t \cdot \rho_{w,t} - \lambda_c \cdot \rho_{w,c}) \cdot b_w \cdot (b_w/2 - b')$. Consequently, the moment that has to be resisted by the compression field $m_{Rd,c}$ (equation (90)) decreases and with it the reduction of the web width Δb_w (equation (89)). However, with $\lambda_c < 1$, the maximum allowable stress in the stirrups on the compression side is limited to $\sigma_s = \lambda_c \cdot f_{sd}$, thus not the entire stirrup resistance is available to equilibrate the vertical component of the compression field. To account for this, the total amount of shear reinforcement in the FE model has to be reduced by the factor λ_m.

This procedure (with $\lambda_c < 1$) leads to a more moderate reduction of the web width (i.e. higher concrete shear strength, $V_{Rd,c}$ ↑), but simultaneously reduces the effective shear reinforcement ($V_{Rd,s}$ ↓). The optimal value for λ_c can be found by iteration, in order to maximise the failure load.

2.4.3 Remarks on the simplified verification method relative to other methods

The stress field layout on the web cross section, *Fig. 66c*, as well as the principle used to equilibrate m_d, is identical to the principles of the RPSF models proposed by Thürlimann [64] and Menn [65] (chapter 2.2). The approaches differ however in the way the required web width is computed, hence the use of difference notations: b_e and $b_{w,eff}$. In the RPSF the width b_e is obtained based on resistance considerations, whereas $b_{w,eff}$ in the simplified verification method is obtained by equilibrium conditions only. In the RPSF models, b_e is the minimum web width necessary to resist the in-plane shear force and thus is computed directly according to the shear strength of concrete $V_{Rd,c}$ (equation (46)). This procedure however requires that the effective strength of concrete $f_{c,eff}$ (i.e. k_c) and the inclination of the compression field θ are known. In the design procedure proposed in the present chapter (2.4), the width $b_{w,eff}$ is chosen in order to obtained the necessary eccentricity e_c to equilibrate the transverse moment $m_{Rd,c}$ with the vertical component of the compression field. The width $b_{w,eff}$ is thus identified only on the basis of equilibrium considerations and does not require hypotheses on critical factors such as k_c. The strength of the element with the reduced web width $b_{w,eff}$ is verified in a separate step using the EPSF FE method, where the concrete strength reduction factors η_ε (equivalent to k_c in RPSF) and the inclinations of the compression field θ are computed automatically from the local state-of-strains in the beam (the EPSF method fulfilling static and kinematic compatibility conditions).

The fact that η_ε and θ are computed on the basis of displacement fields that are compatible with the in-plane boundary conditions generally leads to higher shear strength as RPSF interaction models from the literature (Thürlimann [64], Menn [65]). However, it should be observed that the so obtained (higher) failure load is still a lower bound value of the web strength, because the web reduction Δb_w proposed in equation (89) resides on a RPSF approach where the inclination θ is admitted constant (over b_w) although in reality (when respecting kinematic compatibility in the transverse direction, see ML-EPSF panel element in chapter 2.3.3), the inclination changes over the width of the web and with the intensity of m. A multi-layered approach, as presented for example in chapter 2.3.2, would thus be more pertinent, especially for high transverse bending moments, where, due to the bending compression, the inclination θ of the compression field can reach up to 90°.

If necessary, the presented simplified verification method can be used in combination with the ML-EPSF panel element (chapter 2.3.2), instead of the proposed RP approach. This leads to a more accurate determination of the web width reduction Δb_w (resp. e_c) and effective shear reinforcement cross section. Nevertheless, this verification procedure remains a simplified method leading to a lower bound solution of the shear strength under transverse bending, since the real kinematics of the web in the transverse direction cannot

be represented with the plane EPSF method. An exact solution, and thus the highest shear strength under transvers bending, can be obtained with the ML-EPSF finite element method which respects the in-plane and transverse kinematics of the web, as well as the static theorem of the theory of plasticity. This method is still under development but is briefly presented in chapter 2.5.

2.5 A multi-layered elastic-plastic finite element method for in-plane and out-of-plane shear and transverse bending

The multi-layered elastic-plastic stress field (ML-EPSF) method is an extension of the plane elastic-plastic stress field (EPSF) method by Fernández Ruiz and Muttoni [12] to out-of-plane load situations. The ML-EPSF finite element method allows computing stress fields that are in equilibrium with in-plane as well as out-of-plane forces such as transverse bending moments and out-of-plane shear forces. A detailed description of this method and hypotheses can be found in Backes [77]. As in the EPSF method, the ML-EPSFs are computed on the basis of displacement fields that are compatible with the boundary conditions. The state-of-strain of each element is then used to determine the state-of-stress by means of elastic-plastic material laws for both, steel and concrete. The resulting stress fields thus fulfil simultaneously the static and the kinematic theorem of the theory of plasticity and respect the plastic strength of material in every element of the finite element (FE) model. Consequently, such stress fields represent exact solutions according to the theory of plasticity.

The concerned reinforced concrete members are modelled with different finite elements for concrete and steel, *Fig. 67a*. The concrete is modelled with two combined finite elements: the multi-layered in-plane (ML-IP) concrete element and the out-of-plane (OP) concrete shear element. Together, the two concrete elements ensure the transmission of in-plane forces (normal and shear), constant out-of-plane shear and linearly varying out-of-plane moments. The ML-IP element, in which each layer respects the conditions of the EPSF, carries the in-plane forces and the average out-of-plane bending moments (constant). It is completed at each face by an OP shear element that carries the out-of-plane shear force and the moment variation, *Fig. 67b-c*. The reinforcement is modelled with rebar elements which can be placed with an eccentricity relative to the mid-plane of the concrete elements. This allows modelling the reinforcement at its actual location in the thickness of the element. As in the EPSF method ([12]), the rebar element carries only axial forces (dowel action is neglected) and the bond with the concrete is assumed to be perfect (no slip).

The ML-IP concrete element is a degenerated plane shell element with three nodes and fifteen degrees of freedom (three translations $\{u, v, w\}$ and two rotations $\{\theta_x, \theta_y\}$ at each node, *Fig. 68a*) and each layer behaves like a constant strain triangle. Out-of-plane, the element deforms with a constant curvature and undergoes shear deformations in order to

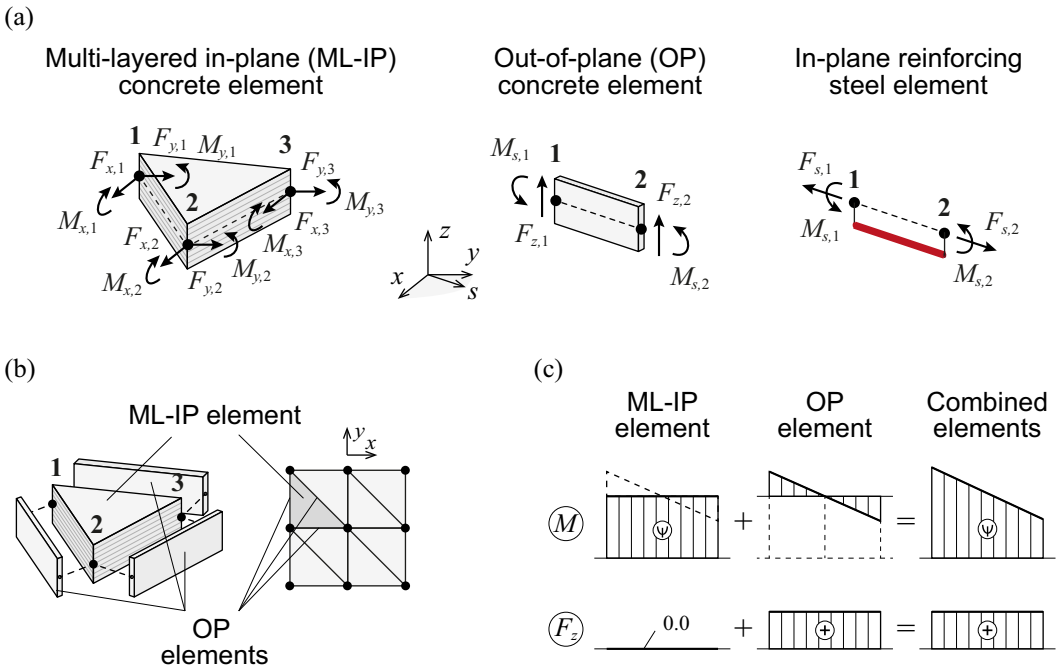

Fig. 67 *The ML-EPSF FE method: (a) FEs for concrete and steel; (b) combined elements for concrete and (c) the internal out-of-plane force concept (schematic representation).*

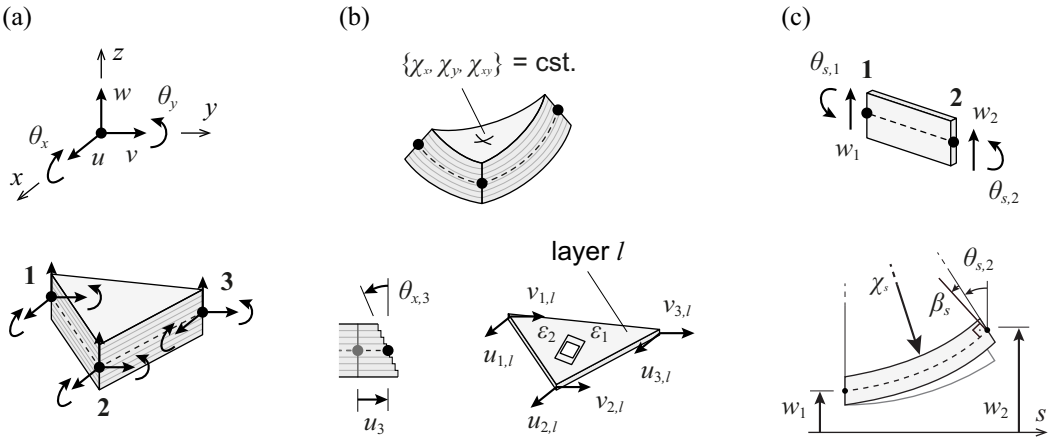

Fig. 68 *Element kinematics: (a) ML-IP element degrees of freedom; (b) ML-IP element kinematics with constant curvature and constant strain per layer; (c) OP shear element degrees of freedom and kinematics with shear deformation.*

ensure C_0 continuity of displacements between elements (displacements are continuous across the boundary of elements but not necessarily its derivatives (slopes), [23]).

The constant curvature, *Fig. 68b*, is a fundamental hypothesis of ML-IP element. Due to this hypothesis, the strain field in each layer is constant (no need for numerical integration points), which is the necessary condition for computing the plane state-of-stress in each layer according to the EPSF method (as in Fernández Ruiz and Muttoni [12]). Furthermore, the ML-IP concrete element accounts for shear deformation according to the Reissner - Mindlin plate bending theory (plane sections remain plane but not necessarily normal to the element reference plane). The shear deformation β is necessary in order to ensure the compatibility between the out-of-plane displacement field $w(x,y)$ with imposed constant curvature and the nodal degrees of freedom (especially w_i, $\theta_{x,i}$ and $\theta_{y,i}$, i = 1,2,3). The shear deformation allows decoupling the rotations θ from the out-of-plane translation w ($\theta \neq$ derivative of w) which leads to independent interpolations of the displacement fields of w and θ, see Mindlin plate in TGC 6 [23]. Mindlin plate elements only require C_0 continuity between elements, thus the element displacement fields $u(x,y)$, $v(x,y)$, $\theta_x(x,y)$ and $\theta_y(x,y)$ are interpolated by linear shape functions. The first order derivatives of the latter lead to the in-plane strain $\{\varepsilon_{x,0}, \varepsilon_{y,0}, \gamma_{xy,0}\}$ at the element mid-plane (plane of the nodes) and the out-of-plane curvatures $\{\chi_x, \chi_y, \chi_{xy}\}$, which are constant. The strains and stresses in each layer are then obtained according to the ML-EPSF method presented in chapter 2.3.1 (only the concrete layers). Eventually, the stress resultants $\{n_x, n_y, n_{xy}, m_x, m_y, m_{xy}\}$ are integrated, similarly to the method presented in Fernández Ruiz and Muttoni [12], in order to obtain the element nodal forces $\{F_{x,i}, F_{y,i}, M_{x,i}, M_{y,i}\}_{i=1,2,3}$.

A consequence of the aforementioned kinematic hypotheses is that the ML-IP element does not carry out-of-plane forces ($F_{z,i}$ = 0, *Fig. 67a*), this is why the element is completed by three OP shear elements. They deform identically to the ML-IP element border to which they are connected to, thus their out-of-plane deformation $w(s)$ is an equation of the second order with a constant a curvature χ_s (= f($\theta_{s,1}$, $\theta_{s,2}$)) and a constant shear deformation β_s (= f(w_1, w_2, χ_s), see *Fig. 68c*). This shear deformation is used to compute the out-of-plane shear force according to a Timoshenko beam approach (see TGC 6 [23]) and nodal moments are applied in order to ensure the equilibrium of forces.

The finite elements for concrete and reinforcing steel presented in this chapter have been developed and implemented into a computer program, Backes [77]. The non-linear displacement based finite element problem is solved by assembling a tangent stiffness matrix and applying a full Newton-Raphson algorithm. The approach appears promising for in-plan actions with constant out-of-plane moments, as well as for out-of-plane shear actions. Further details of the proposed ML-EPSF finite element program can be found in Backes [77].

Bibliography

[1] Gvozdev, A. A., “The determination of the value of the collapse load for statically indeterminate systems undergoing plastic deformation”, International journal of Mechanical Sciences, Vol. 1, 1960, pp. 322-335

[2] Drucker, D.C., On Structural Concrete and the Theorems of Limit Analysis, Publications, International Association for Bridge and Structural Engineering, V.21, Zürich, Switzerland, 1961, pp. 49-59

[3] Muttoni A., Schwartz J., Thürlimann B., Design of Concrete Structures with Stress Fields, Birkhäuser, Basel-Boston-Berlin, Switzerland, 1997, 143 p

[4] Ritter, W. “The Hennebique construction method” (in German, “Die Bauweise Hennebique”), Schweizerische Bauzeitung, XXXIII, N° 7, 1899, pp. 41-61.

[5] Mörsch, E. “Reinforced concrete construction, theory and application” (in German, “Der Eisenbetonbau, seine Theorie und Anwendung”), 3rd Edition, Verlag von Konrad Wittwer, 1908, 376 p.

[6] Leonhardt F., and Walther, R. “Deep beams” (in German, “Wandartige Träger”), Deutscher Ausschuss für Stahlbeton, Heft 178, Berlin, 1966, 159 pp.

[7] Schlaich, J. and Weischede, D. “A practical method for methodical design and building in reinforced concrete” (in German, “Ein praktisches Verfahren zum methodischen Bemessen und Konstruieren im Stahlbetonbau”), Bulletin d’Information n° 150, Comité Euro- International du Béton, 1982, 163 pp.

[8] Schlaich, J., Schäfer, K. and Jennewein, M. “Toward a consistent design of structural concrete“, Prestressed Concrete Institute Journal, May-June, 1987, pp. 75-150.

[9] Chen, W-F, Han, D-J., Plasticity for structural engineers, J. Ross publishing, Fort Lauderdale, USA, 2007, 255 p.

[10] Nielsen, M.P., Hoang, L.C., Limit Analysis and Concrete Plasticity, 3rd edition, CRC Press, 2011, 796 p.

[11] Muttoni A., Fernández Ruiz M., Levels-of-approximation approach in codes of practice, Structural Engineering International, 2012 Vol. 2, Zurich, Switzerland, 2012, pp. 190-194.

[12] Fernández Ruiz M., Muttoni A., On Development of Suitable Stress Fields for Structural Concrete, ACI, Structural Journal, Vol. 104 n°4, Farmington Hills, USA, 2007, pp. 495-50

[13] Muttoni A., Fernández Ruiz M, Niketić F., Design versus assessment of concrete structures using stress fields and strut-and-tie models, *ACI Structural Journal*, Vol. 112, No. 5, 2015, pp. 605-616

[14] Biondini, F., Bontempi, F., Malerba, P.G., Stress path adapting Strut-and-Tie models in cracked and uncracked R.C. elements, Structural Engineering and Mechanics, Vol. 12 , No. 6, 2001, pp. 685-698

[15] Thürlimann, B., Marti, P., Pralong, J., Ritz, P. and Zimmerli, B. “Application of the plasticity theory to reinforced concrete” (in German, “Anwendung der Plastizitätstheorie auf Stahlbeton”), Institut für Baustatik und Konstruction, ETH Zürich, 1983, 252 pp.

[16] Muttoni A., Kostic N., Fernández Ruiz M., Discussion of paper 'Factors affecting strength of elements designed using strut-and-tie models', ACI Structural Journal, Vol. 104, USA, 2008, pp. 233-235

[17] Brown, M.D., Sankovich, C.L., Bayrak, O., Jirsa, J.O., Behaviour and Efficiency of Bottle-Shaped Struts, ACI Structural Journal, Vol. 103, No 3, 2006 pp. 348-354

[18] Lourenco, M. S., Almeida, J. F., Adaptive Stress Field Models: Formulation and Validation, ACI Structural Journal, Vol. 110, No. 1, 2013, pp. 71-81

[19] Muttoni A., The applicability of the theory of plasticity to design of structural concrete (in German: Die Anwendbarkeit der Plastizitätstheorie in der Bemessung von Stahlbeton), Birkhäuser Verlag, Institut für Baustatik und Konstruktion ETH Zürich, 176, Basel, Switzerland, 1990

[20] Campana S., Eléments en béton armé soumis à une combinaison de flexion, effort tranchant et forces de déviation, Thèse EPFL N°5574, Lausanne, 2012, 162 p.

[21] Fédération Internationale du Béton (fib), fib Model Code for Concrete Structures 2010, Ernst & Sohn, 2013, 434 p.

[22] Vecchio F. J., Collins M. P., The Modified Compression-Field theory for Reinforced Concrete Elements Subjected to Shear, ACI Journal, Vol. 83, No. 2, 1986, pp. 219-231

[23] Frey F., Jirousek J. Méthode des éléments finis (TGC volume 6) Analyse des structures et milieux continues, Presses Polytechnique et Universitaires Romandes, 298 p., Lausanne, Suisse, 2001.

[24] SIA 262, Structures en béton, Swiss norm SIA 262:2013, Swiss Society of engineers and Architects, Zurich, Switzerland, 2013, 43 p.

[25] Marti, P., Alvarez, M., Kaufmann, W., and Sigrist, V., Tension Chord Model for Structural Concrete, Structural Engineering International, Vol. 8, No. 4, 1998, pp. 287–298;

[26] EN 1990:2002. Eurocode – Basis of structural design. European Committee for Standardization, CEN, Brussels, 2002.

[27] EN 1992-1-1:2004. Design of concrete structures – General rules and rules for buildings. European Committee for Standardization, CEN, Brussels, 2004.

[28] F. Niketic, On design and assessment of structural concrete using stress field method, PhD Thesis (in preparation), IBETON, EPSF, Lausanne, Switzerland

[29] JCSS - Probabilistic model code, Part 1 - Basis of design, 12th draft, Joint committee on structural safety, Technical University of Denmark, 2001

[30] SIA 269, Existing Structures – Bases, Swiss norm SIA 269:2011, Swiss Society of engineers and Architects, Zurich, Switzerland, 2011

[31] Himsworth F.R, The variability of concrete and its effect on mix design, Proceedings of the Institution of Civil Engineers, PartI, Vol. 3, No. 2, March 1954

[32] Erntroy H.C., The Variation of Works Test Cubes, Cement and Concrete Association, London, Research Report No.10, November 1960

[33] Sándor Popovics, Strength and Related Properties of Concrete: A Quantitative Approach, John Wiley & Sons, Inc, New York, USA, 1998

[34] Tanner P., Lara C.,Prieto M., Semi-probabilistic models for the assessment of existing concrete structures, in Applications of Statistics and Probability in Civil Engineering, Faber, Köhler and Nishijima (eds), Taylor & Francis Group, London, 2011, ISBN 978-0-415-66986-3.

[35] T. C.-K. Chan, «A Study of the behaviour of reinforced concrete dapped end beams», MSc Thesis, University of Washington, Seattle, Washington, USA, 1979.

[36] M. A. Khan, «A study of the behaviour of reinforced concrete dapped-end beams», MSc Thesis, University of Washington, Seattle, Washington, USA, 1981.

[37] W. D. Cook y D. Mitchell, «Studies of disturbed regions near discontinuities in reinforced concrete members», ACI Structural Journal, vol. 85, n.º 2, pp. 206-216, 1988.

[38] R. R. H. Zhu, W. Wanichakorn, T. T. C. Hsu, y J. Vogel, «Crack width prediction using compatibility-aided strut-and-tie model», ACI Structural Journal, vol. 100, n.º 4, pp. 413–421, 2003.

[39] R. Herzinger, “Stud reinforcement in dapped ends of concrete beams”, Thesis, University of Calgary, Calgary, Alberta, Canada, 2008.

[40] J. Mata-Falcón, «Serviceability and Ultimate Behaviour of Dapped-end Beams (In Spanish: Estudio del comportamiento en servicio y rotura de los apoyos a media madera)», PhD Thesis, Universitat Politècnica de València, Valencia, Spain, 2015.

[41] Nagrodzka-Godycka K., Piotrkowski P., Experimental Study of Dapped End Beams Subjected to Inclined Load, ACI, Vol. 109, No. 1, Jan.-Feb. 2012., pp. 11-20

[42] ACI, Building Code Requirements for Structural Concrete (ACI 318M-08) and Commentary, American Concrete Institute, ACI Committee 318, ACI 318-08, 473 p., Farmington Hills, USA, 2008.

[43] AASHTO, AASHTO LRFD Bridge Design Specifications and Commentary, 6th Edition, 1661 p., Washington D.C., USA, 2012.

[44] Rupf, M., Querkraftwiderstand von Stahlbeton - und Spannbetonträgern mittels Spannungsfeldern, PhD Thesis, Ecole Polytechnique Federale de Lausanne, Switzerland, 153pp., 2014.

[45] Rupf, M., Fernandez Ruiz, M. and Muttoni, A., Post-tensioned girders with low amount of shear reinforcement: Shear strength and influence of flanges, Engineering Structures, Vol. 56, pp. 357-371, 2013.

[46] Moore, A. M., Shear Behaviour of Post-Tensioned Spliced Girders, PhD Thesis, The University of Texas at Austin, USA, 268 p., 2014.

[47] Moccia F., Investigation of shear strength of post-tensioned girders, MSc Thesis, École Polytechnique Fédérale de Lausanne, Lausanne, Switzerland, pp. 220, 2015.

[48] Kaufman M.K., Ramirez J.A., Re-evaluation of the Ultimate Shear Behaviour of High Strength Concrete Prestressed I-Beams, ACI Structural Journal, Vol. 85, No. 3, May-June 1988., pp. 295-303

[49] Saqan E. I., Frosch R. J., Influence of flexural reinforcement on shear strength of prestressed concrete beams, ACI Structural Journal, Vol. 106, No. 1, Jan.-Feb.2009., pp. 60-68.

[50] Kuchma, D., Kim, K. S., Nagle, T. J., Sun, S. und Hawkins, N. M., Shear Tests on High-Strength Prestressed Bulb-Tee Girders: Strengths and Key Observations, ACI Structural Journal, Vol. 105, No. 3, May-June 2008., pp. 358-367.

[51] Fernandez Ruiz M., Muttoni A., Shear Strength of Thin-Webbed Post-Tensioned Beams, ACI Structural Journal, Vol. 105, No. 3, May.-June 2008., pp. 308-317.

[52] Wilder K. De, Lava P., Debruyne D., Wang Y., Roeck G. De, Vandewalle L., Stress field based truss model for shear-critical prestressed concrete beams, Engineering Structures, Vol. 3, pp. 28-42, 2015

[53] Leonhardt, F., Walther, R., Dilger, W., Schubversuche an indirekt gelagerten, einfeldrigen und durchlaufenden Stahlbetonbalken, Deutscher Ausschuss für Stahlbeton, Heft 201, Berlin, 1968, 69 pp.

[54] Baumann, T., Rüsch, H., Schubversuche mit indirekter Krafteinleitung, Versuche zum Studium der Verdübelungswirkung der Biegezugbewehrung eines Stahlbetonbalkens, TH München, Deutscher Ausschuss für Stahlbeton, Heft 210, Berlin 1970, pp. 1–41.

[55] Leonhardt, F., Koch, R., Rostásy, F. S., Schubversuche an Spannbetonträgern, Deutscher Ausschuss für Stahlbeton, Heft 227, Berlin, 1973, 179 pp.

[56] Büeler, Ch. und Thoma, K., Indirekt gelagerter Spannbetonträger – Versuchsbericht, CC Konstruktiver Ingenieurbau, Hochschule Luzern – Technik & Architektur, Bericht, 2010, 61 pp.

[57] Thoma K., Seelhofer B., Büeler Ch., Indirekte Lagerung von Betonbrücken - Sachstandbericht (AGB Forschungsbericht No. 660), Bundesamt für Strassen ASTRA, 2014, 93 pp.

[58] Kupfer H., Ewald G. *Überlagerung von Scheibenschub und Plattenbiegung im Spannbetonbrückenbau, Versuchsergebnisse an dem Träger V I/68*, Technische Universität München, Institut für Bauingenieurwesen III, Lehrstuhl für Massivbau, ca. 250 Bl., Munich, Germany, 1973.

[59] Kaufmann J., Menn C. *Versuche über Schub bei Querbiegung*, Institut für Baustatik und Konstruktion ETH Zürich, Birkhäuser Verlag Basel und Stuttgart, N° 7201-1, 92 p., Zürich, Switzerland, December, 1976.

[60] Ewald G. *Überlagerung von Scheiben- und Plattentragwirkung am Beispiel stark profilierter Stahlbeton- und Spannbetonträger bei hoher Schub- und begrenzter Querbiegebeanspruchung*, Institut für Bauingenieurwesen III, Technische Universität München, 211 p., Munich, Germany, 1977.

[61] Gaspar R. *Dimensionamento das almas de pontes celulares*, Tese - Escola Politécnica, University of São Paulo, 250 p., Brazil, 2003.

[62] Kirschner U. *Investigating the behaviour of reinforced concrete shell elements*, PhD Dissertation, 83 p., Toronto, Canada, June, 1986.

[63] Polak M. A., Vecchio F. J. *Reinforced Concrete Shell Elements Subjected to Bending and Membrane Loads*, ACI Structural Journal, Vol. 91, No. 3, pp. 261-268, May, 1994.

[64] Thürlimann B. *Schubbemessung bei Querbiegung*, Schweizerische Bauzeitung, Vol. 95, Heft 26, pp. 478-481, Switzerland, 1977.

[65] Menn C. *Stahlbetonbrücken*, Springer-Verlag, Wien, New York, 533 p., 1986.

[66] Stucchi F. R., Borges L. A. Dimensionamento das almas de vigas celulares, 2. Simpósio EPUSP de estruturas de concreto, pp. 359-401, São Paulo, Brasil, 1990.

[67] CEN *ENV 1992-2 Eurocode 2: Design of concrete structures - Part 2: Concrete Bridges – Design and detailing rules,*, Comité Européen de Normalisation, , Brussels, Belgium, October, 2005.

[68] Marti P. *Design of Concrete Slabs for Transverse Shear*, ACI Structural Journal, Vol. 87 No 2, pp. 180-190, Detroit, USA, March - April, 1990.

[69] Fanti G., Mancini G. *Ultimate limit state design of structural concrete shell elements*, CEB Bulletin d'Information, No. 223, pp. 167-207, Lausanne, Switzerland, June, 1995.

[70] Lourenço P. B., Figueiras J. A. *Solution for the design of reinforced concrete plates and shells*, Journal of Structural Engineering, Vol. 121, Issue 5, pp. 815-823, May, 1995.

[71] Seelhofer H. *Ebener Spannungszustand im Betonbau: Grundlagen und Anwendungen*, Diss. Eidgenössische Technische Hochschule (ETH) Zürich, Nr. 18486, 247 pp., Zürich, Switzerland, 2009.

[72] Giordano L., Mancini G., Napoli P., Recupero A. *Shear-transverse bending interaction in the webs of R.C./P.R.C. box bridges*, First International Conference on Advances in Structural Engineering and Mechanics, pp. 943-948, Seoul, Korea, August, 1999.

[73] SIA *SIA 162/34 : Résistance à la rupture et dimensionnement des structures en béton armé et en béton précontraint, SIA,* 14 p., Zürich, Switzerland, 1976.

[74] CEB *Code modèle pour les structures en béton*, Système international de réglementation technique unifiée des structures, Vol. II, Bulletin d'Information, No. 117, Paris, December, 1976.

[75] Marti P. *Zur plastischen Bemessung von Stahlbeton*, ETH, Dissertation Nr 6602, 176 p., Zürich, Switzerland, November, 1980.

[76] SIA, *SIA162 Betonbauten*, Schweizerischer Ingenieur- und Architektenverein, Zürich, Suisse, 1989.

[77] Backes M.-R. *Interaction of in-plane and out-of-plane forces in reinforced concrete shell elements*, IBETON, EPFL, Thesis Nr. XXXX, Lausanne, Switzerland, 2016.

Glossary

Symbol	Meaning
Upper-case Latin letters	
A	Area of the spreading zone
A_s	Reinforcement area
A_{Mi}	Area of a finite element triangle applied in a i-mesh
A_{spiral}	Area of the spiral reinforcement
A_{sw}, $A_{sw,c}$, $A_{sw,t}$	Shear reinforcement area, on the bending compression ($_{,c}$) and tension ($_{,t}$) side
C_0	Continuity condition
E_c, $E_{s,}$	Modulus of elasticity of concrete ($_c$) and steel ($_s$)
E_h	Hardening modulus of steel
F_{anch}	Anchorage force
F_c	Vertical component of the resultant of the inclined compression field in concrete due to shear, per unit length
$F_{cj,i}$	Nodal force in j-node in i-principle direction coming from concrete
$F_{c,m}$	Bending compression force in the web, vertical, per unit length
$F_{p,\,dev}$	Prestression deviation force
$F_{p,inf}$	Prestress force at an infinite point in time
F_s	Force in the shear reinforcement, per unit length Nodal force in s direction
$F_{s,c}$, $F_{s,t}$	Force in the shear reinforcement on the bending compression ($_{,c}$) and tension ($_{,t}$) side, per unit length
$F_{s,i}$	Nodal force in i-node calculated from a steel finite element
F_{sw}	Force in the shear reinforcement
F_x, F_y, F_z	Nodal force in x, y and z direction
F_y, $F_{y,c}$, $F_{y,t}$	Force in the shear reinforcement at yield, on the bending compression ($_{,c}$), tension ($_{,t}$), side only, per unit length
G_f	Fracture energy
M	Longitudinal bending moment
M_s	Nodal moment in s direction
M_x, M_y	Nodal moment in x and y direction
N	Longitudinal force
Q	Failure load
R	Resultant force of both stirrup forces, per unit length
R_d	Design resistance strength
R_m	Mean resistance strength
R_{spiral}	Radius of the spiral reinforcement
T	Longitudinal torsion moment
V	In-plane (longitudinal) shear force
V_R, $V_{R,c}$, $V_{R,s}$	Shear resistance of the element, of the concrete ($_{,c}$), of the shear reinforcement ($_{,s}$)
V_{R0}	Shear resistance for simultaneous crushing of concrete and yielding of shear reinforcement, $V_{R0} = V_{R,c} = V_{R,s}$
V_{lim}	Shear force, limit between predominant shear and predominant transverse bending
V_w	Total shear force acting on the web (including torsion)

Symbol	Meaning
Lower-case Latin letters	
a_s	Reinforcement area per unit length
a_{nom}	Nominal geometry values
a_{sw}, $a_{sw,c}$, $a_{sw,t}$	Shear reinforcement area per unit length, on the bending compression ($_{,c}$), tension ($_{,t}$), side
$a:b$	Triangle high-to-side ration
b	Width of box cross section Distance between the midpoints of slabs left and right from the rib Width of a steel plate
b_e	Minimum web width to resist the shear force
b_m	Web width to resist the transverse bending compression
b_w	Web width
$b_{w,eff}$	Effective web width
b_{eff}	Effective slab width
$b_{eff,i}$	Slab contribution to effective width left and right from analysed rib
b'	Position of shear reinforcement in the web width, measured from the web surface
$\overline{b}$	Width of box cross section, measured at the web axis
e_c	Eccentricity of the concrete stress resultant relative to the element mid-plane
f_c	Concrete compressive strength (cylinder)
f_{cd}	Design concrete compressive strength
f_{ck}	Characteristic concrete compressive strength
f_{cm}	Mean concrete compressive strength
f_{co}	Concrete compressive strength brittleness limit
f_{cp}	Concrete equivalent plastic strength
f_{ctm}	Mean tensile concrete strength
$f_{cp,confined}$	Confined concrete compressive strength
$f_{c,eff}$	Effective concrete strength
$f_{c,red}$	Reduced concrete strength according to SIA162:1989 [76] (= $k_c{\cdot}f_{cp}$ in SIA262:2013)
f_s	Yield stress of reinforcing steel
f_{sd}	Design steel yield strength
f_{sk}	Characteristic steel yield strength
f_{sm}	Mean steel yield strength
$f_{s,r}$	Reduced steel yielding strength
h	Height of box cross section
$\overline{h}$	Height of box cross section, measured at the flange axis
i	Layer number in the ML-EP model Node number of the finite element
k_c	Concrete strength reduction factor for transverse tensile strain
k_D	Concrete strength reduction factor taking into account the presence of prestressing ducts
l	Layer in the multi-layered finite element Length of a side of a finite element concrete triangle Distance between two points on a reinforcement bar
l_{anch}	Anchorage length
l_0	Distance between the zero points on the moment diagram

Symbol	Meaning
l_{FE}	Length of a finite element
l_x, l_y	Element size/length in x and y direction
m	Transverse (out-of-plane) bending moment in beam webs, per unit length
$m_{R,c}$, $m_{R,s}$	Transverse bending moment resisted by the concrete ($_{,c}$) and by the shear reinforcement ($_{,s}$), per unit length
m_{R0}	Plastic transverse (out-of-plane) bending strength, per unit length
m_c, m_s	Transverse bending moment equilibrated by the concrete ($_{,c}$) and by the shear reinforcement ($_{,s}$), per unit length
m_{lim}	Transverse bending moment, limit between predominant shear and predominant transverse bending, per unit length
m_x, m_y, m_{xy}	Out-of-plane moment in x and y direction and torsion moment, per unit length
$\bar{m}$	Transverse bending moment limit, per unit length
n	Number of concrete layers Compliance factor
n_{cy}	Stress resultant of concrete stresses in y direction, per unit length
n_s	Number of reinforcing layers
n_x, n_y, n_{xy}	In-plane force / stress resultant in x and y, shear force in x-y plane , per unit length
p_f	Probability of failure
r_f	Ratio between reinforcement strength and equivalent plastic strength
s	Spacing of the shear reinforcement Coordinate along element axis
s_{spiral}	Step of the spiral reinforcement
u	Translation in x direction (in-plane)
v	Translation in y direction (in-plane)
w	Translation in z direction (out-of-plane)
w_{lim}	Spalling crack limit width
$w_{lim,lin}$	Spalling crack limit width – assuming liner tensile strength distribution
$w_{lim,plast}$	Spalling crack limit width – assuming plastic tensile strength distribution
x	Coordinate
y	Coordinate
z	Lever arm of internal forces Coordinate along the element normal to the element mid-plane
Upper-case Greek letters	
ΔF	Variation of the force in the stirrups, per unit length
Δb_w	Web width reduction for transverse bending
Δl	Length of a beam segment
Δm	Variation of / supplementary transverse bending moment, per unit length
$\Delta\gamma$	Increment of shear deformation
Lower-case Greek letters	
α	Sensitivity factor
β	Orientation of the reinforcement direction relative to the x direction Shear deformation Characteristic angle of in a node Reliability index
β_1	Reliability index for one year reference period
γ_c	Safety factor for concrete

Symbol	Meaning
γ_C	Partial safety factor for concrete due to material uncertainty
$\gamma_{Rd,c}$	Partial safety factor for concrete due to model uncertainty
γ_d	Global safety factor
γ_s	Partial safety factor for steel
γ_S	Partial safety factor for steel due to material uncertainty
$\gamma_{Rd,s}$	Partial safety factor for steel due to model uncertainty
γ_{xy}, $\gamma_{xy,0}$	Shear deformation in the x-y plane, $(_{,0})$ at the element mid-plane
γ_1	Shear deformation maximising the shear force
δ_1	Deformation of the steel at the yielding
ε	Strain
$\dot{\varepsilon}$	Strain rate
ε_c	Concrete strains
ε_{cu}	Ultimate deformation of concrete
ε_x, $\varepsilon_{x,0}$	Strain in x direction , $(_{,0})$ at the mid-plane of the element
ε_y, $\varepsilon_{y,0}$	Strain in y direction , $(_{,0})$ at the mid-plane of the element
ε_s	Strain in the reinforcement
ε_{su}	Ultimate deformation of reinforcing steel
ε_0	Strain at the mid-plane of the element
ε_1, ε_2	First and second principal strain, $\varepsilon_1 \geq \varepsilon_2$
ζ	Ratio between the force in the stirrup on the bending tension side and the total stirrup force
η_{fc}	Concrete strength reduction factor for brittle failure of high strength concrete
η_ε	Concrete strength reduction factor for transverse tensile strain (= k_c in SIA 262) Concrete compressive strength effectiveness factor
θ	Inclination of the compression field (= α in SIA 262) Inclination of the second principal strain ε_2 relative to the x-axis
θ_s	Nodal rotation in s direction
θ_x, θ_y	Nodal rotation in x and y direction
θ_0	Inclination of the compression field when simultaneous crushing of concrete and yielding of shear reinforcement
λ, λ_c, λ_t, λ_m	Ratio of effective / available amount of shear reinforcement, on the bending compression $(_{,c})$ and tension $(_{,t})$ side, $(_{,m})$ average value
ρ_w, $\rho_{w,c}$, $\rho_{w,t}$	Shear reinforcement ratio in the web, on the bending compression $(_{,c})$, tension $(_{,t})$
$\rho_{w,c,eff}$, $\rho_{w,t,eff}$	Effective shear reinforcement ratio in the web, on the bending compression $(_{,c,})$, tension $(_{,t,})$
σ_c	Concrete compressive stress
$\sigma_{c,confined}$	Confining concrete compressive strength
σ_{cw}	Concrete compressive stress in direction of the inclined strut
σ_{cx}, σ_{cy}	Concrete compressive stress in x and y direction
$\sigma_{p,inf}$	Prestress in at an infinite point in time
σ_{sx}, σ_{sy}	Reinforcement stress in x and y direction
σ_{s1}, σ_{s2}	Reinforcement stress on the bending tension $(_{,1})$ and compression $(_{,2})$ side
σ_x, σ_y	Stress in x and y direction
σ_s	Stress in the reinforcing bar
σ_v	Vertical component of the inclined concrete compressive stress

Symbol	Meaning
σ_1, σ_2	First and second principal stress in concrete, $\sigma_1 \geq \sigma_2$
τ	Nominal tangential stress
τ_{b0}	Concrete bond strength prior to yielding
τ_{b1}	Concrete bond strength after to yielding
τ_{cxy}	Concrete shear stress in the x-y plane
τ_{sxy}	Reinforcement shear stress in the x-y plane
τ_{xy}	Shear stress in the x-y plane
$\emptyset$	Reinforcement bar diameter Normal distribution function
$\emptyset_D$	Diameter of prestressing duct
χ	Curvature
χ_s	Curvature in s direction
χ_x, χ_y, χ_{xy}	Curvature in x and y direction, torsion curvature
Additional symbols and abbreviations	
→	Value tends to
↑	Increasing value
↓	Decreasing value
1D	One dimensional
2D	Two dimensional
3PB	Three point bending
4PB	Four point bending
COV	Coefficient of variation
CLCP	Concentrated load on continuous beams
DEB	Dapped-end beams
EP	Elastic-plastic
EPSF	Elastic-plastic stress field
FE	Finite element
FEM	Finite element method
GSF	Global safety format
LoA	Levels of approximation
ML-EP	Multi-layered elastic-plastic
ML-EPSF	Multi-layered elastic-plastic stress field
ML-IP	Multi-layered in-plane concrete element
OP	Out-of-plane concrete element
PB	Pure bending
PC	Prestressed concrete
PSF	Partial safety format
Re-bar	Reinforcement bar
Rec. CS	Rectangular cross-section
RC	Reinforced concrete
RP	Rigid-plastic
RPSF	Rigid-plastic stress field
SF	Stress field
SLS	Serviceability limit state

Symbol	Meaning
std	Standard deviation
STM	Strut-and-tie model
SBCL	Simple beams subjected to continuous load
TCM	Tension cord model
T CS	T cross section
TT CS	Double T cross-section
ULS	Ultimate limit state
Indices	
$_{,1\ ,2}$	The principle directions
$_{,Rd}$	Design value of the resistance
$_{,\text{SIA 262:2013}}$	According to Swiss code SIA 262:2013 [24]
$_{,a}$	Cross section a-a
$_{,b}$	Cross section b-b
$_{,d}$	Design value
$_{,def,i}$ $_{,def,ref}$	i-distorted mesh reference mesh
$_{,fc}$	Of concrete compressive strength
$_{,fs}$	Of steel yield strength
$_{,EPSF}$	Estimated using elastic-plastic stress field method
$_{,geometry,c}$	Geometry properties of concrete
$_{,geometry,s}$	Geometry properties of steel
$_{,i}$	Number of the layer Principal stress direction Bar finite element
$_{,l}$	Layer in the multi-layered finite element
$_{Mi}$	Referring to an i-mesh
$_{,max}$	Maximum value
$_{,model}$	Related to a model
$_{,orient,i}$	i-mesh orientation
$_{,previous}$	Value at previous iteration
$_{,test}$	Measured value
$_{,ult}$	At ultimate limit state

Project closure

Schweizerische Eidgenossenschaft
Confédération suisse
Confederazione Svizzera
Confederaziun svizra

Département fédéral de l'environnement, des transports, de l'énergie et de la communication DETEC
Office fédéral des routes OFROU

RECHERCHE DANS LE DOMAINE ROUTIER DU DETEC

Version du 09.10.2013

Formulaire N° 3 : Clôture du projet

établi / modifié le : 30 juin 2016

Données de base

Projet N° : AGB 2009-009

Titre du projet : Vérification de structures existantes par la méthode des champs de contraintes élastiques-plastiques - Modélisation de détails critiques et analyse de l'interaction entre l'effort tranchant et la flexion transversale

Echéance effective :

Textes :

Résumé des résultats du projet :

La première partie du rapport présente des sujets liés aux champs de contraintes élastiques-plastiques (EPSF) qui n'avaient pas encore été étudiés de façon détaillée précédemment. Il fournit une aide pratique pour la modélisation adéquate de détails critiques de ponts : entretoises et voiles croisées, zones d'introduction d'efforts concentrés, zones d'introduction des forces de précontrainte, joints Gerber et poutres avec discontinuités géométriques. Il est également montré comment considérer l'adhérence béton-armature en cas de longueur d'ancrage insuffisante et comment traiter les problèmes d'éclatement du béton d'enrobage avec les EPSF. Certains problèmes de la méthode aux éléments finis (MEF) utilisée pour la résolution des EPSF sont étudiés en détail. L'étude de sensibilité du maillage a montré que l'orientation des éléments finis (EF) triangulaires peut être un paramètre important. Il importe d'éviter une orientation préférentielle des éléments triangulaires et de préférer plutôt une disposition en forme de zigzag ou en bloc de quatre éléments. Par contre, la taille et la forme des éléments triangulaires n'ont généralement que peu d'influence sur le résultat global. Comme règles de bonne pratique, il faudrait limiter, si possible, l'élancement des EF triangulaires à 1:3 (rapport largeur-hauteur) et utiliser l'espacement des étriers comme dimension de base pour la génération du maillage. L'étude de la convergence de la MEF a montré qu'un calcul à 250 itérations est suffisant pour obtenir des résultats satisfaisants. La MEF et les EPSF, avec les recommandations proposées, ont été validés de manière rigoureuse en les comparant à 315 essais effectués en laboratoire et décrits dans la littérature scientifique. Les EPSF permettent une très bonne estimation de la charge de rupture réelle (charge de rupture mesurée/charge de rupture calculée = 1.03 en moyenne, COV 8%) et une prédiction cohérente du mode de rupture.
Une étude du format de sécurité a montré que l'approche à facteurs partiels, tel que définie dans les normes SIA 260:2013 et SIA262:2013, est à appliquer de préférence pour les calculs avec les EPSF. Une méthode permettant d'adapter les facteurs partiels pour les EPSF tenant compte du facteur de modèle réduit est présentée. Cependant, les facteurs de sécurités réduits qui en résultent doivent être utilisés avec beaucoup de précaution.
La deuxième partie du rapport porte sur l'effet de la flexion transversale sur la résistance à l'effort tranchant des âmes des ponts caissons. D'abord, des modèles de la littérature basés sur les champs de contraintes rigides-plastiques (RP) sont étudiés et présentés en détail. Ces modèles d'interaction sont simples à utiliser et illustrent élégamment l'effet de la flexion transversale sur le champ de contraintes, mais prédisent une réduction importante de la résistance à l'effort tranchant. Une étude avancée avec un nouveau modèle multi-couches basé sur les EPSF (ML-EP) a permis de montrer que l'interaction est sensiblement moins prononcée, surtout pour des moments transversaux faibles, ce qui augmente notablement la résistance prédite. En effet, le modèle ML-EP a montré que sous l'effet de la flexion transversale, le champ de contraintes n'est pas uniforme sur l'épaisseur de l'âme. L'inclinaison et le facteur kc augmentent fortement vers la face comprimée jusqu'à atteindre des valeurs qui peuvent aller au-delà de ce qui est généralement admis pour les champs de contraintes RP. Malgré son temps de calcul plus important, l'approche ML-EP est donc un outil précieux dans les cas où une évaluation précise du champ de contraintes et de la résistance à l'effort tranchant en présence d'un moment transversale est requise.
Finalement, une approche simplifiée, qui combine les principes des modèles d'interaction RP avec la MEF des EPSF, est présentée. Elle permet d'étudier le comportement global de l'élément tout en prenant en compte, de manière simplifiée, l'effet de la flexion transversale. Cette approche conduit généralement à une résistance plus élevée que les modèles d'interaction RP tout en étant une borne inférieure de la résistance réelle. Le rapport donne finalement un aperçu sur une extension de la méthode des EPSF qui consiste en un élément fini élastique-plastique multi-couches.

Schweizerische Eidgenossenschaft
Confédération suisse
Confederazione Svizzera
Confederaziun svizra

Département fédéral de l'environnement, des transports, de l'énergie et de la communication DETEC
Office fédéral des routes OFROU

Atteinte des objectifs :

Les objectifs du projet ont été atteints. La recherche a démontré que la méthode des champs de contraintes élastiques-plastiques (EPSF) est un outil fiable et efficace pour la vérification détaillée des structures existantes. Les règles de modélisation décrites dans ce rapport devraient permettre aux ingénieurs de la pratique d'utiliser cette méthode de façon fiable et efficace pour la vérification des détails critiques des ponts en béton armé et précontraint.

L'étude de l'interaction entre l'effort tranchant et la flexion transversale dans les âmes de ponts par le biais des champs de contraintes élastiques plastiques a montré que cet effet est moins important de ce qui est préconisé par les méthodes simplifiées utilisées couramment.

Déductions et recommandations :

La méthode des EPSF est fiable et permet de déterminer la résistance des détails de structure critiques avec une bonne précision. Cette méthode peut être utilisée dans la pratique par des ingénieurs suffisamment compétents pour la vérification de détails critiques présentant une armature minimale suffisante pour permettre la redistribution des efforts.

Le format de sécurité tel que défini dans les normes SIA 260:2013 et SIA 262:2013 peut être appliqué pour les calculs avec les EPSF. Si nécessaire, les facteurs partiels pourraient encore être adaptés selon les indications de la norme SIA 269:2011. Dans ce contexte, une approche permettant de considérer la bonne fiabilité des EPSF en réduisant le facteur de modèle est indiquée. Cependant, cette adaptation est à appliquer avec précaution.

Publications :

Muttoni A., Fernández Ruiz M, Niketić F., Design versus assessment of concrete structures using stress fields and strut-and-tie models, ACI Structural Journal, Vol. 112, No. 5, 2015, pp. 605-616

Backes M.-R., Fernández Ruiz M., Muttoni A. Interaction between in-plane shear forces and transverse bending moments in concrete bridge webs, Proc. of the 10th fib International PhD Symposium in Civil Engineering, Quebec, pp. 403-408, Canada, 2014.

en préparation :
Backes M.-R. Interaction of in-plane and out-of-plane forces in reinforced concrete shell elements, IBETON, EPFL, Lausanne, Switzerland, 2016.

Chef/cheffe de projet :

Nom : Muttoni Prénom : Aurelio

Service, entreprise, institut : Ecole Polytechnique Fédérale de Lausanne, Laboratoire de Construction en Béton (IBETON)

Signature du chef/de la cheffe de projet :

Schweizerische Eidgenossenschaft
Confédération suisse
Confederazione Svizzera
Confederaziun svizra

Département fédéral de l'environnement, des transports, de l'énergie et de la communication DETEC
Office fédéral des routes OFROU

RECHERCHE DANS LE DOMAINE ROUTIER DU DETEC
Formulaire N° 3 : Clôture du projet

Appréciation de la commission de suivi :

Evaluation :

La commission d'accompagnement juge très positivement la démarche effectuée dans le projet et relève que des objectifs importants ont été atteints, notamment aux niveaux suivants :
- la démonstration de la fiabilité et de l'efficacité respectivement de l'usage qu'il peut être fait, dans la pratique et en tenant compte des recommandations formulées pour la modélisation, de la méthode des champs de contraintes élastiques - plastiques (EPSF) pour la vérification détaillée des structures existantes, en particulier des détails critiques des ponts en béton;
- l'évaluation de l'effet de l'interaction entre l'effort tranchant et la flexion transversale dans les âmes de ponts;
- l'application du format de sécurité partiel selon SIA 260:2013 et SIA 262:2013, ainsi que le développement d'une méthode permettant l'adaptation de ces facteurs partiels de sécurité, méthode dont le cadre d'application et les limites sont précisés;
- l'approche simplifiée permettant l'étude du comportement global de l'élément en prenant en compte, de manière simplifiée, l'effet de la flexion transversale;
- l'aperçu sur une extension de la méthode des EPSF consistant en un élément fini élastique-plastique multicouches.

Mise en oeuvre :

La méthode des EPSF peut être utilisée dans la pratique par les ingénieurs, à la condition qu'ils disposent des compétences suffisantes, pour la vérification de détails critiques présentant une armature minimale suffisante pour permettre la redistribution des efforts.
Elle permet une très bonne estimation de la charge de rupture réelle, comme l'attestent les résultats des nombreux essais réalisés.

Le format de sécurité tel que défini dans les normes SIA 260:2013 et SIA 262:2013 peut être appliqué dans les calculs avec la méthode des EPSF et les facteurs partiels pourraient encore être adaptés selon les indications de la norme SIA 269:2011. Une approche permettant de considérer la bonne fiabilité des EPSF en réduisant le facteur de modèle est possible; son application doit toutefois s'accompagner des précautions nécessaires.

Besoin supplémentaire en matière de recherche :

Pas de besoin mis en évidence.

Influence sur les normes :

Pas d'influence mise en évidence.

Président/Présidente de la commission de suivi :

Nom : Putallaz Prénom : Jean-Christophe

Service, entreprise, institut : Service des routes, transports et cours d'eau / DTEE - Etat du Valais

Signature du président/ de la présidente de la commission de suivi :

Recherche dans le domaine routier du DETEC : Formulaire 3 **Page 3 / 3**

Index des rapports de recherche en matière de route

Etat: 15.03.2016

no. de rapport.	no. de projet	titre	année
1557	SVI 2010/001	Reklame im Strassenverkehr	2016
1555	SVI 2004/049	Sichere Schulwege – Gefahrenanalyse und Massnahmenplanung	2016
1554	VSS 2011/501	Evaluation des Frosttaumittelwiderstands von Beton – Vergleich von vier Prüfverfahren	2016
1551	VSS 2012/207	Akustische Installationen im Strassentunnel	2016
1550	VSS 2012/311	SERFOR: Voranalyse "Self Explaining and Forgiving Roads"	2016
1549	SVI 2011/015	Anforderungen an zukünftige Mobilitätserhebungen	2016
1548	VSS 2010/404	Grundlagen für die Anforderungen an Schutzgeokunststoffe auf der Basis von neuen EN-Prüfmethoden	2016
1547	ASTRA 2011/012_OBF	Development of a self-healing asphalt road via induction heating	2015
1545	ASTRA 2011/013_OBF	Vergleich verschieden starker Asphalt-Belagsaufbauten: Ermittlung der Versagensgrenze eines T3-Normbelages mit der mobilen Grossversuchsanlage MLS10	2015
1544	VSS 2007/302	Rampenbewirtschaftung: Anforderungen an Regelungsverfahren	2015
1543	VSS 2012/402	Machbarkeitsstudie zur Reduktion von Feinstaub oder seiner Vorläufergase mittels spezieller Strassenbeläge	2015
1542	VSS 2011/713	Forschungspaket Nutzensteigerung für die Anwender des SIS: EP3: Transformationskonzepte zwischen Bezugssystemen	2015
1541	VSS 2010/301	Verkehrssicherheit zweistreifiger Kreisel	2015
1540	AGE 2013/001_ENG	TOSA - Transport par bus avec Optimisation du Système d'Alimentation	2015
1539	FGU 2010/007	Modelling of anhydritic swelling claystones	2015
1538	SVI 2011/021	Forschungspaket Verkehr der Zukunft (2060): Initialprojekt	2015
1537	FGU 2010/007	Geotechnischer Indexwert für die Beurteilung des Potentials zur Quarzstaubbelastung	2015
1536	VSS 2012/201	Wirkungskontrolle von Strassenprojekten	2015
1535	VSS 2012/403	Einfluss der Gesteinskörnung auf den Chloridwiderstand von Beton	2015
1534	VSS 2009/102	Forschungsbündel Erhebung verkehrsplanerischer Grundlagedaten: Teilprojekt 2: Methoden der Verkehrsbeobachtung	2015
1533	VSS 2009/101	Forschungsbündel Erhebung verkehrsplanerischer Grundlagedaten: Synthesebericht	2015
1532	VSS 2009/101	Forschungsbündel Erhebung verkehrsplanerischer Grundlagedaten: Teilprojekt 1: Systematik und Glossar	2015
1531	VSS 2011/906	Datenaustausch zwischen Strasseninformationssystemen und Verkehrsmodellen	2015
1530	VSS 2010/402	Einfluss biogener Öle auf die Ökobilanz von Strassenbaubindemittel	2015
1529	VSS 2005/404	Beschleunigte Alterungsmethode von heiss verarbeitbaren Fugenmassen zur Simulation des Einbaus	2015
1528	VSS 2011/308	Verkehrsablauf an ungesteuerten Knoten innerorts unter Berücksichtigung der verschiedenen Verkehrsarten; Ermittlung repräsentativer Richtwerte und Zusammenhänge	2015
1527	VSS 2006/510	Forschungspaket Brückenabdichtungen: Synthesebericht	2015
1526	VSS 2005/456	Paquet de recherche de recyclage des matériaux bitumineux de démolition des routes dans des enrobés à chaud : EP5: Formulation des enrobés avec matériaux recyclés	2015
1525	SVI 2004/058	Verträglichkeitskriterien für den Strassenraum innerorts	2015
1524	ASTRA 2012/003	Erarbeitung von Grundlagen zur Bemessung von Steinschlagschutzdämmen	2015
1523	VSS 2011/104	Monetarisierung des statistischen Lebens im Strassenverkehr	2015
1522	VSS 2011/106	Normierte gesamtverkehrliche Erschliessungsqualitäten - Grundlagenbericht	2015
1521	VSS 2006/514_OBF	Forschungspaket Brückenabdichtungen: EP4 - Zerstörungsfreie Prüfungen von Verbund und Oberflächen	2015
1520	ASTRA 2008/013_OBF	Nächtliche Immissionsprognosen von Strassenlärm (Hochleistungsstrassen)	2015
1519	VSS 2009/201	Lärmimmissionen bei Knoten und Kreiseln	2015

no. de rapport.	no. de projet	titre	année
1518	SVI 2011/024	Langsamverkehrsfreundliche Lichtsignalanlagen	2015
1517	VSS 2011/103	Bemessungsverkehrsstärken: Ein neuer Ansatz	2015
1516	VSS 2011/711	Forschungspaket Nutzensteigerung für die Anwender des SIS: EP1: Zeitaspekte und Historisierung	2015
1515	SVI 2011/034	Längere Umsteigezeiten und Haltestellenaufenthaltszeiten - Auswirkungen und Massnahmen	2015
1514	VSS 2006/513_OBF	Forschungspaket Brückenabdichtungen: EP3 - Langzeitverhalten des Verbundes	2015
1513	VSS 2005/403	Fliesskoeffizienten von feinen Gesteinskörnungen aus der Schweiz	2015
1512	SVI 2004/069	Veloverkehr in den Agglomerationen - Einflussfaktoren, Massnahmen und Potenziale	2015
1511	VSS 2012/601	Die Physik zwischen Salz, Schnee und Reifen	2015
1510	VSS 2005/453	Forschungspaket Recycling von Ausbauasphalt in Heissmischgut: EP2: Mehrfachrecycling von Strassenbelägen	2015
1509	ASTRA 2010/022	Markt- und Nutzermonitoring Elektromobilität (MANUEL)	2015
1508	VSS 2011/716	Forschungspaket Nutzensteigerung für die Anwender des SIS: EP6: Schnittstellen aus den Auswertungssystemen SIS (SIS-DWH)	2015
1507	FGU 2007/004	TBM Tunneling in Faulted and Folded Rocks	2015
1506	VSS 2006/512_OBF	Forschungspaket Brückenabdichtungen: EP2 - Flüssigkunststoff-Abdichtungen, Erfassen der Verbundproblematik	2015
1505	VSS 2006/509	Abdichtungssysteme und bitumenhaltige Schichten auf Betonbrücken - Initialprojekt	2014
1504	VSS 2005/504	Druckschwellversuch zur Beurteilung des Verformungsverhaltens von Belägen	2014
1503	VSS 2006/515_OBF	Research Package on Bridge Deck Waterproofing Systems: EP5-Mechanisms of Blister Formation	2014
1502	VSS 2010/502	Road – landside interaction : Applications	2014
1501	VSS 2011/705	Grundlagen zur Anwendung von Lebenszykluskosten im Erhaltungsmanagement von Strassenverkehrsanlagen	2014
1500	ASTRA 2010/007	SURPRICE (Sustainable mobility through road user charging) - Swiss contribution: Equity effects of congestion charges and intra-individual variation in preferences	2015
1499	ASTRA 2011/010	Stauprognoseverfahren und -systeme	2014
1498	VSS 2011/914	Coordinated Ramp Metering Control with Variable Speed Limits for Swiss Freeways	2014
1497	VSS 2009/705	Verfahren zur Bildung von homogenen Abschnitten der Strassenverkehrsanlage für das Erhaltungsmanagement Fahrbahnen	2014
1496	VSS 2010/601	Einfluss von Lärmschutzwänden auf das Raumnutzungsverhalten von Reptilien	2014
1495	VSS 2009/703	Zusammenhang Textur und Griffigkeit von Fahrbahnen und Einflüsse auf die Lärmemission	2014
1494	VSS 2010/704	Erhaltungsmanagement der Strassen - Erarbeiten der Grundlagen und Schadenkataloge zur systematischen Zustandserhebung und -bewertung von zusätzlichen Objekten der Strassen	2014
1493	VSS 2006/001	Neue Methoden zur Beurteilung der Tieftemperatureigenschaften von bitumenhaltigen Bindemitteln	2014
1492	SVI 2004/029	Kombiniertes Verkehrsmittel- und Routenwahlmodell	2014
1491	VSS 2007/704	Gesamtbewertung von Kunstbauten	2014
1490	FGU 2004/002	Langzeit-Beständigkeit von Tunnel-Abdichtungssystemen aus Kunststoffen (Best TASK)	2014
1489	VSS 2006/516_OBF	Forschungspaket Brückenabdichtungen: EP6 - Anschlüsse von Brückenabdichtungen	2014
1488	SVI 2007/020	Methodik zur Nutzenermittlung von Verkehrsdosierungen	2014
1487	SVI 2008/001	Erfahrungsbericht Forschungsbündel	2014
1486	SVI 2004/005	Partizipation in Verkehrsprojekten	2014
1485	VSS 2007/401	Anforderungen an Anschlussfugensysteme in Asphaltdecken - Teil 1: Praxiserfahrung	2014
1484	FGU 2010/003	Misestimating time of collision in the tunnel entrance due to a disturbed adaptation	2014
1483	VSS 2005/452	Forschungspaket Recycling von Ausbauasphalt in Heissmischgut: EP1: Optimaler Anteil an Ausbauasphalt	2014
1482	ASTRA 2010/018	SURPRICE: Sustainable mobility through road user charges Swiss contribution: Comprehensive road user charging (RUC)	2015

no. de rapport.	no. de projet	titre	année
1481	VSS 2001/702	Application des méthodes de représentation aux données routières	2014
1480	ASTRA 2008/004	Prozess- und wirkungsorientiertes Management im betrieblichen Strassenunterhalt Modell eines siedlungsübergreifenden Unterhalts	2014
1479	ASTRA 2005/004	Entscheidungsgrundlagen & Empfehlungen für ein nachhaltiges Baustoffmanagement	2014
1478	VSS 2005/455	Research Package on Recycling of Reclaimed Asphalt in Hot Mixes - EP4: Evaluation of Durability	2014
1477	VSS 2008/503	Feldversuch mit verschiedenen Pflästerungen und Plattendecken	2014
1476	VSS 2011/202	Projet initial pour la conception multi-usagers des carrefours	2014
1475	VSS 1999/125	Ringversuch "Eindringtiefe eines ebenen Stempels, statische Prüfung an Gussasphalt"	2014
1474	VSS 2009/704	Wechselwirkung zwischen Aufgrabungen, Zustand und Alterungsverhalten im kommunalen Strassennetz-Entwicklung eines nachhaltigen Aufgrabungsmanagement	2014
1473	VSS 2011/401	Forschungspaket "POLIGRIP - Einfluss der Polierbarkeit von Gesteinskörnungen auf die Griffigkeit von Deckschichten - Initialprojekt"	2014
1472	SVI 2010/003	Einfluss der Verlässlichkeit der Verkehrssysteme auf das Verkehrsverhalten	2014
1471	ASTRA 2008/011	Strategien zum wesensgerechten Einsatz der Verkehrsmittel im Güterverkehr Forschungspaket UVEK/ASTRA - Synthese	2014
1470	VSS 2011/907	Initialprojekt für ein Forschungspaket "Kooperative Systeme für Fahrzeug und Strasse"	2014
1469	VSS 2008/902	Untersuchungen zum Einsatz von Bewegungssensoren für fahrzeitbezogene Verkehrstelematik-Anwendungen	2014
1468	VSS 2010/503	Utilisation des géostructures énergétiques pour la régulation thermique et l'optimisation énergétique des infrastructures routières et ouvrages d'art	2014
1467	ASTRA 2010/021	Sekundärer Feinstaub vom Verkehr	2014
1466	VSS 2010/701	Grundlagen zur Revision der Normen über die visuelle Erhebung des Oberflächenzustands	2014
1465	ASTRA 2000/417	Erfahrungen mit der Sanierung und Erhaltung von Betonoberflächen	2014
1464	VSS 2002/403	Récupération de liants modifiés aux polymères issus d'échantillons d'enrobés	2014
1463	VSS 2006/511_OBF	Forschungspaket Brückenabdichtungen: EP1 – Standfester Gesamtaufbau, Prüfung und Bewertung	2014
1462	ASTRA 2011/004	Ermittlung der Versagensgrenze eines T2 Norm-Belages mit der mobiles Grossversuchsanlage MLS10	2014
1461	VSS 2001/506	Einfluss der Verdichtungstemperatur auf die Ergebnisse der Marshall-Prüfung und der Einbaukontrolle	2014
1460	SVI 2007/017	Nutzen der Verkehrsinformation für die Verkehrssicherheit	2014
1459	VSS 2002/501	Leichtes Fallgewichtsgerät für die Verdichtungskontrolle von Fundationsschichten	2014
1458	VSS 2010/703	Umsetzung Erhaltungsmanagement für Strassen in Gemeinden - Arbeitshilfen als Anhang zur Norm 640 980	2014
1457	SVI 2012/006	Forschungspaket VeSPA Teilprojekt 5: Medizinische Folgen des Strassenunfallgeschehens	2014
1456	SVI 2012/005	Fotschungspaket VeSPA Teilprojekt 4: Einflüsse des Wetters auf das Strassenunfallgeschehen	2014
1455	SVI 2012/004	Forschungspaket VeSPA Teilprojekt 3: Einflüsse von Fahrzeugeigenschaften auf das Strassenunfallgeschehen	2014
1454	SVI 2012/003	Forschungspaket VeSPA Teilprojekt 2: Einflüsse von Situation und Infrastruktur auf das Strassenunfallgeschehen: Phase 1	2014
1453	SVI 2012/002	Forschungspaket VeSPA Teilprojekt 1: Einflüsse von Mensch und Gesellschaft auf das Strassenunfallgeschehen: Phase 1	2014
1452	SVI 2012/001	Forschungspaket VeSPA: Synthesebericht Phase 1	2014
1451	FGU 2010/006	Gasanalytik zur frühzeitigen Branddetektion in Tunneln	2013
1450	VSS 2002/401	Kaltrecycling von Ausbauasphalt mit bituminösen Bindemitteln	2014
1449	ASTRA 2010/024	E-Scooter - Sozial- und naturwissenschaftliche Beiträge zur Förderung leichter Elektrofahrzeuge in der Schweiz	2013
1448	SVI 2009/008	Anforderungen der Güterlogistik an die Netzinfrastruktur und die langfristige Netzentwicklung in der Schweiz. Forschungspaket UVEK/ASTRA "Strategien zum	2014

no. de rapport.	no. de projet	titre	année
		wesensgerechten Einsatz der Verkehrsmittel im Güterverkehr der Schweiz", Teilprojekt C	
1447	SVI 2009/005	Informationstechnologien in der zukünftigen Gütertransportwirtschaft Forschungspaket UVEK/ASTRA "Strategien zum wesensgerechten Einsatz der Verkehrsmittel im Güterverkehr der Schweiz", Teilprojekt E	2013
1446	VSS 2005/454	Forschungspaket Recycling von Ausbauasphalt in Heissmischgut: EP3: Stoffffluss- und Nachhaltigkeitsbeurteilung	2013
1445	VSS 2009/301	Öffnung der Busstreifen für weitere Verkehrsteilnehmende	2013
1444	VSS 2007/306	Verkehrsqualität und Leistungsfähigkeit von Anlagen des leichten Zweirad- und des Fussgängerverkehrs	2013
1443	VSS 2007/305	Verkehrsqualität und Leistungsfähigkeit des strassengebundenen ÖV	2013
1442	SVI 2010/004	Messen des Nutzens von Massnahmen mit Auswirkungen auf den Langsamverkehr - Vorstudie	2013
1441_2	SVI 2009/010	Zielsystem im Güterverkehr. Forschungspaket UVEK/ASTRA Strategien zum wesensgerechten Einsatz der Verkehrsmittel im Güterverkehr der Schweiz - Teilprojekt G	2013
1441_1	SVI 2009/010	Effizienzsteigerungspotenziale in der Transportwirtschaft durch integrierte Bewirtschaftungsinstrumente aus Sicht der Infrastrukturbetreiber Synthese der Teilprojekte B3, C, D, E und F des Forschungspakets Güterverkehr anhand eines Zielsystems für den Güterverkehr	2013
1440	SVI 2009/006	Benchmarking-Ansätze im Verkehrswesen	2013
1439	SVI 2009/002	Konzept zur effizienten Erfassung und Analyse der Güterverkehrsdaten Forschungspaket UVEK/ASTRA Strategien zum wesensgerechten Einsatz von Verkehrsmitteln im Güterverkehr der Schweiz TP A	2013
1438_2	SVI 2009/011	Ortsbezogene Massnahmen zur Reduktion der Auswirkungen des Güterverkehrs - Teil 2. Forschungspaket UVEK/ASTRA Strategien zum wesensgerechten Einsatz der Verkehrsmittel im Güterverkehr der Schweiz TP H	2013
1438_1	SVI 2009/011	Ortsbezogene Massnahmen zur Reduktion der Auswirkungen des Güterverkehrs - Teil 1. Forschungspaket UVEK/ASTRA Strategien zum wesensgerechten Einsatz der Verkehrsmittel im Güterverkehr der Schweiz TP H	2013
1437	VSS 2008/203	Trottoirüberfahrten und punktuelle Querungen ohne Vortritt für den Langsamverkehr	2013
1436	VSS 2010/401	Auswirkungen verschiedener Recyclinganteile in ungebundenen Gemischen	2013
1435	FGU 2008/007_OBF	Schadstoff- und Rauchkurzschlüsse bei Strassentunneln	2013
1434	VSS 2006/503	Performance Oriented Requirements for Bitumainous Mixtures	2013
1433	ASTRA 2010/001	Güterverkehr mit Lieferwagen: Entwicklungen und Massnahmen Forschungspaket UVEK/ASTRA Strategien zum wesensgerechten Einsatz der Verkehrsmittel im Güterverkehr der Schweiz TP B3	2013
1432	ASTRA 2007/011	Praxis-Kalibrierung der neuen mobilen Grossversuchanlage MLS10 für beschleunigte Verkehrslastsimulation auf Strassenbelägen in der Schweiz	2013
1431	ASTRA 2011/015	TeVeNOx - Testing of SCR-Systems on HD-Vehicles	2013
1430	ASTRA 2009/004	Impact des conditions météorologiques extrêmes sur la chaussée	2013
1429	SVI 2009/009	Einschätzungen der Infrastrukturnutzer zur Weiterentwicklung des Regulativs Forschungspaket UVEK/ASTRA Strategien zum wesensgerechten Einsatz der Verkehrsmittel im Güterverkehr der Schweiz TP F	2013
1428	SVI 2010/005	Branchenspezifische Logistikkonzepte und Güterverkehrsaufkommen sowie deren Trends Forschungspaket UVEK/ASTRA Strategien zum wesensgerechten Einsatz der Verkehrsmittel im Güterverkehr der Schweiz TP B2	2013
1427	SVI 2006/002	Begegnungszonen - eine Werkschau mit Empfehlungen für die Realisierung	2013
1426	ASTRA 2010/025_OBF	Luftströmungsmessung in Strassentunneln	2013
1425	VSS 2005/401	Résistance à l'altération des granulats et des roches	2013
1424	ASTRA 2006/007	Optimierung der Baustellenplanung an Autobahnen	2013

no. de rapport.	no. de projet	titre	année
1423	ASTRA 2010/012	Forschungspaket: Lärmarme Beläge innerorts EP3: Betrieb und Unterhalt lärmarmer Beläge	2013
1422	ASTRA 2011/006_OBF	Fracture processes and in-situ fracture observations in Gipskeuper	2013
1421	VSS 2009/901	Experimenteller Nachweis des vorgeschlagenen Raum- und Topologiemodells für die VM-Anwendungen in der Schweiz (MDATrafo)	2013
1420	SVI 2008/003	Projektierungsfreiräume bei Strassen und Plätzen	2013
1419	VSS 2001/452	Stabilität der Polymere beim Heisseinbau von PmB-haltigen Strassenbelägen	2013
1418	VSS 2008/402	Anforderungen an hydraulische Eigenschaften von Geokunststoffen	2012
1417	FGU 2009/002	Heat Exchanger Anchors for Thermo-active Tunnels	2013
1416	FGU 2010/001	Sulfatwiderstand von Beton: verbessertes Verfahren basierend auf der Prüfung nach SIA 262/1, Anhang D	2013
1415	VSS 2010/A01	Wissenslücken im Infrastrukturmanagementprozess "Strasse" im Siedlungsgebiet	2013
1414	VSS 2010/201	Passive Sicherheit von Tragkonstruktionen der Strassenausstattung	2013
1413	SVI 2009/003	Güterverkehrsintensive Branchen und Güterverkehrsströme in der Schweiz Forschungspaket UVEK/ASTRA Strategien zum wesensgerechten Einsatz der Verkehrsmittel im Güterverkehr der Schweiz Teilprojekt B1	2013
1412	ASTRA 2010/020	Werkzeug zur aktuellen Gangliniennorm	2013
1411	VSS 2009/902	Verkehrstelematik für die Unterstützung des Verkehrsmanagements in ausserordentlichen Lagen	2013
1410	VSS 2010/202_OBF	Reduktion von Unfallfolgen bei Bränden in Strassentunneln durch Abschnittsbildung	2013
1409	ASTRA 2010/017_OBF	Regelung der Luftströmung in Strassentunneln im Brandfall	2013
1408	VSS 2000/434	Vieillissement thermique des enrobés bitumineux en laboratoire	2012
1407	ASTRA 2006/014	Fusion des indicateurs de sécurité routière : FUSAIN	2012
1406	ASTRA 2004/015	Amélioration du modèle de comportement individuell du Conducteur pour évaluer la sécurité d'un flux de trafic par simulation	2012
1405	ASTRA 2010/009	Potential von Photovoltaik an Schallschutzmassnahmen entlang der Nationalstrassen	2012
1404	VSS 2009/707	Validierung der Kosten-Nutzen-Bewertung von Fahrbahn-Erhaltungsmassnahmen	2012
1403	SVI 2007/018	Vernetzung von HLS- und HVS-Steuerungen	2012
1402	VSS 2008/403	Witterungsbeständigkeit und Durchdrückverhalten von Geokunststoffen	2012
1401	SVI 2006/003	Akzeptanz von Verkehrsmanagementmassnahmen-Vorstudie	2012
1400	VSS 2009/601	Begrünte Stützgitterböschungssysteme	2012
1399	VSS 2011/901	Erhöhung der Verkehrssicherheit durch Incentivierung	2012
1398	ASTRA 2010/019	Environmental Footprint of Heavy Vehicles Phase III: Comparison of Footprint and Heavy Vehicle Fee (LSVA) Criteria	2012
1397	FGU 2008/003_OBF	Brandschutz im Tunnel: Schutzziele und Brandbemessung Phase 1: Stand der Technik	2012
1396	VSS 1999/128	Einfluss des Umhüllungsgrades der Mineralstoffe auf die mechanischen Eigenschaften von Mischgut	2012
1395	FGU 2009/003	KarstALEA: Wegleitung zur Prognose von karstspezifischen Gefahren im Untertagbau	2012
1394	VSS 2010/102	Grundlagen Betriebskonzepte	2012
1393	VSS 2010/702	Aktualisierung SN 640 907, Kostengrundlage im Erhaltungsmanagement	2012
1392	ASTRA 2008/008_009	FEHRL Institutes WIM Initiative (Fiwi)	2012
1391	ASTRA 2011/003	Leitbild ITS-CH Landverkehr 2025/30	2012
1390	FGU 2008/004_OBF	Einfluss der Grundwasserströmung auf das Quellverhalten des Gipskeupers im Belchentunnel	2012
1389	FGU 2003/002	Long Term Behaviour of the Swiss National Road Tunnels	2012
1388	SVI 2007/022	Möglichkeiten und Grenzen von elektronischen Busspuren	2012
1387	VSS 2010/205_OBF	Ablage der Prozessdaten bei Tunnel-Prozessleitsystemen	2012
1386	VSS 2006/204	Schallreflexionen an Kunstbauten im Strassenbereich	2012

no. de rapport.	no. de projet	titre	année
1385	VSS 2004/703	Bases pour la révision des normes sur la mesure et l'évaluation de la planéité des chaussées	2012
1384	VSS 1999/249	Konzeptuelle Schnittstellen zwischen der Basisdatenbank und EMF-, EMK- und EMT-DB	2012
1383	FGU 2008/005	Einfluss der Grundwasserströmung auf das Quellverhalten des Gipskeupers im Chienbergtunnel	2012
1382	VSS 2001/504	Optimierung der statischen Eindringtiefe zur Beurteilung von harten Gussasphaltsorten	2012
1381	SVI 2004/055	Nutzen von Reisezeiteinsparungen im Personenverkehr	2012
1380	ASTRA 2007/009	Wirkungsweise und Potential von kombinierter Mobilität	2012
1379	VSS 2010/206_OBF	Harmonisierung der Abläufe und Benutzeroberflächen bei Tunnel-Prozessleitsystemen	2012
1378	SVI 2004/053	Mehr Sicherheit dank Kernfahrbahnen?	2012
1377	VSS 2009/302	Verkehrssicherheitsbeurteilung bestehender Verkehrsanlagen (Road Safety Inspection)	2012
1376	ASTRA 2011/008_004	Erfahrungen im Schweizer Betonbrückenbau	2012
1375	VSS 2008/304	Dynamische Signalisierungen auf Hauptverkehrsstrassen	2012
1374	FGU 2004/003	Entwicklung eines zerstörungsfreien Prüfverfahrens für Schweissnähte von KDB	2012
1373	VSS 2008/204	Vereinheitlichung der Tunnelbeleuchtung	2012
1372	SVI 2011/001	Verkehrssicherheitsgewinne aus Erkenntnissen aus Datapooling und strukturierten Datenanalysen	2012
1371	ASTRA 2008/017	Potenzial von Fahrgemeinschaften	2011
1370	VSS 2008/404	Dauerhaftigkeit von Betonfahrbahnen aus Betongranulat	2011
1369	VSS 2003/204	Rétention et traitement des eaux de chaussée	2012
1368	FGU 2008/002	Soll sich der Mensch dem Tunnel anpassen oder der Tunnel dem Menschen?	2011
1367	VSS 2005/801	Grundlagen betreffend Projektierung, Bau und Nachhaltigkeit von Anschlussgleisen	2011
1366	VSS 2005/702	Überprüfung des Bewertungshintergrundes zur Beurteilung der Strassengriffigkeit	2010
1365	SVI 2004/014	Neue Erkenntnisse zum Mobilitätsverhalten dank Data Mining?	2011
1364	SVI 2009/004	Regulierung des Güterverkehrs Auswirkungen auf die Transportwirtschaft Forschungspaket UVEK/ASTRA Strategien zum wesensgerechten Einsatz der Verkehrsmittel im Güterverkehr der Schweiz TP D	2012
1363	VSS 2007/905	Verkehrsprognosen mit Online -Daten	2011
1362	SVI 2004/012	Aktivitätenorientierte Analyse des Neuverkehrs	2012
1361	SVI 2004/043	Innovative Ansätze der Parkraumbewirtschaftung	2012
1360	VSS 2010/203	Akustische Führung im Strassentunnel	2012
1359	SVI 2004/003	Wissens- und Technologientransfer im Verkehrsbereich	2012
1358	SVI 2004/079	Verkehrsanbindung von Freizeitanlagen	2012
1357	SVI 2007/007	Unaufmerksamkeit und Ablenkung: Was macht der Mensch am Steuer?	2012
1356	SVI 2007/014	Kooperation an Bahnhöfen und Haltestellen	2011
1355	FGU 2007/002	Prüfung des Sulfatwiderstandes von Beton nach SIA 262/1, Anhang D: Anwendbarkeit und Relevanz für die Praxis	2011
1354	VSS 2003/203	Anordnung, Gestaltung und Ausführung von Treppen, Rampen und Treppenwegen	2011
1353	VSS 2000/368	Grundlagen für den Fussverkehr	2011
1352	VSS 2008/302	Fussgängerstreifen (Grundlagen)	2011
1351	ASTRA 2009/001	Development of a best practice methodology for risk assessment in road tunnels	2011
1350	VSS 2007/904	IT-Security im Bereich Verkehrstelematik	2011
1349	VSS 2003/205	In-Situ-Abflussversuche zur Untersuchung der Entwässerung von Autobahnen	2011
1348	VSS 2008/801	Sicherheit bei Parallelführung und Zusammentreffen von Strassen mit der Schiene	2011
1347	VSS 2000/455	Leistungsfähigkeit von Parkierungsanlagen	2010
1346	ASTRA 2007/004	Quantifizierung von Leckagen in Abluftkanälen bei Strassentunneln mit konzentrierter Rauchabsaugung	2010
1345	SVI 2004/039	Einsatzbereiche verschiedener Verkehrsmittel in Agglomerationen	2011

no. de rapport.	no. de projet	titre	année
1344	VSS 2009/709	Initialprojekt für das Forschungspaket "Nutzensteigerung für die Anwender des SIS"	2011
1343	VSS 2009/903	Basistechnologien für die intermodale Nutzungserfassung im Personenverkehr	2011
1342	FGU 2005/003	Untersuchungen zur Frostkörperbildung und Frosthebung beim Gefrierverfahren	2010
1341	FGU 2007/005	Design aids for the planning of TBM drives in squeezing ground	2011
1340	SVI 2004/051	Aggressionen im Verkehr	2011
1339	SVI 2005/001	Widerstandsfunktionen für Innerorts-Strassenabschnitte ausserhalb des Einflussbereiches von Knoten	2010
1338	VSS 2006/902	Wirkungsmodelle für fahrzeugseitige Einrichtungen zur Steigerung der Verkehrssicherheit	2009
1337	ASTRA 2006/015	Development of urban network travel time estimation methodology	2011
1336	ASTRA 2007/006	SPIN-ALP: Scanning the Potential of Intermodal Transport on Alpine Corridors	2010
1335	VSS 2007/502	Stripping bei lärmmindernden Deckschichten unter Überrollbeanspruchung im Labormassstab	2011
1334	ASTRA 2009/009	Was treibt uns an? Antriebe und Treibstoffe für die Mobilität von Morgen	2011
1333	SVI 2007/001	Standards für die Mobilitätsversorgung im peripheren Raum	2011
1332	VSS 2006/905	Standardisierte Verkehrsdaten für das verkehrsträgerübergreifende Verkehrsmanagement	2011
1331	VSS 2005/501	Rückrechnung im Strassenbau	2011
1330	FGU 2008/006	Energiegewinnung aus städtischen Tunneln: Systemeevaluation	2010
1329	SVI 2004/073	Alternativen zu Fussgängerstreifen in Tempo-30-Zonen	2010
1328	VSS 2005/302	Grundlagen zur Quantifizierung der Auswirkungen von Sicherheitsdefiziten	2011
1327	VSS 2006/601	Vorhersage von Frost und Nebel für Strassen	2010
1326	VSS 2006/207	Erfolgskontrolle Fahrzeugrückhaltesysteme	2011
1325	SVI 2000/557	Indices caractéristiques d'une cité-vélo. Méthode d'évaluation des politiques cyclables en 8 indices pour les petites et moyennes communes.	2010
1324	VSS 2004/702	Eigenheiten und Konsequenzen für die Erhaltung der Strassenverkehrsanlagen im überbauten Gebiet	2009
1323	VSS 2008/205	Ereignisdetektion im Strassentunnel	2011
1322	SVI 2005/007	Zeitwerte im Personenverkehr: Wahrnehmungs- und Distanzabhängigkeit	2008
1321	VSS 2008/501	Validation de l'oedomètre CRS sur des échantillons intacts	2010
1320	VSS 2007/303	Funktionale Anforderungen an Verkehrserfassungssysteme im Zusammenhang mit Lichtsignalanlagen	2010
1319	VSS 2000/467	Auswirkungen von Verkehrsberuhigungsmassnahmen auf die Lärmimmissionen	2010
1318	FGU 2006/001	Langzeitquellversuche an anhydritführenden Gesteinen	2010
1317	VSS 2000/469	Geometrisches Normalprofil für alle Fahrzeugtypen	2010
1316	VSS 2001/701	Objektorientierte Modellierung von Strasseninformationen	2010
1315	VSS 2006/904	Abstimmung zwischen individueller Verkehrsinformation und Verkehrsmanagement	2010
1314	VSS 2005/203	Datenbank für Verkehrsaufkommensraten	2008
1313	VSS 2001/201	Kosten-/Nutzenbetrachtung von Strassenentwässerungssystemen, Ökobilanzierung	2010
1312	SVI 2004/006	Der Verkehr aus Sicht der Kinder: Schulwege von Primarschulkindern in der Schweiz	2010
1311	VSS 2000/543	VIABILITE DES PROJETS ET DES INSTALLATIONS ANNEXES	2010
1310	ASTRA 2007/002	Beeinflussung der Luftströmung in Strassentunneln im Brandfall	2010
1309	VSS 2008/303	Verkehrsregelungssysteme - Modernisierung von Lichtsignalanlagen	2010
1308	VSS 2008/201	Hindernisfreier Verkehrsraum - Anforderungen aus Sicht von Menschen mit Behinderung	2010
1307	ASTRA 2006/002	Entwicklung optimaler Mischgüter und Auswahl geeigneter Bindemittel; D-A-CH - Initialprojekt	2008
1306	ASTRA 2008/002	Strassenglätte-Prognosesystem (SGPS)	2010
1305	VSS 2000/457	Verkehrserzeugung durch Parkierungsanlagen	2009
1304	VSS 2004/716	Massnahmenplanung im Erhaltungsmanagement von Fahrbahnen	2008

no. de rapport.	no. de projet	titre	année
1303	ASTRA 2009/010	Geschwindigkeiten in Steigungen und Gefällen; Überprüfung	2010
1302	VSS 1999/131	Zusammenhang zwischen Bindemitteleigenschaften und Schadensbildern des Belages?	2010
1301	SVI 2007/006	Optimierung der Strassenverkehrsunfallstatistik durch Berücksichtigung von Daten aus dem Gesundheitswesen	2009
1300	VSS 2003/903	SATELROU Perspectives et applications des méthodes de navigation pour la télématique des transports routiers et pour le système d'information de la route	2010
1299	VSS 2008/502	Projet initial - Enrobés bitumineux à faibles impacts énergétiques et écologiques	2009
1298	ASTRA 2007/012	Griffigkeit auf winterlichen Fahrbahnen	2010
1297	VSS 2007/702	Einsatz von Asphaltbewehrungen (Asphalteinlagen) im Erhaltungsmanagement	2009
1296	ASTRA 2007/008	Swiss contribution to the Heavy-Duty Particle Measurement Programme (HD-PMP)	2010
1295	VSS 2005/305	Entwurfsgrundlagen für Lichtsignalanlagen und Leitfaden	2010
1294	VSS 2007/405	Wiederhol- und Vergleichspräzision der Druckfestigkeit von Gesteinskörnungen am Haufwerk	2010
1293	VSS 2005/402	Détermination de la présence et de l'efficacité de dope dans les bétons bitumineux	2010
1292	ASTRA 2006/004	Entwicklung eines Pflanzenöl-Blockheizkraftwerkes mit eigener Ölmühle	2010
1291	ASTRA 2009/005	Fahrmuster auf überlasteten Autobahnen Simultanes Berechnungsmodell für das Fahrverhalten auf Autobahnen als Grundlage für die Berechnung von Schadstoffemissionen und Fahrzeitgewinnen	2010
1290	VSS 1999/209	Conception et aménagement de passages inférieurs et supérieurs pour piétons et deux-roues légers	2008
1289	VSS 2005/505	Affinität von Gesteinskörnungen und Bitumen, nationale Umsetzung der EN	2010
1288	ASTRA 2006/020	Footprint II - Long Term Pavement Performance and Environmental Monitoring on A1	2010
1287	VSS 2008/301	Verkehrsqualität und Leistungsfähigkeit von komplexen ungesteuerten Knoten: Analytisches Schätzverfahren	2009
1286	VSS 2000/338	Verkehrsqualität und Leistungsfähigkeit auf Strassen ohne Richtungstrennung	2010
1285	VSS 2002/202	In-situ Messung der akustischen Leistungsfähigkeit von Schallschirmen	2009
1284	VSS 2004/203	Evacuation des eaux de chaussée par les bas-cotés	2010
1283	VSS 2000/339	Grundlagen für eine differenzierte Bemessung von Verkehrsanlagen	2008
1282	VSS 2004/715	Massnahmenplanung im Erhaltungsmanagement von Fahrbahnen: Zusatzkosten infolge Vor- und Aufschub von Erhaltungsmassnahmen	2010
1281	SVI 2004/002	Systematische Wirkungsanalysen von kleinen und mittleren Verkehrsvorhaben	2009
1280	ASTRA 2004/016	Auswirkungen von fahrzeuginternen Informationssystemen auf das Fahrverhalten und die Verkehrssicherheit Verkehrspsychologischer Teilbericht	2010
1279	VSS 2005/301	Leistungsfähigkeit zweistreifiger Kreisel	2009
1278	ASTRA 2004/016	Auswirkungen von fahrzeuginternen Informationssystemen auf das Fahrverhalten und die Verkehrssicherheit - Verkehrstechnischer Teilbericht	2009
1277	SVI 2007/005	Multimodale Verkehrsqualitätsstufen für den Strassenverkehr - Vorstudie	2010
1276	VSS 2006/201	Überprüfung der schweizerischen Ganglinien	2008
1275	ASTRA 2006/016	Dynamic Urban Origin - Destination Matrix - Estimation Methodology	2009
1274	SVI 2004/088	Einsatz von Simulationswerkzeugen in der Güterverkehrs- und Transportplanung	2009

no. de rapport.	no. de projet	titre	année
1273	ASTRA 2008/006	UNTERHALT 2000 - Massnahme M17, FORSCHUNG: Dauerhafte Materialien und Verfahren SYNTHESE - BERICHT zum Gesamtprojekt "Dauerhafte Beläge" mit den Einzelnen Forschungsprojekten: - ASTRA 200/419: Verhaltensbilanz der Beläge auf Nationalstrassen - ASTRA 2000/420: Dauerhafte Komponenten auf der Basis erfolgreicher Strecken - ASTRA 2000/421: Durabilité des enrobés - ASTRA 2000/422: Dauerhafte Beläge, Rundlaufversuch - ASTRA 2000/423: Griffigkeit der Beläge auf Autobahnen, Vergleich zwischen den Messergebnissen von SRM und SCRIM - ASTRA 2008/005: Vergleichsstrecken mit unterschiedlichen oberen Tragschichten auf einer Nationalstrasse	2008
1272	VSS 2007/304	Verkehrsregelungssysteme - behinderte und ältere Menschen an Lichtsignalanlagen	2010
1271	VSS 2004/201	Unterhalt von Lärmschirmen	2009
1270	VSS 2005/502	Interaktion Strasse Hangstabilität: Monitoring und Rückwärtsrechnung	2009
1269	VSS 2005/201	Evaluation von Fahrzeugrückhaltesystemen im Mittelstreifen von Autobahnen	2009
1268	ASTRA 2005/007	PM10-Emissionsfaktoren von Abriebspartikeln des Strassenverkehrs (APART)	2009
1267	VSS 2007/902	MDAinSVT Einsatz modellbasierter Datentransfernormen (INTERLIS) in der Strassenverkehrstelematik	2009
1266	VSS 2000/343	Unfall- und Unfallkostenraten im Strassenverkehr	2009
1265	VSS 2005/701	Zusammenhang zwischen dielektrischen Eigenschaften und Zustandsmerkmalen von bitumenhaltigen Fahrbahnbelägen (Pilotuntersuchung)	2009
1264	SVI 2004/004	Verkehrspolitische Entscheidfindung in der Verkehrsplanung	2009
1263	VSS 2001/503	Phénomène du dégel des sols gélifs dans les infrastructures des voies de communication et les pergélisols alpins	2006
1262	VSS 2003/503	Lärmverhalten von Deckschichten im Vergleich zu Gussasphalt mit strukturierter Oberfläche	2009
1261	ASTRA 2004/018	Pilotstudie zur Evaluation einer mobilen Grossversuchsanlage für beschleunigte Verkehrslastsimulation auf Strassenbelägen	2009
1260	FGU 2005/001	Testeinsatz der Methodik "Indirekte Vorauserkundung von wasserführenden Zonen mittels Temperaturdaten anhand der Messdaten des Lötschberg-Basistunnels	2009
1259	VSS 2004/710	Massnahmenplanung im Erhaltungsmanagement von Fahrbahnen - Synthesebericht	2008
1258	VSS 2005/802	Kaphaltestellen Anforderungen und Auswirkungen	2009
1257	SVI 2004/057	Wie Strassenraumbilder den Verkehr beeinflussen Der Durchfahrtswiderstand als Arbeitsinstrument bei der städtebaulichen Gestaltung von Strassenräumen	2009
1256	VSS 2006/903	Qualitätsanforderungen an die digitale Videobild-Bearbeitung zur Verkehrsüberwachung	2009
1255	VSS 2006/901	Neue Methoden zur Erkennung und Durchsetzung der zulässigen Höchstgeschwindigkeit	2009
1254	VSS 2006/502	Drains verticaux préfabriqués thermiques pour la consolidation in-situ des sols	2009
1253	VSS 2001/203	Rétention des polluants des eaux de chausées selon le système "infilitrations sur les talus". Vérification in situ et optimisation	2009
1252	SVI 2003/001	Nettoverkehr von verkehrsintensiven Einrichtungen (VE)	2009
1251	ASTRA 2002/405	Incidence des granulats arrondis ou partiellement arrondis sur les propriétés d'ahérence des bétons bitumineux	2008
1250	VSS 2005/202	Strassenabwasser Filterschacht	2007
1249	FGU 2003/004	Einflussfaktoren auf den Brandwiderstand von Betonkonstruktionen	2009
1248	VSS 2000/433	Dynamische Eindringtiefe zur Beurteilung von Gussasphalt	2008
1247	VSS 2000/348	Anforderungen an die strassenseitige Ausrüstung bei der Umwidmung von Standstreifen	2009

no. de rapport.	no. de projet	titre	année
1246	VSS 2004/713	Massnahmenplanung im Erhaltungsmanagement von Fahrbahnen: Bedeutung Oberflächenzustand und Tragfähigkeit sowie gegenseitige Beziehung für Gebrauchs- und Substanzwert	2009
1245	VSS 2004/701	Verfahren zur Bestimmung des Erhaltungsbedarfs in kommunalen Strassennetzen	2009
1244	VSS 2004/714	Massnahmenplanung im Erhaltungsmanagement von Fahrbahnen - Gesamtnutzen und Nutzen-Kosten-Verhältnis von standardisierten Erhaltungsmassnahmen	2008
1243	VSS 2000/463	Kosten des betrieblichen Unterhalts von Strassenanlagen	2008
1242	VSS 2005/451	Recycling von Ausbauasphalt in Heissmischgut	2007
1241	ASTRA 2001/052	Erhöhung der Aussagekraft des LCPC Spurbildungstests	2009
1240	ASTRA 2002/010	L'acceptabilité du péage de congestion : Résultats et analyse de l'enquête en Suisse	2009
1239	VSS 2000/450	Bemessungsgrundlagen für das Bewehren mit Geokunststoffen	2009
1238	VSS 2005/303	Verkehrssicherheit an Tagesbaustellen und bei Anschlüssen im Baustellenbereich von Hochleistungsstrassen	2008
1237	VSS 2007/903	Grundlagen für eCall in der Schweiz	2009
1236	ASTRA 2008/008_07	Analytische Gegenüberstellung der Strategie- und Tätigkeitsschwerpunkte ASTRA-AIPCR	2008
1235	VSS 2004/711	Forschungspaket Massnahmenplanung im EM von Fahrbahnen - Standardisierte Erhaltungsmassnahmen	2008
1234	VSS 2006/504	Expérimentation in situ du nouveau drainomètre européen	2008
1233	ASTRA 2000/420	Unterhalt 2000 Forschungsprojekt FP2 Dauerhafte Komponenten bitumenhaltiger Belagsschichten	2009
676	AGB 2011/002	Modelling the corrosion initiation of reinforced concrete exposed to deicing salts	2016
674	AGB 2010/006	Einfluss des Asphaltbelages auf die Dynamik von Fussgängerbrücken aus Beton und Stahl	2015
673	AGB 2006/017	Dynamic structural capacity of reinforced concrete slabs due to rockfall	2015
671	AGB 2009/008	Résistance à l'effort tranchant de dalles de roulement sous actions statiques et de fatigue	2015
670	AGB 2012/013	Optimierung und Validierung von Verfahren zur Bestimmung der Korrisionsgeschwindigkeit in Stahlbeton	2015
669	AGB 2008/007	Zentrale Dokumentation der mechanischen Eigenschaften alter Bewehrungen	2015
668	AGB 2009/004_OBF	Multifunktionaler Hochleistungsoberflächenschutz für Kunstbauten	2015
667	AGB 2008/004	Résistance au déversement des poutres métalliques de pont	2015
666	AGB 2012/015	Structural Identification for Condition Assessment of Swiss Bridges	2015
665	AGB 2011/001	Wirksamkeit und Prüfung der Nachbehandlungsmethoden von Beton	2014
664	AGB 2009/005	Charges de trafic actualisées pour les dalles de roulement en béton des ponts existants	2014
663	AGB 2003/014	Seismic Safety of Existing Bridges	2014
662	AGB 2008/001	Seismic Safety of Existing Bridges - Cyclic Inelastic Behaviour of Bridge Piers	2014
661	AGB 2010/002	Fatigue limit state of shear studs in steel-concrete composite road bridges	2014
660	AGB 2008/002	Indirekt gelagerte Betonbrücken - Sachstandsbericht	2014
659	AGB 2009/014	Suizidprävention bei Brücken: Follow-Up	2014
658	AGB 2006/015_OBF	Querkraftwiderstand vorgespannter Brücken mit ungenügender Querkraftbewehrung	2014
657	AGB 2003/012	Brücken in Holz: Möglichkeiten und Grenzen	2013
656	AGB 2009/015	Experimental verification oif integral bridge abutments	2013
655	AGB 2007/004	Fatigue Life Assessment of Roadway Bridges Based on Actual Traffic Loads	2013
654	AGB 2005-008	Thermophysical and Thermomechanical Behavior of Cold-Curing Structural Adhesives in Bridge Construction	2013
653	AGB 2007/002	Poinçonnement des pontsdalles précontraints	2013
652	AGB 2009/006	Detektion von Betonstahlbrüchen mit der magnetischen Streufeldmethode	2013
651	AGB 2006/006_OBF	Instandsetzung und Monitoring von AAR-geschädigten Stützmauern und Brücken	2013
650	AGB 2005/010	Korrosionsbeständigkeit von nichtrostenden Betonstählen	2012
649	AGB 2008/012	Anforderungen an den Karbonatisierungswiderstand von Betonen	2012

no. de rapport.	no. de projet	titre	année
648	AGB 2005/023 + AGB 2006/003	Validierung der AAR-Prüfungen für Neubau und Instandsetzung	2011
647	AGB 2004/010	Quality Control and Monitoring of electrically isolated post- tensioning tendons in bridges	2011
646	AGB 2005/018	Interactin sol-structure : ponts à culées intégrales	2010
645	AGB 2005/021	Grundlagen für die Verwendung von Recyclingbeton aus Betongranulat	2010
644	AGB 2005/004	Hochleistungsfähiger Faserfeinkornbeton zur Effizienzsteigerung bei der Erhaltung von Kunstbauten aus Stahlbeton	2010
643	AGB 2005/014	Akustische Überwachung einer stark geschädigten Spannbetonbrücke und Zustandserfassung beim Abbruch	2010
642	AGB 2002/006	Verbund von Spanngliedern	2009
641	AGB 2007/007	Empfehlungen zur Qualitätskontrolle von Beton mit Luftpermeabilitätsmessungen	2009
640	AGB 2003/011	Nouvelle méthode de vérification des ponts mixtes à âme pleine	2010
639	AGB 2008/003	RiskNow-Falling Rocks Excel-basiertes Werkzeug zur Risikoermittlung bei Steinschlagschutzgalerien	2010
638	AGB2003/003	Ursachen der Rissbildung in Stahlbetonbauwerken aus Hochleistungsbeton und neue Wege zu deren Vermeidung	2008
637	AGB 2005/009	Détermination de la présence de chlorures à l'aide du Géoradar	2009
636	AGB 2002/028	Dimensionnement et vérification des dalles de roulement de ponts routiers	2009
635	AGB 2004/002	Applicabilité de l'enrobé drainant sur les ouvrages d'art du réseau des routes nationales	2008
634	AGB 2002/007	Untersuchungen zur Potenzialfeldmessung an Stahlbetonbauten	2008
633	AGB 2002/014	Oberflächenschutzsysteme für Betontragwerke	2008
632	AGB 2008/201	Sicherheit des Verkehrssystem Strasse und dessen Kunstbauten Testregion - Methoden zur Risikobeurteilung Schlussbericht	2010
631	AGB 2000/555	Applications structurales du Béton Fibré à Ultra-hautes Performances aux ponts	2008
630	AGB 2002/016	Korrosionsinhibitoren für die Instandsetzung chloridverseuchter Stahlbetonbauten	2010
629	AGB 2003/001 + AGB 2005/019	Integrale Brücken - Sachstandsbericht	2008
628	AGB 2005/026	Massnahmen gegen chlorid-induzierte Korrosion und zur Erhöhung der Dauerhaftigkeit	2008
627	AGB 2002/002	Eigenschaften von normalbreiten und überbreiten Fahrbahnübergängen aus Polymerbitumen nach starker Verkehrsbelastung	2008
626	AGB 2005/110	Sicherheit des Verkehrssystems Strasse und dessen Kunstbauten: Baustellensicherheit bei Kunstbauten	2009
625	AGB 2005/109	Sicherheit des Verkehrssystems Strasse und dessen Kunstbauten: Effektivität und Effizienz von Massnahmen bei Kunstbauten	2009
624	AGB 2005/108	Sicherheit des Verkehrssystems / Strasse und dessen Kunstbauten / Risikobeurteilung für Kunstbauten	2010
623	AGB 2005/107	Sicherheit des Verkehrssystems Strasse und dessen Kunstbauten: Tragsicherheit der bestehenden Kunstbauten	2009
622	AGB 2005/106	Rechtliche Aspekte eines risiko- und effizienzbasierten Sicherheitskonzepts	2009
621	AGB 2005/105	Sicherheit des Verkehrssystems Strasse und dessen Kunstbauten Szenarien der Gefahrenentwicklung	2009
620	AGB 2005/104	Sicherheit des Verkehrssystems Strasse und dessen Kunstbauten: Effektivität und Effizienz von Massnahmen	2009
619	AGB 2005/103	Sicherheit des Verkehrssystems / Strasse und dessen Kunstbauten / Ermittlung des Netzrisikos	2010
618	AGB 2005/102	Sicherheit des Verkehrssystems Strasse und dessen Kunstbauten: Methodik zur vergleichenden Risikobeurteilung	2009

no. de rapport.	no. de projet	titre	année
617	AGB 2005/100	Sicherheit des Verkehrssystems Strasse und dessen Kunstbauten Synthesebericht	2010
616	AGB 2002/020	Beurteilung von Risiken und Kriterien zur Festlegung akzeptierter Risiken in Folge aussergewöhnlicher Einwirkungen bei Kunstbauten	2009